DESIGN OF A LUNAR PROPELLANT PROCESSING FACILITY

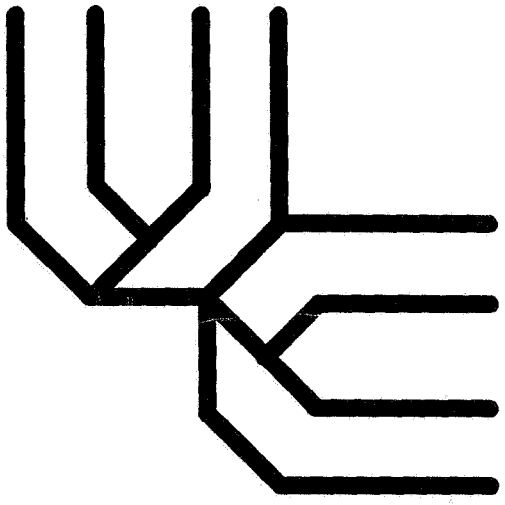

University of Cincinnati Space Engineering Research Center
NASA/USRA Advanced Design Program
Cincinnati, Ohio 45221-0343

July 28, 1993

ABSTRACT

Mankind's exploration of space will eventually lead to the establishment of a permanent human presence on the Moon. Essential to the economic viability of such an undertaking will be prudent utilization of indigenous lunar resources. The design of a lunar propellant processing system is presented. The system elements include facilities for ore processing, ice transportation, water splitting, propellant storage, personnel and materials transportation, human habitation, power generation, and communications.

The design scenario postulates that ice is present in the lunar polar regions, and that an initial lunar outpost has been established. Mining, ore processing, and water transportation operations are located in the polar regions. Water processing and propellant storage facilities are positioned near the equator. A general description of design operations is outlined below.

Regolith containing the ice is mined from permanently-shaded polar craters. Water is separated from the ore using a microwave processing technique, and refrozen into projectiles for launch to the equatorial site via railgun. A mass-catching device retrieves the ice. This ice is processed using fractional distillation to remove impurities, and the purified liquid water is fed to an electrolytic cell that splits the water into vaporous hydrogen and oxygen. They hydrogen and oxygen are condensed and stored separately in a tank farm.

Electric power for all operations is supplied by SP-100 nuclear reactors. Transportation of materials and personnel is accomplished primarily using chemical rockets. Modular living habitats are used which provide flexibility for the placement and number of personnel. A communications system consisting of lunar surface terminals, a lunar relay satellite, and terrestrial surface stations provides capabilities for continuous Moon-Moon and Moon-Earth transmissions of voice, picture, and data.

DESIGN OF A LUNAR PROPELLANT PROCESSING FACILITY

FINAL REPORT

NASA/USRA Advanced Design Program

Prepared By

Rajesh Batra
Jason Bell
J. Matt Campbell
Tom Cash
John Collins
Brian Dailey
Angelique France
Will Gareau
Mark Gleckler
Charles Hamilton
Kurt Hanson
Randall Hardin
Bobbi Hartwell
Steve Hudepohl
William Hull
Ken Koller
Larry Kruger
Rich Listo
John Papp
Bill Patrizio
John Penix
Chris Pickrell
Kathy Reicosky
Sherif Sakr
Greg Schreppel
Ed Schulte
Chris Staneluis
Tim Taulbee
Tom Walker
Heather Walls

Lead Instructor

Dr. Larry Cooper

Teaching Assistant

Joe Lemanski

Assistant Instructors

James Anno
Amy Ciric
Dave Greenberg
Arthur Helmicki
H. Thurman Henderson
Ray Lin
Joseph Nevin
Frank Weisgerber
Trevor Williams
Richard Wysong

University of Cincinnati Space Engineering Research Center
NASA/USRA Advanced Design Program
Cincinnati, Ohio 45221-0343

July 28, 1993

PREFACE

This year was the University of Cincinnati's initiation into the NASA/USRA Advanced Design Program. This association was initiated by the University of Cincinnati NASA Space Engineering Research Center to expose undergraduate students to space-related design opportunities.

More than fifty students and ten faculty from the Departments of Aerospace Engineering and Engineering Mechanics, Chemical Engineering, Civil and Environmental Engineering, Electrical and Computer Engineering, Materials Science and Engineering, and Nuclear and Power Engineering collaborated under the leadership of the NASA Space Engineering Research Center in a unique design effort. This interdisciplinary approach to design is intended to provide the students with a "real-world" experience; it was the first opportunity for most of the students to work with people outside their respective disciplines on a common project.

During Fall Quarter, experts from NASA, industry, and academia gave seminars on space-related topics. The students were presented with an overall design goal, and divided into design teams to identify key technologies and parametrics associated with achieving this goal. Most of the actual design work was accomplished during Winter Quarter. Spring Quarter was devoted to report writing and preparing for the USRA/ADP Annual Conference. Weekly meetings attended by students and faculty were held to address problems and project direction. The students also submitted weekly progress reports.

Our presentation at the NASA/USRA ADP Ninth Annual Conference in Houston, TX on June 16, 1993 was well received by attendees from NASA, USRA, industry, and academia. The students viewed their participation in the program as an invaluable experience, and several students reported that talking about the experience during job interviews drew great interest from the interviewers.

Joe Lemanski, Teaching Assistant
July 20, 1993

ACKNOWLEDGMENTS

The students would like to thank all professors listed and unlisted whose help and guidance were invaluable to the completion of this design project. A special thanks goes to Larry Cooper from the University of Cincinnati NASA Space Engineering Research Center, whose efforts made this project possible and exciting to work on.

Assistance was received from several industrial sources. In particular, the chemical engineering group would like to acknowledge James McElroy of United Technologies Hamilton Standard Division for his assistance on electrolyzer technology and design.

A final thanks to the USRA and center mentor Keith Henderson of NASA Johnson Space Center for making this experience available.

TABLE OF CONTENTS

1.0 EXECUTIVE SUMMARY

Joe Lemanski, Teaching Assistant

TABLE OF CONTENTS

1.1 INTRODUCTION

As currently envisioned, payloads for manned missions to the moon are dominated by propellant requirements. NASA's "Report on the 90-Day Study on the Human Exploration of the Moon and Mars" estimated that the mass launched to LEO for colonization of the Moon could be reduced by several hundred tons per year if propellant were produced on the Moon. This corresponds to savings in the $50 billion range, which justifies careful study of lunar in-situ propellant production. This work summarizes the design of a lunar propellant production facility and related operations.

1.2 DESIGN SCENARIO

This study assumes that ice containing frozen water and ammonia is present in permanently-shaded lunar polar regions [Arnold, J.R., "Ice in the Lunar Polar Regions, *J Geophysical Research* **84**, 5661 (1979)]. A second major assumption is that a preliminary lunar outpost has been established in an equatorial region that contains established habitats, emergency medical facilities, communication facilities, offloading equipment, and other items of infrastructure useful to the construction and operation of the proposed processing facility.

The design goal is to produce 15 metric tons of liquid oxygen and 2 metric tons of liquid hydrogen per month from the water and ammonia present at the north lunar pole for use as propellant at the lunar equator.

1.3 DESIGN OVERVIEW

The major systems designed to accomplish the design goal are shown in Figure 1.1 . Regolith containing the ice is mined at the north lunar pole. The resulting ore is fed to a microwave processing unit which separates the water, ammonia, and any other volatiles present from the regolith. The water and ammonia are refrozen into small projectiles at a railgun (ice-launcher) facility. The railgun converts electrical energy into mechanical energy and launches the ice projectiles toward a catching site at the equator.

A mobile mass catcher (much like a large funnel) tracks the incoming projectile and moves to the anticipated landing location to retrieve the ice. The resultant ice is sent to a processing facility. At this facility, the water and ammonia are separated using a cryogenic distillation column. The purified water is split into molecular oxygen and hydrogen using an electrolyzer. The ammonia is split into molecular hydrogen and nitrogen by heating the ammonia to high temperatures. The product gases are separately liquefied by compression and sent to a storage facility. The oxygen and hydrogen are used as propellant by a lunar transport vehicle, and the nitrogen is used both as a heat transfer medium and to maintain pressures in habitats.

A lunar transport vehicle (LTV) was designed to ferry equipment and personnel between the polar and equatorial processing sites. The LTV is constructed using a lightweight truss structure and uses four chemical rockets to transport up to four personnel.

Electricity is produced to support all operations using SP-100 nuclear reactors. Each reactor can produce about 1 MW. Communications are supported by the Deep Space Network with an additional lunar relay satellite.

Two different, modular lunar habitats were designed to support personnel at the polar and equatorial locations. Both habitats have a rigid structure capable of supporting a regolith shield for radiation protection.

1.4 ECONOMICS

For costing purposes, the composite rate for materials delivered to the polar region was assumed to be $50,000 per pound and to the equatorial region the rate is $35,000 per pound. Major equipment items were sized and costed for each system. The anticipated total project cost for purchasing major equipment items and delivering them to their respective sites was estimated to be $100 billion.

Process Flowchart

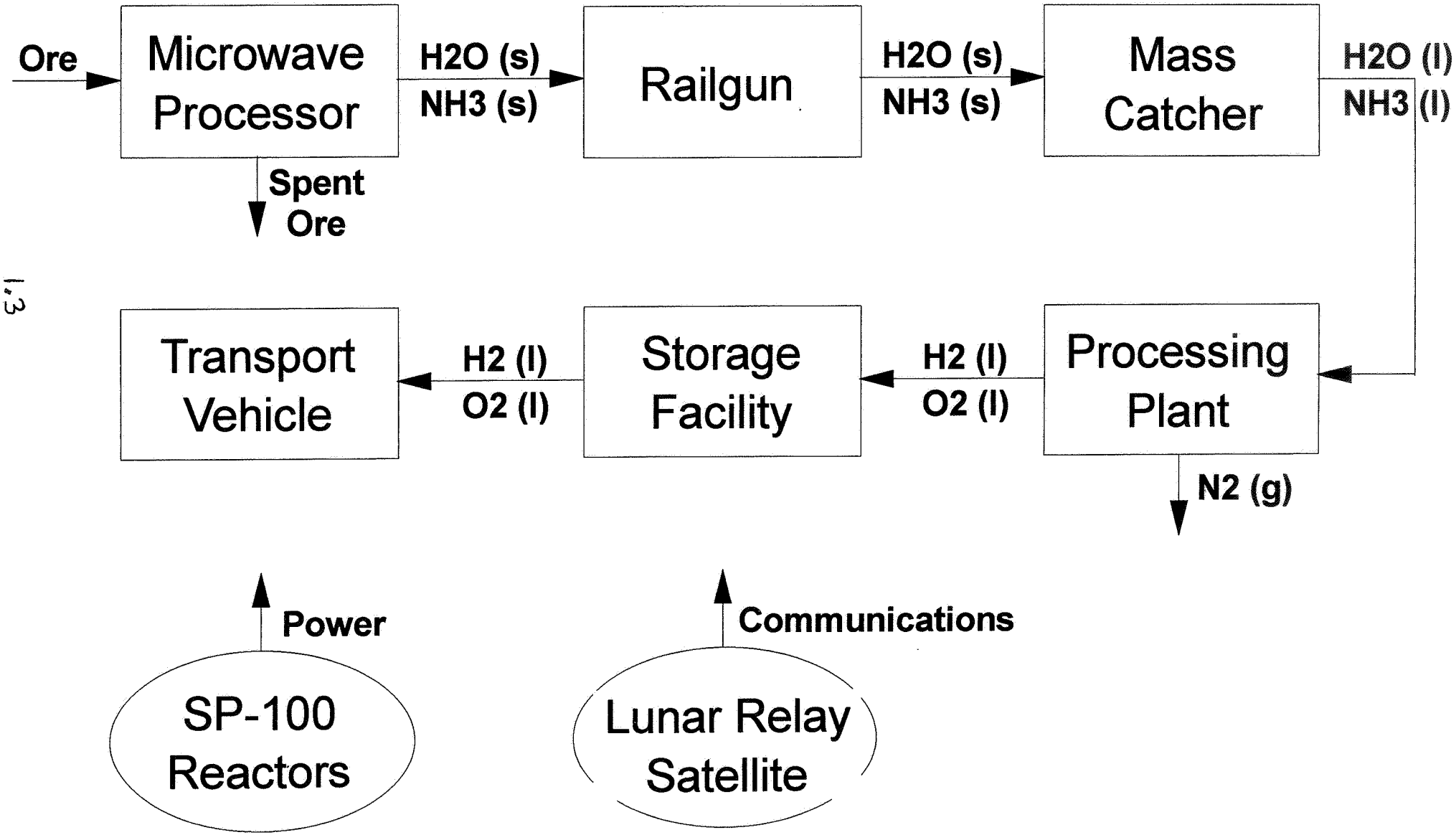

2.0 REGOLITH BENEFICIATION

Department of Materials Science and Engineering
Tom Cash
Tom Waters

TABLE OF CONTENTS

Tables and Figures

Table of Variables

Variable	Description
i	compound or element
X	mole fraction
P^o	vapor pressure
n	number of moles
(s)	solid
(l)	liquid
(v)	vapor
P_{fur}	pressure in furnace
P_{tan}	pressure in water storage tank
ΔH	enthalpy change per unit mass
ΔKE	kinetic energy change per unit mass
ΔPE	potential energy change per unit mass
Q	total energy of the system
W_s	work done by the system
h_f	friction forces

I. Abstract:

The basis for a lunar base to be successful will be its' ability to be self sufficient. To accomplish this, utilization of lunar resources for construction, fuel and life support will have to be demonstrated. As materials engineers, our responsibility will focus on the feasibility for the beneficiation of water and ammonia from the lunar regolith. The beneficiation facility will utilize a microwave heating technique in a batch furnace followed by a condensation process to extract water and ammonia from the lunar regolith. Based on the energy requirements, thermodynamics and kinetics of this extraction process, it is feasible to use microwave energy as a vaporization technique followed by a condensation process for the recovery of the volatiles.

II. Background:

One of the most convincing theories on how the moon was formed is a collision between the early Earth and a Mars-sized rocky planet about 4.5-billion years ago. The collision of this planet with the Earth threw a cloud of vaporized debris into orbit around Earth. This debris, which came mostly from the rocky parts of the impacting planet, formed a disk-like body in Earth's' orbit much like the rings around Saturn, this quickly collected into a single, large body which is now the moon.

The rapid rate of lunar assembly released large amounts of heat which produced near-global melting. As minerals began to crystallize in these "oceans of magma", the low-density aluminum-rich minerals floated upward, forming the lunar crust which is approximately 70 km thick. The high-density iron-rich minerals crystallized in the lower levels of the magma ocean, forming the lunar mantle which by mass, comprises most of the moon. This separation between the lunar crust and mantle

occurred about 4.5 to 4.4 billion years ago. Over the next 300 million years, bodies of molten rock continued to make its way through the crust producing layered bodies of a wide variety of different types of rocks. The dark plains that dominate the near side of the moon are lava flows that erupted mostly between 3.8 and 3.0 billion years ago.

The main process operating on the moon for the last 3 billion years has been impact cratering by microscopic meteorites. These showers of meteorites have ground up the lunar surface into powdery masses, fine debris and rock fragments that are several meters thick. This material is known as regolith and is characterized by particles less than 1 cm in diameter. Regolith is mostly a type of powder that is analogous to concrete powder in color, behavior and consistency. This resemblance to concrete powder brings about several important considerations. The regolith has a tendency to float in the small gravitational field of the moon and attaches itself to everything. This thin coating of regolith tends to cause problems among movable parts on machinery such as bearings, joints, etc. Tables 1 [8] and 2 [9] show average compositions of the lunar soil as reported from two seperate publications. This consistensy between reported values allows some confidence in using these compositions. Table 3 [10] shows some physical parameters of the regolith.

Table 1 Chemical compositions of lunar soil samples brought to Earth

Compound	Basaltic rock "Luna-16"	Fine Fraction "Luna-16"	Basaltic Rock "Apollo-12"	Fine Fraction "Apollo-12"
SiO2	43.8	41.7	40	42
TiO2	4.9	3.39	3.7	3.1
Al2O3	13.65	15.32	11.2	14
FeO	19.35	16.8	21.3	17
MgO	7.05	8.73	11.7	12
CaO	10.4	12.2	10.7	10
Na2O	.33	.37	.45	.40
K2O	.15	.10	.065	.18
MnO	.2	.21	.26	.25
Cr2O3	.28	.31	.55	.41
ZrO2	.04	.015	.023	.009

Table 2 Average composition of soil samples (<1 mm fraction).

	Apollo					Luna	
	11	12	14	15	16	16	20
SiO2	42.04	46.40	47.93	46.61	44.94	41.70	45.40
TiO2	7.48	2.66	1.74	1.36	.58	3.38	.47
Al2O3	13.92	13.50	17.60	17.18	26.71	15.33	23.44
FeO	15.74	15.50	10.37	11.62	5.49	16.64	7.37
MgO	7.90	9.73	9.24	10.46	5.96	8.78	9.19
CaO	12.01	10.5	11.19	11.64	15.57	12.50	13.38
Na2O	.44	.59	.68	.46	.48	.34	.29
K2O	.14	.32	.55	.20	.13	.10	.07
P2O5	.12	.40	.53	.19	.12	-----	.06
MnO	.21	.21	.14	.16	.07	.21	.10
Cr2O3	.30	.40	.25	.25	.12	.28	.14

Table 3

Conductivity (k) = 2x10^-6 cal/(cm sec K)
Density (p) = 1.65 g/cc
Specific Heat (c) = .06 - .20 cal/(g K)

An aspect that must be considered when constructing facilities on the moon is the range in temperatures. At the equator, the temperature on the near side of the moon reaches approximately 400 K. At the poles of the moon, the temperature falls to approximately 100 K. The temperature range is a major consideration for materials that are to be used for construction on the moon. Another consideration is

whether the construction will see an eclipse during its lifetime. Figure 1 [10] on page 9 illustrates the changes in temperatures at different depths in the lunar surface as a function of time during an eclipse of the moon. It is clearly be seen from the graph that the temperature on the surface of the moon drastically decreases from approximately 400 K to 200 K in the first hour during an eclipse. Thus, any materials exposed to this rapid change in temperature must have comparable thermal expansion coefficients and must not be susceptible to thermal shock. Also note that materials embedded in the lunar surface, such as those used for construction, will experience a wide range in temperature from a depth of a few meters to the surface.

The discovery of ice on the moon provides the major significant source of lunar hydrogen. Among the scores of other uses, the hydrogen could be used along with oxygen to fuel rockets - both those taking supplies between Earth and the moon and those outbound to other planets. To date, all fuel has necessarily been carried from Earth. Launching an item from the Earth takes a great deal of energy. Most of what is launched is the fuel needed for acceleration the first few hundred kilometers above the surface of the Earth. If materials can be produced on the moon, rather than bringing them from Earth, all the extra mass launched as fuel to get them back to the Earth or to another outpost would no longer be required.

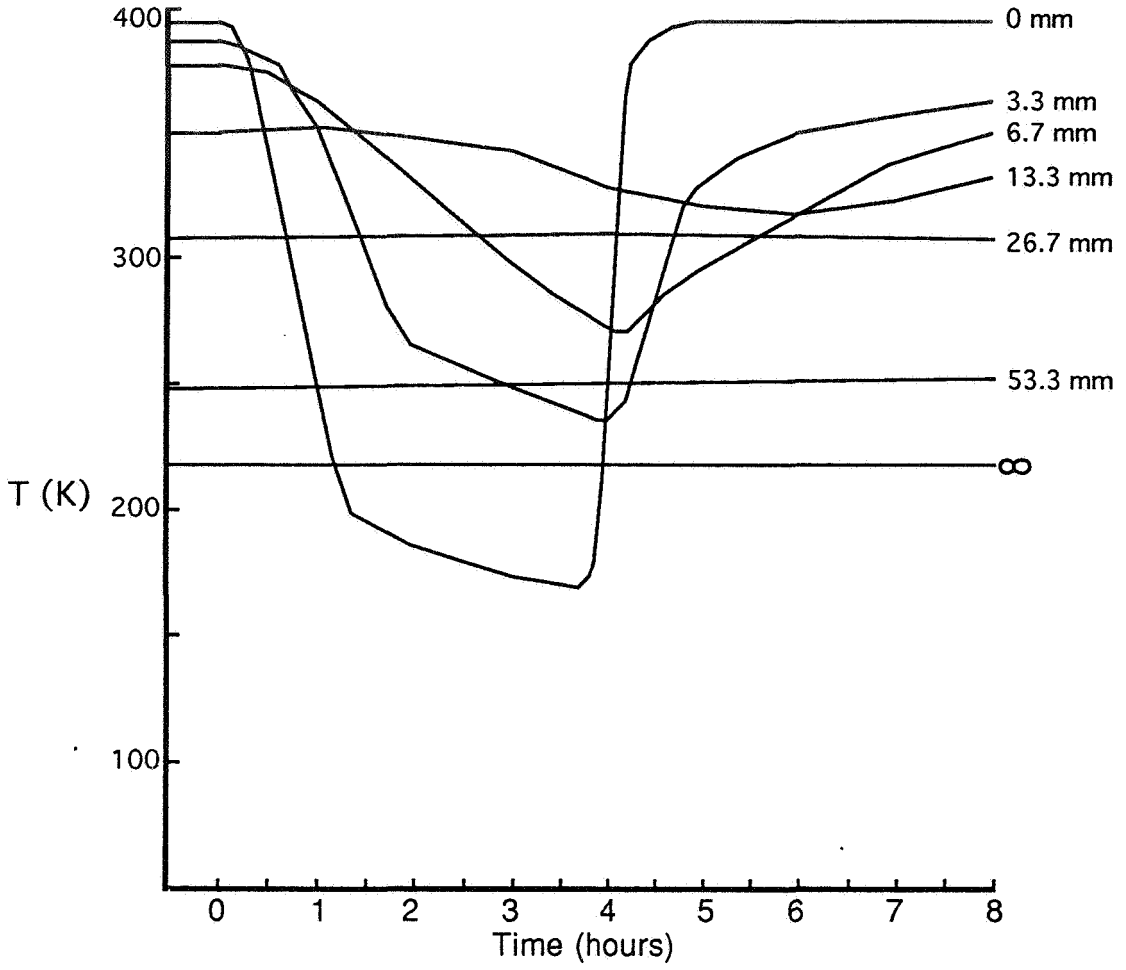

Figure 1.

Computed surface and subsurface temperatures, T, at points in the lunar thermal equator, during an eclipse of the moon. The numbers by individual curves refer, in each case, to the depth below the surface. A value of $\beta = 10^3\ cm^2\ sec^{1/2}\ K\ cal^{-1}$ has been assumed in each case. (From unpublished calculations by D. O. Gough).

The ice has been found no more than 200 km from the northern polar region of the moon, where the lunar surface is permanently in the shade. The temperatures there are about 100 K. It is expected that ice may be found at the southern region as well, but exploration of the region has not yet started. The ice is composed of frozen water and ammonia, along with traces of other substances, interspersed in the regolith from 0.5 to 10 meters beneath the surface.

The average concentration of ice in the ice fields is at least 0.25 kilograms(mass) per cubic meter regolith and 0.03 kilograms(mass) per cubic meter regolith.

For several reasons mentioned above, it is desired to process the ice into hydrogen and oxygen, and store these products in the vicinity of the existing Lunar Research Center which is located near the crater Davinci (Longitude 42 E, Latitude 10.5 N) in the equatorial region of the moon. At this site there are habitats, emergency medical facilities, communication facilities, off loading equipment and other items of infrastructure useful to the construction and operation of the proposed propellant processing facility. The mining site is located near the Roshdestrensky Crater in the northern polar region of the moon (Longitude 15 W, Latitude 86 N), which is approximately 1500 miles from the Lunar Research Center. Near the mining site, a beneficiation facility must be designed to extract the ice from the regolith.

III. Introduction:

As manned efforts proceed toward the colonization of the moon, propulsion and life support systems will place the greatest demands on technology and resources. Since the most advanced chemical propulsion systems use hydrogen and oxygen as propellants, the availability of these elements is a very important issue. A solution is to extract water from the lunar regolith for decomposition into hydrogen and oxygen.

A batch system using microwave energy to evaporate ice from the regolith is being designed. The microwave system uses electrical energy from a nuclear reactor, so that using the hydrogen and oxygen produced is unnecessary, which is a very attractive feature in the use of this system.

IV. Beneficiation Facility:

The purpose of this facility is to provide the hydrogen/oxygen production plant with a requisite amount of water to meet the production requirements imposed . One of the few details established is that the plant will not be justified unless it can produce a minimum of 15000 kg of oxygen and 2000 kg of hydrogen per month for a life span of twenty years. It must also have a surge capacity to support twice the nominal amount one month per year.

IV.1. *Processing Amounts:*

The beneficiation facility extracts the ice from the regolith by evaporation. To produce the amount of water required, the beneficiation facility will need to process 71327 cubic meters of regolith per month. This translates into 17832 kilograms of water per month. At 100% efficiency, this will produce 2000 kg of hydrogen and 15832 kg of oxygen per month. But, by using a vaporization process, 2140 kilograms of ammonia will also be extracted from the regolith. By using the hydrogen from the ammonia, hydrogen becomes the limiting element. Thus, in order to produce the required amount of liquid substance, 67580 cubic meters of regolith will need to be processed per month. This will produce 16895 kilograms of water mixed with 2027 kilograms of ammonia per month. These amounts translate into 2255 kg of hydrogen and 15000 kg of oxygen per month. Table 4 shows the advantage in processing ammonia.

Processing/Production per Month					
Extracting Hydrogen	From Water Only		Extracting Hydrogen	From Ammonia Also	
Regolith	Water	Ammonia	Regolith	Water	Ammonia
71327 m^3	17.8 m^3	2.8 m^3	67580 m^3	16.9 m^3	2.6 m^3
90228655 kg	17832 kg	2140 kg	85488368 kg	16895 kg	2027 kg
	4693 gallons	733 gallons		4446 gallons	695 gallons
Produces-	Oxygen:	15832 kg	Produces-	Oxygen:	15000 kg
	Hydrogen:	2000 kg		Hydrogen:	2255 kg

Table 4.
Advantages in processing ammonia.

Due to factors in the process, an estimation of 80% of the ice will be processed. Thus, a volume of 84475 m^3 of regolith will need to be processed per month to produce the required amount of oxygen and hydrogen.

IV.2. *Application of Microwave Energy :*

The use of microwave energy will provide a very efficient method of heating lunar regolith. Not only can regolith be heated with less energy than conventional methods, but the heating will be accomplished in a controlled manner and in much less time. This is due in part to the ability to control field intensities, heating rates, and maximum temperatures during microwave heating. Also, microwave energy tends to heat the regolith volume uniformly. High absorption rates of microwave energy are desirable if the process is to be feasible. In the application of microwave heating for regolith, knowledge of the dielectric properties is required to predict heating behavior. The absorption of microwave energy is determined by the relative complex permittivity, consisting of the dielectric constant and the product of the loss tangent and dielectric loss factor.

Dielectric constant = E'
Dielectric loss factor = E"
Loss tangent = j
Relative complex permittivity (E) = E' + jE"

Energy absorption of microwaves in a dielectric material increases with frequency and also with the product of the loss tangent and dielectric loss factor. The loss tangent shows higher variation with frequency than the dielectric constant does and is therefore the main factor in considering dielectric losses.

Insulating materials such as basalt, ilmenite, and feldspars, which are present in the in the lunar regolith (ilmenite being the most common lunar mineral [11]), couple at microwave frequencies of 2.45 GHz which increases microwave absorption [7]. Thus, high heating rates can be achieved. With respect to lunar processing, this

fact may be exploited commercially by not having to transport coupling agents into space.

Figure 2 shows the variations of the dielectric constant (E') and the dielectric loss factor (E") for ilmenite at a microwave frequency corresponding to 2.45 GHz for several densities [4]. Since the mean density of the lunar soil is 1.65 g/cm^3 [10], the values for the dielectric constant and the dielectric loss factor can be estimated at 3.99 and 1.71 , respectively. Figure 3 shows the dielectric loss tangent at a frequency of 2.45 GHz for several densities. At a density of 1.65 g/cm^3 the loss tangent has a value of approximately 0.254.

To obtain the amount of oxygen and hydrogen required with an 80% efficiency, a volume of 1.955 m^3 must be processed each minute. The amount of power output needed to heat a volume of 0.1 m^3 (1 meter length x 2 meter width x 0.05 meter depth) from 100 K to 473 K is approximately 9305 watts. This power output produces an electric field value of 4893 volts/meter. Thus, a series of twenty 15000 watt magnetrons will be used each being placed one meter apart along the length of each chamber. Each magnetron will be run at 62% of its total power output and will need a supply of 18.6 kilovolts.

Ilmenite

Figure 2

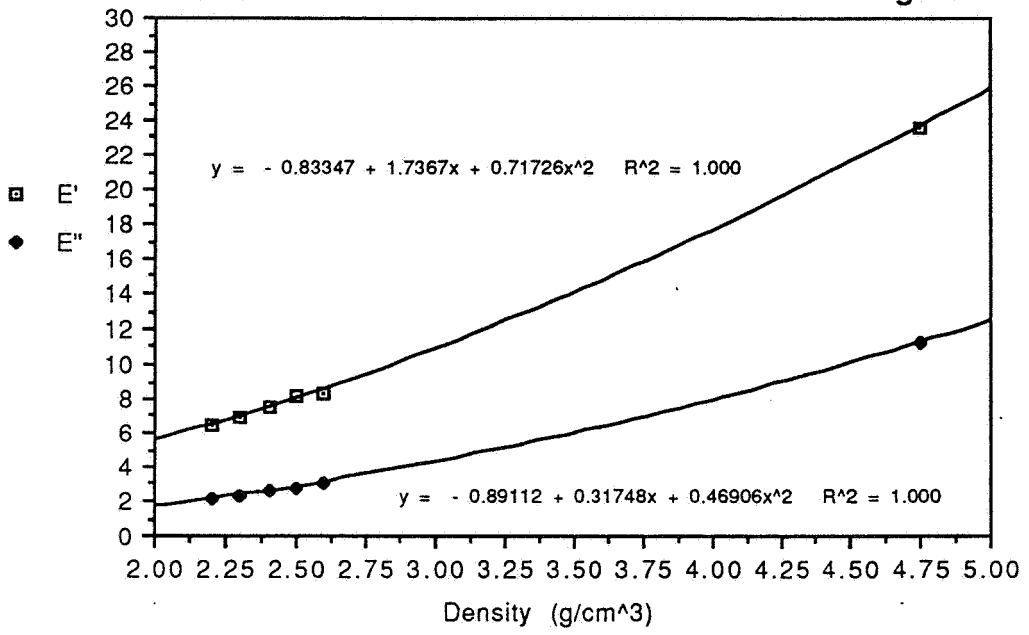

Ilmenite

Figure 3

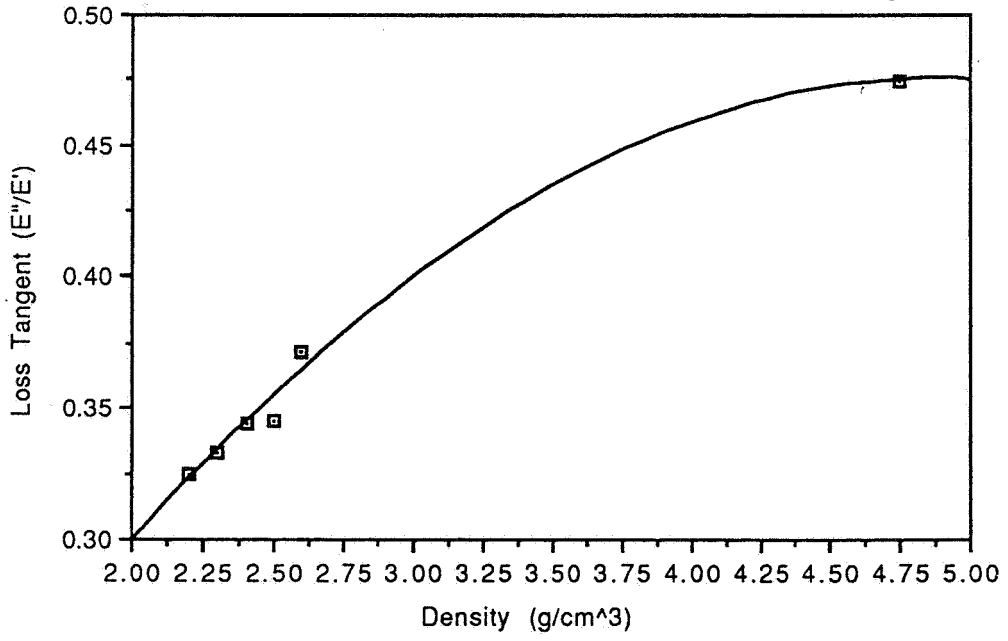

IV.3. *The Condensation Process:*

Condensation is a thermodynamic process that transforms a compound and/or element from the vapor phase to the liquid phase. The constituents of this system are water and ammonia. The vapor will condense to a liquid after the required amount of heat (energy) is removed from the system. The energy to be extracted from the system to condense the vapor is dependent on the specific heat, heat of vaporization and the mass of the vapor in the system. The rate of condensation will be dependent of the rate that the heat can be extracted from the system.

IV.4. *Facility Design and Processing:*

The batch conveyorized microwave system shown in Figure 3 (Appendix) is composed of a hopper (A) and two aluminum chambers (B & C) which are separated by doors. One door (AB) seals off the hopper from chamber (B), and one door (BC) seals off chamber (B) from chamber (C) during the heating process. Each chamber will have a length of 20 meters, a width of 2.1 meters, and a depth of 0.2 meter. Each of the chambers also has its own steel cord conveyor belt (1b & 1c) to move the regolith through the furnace.

The hopper is a holding compartment for the regolith yet to be processed. Mined regolith is delivered into the hopper from the mining site. Inside the hopper is a pulverizer (1a) which grounds the regolith into smaller particles to insure a uniform heating and to release any ice that may be trapped within clustered balls of regolith. Towards the bottom of the hopper is a finned roller (2a) which prevents clogging and spreads a uniform layer of regolith over the moving conveyor belt below. Chamber (B) is the initial heating station where most of the water will be

evaporated. Above the conveyors are a series of twenty 15000 watt magnetrons (D) which convert electrical energy into microwave energy. Microwaves are fed into the microwave cavities (1d) and dispersed throughout the chamber by wave guides (2d) to heat the regolith to approximately 200 degrees Celsius on the conveyor belt below. The walls of the chamber will have a thin coating of plasma sprayed regolith. This allows the walls of the chamber to moderately absorb a small fraction of the microwave energy effectively maintaining a wall temperature hot enough to prevent the condensation of liquid on the chamber walls. Located at the top of the chamber is a series of valves (E) to allow the flow of vapor into heat exchangers (F) that run along the outside wall of each chamber. (The condensation process will be covered in detail in section IV.4.) Covering each of the vapor flow openings in the chamber is a porous material that prevents microwaves from entering while allowing the vapor to flow into the heat exchangers. This cover will also be heated by the microwaves to prevent vapor condensation.

Most of the water trapped in the regolith will be exposed when transferred from the conveyor in chamber (B) to the conveyor in chamber (C) due to the inversion and mixing action caused by such transfer. Chamber (C) is the final heating stage which evaporates any ice left after the initial vaporization in chamber (B). All other principles in chamber (C) are analogous to those in chamber (B). Included in chambers (B) and (C) are optical pyrometers continuously monitoring the temperature of the regolith. These pyrometers will provide feedback to the control system so that the magnetrons in each chamber will maintain the temperature of the product within a designated temperature range.

Since the outside temperature at the location of the beneficiation facility is approximately 100 K, the water storage tank will be heated with the heat given off by the nuclear reactors' cooling system to prevent solidification. After the final stage of

heating, the regolith is dumped into vessels which the mining facility will transfer back to the mining site and the water stored in the tanks will be readily accessible to the transportation facility through a drainage valve (H).

The regolith will be heated in the furnace as described earlier in the paper. Figure 5 on page A2 describes the thermodynamic steps for the ice and ammonia throughout the process. As the system in step1 is heated from an initial 100 K, the first transformation will take place at 240 K. Here the ammonia (NH_3) will begin to vaporize until most of the NH_3 is in the gaseous phase. As heating continues, the pressure in the furnace will be governed by Raoult's Law:

$$P_{total} = X(NH_3) \times P^o(NH_3) + X(H_2O) \times P^o(H_2O)$$

Since the composition of the vapor at this point is nearly 100% NH3 and all the NH3 is now a gas, the mole fraction of NH3 will be the total number of moles in the system and the equation reduces to:

$$P_{total} = n(NH_3) \times P^o(NH_3)$$

The system is now in a dynamic state with the temperature and pressure increasing with time. The pressure in the system will be less than the vapor pressure of water from 240 K to 473 K such that the process will continue to step 3. At some point to be determined during this dynamic state, the valve will be opened to allow the $H_2O(v)$ and $NH_3(v)$ to pass through the heat exchanger(5) starting the condensation process. The $H_2O(v)$ will condense due to the loss of heat through the heat exchanger. The condensation will produce a thermosyphon which will be the driving force for the mass transport of vapor from the furnace to the tank. The

thermosyphoning will continue until the pressure in the furnace is equal to that of the pressure in the storage tank.

$$P_{fur} = X(H_2O) \times P^o(H_2O) \quad \text{at 473 K}$$

$$P_{tan} = n(NH_3) \times P^o(NH_3) \quad \text{at 278 K}$$

The temperature in the condensate tank will be kept at a temperature of 278 K in step 6. At this temperature, the NH_3 will still be in the vapor phase and can be extracted in step 7 and stored in a separate tank(8). The NH_3 tank will be stored at a location nearby on the lunar surface where the temperature is a nominal 100 K which is below the saturation point of liquid ammonia.

The number of moles of H_2O left in the furnace and essentially the amount left in the regolith after one cycle is completed.

$$X(H2O) = \frac{X(NH_3) \times P^o(NH_3) \text{ at 278 K}}{P^o(H_2O) \text{ at 473 K}}$$

The rate of heat removal will be the rate determining step in the beneficiation process. This will be determined by the size of the heat exchanger(s) that can be provided with current technology. The mass of H_2O to be condensed in a given cycle time can then be determined based on the application of Bernoulli's Equation for a compressible fluid between points 1 and 2 in Figure 6 on page A3.

$$\Delta H + \Delta KE + \Delta PE = Q + W_S - h_f$$

The kinetic energy change, potential energy change, shaft work and friction losses will be assumed to be negligible compared to the enthalpy change and the heat transfer such that the equation reduces to:

$$\Delta H = Q$$

This will provide the energy per unit mass per unit time needed for the condensation process.

V. Conclusions:

1. Microwave energy is a feasible method of heating the regolith for the vaporization of the water and ammonia.

2. The use of heat exchangers to condense the water vapor and separate the ammonia gas is possible.

3. The use of current technology for the beneficiation facility will reduce the lead time for the implementation of said facility.

VI. Recommendations:

1. Final decisions on the sizing of magnetrons, heat exchangers, tanks must be completed so that decisions on materials of construction, failure analysis and cost for construction on the lunar surface can be accomplished.

2. A lab scale prototype should be manufactured to analyze the heating, thermodynamics and kinetics of the current designed process for the proper scale-up to production equipment.

VII. References:

1. R. V. Decareau, *Microwaves in the Food Processing Industry,* Academic Press, New York, New York, 1985.

2. D. A. Copson, *Microwave Heating in Freeze-Drying, Electronic Ovens , and Other Applications,* AVI Publishing Company, Westport, CN, 1962.

3. K. G. Budinski, *Engineering Materials , Properties & Selection,* Prentice Hall, Englewood Cliffs, NJ, 1979.

4. S. Nelson, D. Lindroth, R. Blake, *Dielectric Properties of Selected and Purified Minerals at 1 to 22 GHz,* Journal of Microwave Power, V4, N4 1989, pp213-20.

5. J. Sochanski, J. Goyette, T. Bose, C. Akyel, R. Bosisio, *Freeze-Drying of Yhin Plates by Microwave,* Journal of Microwave Power, V26, N2 1991, pp91-100.

6. I. Turner, P. Jolly, *The Effect of Dielectric Properties on Microwave Drying Kinetics,* Journal of Microwave Power, V25, N4 1990, pp211-23

7. D.S. Tucker, D.T. Vaniman, J.L. Anderson, F.W. Clinard, jr., R.C. Feber, jr., H.M. Frost, T.T. Meek, T.C. Wallace, *Hydrogen Recovery from Extraterrestrial Materials using Microwave Energy,* Papers from a NASA-sponsored, public symposium, Oct. 29-31, 1984, pp 583-590.

8. Edited by A. Yu. Ishlinskii, *Lunar Soil Science,* Keterpress Enterprises, Jerusalem, 1975.

9. Stuart Ross Taylor, *Lunar Science: A Post-Apollo View,* Pergamon Press Inc., New York, 1975.

10. Edited by G. Fielder, *Geology and Physics of the Moon,* Elsevier Publishing Inc., Amsterdam, The Netherlands, 1971.

11. J.W. Frondel, *A Glossary of Luanr Materials,* John Wiley, New York, 1973, p 72.

APPENDIX

Cost Analysis:

System	Amount	Mass (kg)	Cost per item($)	Cost($)
Outer Furnace	2	2530	7,500	15, 000
Internal Microwave	2	1,000	1,000,000	2,000,000
Heat Exchangers	60	35	350	21, 000
Piping	120 meters	1875	70 per meter	8, 400
Primary Water Tank	2	1215	5,000	10, 000
Secondary Tank	2	486	3,500	7, 000
Ammonia Tank	2	243	2,000	4, 000

	Mass (kg)	Cost ($)
Sub Totals	14,923	2,065,400
Transportation cost:	$110,230 per kg	1,644,962,290

TOTAL COST OF BENEFICIATION FACILITY **$ 1,647,027,690**

Conveyorized Batch Microwave System

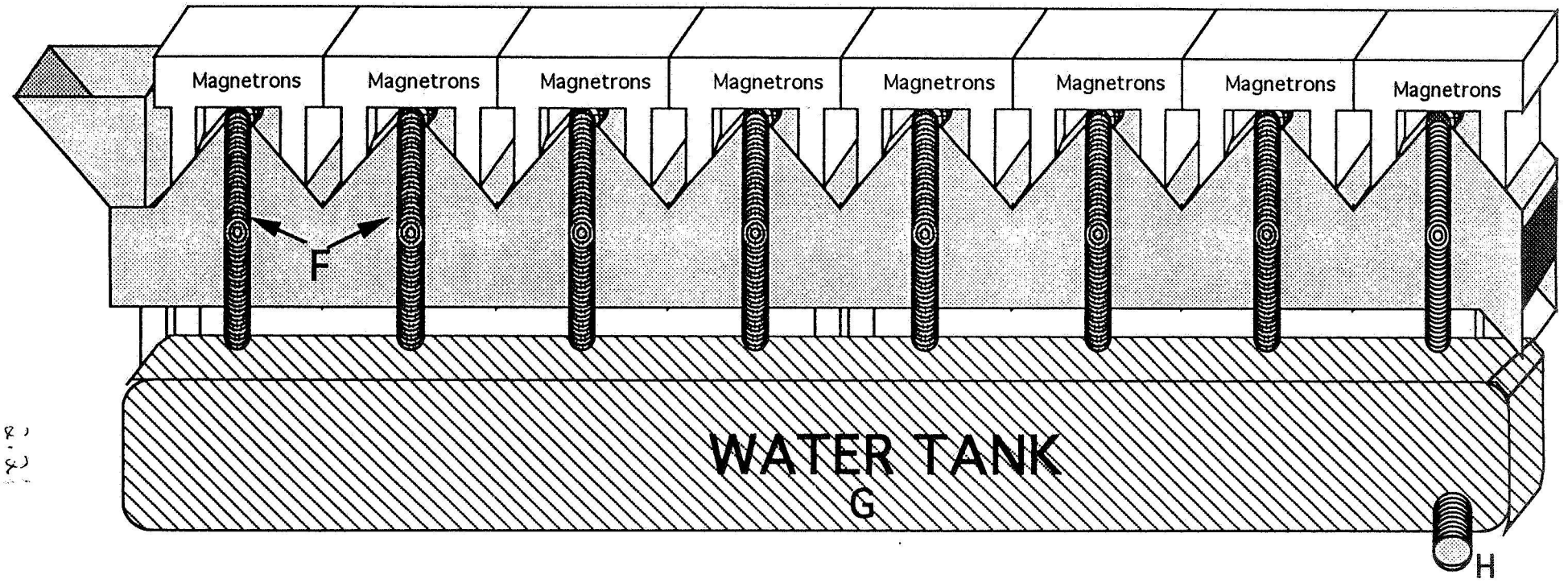

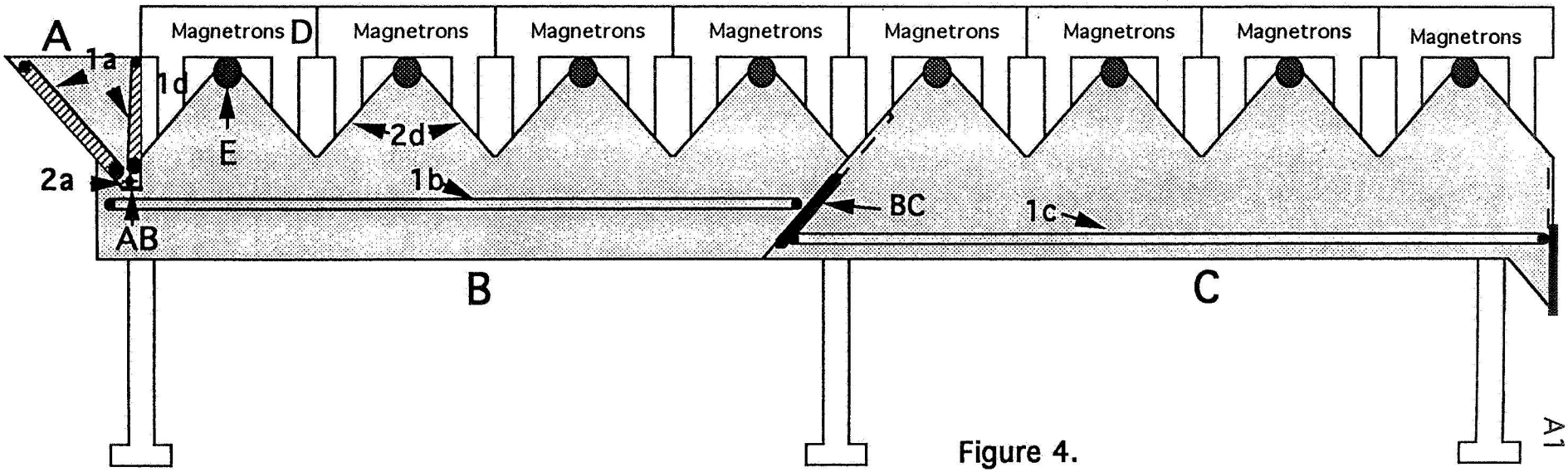

Figure 4.

A1

Flow Chart

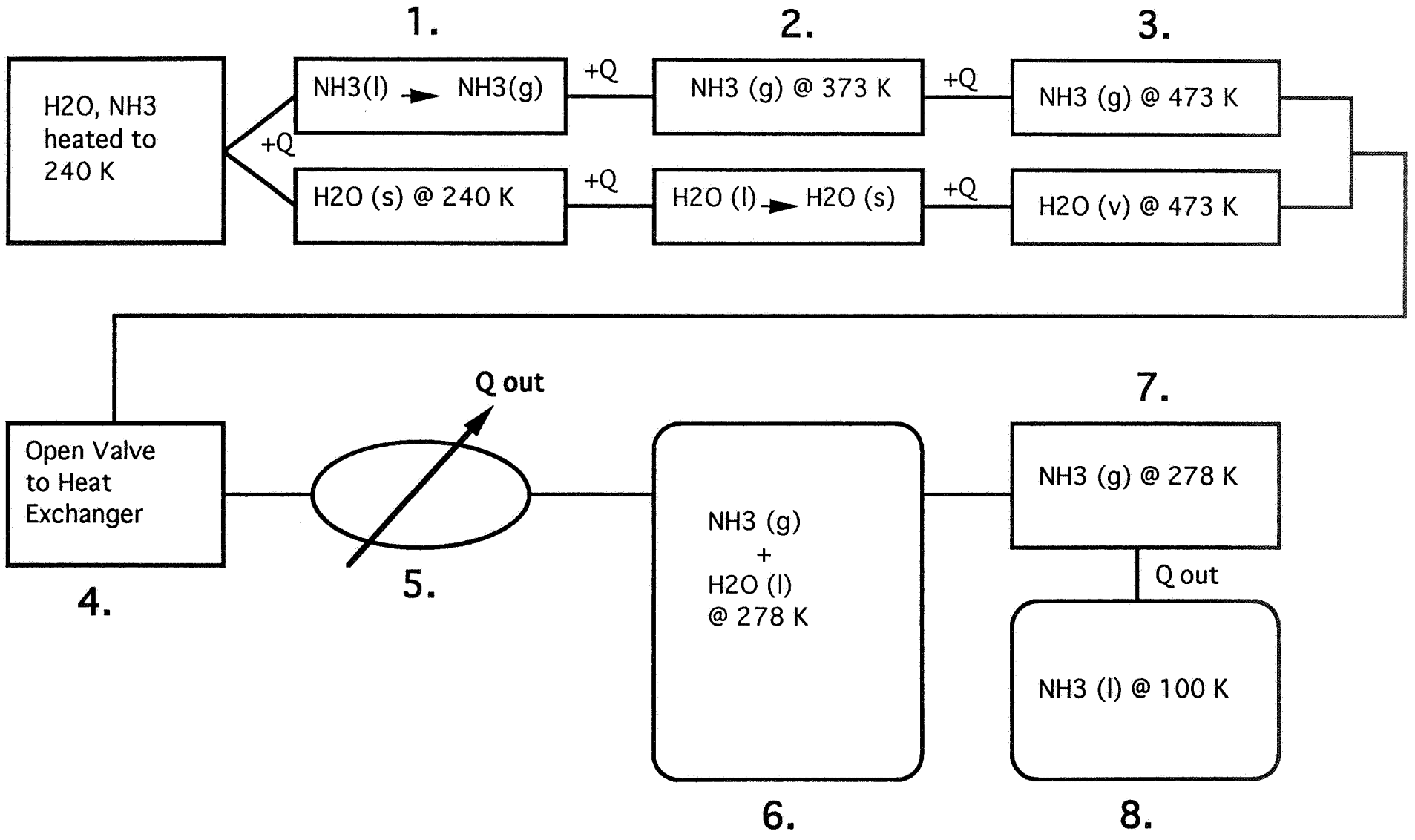

Figure 5.

Temperature - Pressure Relationship Between
Furnace and Water/Ammonia Storage Tank

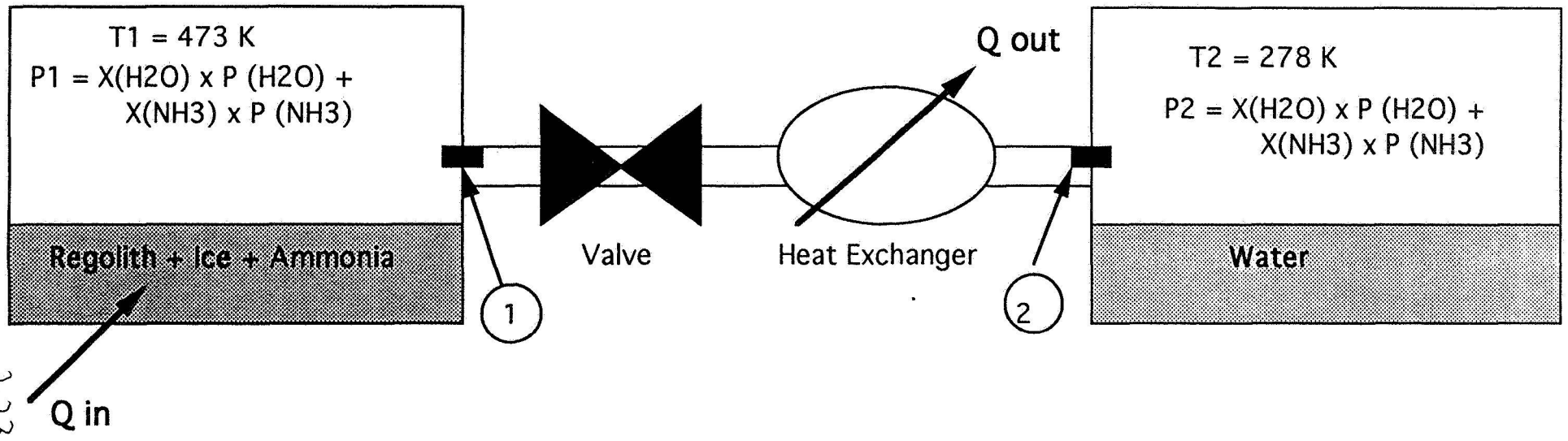

2.23

Figure 6.

3.0 TRANSPORTATION

Department of Aerospace Engineering and Engineering Mechanics
Rajesh Batra
Jason Bell
John Collins
Brian Dailey
Angelique France
Charles Hamilton
Kurt Hanson
William Hull
Kenneth Koller
John Papp

TABLE OF CONTENTS

HUMAN TRANSPORTATION

Abstract

The recent discovery of ice at the northern polar regions of the Moon provides the only known source of lunar hydrogen. This monumental discovery is quite possibly one of the most important results of lunar exploration to date, as it could provide water for life support at the various lunar bases, and a plentiful supply of hydrogen. Up to this date, the only other source of lunar hydrogen was the highly volatile "free hydrogen," which is carried by the solar wind and trapped in extremely low concentrations in the lunar regolith. Hydrogen and oxygen extracted from the lunar ice could be used as a propellant to fuel rocket propelled vehicles - those ferrying people, equipment, and supplies from base to base or between the Earth and the Moon, and, eventually, those vehicles destined for other planets. Also, the oxygen produced could be used to supplement life-support systems at the various lunar bases.

It is desired to extract hydrogen and oxygen from the lunar ice. The main processing plant and storage facilities are located in the Lunar Industrial Park, adjacent to the Lunar Research Center (LRC), which is just outside Jordy City, near the crater Davinci in the equatorial region of the Moon (Longitude 42 E, Latitude 10.5 N). This centralized site has existing habitats, emergency medical facilities, communication facilities, and other infrastructure items necessary for life-support and the processing of the lunar ice. Since the mining site is located in the northern polar region (near the Roshdestrensky Crater - Longitude 150 W, Latitude 86 N), approximately 1500 miles from the LRC, a lunar transportation system must be designed and implemented in order to provide for transportation of the lunar ice, people, equipment, and supplies from pole to equator and back.

Aerospace Design Group Task

The Aerospace Design Group is divided into two subgroups: one to examine the transportation of the mined lunar regolith from the mining site in the northern polar region to the LRC, and another to investigate the transporting of people and/or equipment between the mining site and the LRC, as well as other exploratory missions. Our design assessment resulted in following conclusions:

(1) The mined regolith will be transported from the mining site to the vicinity of the Lunar Research Center by an electromagnetically powered railgun-catcher system. This system will launch the 177 lb (80 kg) "bundles" of mined material approximately 10 times a day (i.e., 24 Earth-hour period).

(2) Skilled personnel and/or specialized equipment and supplies will be transported to and from the two sites by means of a Lunar Transportation Vehicle (LTV). This

sophisticated, reusable vehicle is designed to carry a standard payload of four (4) crew persons at 400 lb (178.5 kg) each, and 1000 lb (446 kg) of cargo.

This report addresses the design, construction, and maintenance of these two systems and their corresponding subsystems.

1.0 Railgun Introduction

There are many reasons to choose a railgun for bulk ice transport over the various other options available. Given the fact that a continuous transportation system could be prone to breakdowns at inconvenient or even dangerous locations and considering that a design of this type would require massive amounts of raw materials to traverse the almost 1500 miles from the lunar pole to the equator, the concepts of a lunar railway, pipeline, tramway, etc. were discarded as an option. Similar complications arise with more versatile mobile surface transportation systems such as lunar rovers, trucks, and 'hopping' vehicles[10]. Additionally, difficulties such as lunar dust contamination, massive road construction projects, and possible long detour routes around lunar surface obstructions are introduced. A decision was made to limit the bulk ice transportation system to a point-to-point method involving either rocket or ballistic transportation and thus isolate breakdown and maintenance to two specific points--the take off and landing locations. Preliminary calculations revealed that ice transportation by a conventional chemical rocket required more fuel than could be processed from the transported ice. Consequently, the option of ballistic transportation was examined more closely. Of the many ballistic means of ice transportation, the choice of the electromagnetic railgun is preferred due to its high projectile exit velocity, use of readily available electric power, and expandability to new mission parameters such as surface-to-orbit or Moon-to-Earth bulk transportation.

The use of a railgun for the acceleration of a projectile is a concept that has been analyzed both experimentally and theoretically for more than a two decades. Experiments conducted in the seventies[3] and theoretical reports from the early eighties[11] began to show the advantages of a railgun design. More recent reports[9] have improved upon these early analysis and offer solutions to the enormous energy requirements of railgun designs[5][13] with ever increasing efficiency. All these combine to show the effectiveness of a railgun in achieving the requirements necessary for the proposed design criteria.

A railgun is very similar to a conventional canon; the only difference is the form of propulsive force. For the canon, it is the chemical reaction of gun powder and air; while for the railgun, it is the simple physical principle of current loops through a magnetic field. Both achieve the same goal--supply extremely large values of propulsive force producing high exit velocities. The components of a simple railgun are two parallel, current carrying plates, a power supply, an armature, and the projectile. By connecting the power source to the current carrying plates and armature, a current loop is created along with an induced magnetic field. The interaction between the current and induced magnetic field produces the force on the projectile. By applying a large power supply, tremendous exit

velocities of up to several kilometers per second for small masses can be attained. [3] [9] [11].

The initial railgun design used basic electromagnetic theory to conceptualize and parameterize important variables such as railgun length, power requirements, achievable exit velocity, and launch mass dependency. The resulting parameters proved somewhat intimidating, i.e., extremely large power, force, current, and voltage values. Therefore, a new means of improving railgun design and performance is investigated. The result is the Distributed Energy Source (DES) railgun concept[7][9][11]. By dividing the original one-piece railgun into seperate, powered sections, certain parameters such as power, exit velocity, and efficiency are more readily controlled and improved. This concept also allows for the expandability to surface-to-orbit or Moon-to-Earth launches by the addition of powered sections and increasing the exit velocity of the projectile. Furthemore, because the designed railgun system is modular, it is easily assembled and disassembled to offer portability in case there is a discovery of new ice locations. With the DES railgun chosen as the primary launch means for the raw ice, the repeatability and accuracy of such a launch scheme is investigated. The methods and final results of this design are presented in the following sections.

1.1 The Railgun Design for Transport of Bulk Lunar Ice

A quick introduction of the basic principles behind the dynamics of a railgun is necessary to understand concepts used further in this report. Initially, the idealized, frictionless, one dimensional railgun model is investigated. The basic principles of a one-dimensional railgun is then expanded to a two dimensional model. Finally, the advanced concept of distributed energy sources for the design of a more efficient railgun is introduced. This concept is then used to design a railgun meeting the requirements for bulk ice transportation.

1.1.1 The One Dimensional Railgun

A simple model of a one dimensional railgun is shown in Figure 1.1.1 The components of this 1D model are two current carrying wires, an armature, and a power source. As can be seen, a 1D railgun is simply a current loop in a magnetic field with a moveable armature.

One dimensional railgun visualization

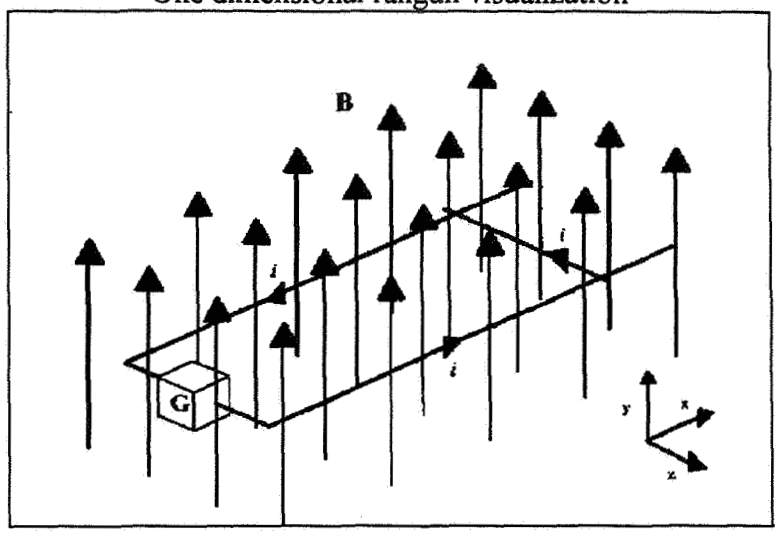

Figure 1.1.1

Inherently, a moving current immersed in a magnetic field produces a force acting on the object conducting the current. This physical concept is described by the governing equation for a 1D railgun

$$\mathbf{F} = I\mathbf{L} \times \mathbf{B} \tag{1.1.1}$$

where **F** is the vector force in Newtons, **I** is the current vector in amps pointing in the direction of current flow, L is the length magnitude in meters, and **B** is the magnetic field vector in Teslas. Immediate deduction shows that the current vector must be at right angles to the magnetic field to produce the maximum propelling force on the projectile.

Figure 1.1.2 shows the resulting forces acting on the wires in a 1D railgun.

Resulting forces on simplified, 1D railgun

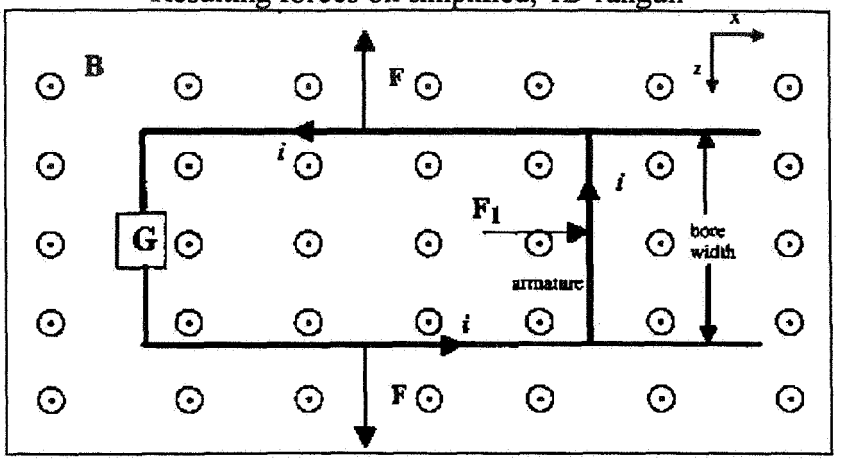

Figure 1.1.2

The result of summing the forces is a net force acting on the sliding wire or armature. It can then be imagined that if this sliding armature were to push a mass, the mass could be accelerated by a force dependent on the strength of the current through the wires, the magnetic field the wires are emersed in (hence the size of the power source), and the length of the armature.

From equation (1.1.1), it is simple to compute the force if the current magnitude and magnetic field are known. However, a current carrying wire also induces a magnetic field. This magnetic field is found using Ampere's law simplified to the current carrying wire

$$\mathbf{B} = \frac{\mu_0 i}{2\pi r}\hat{e}_\theta \qquad (1.1.2)$$

where **B** is the magnetic field vector, μ_0 is the permeability constant, i is the current magnitude running through the wire, r is the radial distance from the wire, and $\hat{e}_\theta$ is a unit vector in the axial direction governed by the right hand rule. Thus, a current carrying wire produces concentric magnetic field circles with decreasing magnitude as the radial distance, r, from the wire increases. It is discovered that the magnetic field produced by the current carrying wires intern applies the force on the armature. Computing the magnetic field created by two wires (ignoring the armature for simplicity) and then substituting this value into equation (1.1.1) will allow the calculation of the total force acting on the armature. For two current carrying wires, the magnetic field is found by

applying equation (1.1.2) to each of them seperately and then combining the magnetic fields by superposition. The final equation in Cartesian coordinates is

$$B(x) = \frac{\mu_0 i}{2\pi}\left(\frac{1}{z} + \frac{1}{(\text{bore width} - z)}\right) \tag{1.1.3}$$

Figure 1.1.3 is a plot of equation (1.1.3) for two current carrying wires.

Magnetic field magnitude between two opposing current carrying wires.

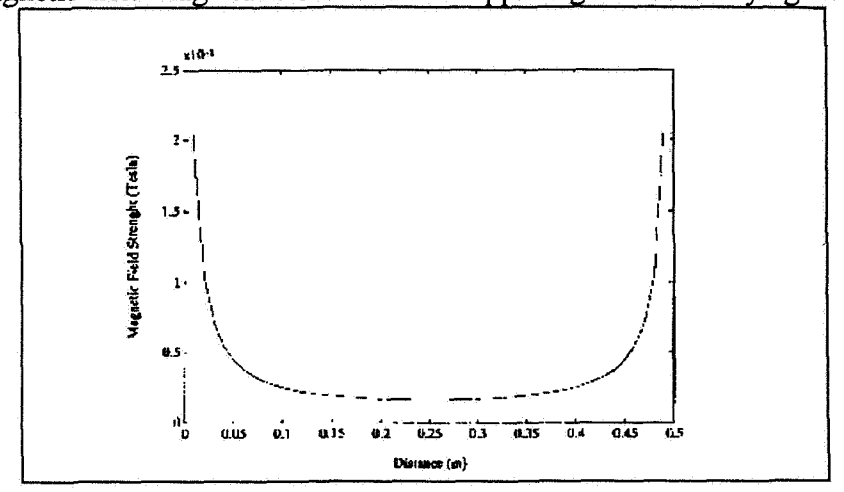

Figure 1.1.3

By integrating equation (1.1.1) over the bore width an initial net force can be computed on the armature.

Expanding, the magnetic field produced by two wires in two dimensions can be extracted from equation (1.1.2) by separating $\hat{e}_\theta$ into its Cartesian $\hat{i}$ and $\hat{j}$ coordinates for each wire and then again superimposing the two solutions. The configuration employed is shown in Figure 1.1.4.

Cartesian coordinate representation of the magnetic field between two current carrying wires.

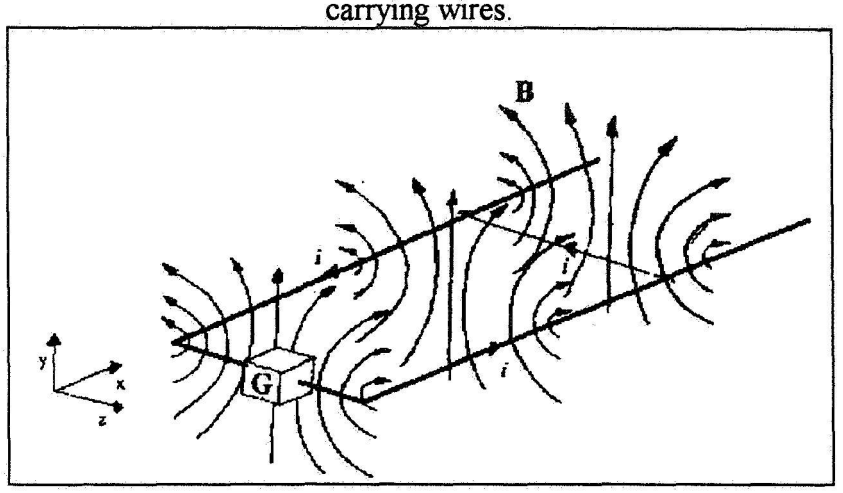

Figure 1.1.4

The result is shown in Figure 1.1.5 where the third dimension represents magnetic field strength in the y($\hat{j}$) direction because only a magnetic field in the y($\hat{j}$) direction produces a net force on the armature in the in the desired x($\hat{i}$) direction (equation 1.1.1)).

Three-dimensional interpretation of y($\hat{j}$) direction magnetic field magnitude

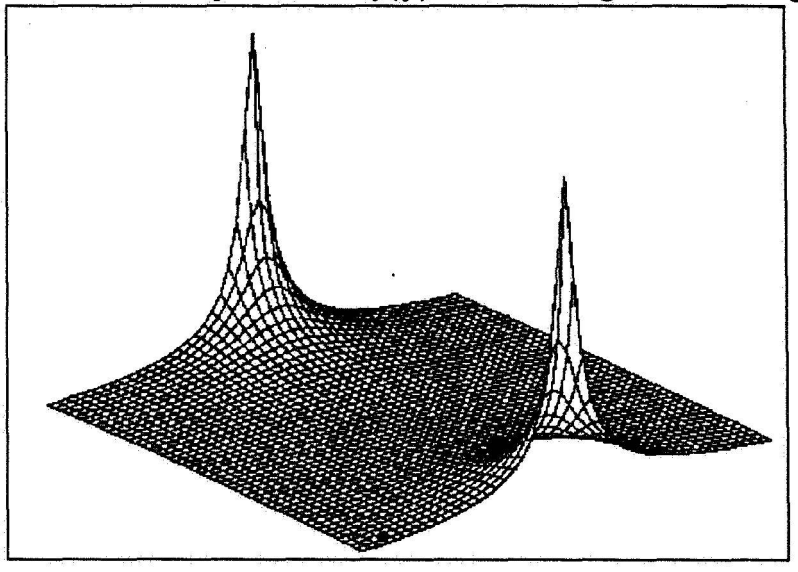

Figure 1.1.5

Note the expected high magnetic field near the wire surface and its gradually decreasing magnitude further away.

1.1.2 Two Dimensional Railgun

Equation (1.1.1) expanded to a 2D system is simply

$$\mathbf{F} = \mathbf{J} \times \mathbf{B} \tag{1.1.4}$$

where **J** represents a vector current density-length (in amps-meter/meter^2). By assuming two flat plates instead of two wires, a force can be computed on the armature (which itself is a flat plate instead of a wire). A diagram of this 2D system is shown in Figure 1.1.6.

Two dimensional railgun visualization

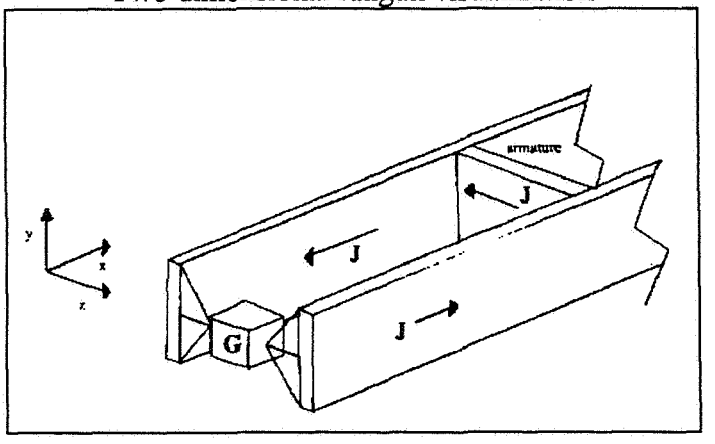

Figure 1.1.6

Again, similar to a wire railgun, the current carrying plates induce a magnetic field. This magnetic field is again governed by Ampere's law and is somewhat complicated when put in Cartesian form and will not be presented here. As with the wires, the magnetic field for each of the plates is then superimposed to produce the full 2D magnetic field. A three dimensional visualization of the magnetic field similar to that shown for the two wires (Figure 1.1.5) is plotted in Figure 1.1.7. Again, the higher field strengths are located near the plate surfaces.

Three-dimensional interpretation of magnetic field magnitude

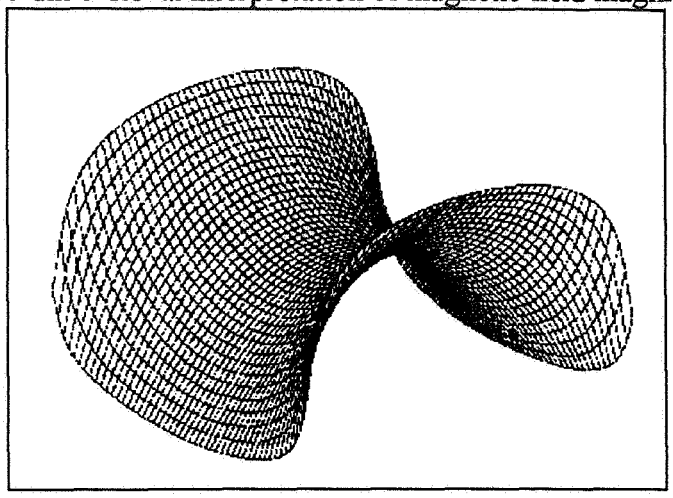

Figure 1.1.7

With the magnetic field density known between the two flat plates, the force can be computed by integrating the magnetic field over the armature area (again ignoring the magnetic field induced by the armature). Each infinitesimal force is governed by

$$d\mathbf{F} = \mathbf{J} \times d\mathbf{B}\, dx\, dy\, dz \tag{1.1.4a}$$

and adding these forces together produces the overall force on the armature.

1.1.3 Summary of the Simplified Railgun Models

The previous sections briefly described the most simplified versions of possible railgun configurations. These simplifications are at the expence of efficiency. The best theoretical transfer of electrical energy to kinetic energy from a single, two dimensional railgun configuration is 50%[11] due to the wasted inductive energies remaining within the plates. Also, there are tremendous rail resistance losses as the gun is increased in size to accommodate increased projectile exit velocities[11]. The alternative discovered to avoid these circumstances is to divide the railgun into seperately powered but connected sections. By implimenting this separation method, the energy transfer efficiency is increased while resistive losses remain controlable as the bore length increases. The result is the Distributed Energy Source (DES) railgun.

1.1.4 The Distributed Energy Source Railgun

The following paragraphs summarize the processes and procedures implemented in the performance calculations of a DES railgun. First, the governing railgun equations are introduced. They are then non-dimensionalized and simiplified to reduce the number of adjustable parameters and increase the applicability of a single, non-dimensional solution to many physical solutions. Finally, the non-dimensional governing equations are solved and optimized for the case at hand using chosen design parameters.

The basis of the DES railgun design is the placement of multiple energy sources along its length[11]. By strategically releasing the energy ('firing' or 'tripping' the stage) stored in each stage, the projectile is propelled to the required speed much more efficiently than a conventional one-piece railgun design. The principle behind the DES railgun is as follows. Each section of the railgun has its own stored power system. The system may contain an inductor, resistor, and capacitor in series forming an LRC circuit (Fig 1.1.8a and 1.1.8b). However, the current design idealizes the conditions and assumes no resistive losses.

Stage circuit design with resistance. Reprinted from [11]

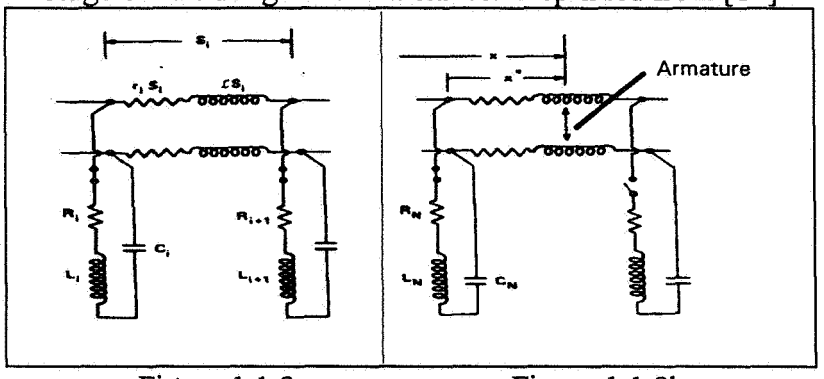

Figure 1.1.8a Figure 1.1.8b

The capacitors in each section are charged by a voltage predetermined by the amount of acceleration needed. When the projectile is in the appropriate section, the circuit is tripped and the current is allowed to discharge as an LC circuit into the rails, inducing the magnetic field which propels the mass. The equation describing a tripped stage (a stage in which the mass has already passed - see Fig. 1.1.8 a) is

$$\frac{q_i}{C_i} + R_i\dot{q}_i + L_i\ddot{q}_i + r_i S_i \sum_{k=1}^{i} \dot{q}_k + \ell\, S_i \sum_{k=1}^{i} \ddot{q}_k - \frac{q_{i+1}}{C_{i+1}} - R_{i+1}\dot{q}_{i+1} - L_{i+1}\ddot{q}_{i+1} = 0 \qquad \text{for } i \le 1 \le N-1 \tag{1.1.5}$$

where q, $\dot{q}$, and $\ddot{q}$ are the charge, current, and rate change of current, C is the capacitance, R is the resistance, L is the inductance, S is the stage length, and i the maximum number of stages (energy sources) ranging from 1 to N-1. The equation describing the tripped circuit which still contains the mass (Fig. 1.1.8 b) is

$$\frac{q_N}{C_N} + R_N\dot{q}_N + L_N\ddot{q}_N + (rx^* + \ell\,\dot{x}) \sum_{k=1}^{N} \dot{q}_k + \ell\, x^* \sum_{k=1}^{N} \ddot{q}_k = 0 \qquad \text{for } i \le N \tag{1.1.6}$$

where N is the maximum number of stages in the railgun and x^* is distance from the beginning of the stage to the location of the mass. Subsequently, the force equation is

$$m\ddot{x} = \frac{1}{2}\,\ell \left(\sum_{k=1}^{N} \dot{q}_k \right)^2 - F_D \tag{1.1.7}$$

where F_D is the frictional drag force on the projectile. To further simplify this analysis, the frictional drag is assumed negligible since studies have shown that drag forces are usually four to five orders of magnitude smaller than the propelling force[11]. However, this by no means reduces the applicability of the equations to physical uses.

Equation (1.1.7) inherently limits the amount of current allowed through the system by relating it to the force produced. Consequently, the speed of the projectile is governed by the maximum force allowed to propel the mass without crushing it. The correlating equations are

$$\frac{1}{2}\,\ell\, I_{\max}^2 \le P_m A \tag{1.1.8}$$

and

$$\left(\sum_{k=1}^{N} \dot{q} \right)^2 \le \left[\frac{2P_m A}{\ell} \right]. \tag{1.1.9}$$

Equations (1.1.5) through (1.1.9) form a system of equations that describe the dynamics of the DES railgun. There are N+1 equations and N+1 unknowns, (q_i, x), which allows for a unique solution to the system. The initial conditions to the above equations are

$$q_1(0) = q_0, \;\; \dot{q}_1(0) = 0, \;\; x(0) = 0, \;\; \dot{x}(0) = v_0 \tag{1.1.10}$$

Equations (1.1.7)-(1.1.9) can be recognized as simple ordinary differential equations which can be solved using proven computer methods.

The governing equations are non-dimensionalized to expand their usefulness to a wide variety of problems[11]. By introducing the dimensionless variables

$$\xi = \frac{2m}{\ell\, q_0^2} x, \;\; y_i = \frac{q_i}{q_0}, \;\; \tau = t \Big/ \sqrt{\ell\, C_1 S_1} \tag{1.1.11}$$

equations (1.1.5)-(1.1.9) are non-dimensionalized and simplified assuming no resistive losses, constant-energy-per-stage design, and equal stage lengths to

$$\lambda_i y_i'' + \Omega_i^2 y_i + \sigma_i \sum_{k=1}^{i} y_k'' - \left[\lambda_{i+1} y_{i+1}'' + \Omega_{i+1}^2 \sigma y_{i+1}\right] = 0 \tag{1.1.5a}$$

$$\lambda_N y_N'' + N\sigma y_N + \xi' \sum_{k=1}^{N} y_k' + \left(\xi - (N-1)\sigma\right) \sum_{k=1}^{N} y_k'' = 0 \tag{1.1.6a}$$

$$\xi'' = \left(\sum_{k=1}^{N} y_k' \right)^2 \tag{1.1.7a}$$

$$\left[\sum_{k=1}^{N} y_k' \right]^2 \le \frac{P_m A S}{q_0^2 \Big/ 2C_1} \equiv \beta \tag{1.1.9a}$$

where,

$$\lambda_i = \frac{2mL_i}{\ell^{\,2} q_0^2}, \;\; \sigma = \frac{2mS}{\ell\, q_0^2}, \;\; \Omega_i^2 = \frac{C_1}{C_i}\sigma \tag{1.1.12}$$

The initial conditions for equations (1.1.5a)-(1.1.9a) for the first stage (i=1) are

$$y_1 = 1, \; y_1' = 0, \; \xi = 0, \; \xi' = 0 \tag{1.1.13}$$

Equations (1.1.5a)-(1.1.9a), along with the initial conditions given by equation (1.1.13), are used to analyze a no-loss DES railgun design.

The numerical solution to the DES railgun begin with equations (1.1.5a) and (1.1.7a), which together represent the case where the mass is within the first stage (i=1). The equations with the initial conditions are then numerically integrated using a fourth order accurate Runge-Kutta scheme until the projectile had passed to the next stage. These computed values are then used as initial conditions in conjunction with the initial conditions for the next stage. This iterative process continues until the last stage is completed and the final numerical solution is calculated. A more detailed description of the solution method and code listing are available in Appendix A.

1.1.5 DES Railgun Efficiencies

Before proceding further with validation studies and parameter optimization, an introduction to certain railgun efficiencies and their significance is necessary. The first efficiency is defined as the ratio of kinetic energy imparted to the projectile to the total stored electrical energy. In dimensional form this overall efficiency is

$$\bar{\varepsilon} = \frac{m\left(v_f^2 - v_o^2\right)}{\sum_i^N \left[q_i^2(0)/C_i\right]} \tag{1.1.14}$$

where m is the mass of the projectile, v_f and v_o are the final and initial velocities of the projectile, $q_i(0)$ is the initial charge on the capacitors, N is the number of stages, and C_i is the capacitance for each stage. In non-dimensional form, this becomes

$$\bar{\varepsilon} = \frac{\bar{\xi}_f^2 - \bar{\xi}_o^2}{2\sum_i^N \Omega_i^2 y_i^2(0)} \tag{1.1.14a}$$

There is also an efficiency comparing the calculated final kinetic energy to the maximum feasible kinetic energy. This mean space utilization (MSU) efficiency in dimensional form is defined as

$$\varepsilon^S = \frac{m\left(v_f^2 - v_o^2\right)}{2P_m A\sum_{i=1}^N S_i} \tag{1.1.15}$$

where P_m is the maximum allowable pressure force on the projectile, A is the area which this force is acting on the projectile, and S_i is the length of each section of rail. In non-dimensional form, this becomes

$$\varepsilon^S = \frac{\bar{\xi}_f^2 - \bar{\xi}_o^2}{2\beta\sum_{i=1}^N \sigma_i} \tag{1.1.15a}$$

With these efficiencies defined, some choices about certain adjustable parameters are made. For instance, the choice of σ, given as

$$\varepsilon_i = \left(\frac{\sigma}{2}\right)^{1/2} \tag{1.1.16}$$

where ε_i is the efficiency per stage of the railgun (the average value of ε_i is ε^S), shows that a choice of σ=2 would produce 100% efficiency per stage and that choices of σ>2 would produce stage efficiencies greater than 100%. However, efficiencies greater than 100% are physically impossible and this fact is evident when the governing equations are solved

using $\sigma>2$. The solutions produced are highly unstable and diverging and cannot be applied to actual physical situations (See section 1.1.6 for visual results)[11].

These efficiencies are now applied to analyzing dimensional conditions such as stage capacitance, charge, inductance, current, and voltage. From the validation cases completed, it was discovered that the critical limiting factor in the railgun design is capacitance per stage. By using the definition of β given by equation (1.1.7a), substituting in for P_m using equation (1.1.15), for q_o^2 using equation (1.1.12), and solving for C_1 produces

$$C_1 = \frac{2}{\mu_o \sigma_i v_f^2} \cdot S_N \beta \varepsilon^s \qquad (1.1.17)$$

where μ_o is the inductance per meter for a square bore railgun (permeability constant)[11], σ_i is the non-dimensionalized railgun stage length (constant), v_f the exit velocity (constant), S_N is the total powered railgun length, β is the non-dimensional force parameter, and ε^s the mean space utilization efficiency.

Two observations are made from equation (1.1.17). One is that capacitance is independent of mass. Another more important observation is that the only adjustable variables which have an effect on initial stage capacitance are S_N, β and ε^s. In other words, to reduce the capacitance, the force parameter, efficiency, and total gun length are the only feasible parameters that can be adjusted and optimized. Equation (1.1.17) also indicates that the maximum efficiency may not be the most optimal condition for constructing a physical railgun; however, a more rigorous investigation of the values in equation (1.1.17) can limit the optimizing variables to just β. Using equation (1.1.15), it is seen that S_N and ε^s are inversely proportional to P_m and that decreasing these values by the amount necessary to reduce the capacitance would also increase the amount of force applied to the projectile significantly. Therefore, the only quasi-independent variable that could be adjusted without adverse effects on other parameters is β, which is related to maximum current flowing through the railgun.

These and other non-adjustable parameters chosen to calculate performance are summarized in Table 1.1.1 below. The initial parameters are based on the Request For Proposal (RFP) and mechanical circumstances discussed above. For instance, the launch mass is chosen to fulfill the required amount of hydrogen/oxygen production per Earth month assuming approximately ten launches per Earth day with three days for maintenance. The number of stages is chosen to limit the amount of stage transportation necessary to complete the gun and allow for the trial and error process in minimizing β.

Excessive stages would add too many additional variables and would be difficult to optimize by the trial and error approach. The powered gun length is initially chosen to accommodate the yield strength of the projectile and gun through calculation of P_m. The σ parameter is chosen to produce a high mean space utilization efficiency through use of equation (1.1.16). Finally, the exit velocity is chosen 10% higher than needed to account for the lack of a velocity control system within the powered railgun.

Initial Constant Railgun Parameters

Total Projectile Mass (m)	120 kg
Ice Projectile Mass	80 kg
Number of Launches/Day	10
Number of Stages	10
Efficiency Parameter σ_i	1.8
Total Railgun Length (S_N)	100 m
Initial Projectile Velocity (v_i)	0 m/s
Final Projectile Velocity (v_f)	1650 m/s
Bore Dimension	0.5m X 0.5m
Bore Area	0.25 m^2

Table 1.1.1

1.1.6 DES Railgun Validation Cases

Before applying the observations and parameterizations made in the previous section, several validation cases are computed for both an ideal, lossless case and a case involving resistance within the circuit. These results are then compared to a theoretical study conducted by Jerald V. Parker[11]. The method of comparison is both visual and numerical with results given in the Parker report. Additionally, there is a visual example of the unstable solution to the governing equations when efficiency values defined from equation (1.1.16) excede 100%.

First, an ideal, lossless validation case is computed using an initial, non-dimensional velocity $\xi'(0)=0.0$, a $\sigma=0.7$, and a $\lambda=1.0$, where σ and λ are constant for all stages. Table 1.1.2 summarizes the numerical results of both the report and computational cases with the percent difference between the two.

Comparison of Report and Computational Case (ξ'=0, σ=0.7, λ=1.0)

	Report Case	Computational Case	% Difference
Synchronous velocity (ξ'_N)	0.900 $N^{1/2}$	0.932 $N^{1/2}$	3.55
Projectile Current (I_p)	0.772	0.787	1.94
Maximum Force Parameter (β)	0.596	0.620	4.03
Overall Electrical Efficiency ($\bar{\varepsilon}$)	0.578	0.585	1.21
Mean Space Utilization (MSU) Efficiency	0.970	0.959	1.13
Force Variation	0.003	0.003	0.00

Table 1.1.2

Figure 1.1.9a and 1.1.9b shows a comparison between the non-dimensional projectile current value, Ip, for the report and computational case.

Projectile current value versus time comparison between report and computational case for ξ'=0, σ=0.7, λ=1.0

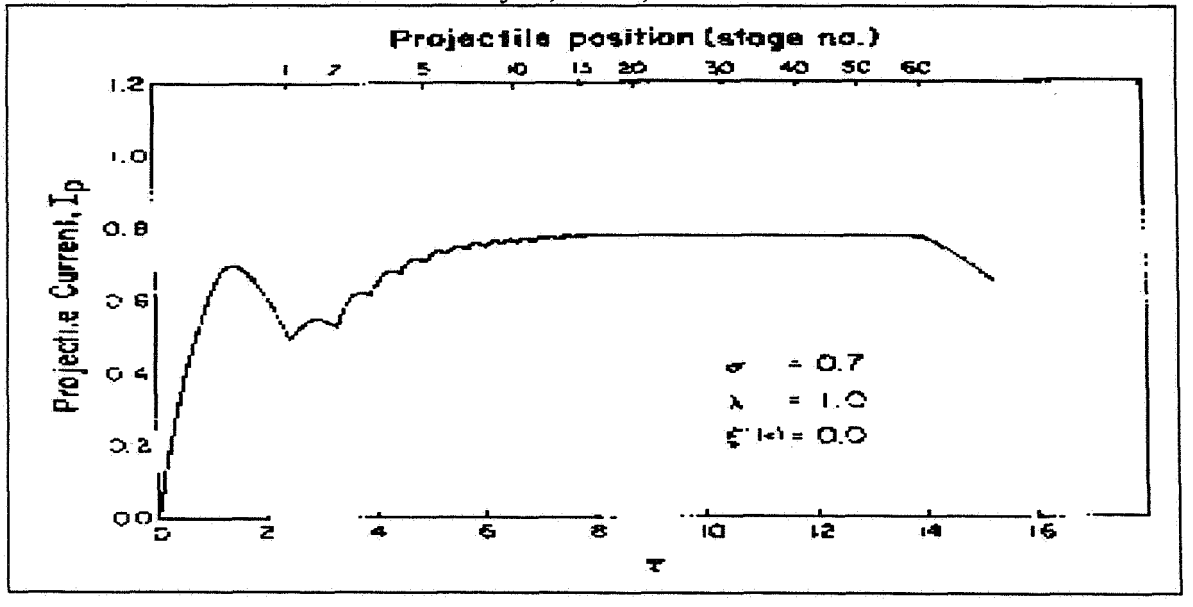

Figure 1.1.9a. Reprinted from [11]

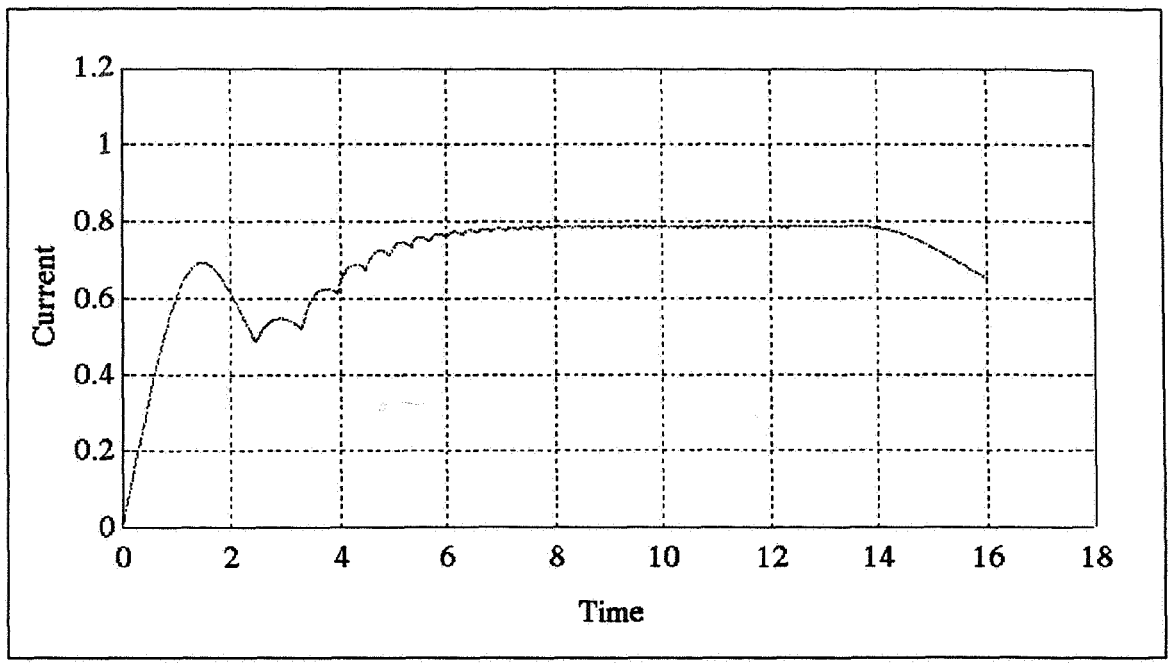

Figure 1.1.9b

Just from the numerical results, the code is within 3% difference for all values compared. Visually, the difference is not even descernable exept for the method of computing to zero current where a slight difference is noted after the last stage (t>14). This is found to become less evident as the σ value is increased. The descrepency between the two cases can be attributed to computational variation and machine round off; but, because of its extremely small size (referenced from the percent differences), can be ignored and the two solutions considered close enough to be the same.

Second, a case involving resistance losses is compared to the report values. The parameters for this case are σ=1.85, λ=0.5, a friction factor γ_0=0.15, and an initial velocity condition $\xi'(0)$=0.1. The comparison is again of non-dimensionalized current versus time and is shown in Figures 1.1.10a and 1.1.10b for report and computational case respectively.

Projectile current versus time comparison between report and computational case for σ=1.85, λ=0.5, γ_0=0.15, and $\xi'(o)$=0.1

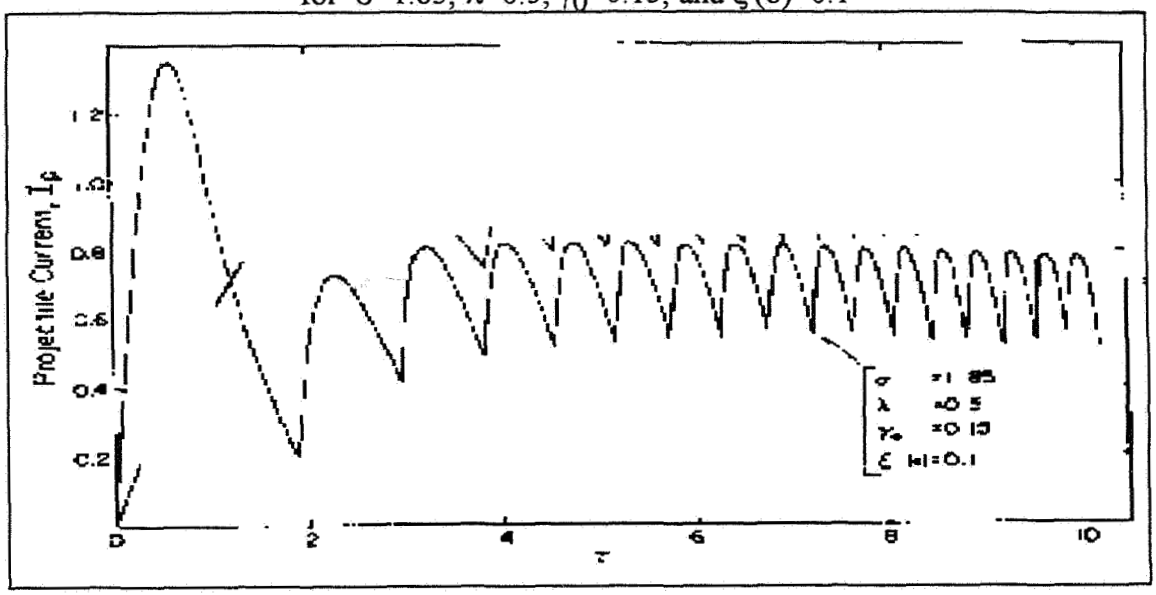

Figure 1.1.10a. Reprinted from [11]

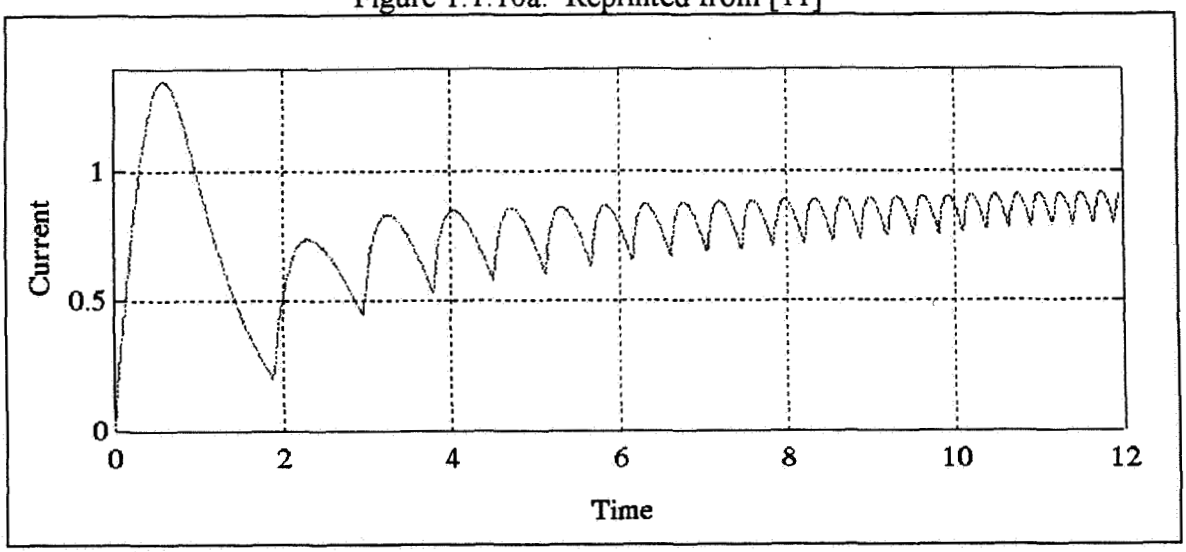

Figure 1.1.10b

Again, the comparisons are quite good although not as close as those observed for the ideal, resistanceless case. This can be attributed to computational method differences and machine round off error. An additional observation can be made regarding the two visual solutions. Because of the proximity of the σ value to two, there is a slight divergent characteristic of the report case that is not evident in the computational case (This divergent phenomenon will be detailed in the following paragraph). Inherently this could

again be attributed to machine round off error or computational method differences but might represent a more forgiving nature within the code written for this study.

Finally, an example of the unstable solution of the governing equations for efficiencies equal to or greater than 100% (equation (1.1.16)) is represented below. In Figure 1.1.11, non-dimensionalized current versus time plot for σ=2.5, λ=0.5, and $\xi'(0)$=0.0 is plotted.

Unstable solution example for σ=2.5, λ=0.5, and $\xi'(0)$=0.0

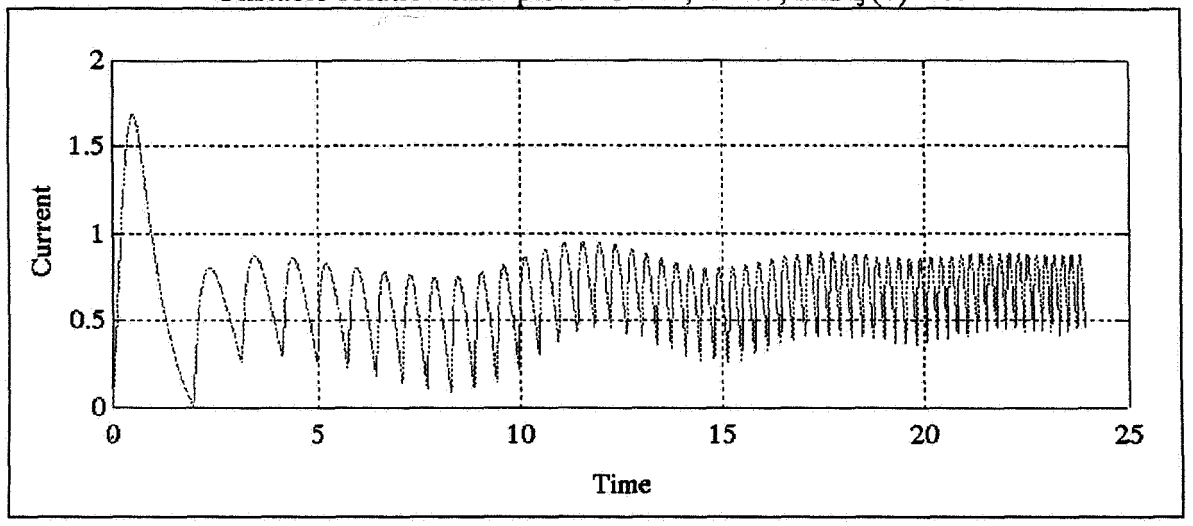

Figure 1.1.11

As can be seen, there is a computed solution for this case, i.e., the code does not abnormally terminate, but the force variation represented by the ratio of maximum to minumum current is extremely large. Furthermore, this oscillation does not damp out to a converged solution as can be witnessed by the almost constant current minimum/maximum difference for each stage. Additionally, there is the formation of a secondary oscillation caused by the high σ value. As stated earlier, it can be concluded that values of σ>2 produces unstable numerical results that cannot be applied to physcal situations.

With code validation complete and exceptionally good comparisons obtained, confidence is high that the code will produce accurate results when applied to the design project at hand.

1.1.7 Numerical Results

Because the number of stages chosen is small, a trial and error process is used to minimize β and force variation, F_v, on the projectile. By adjusting the inductance and initial stored charge per stage, β is reduced to a value that produces a feasible capacitance

as presented in section 1.1.4. Dimensional values are obtained using the constant parameters given in Table 1.1.1 and the definitions of equation (1.1.12). Plots of current, position, velocity, and acceleration versus time are shown in Figures 1.1.12a-d.

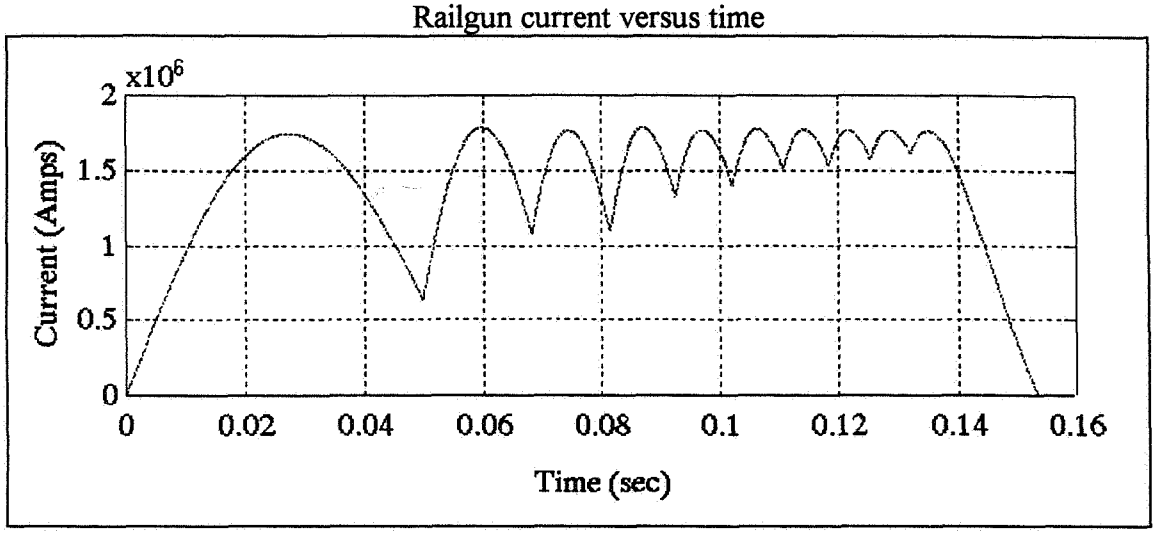

Figure 1.1.12a

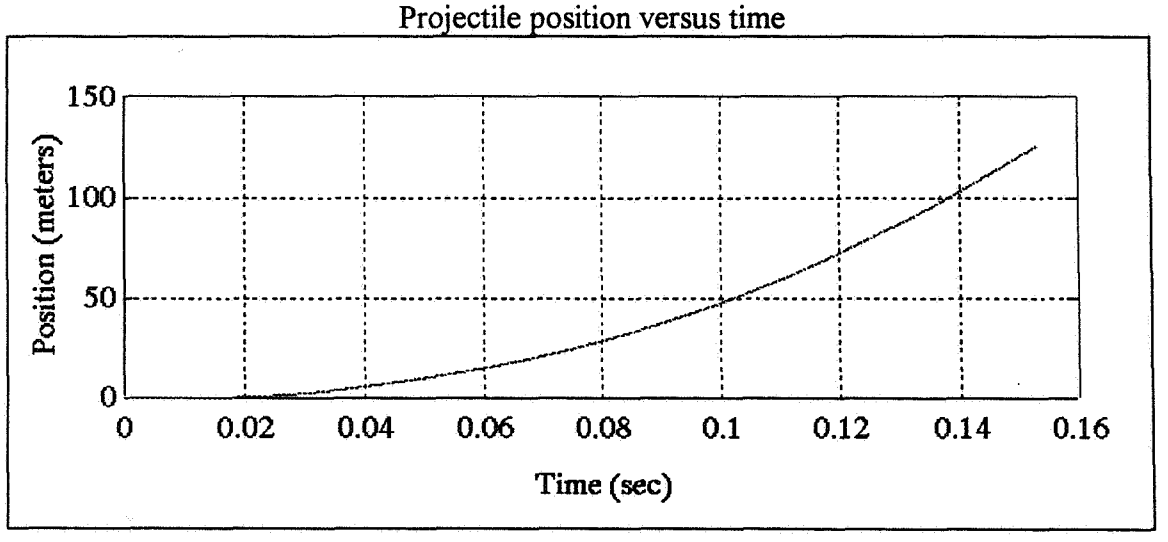

Figure 1.1.12b

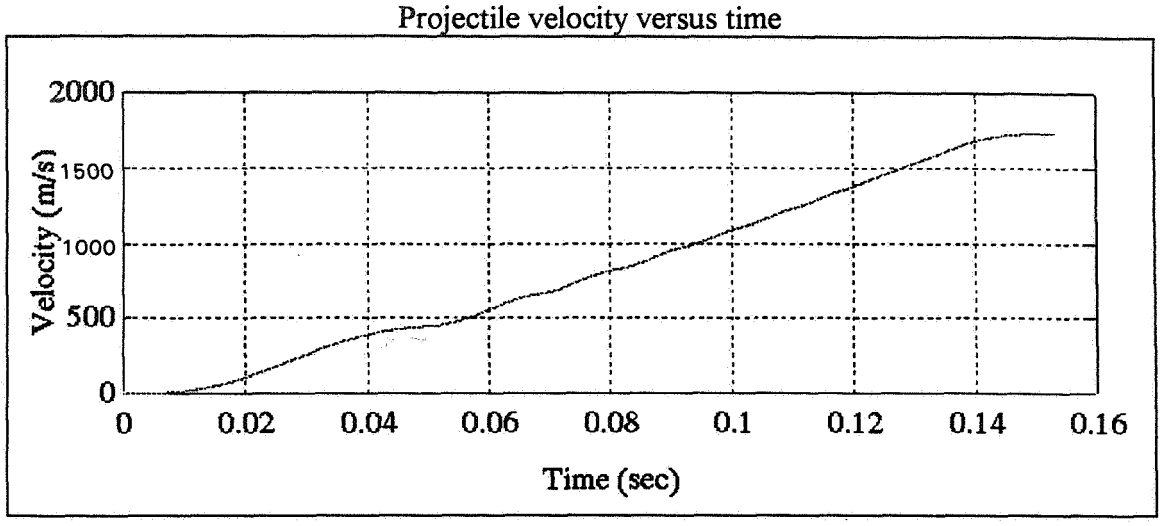

Figure 1.1.12c

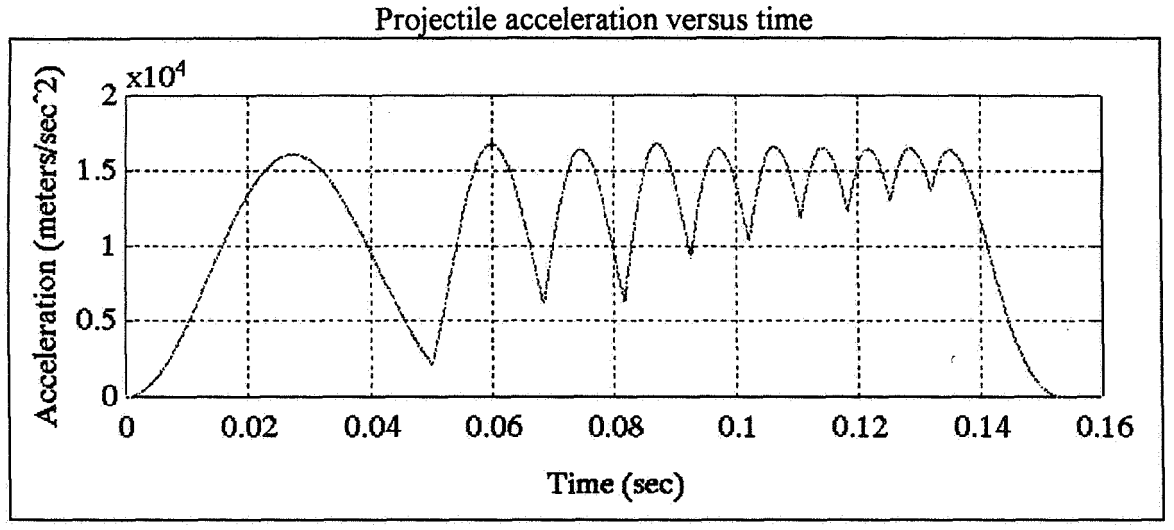

Figure 1.1.12d

Table 1.1.3 summarizes stage conditions while Table 1.1.4 summarizes some output results and efficiencies.

Stage Condition and Efficiency Summary

	Initial Inductance (μH)	Initial Charge (kC)	Capacitance (F)	Voltage (kV)
stage 1	77.0	32.4	4.23	7.65
stage 2	36.4	22.9	2.12	10.8
stage 3	41.3	22.9	1.41	16.24
stage 4	49.0	22.9	1.06	21.60
stage 5	59.5	19.4	0.846	22.93
stage 6	61.5	16.2	0.705	22.98
stage 7	70.0	13.0	0.604	21.52
stage 8	73.5	11.3	0.529	21.36
stage 9	87.5	10.8	0.470	22.98
stage 10	108.9	10.2	0.423	24.11

Table 1.1.3

Efficiency and Output Summary

Efficiencies		Output Parameters	
Overall Eff.	0.11773	Beta	0.16162
MSU Eff.	0.80923	Maximum F_V	88%
		Minimum F_V	11%
		Avg. Pressure P_m	8.07×10^6 Pa
		Avg. Applied Force	2.02×10^6 N
		Transit Time	153.5 ms
		Total Length	121 m
		Exit Velocity	1736 m/s
		Stored Energy	361 MJ
		Overall Power	2.29 GW

Table 1.1.4

Some discussion of these results are in order. The MSU efficiency, or average efficiency per stage, agreed with the expected theoretical result defined by equation

(1.1.16). Unfortunately, minimizing β dramatically decreases the overall efficiency of the system. A system with a higher overall efficiency was analyzed but increased the capacitance value by an order of magnitude. Although overall efficiency is low, it is a sacrifice necessary to maintain a decidedly low capacitance per stage. Increasing the amount of stages could increase overall efficiency but would jeopardize the trial and error process of minimizing β. The force variations are relatively large but the pressure and applied forces are within the yield strengths of the metals to be used for module construction. The exit velocity and railgun length are somewhat higher than the expected 1650 m/s and 100 m, respectively. This is due to integrating the current down to zero to reduce erosion caused by the extremely large current values left in the railgun if the projectile were ejected at 100 m [11]. From the stored energy and power requirements predicted by the equations, it can be deduced that the only feasible source was a capacitor based discharge system.

The physical implications of the results may be intimidating. For instance, although β was optimized, the capacitance for each stage is still on the order of a Farad. However, by using multiple capacitors with dielectrics, a total capacitance of this order is achievable. A more critical situation arises from the massive amounts of current produced by the fully charged system. Any resistance in the line would immediately vaporize switches, power lines, and possibly other components. The only option may be to super-cool the entire power system (including the railgun) to reduce the temperature to a super-conductive, zero resistance state. Although the super-conducting method has not been stated explicitly, it has been assumed by eliminating resistance terms in the governing equations. Maintaining a super-conducting state is a massive undertaking under 'normal' Earth circumstances. However, since the only source of heat on the lunar surface is radiation, the temperature should drop to the mean space temperature of 4K if the system were shielded from the Sun and lunar surface. At this temperature, most commonly used metals achieve superconductivity.

1.1.8 Railgun Launch Control System

To accurately launch the ice material, a control system is designed to account for railgun exit velocity perturbations, ice mass inconsistencies, and Earth-Moon-Sun gravitational effects. Basically, this control system uses diode sensors placed on the ice module and a reflective material placed on the launch rail to calculate the instantaneous velocity of the module. Servo motors point the ice pod at the elevation and azimuth angle required and at a predetermined speed, the ice is released in the proper direction. A plasma armature is used as an alternative to a mechanical one to reduce the effect of

friction and also save on general wear and tear on the railgun bore itself by minimizing physically touching parts. A more detailed discussion of each component follows.

The module is shown in Fig. 1.1.13. The module basically houses the servo motor for the small azimuth angle control of the ice pod (A). The wheels included on the module are actually solid balls that will be free to rotate in any direction through the use of bearings. The design reduces or eliminates shear forces that would plague disk-type wheels if the module were to shift within the bore or outside on the rails. Also, the use of these 'bearing wheels' reduces the number of wheels necessary from 12 to 6 and reduces the overall weight of the module. The rear of the module (B) consists of a concave indentation to contain the plasma and reduce plasma leakage. The diode sensor is also shown on the side of the module (C). The locations for cable attachment are not shown on this diagram but exist on the module and are located on the underside of the module forward of the center of mass of the ice pod module system.

Schematic of module and pod

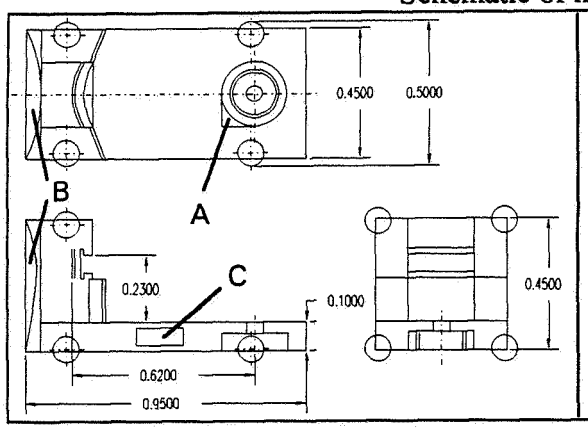

Figure 1.1.13

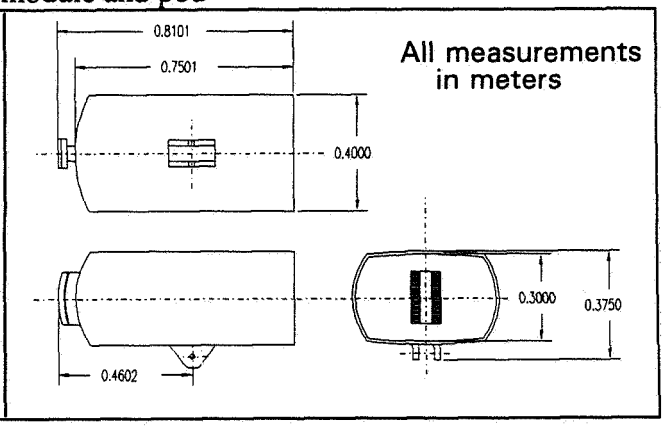

Figure 1.1.14

Schematic of disk and azimuth servo control

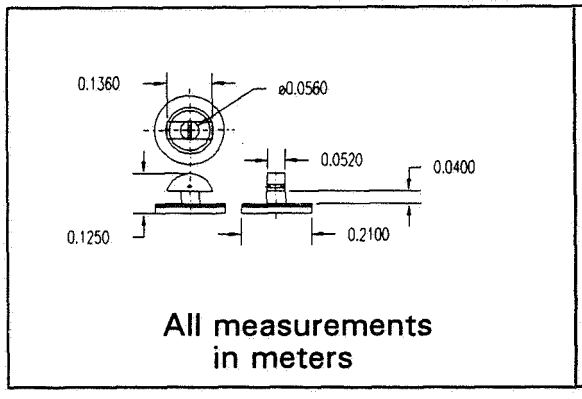

Figure 1.1.15

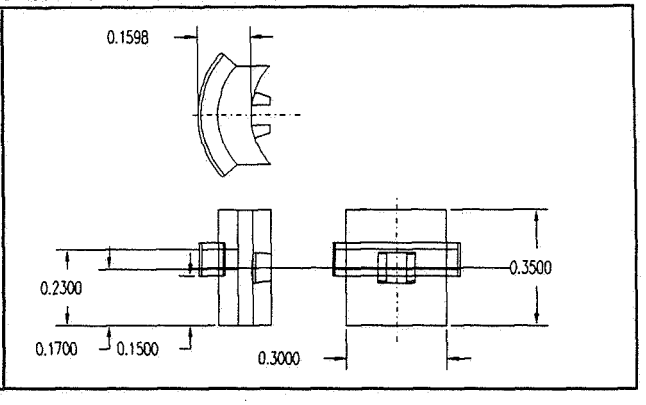

Figure 1.1.16

The ice carrying pod (Fig. 1.1.14) is designed to carry approximately 80 kg of ice and will be attached to the module by the disk pictured in Fig. 1.1.15. Through this design, the pod will be allowed to rotate in the azimuth angle direction by the servo motor located in the base of the module. Simultaneously, the servo control unit (Fig. 1.1.16) will rotate the pod to the proper elevation. The ice pod, itself, will have plates retaining the ice (Fig. 1.1.17) and have a layer of low friction substance to allow the ice to easily separate when the correct velocity and direction are achieved.

Schematic of pod doors

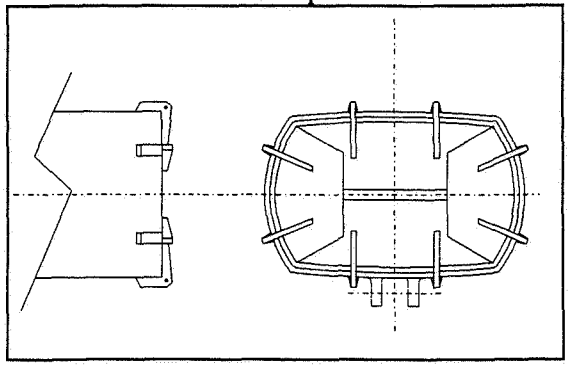

Figure 1.1.17

The assembled platform is shown in Fig. 1.1.18. With this platform, accurate directional control should be achievable. It is also possible to accommodate changing conditions by performing the fine tuning necessary under the more accurate control of the servo motors. This kind of directional accuracy is impossible to achieve using the railgun alone.

Assembly view of platform

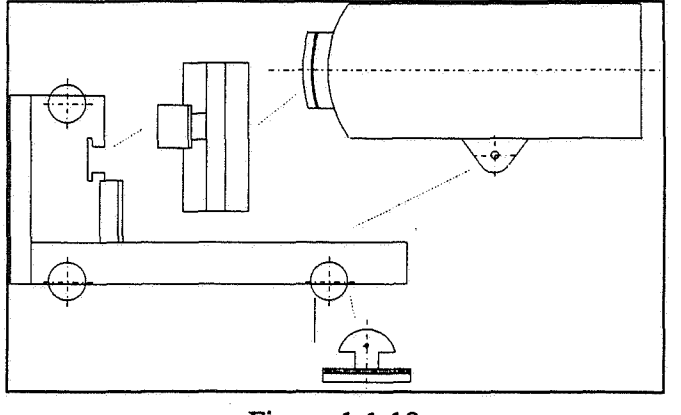

Figure 1.1.18

Velocity measurement will be attained by reflecting LED light off strips on the launch track to be picked up by sensors on the module. The information will be transmitted back to a computer controlling the braking cables which attach to the underside of the module after it has exited the railgun. There will be four cables attached to the underside of the module--a pair connected to a motor for controlled braking and a pair connected to two generators for power supply to the motor (Fig. 1.1.19).

Simplified interpretation of cable braking system and velocity measurement

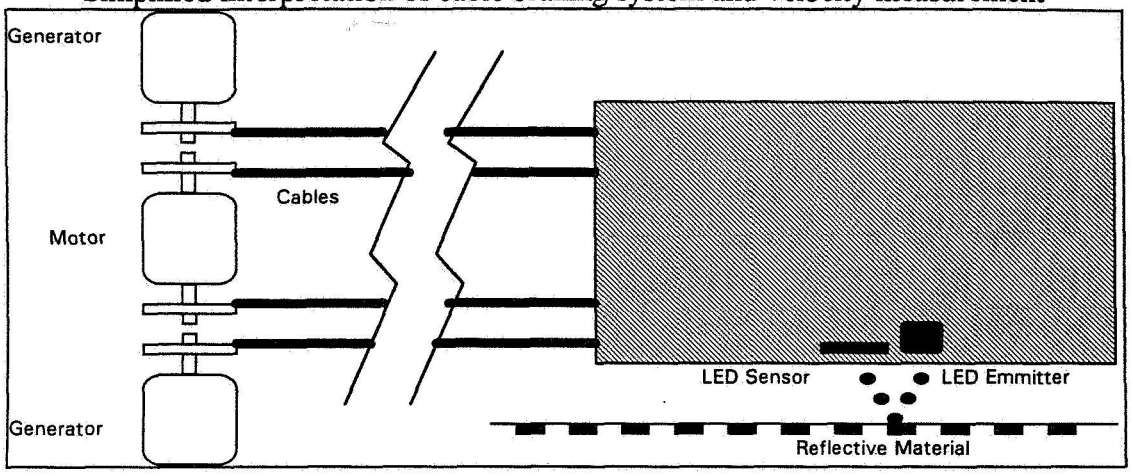

Figure 1.1.19

Cable yield strengths vary from 1.27 GPa to 1.96 GPa depending on strand type and rope construction[2][12]. Assuming cables with diameters ranging from 4 cm to 8 cm, the maximum force that can be applied ranges from 1.60 MN to 9.8 MN. For four cables assumed attached to the module, this translates to a maximum braking force of 6.40 MN to 39.4 MN. The force applied to the module within the railgun is only 2.02 MN (Table 1.1.4), which lies below the maximum yield force of the cables even with a standard safety factor. So if it were necessary, the module could be stopped in 100 meters. Unfortunately, the limitation to braking will be the electric motor and current supply from the electric generators. Initially, there will be a large force on the cables due to the momentum of the exiting module but because neither the motor or the generators are 100% efficient (the best efficiency that can be achieved is close to 90%[1][6]), the current from the generators will gradually decrease as will the braking force by the motor. An estimation of motor size through an average power requirement can be calculated using the average velocity of the module during braking. Multiplying this by the maximum force necessary to stop the module produces an average power of 876 MW. It should be noted that this is a very rough estimate and needs further consideration.

The hope of this type of control system is that the module braking will be more precisely controlled by monitoring the current to the motor and also recapturing some of the kinetic energy imparted to the projectile. However, the exact uncertainties involved in angle and velocity values are unknown. Certain variables such as friction, force perturbations, and the general dynamics of the system make it next to impossible to predict the accuracy required for a precision launch. The main purpose of this method is to attain reproducibility of a launch without wild fluctuations with braking forces and rotational angles. Calibration will be necessary to increase the accuracy of a launch.

A typical launch scenario is pictured in Fig. 1.1.20. It is assumed that all the capacitors are charged to the correct value governed by the DES railgun equations.

Overview of launch scenario

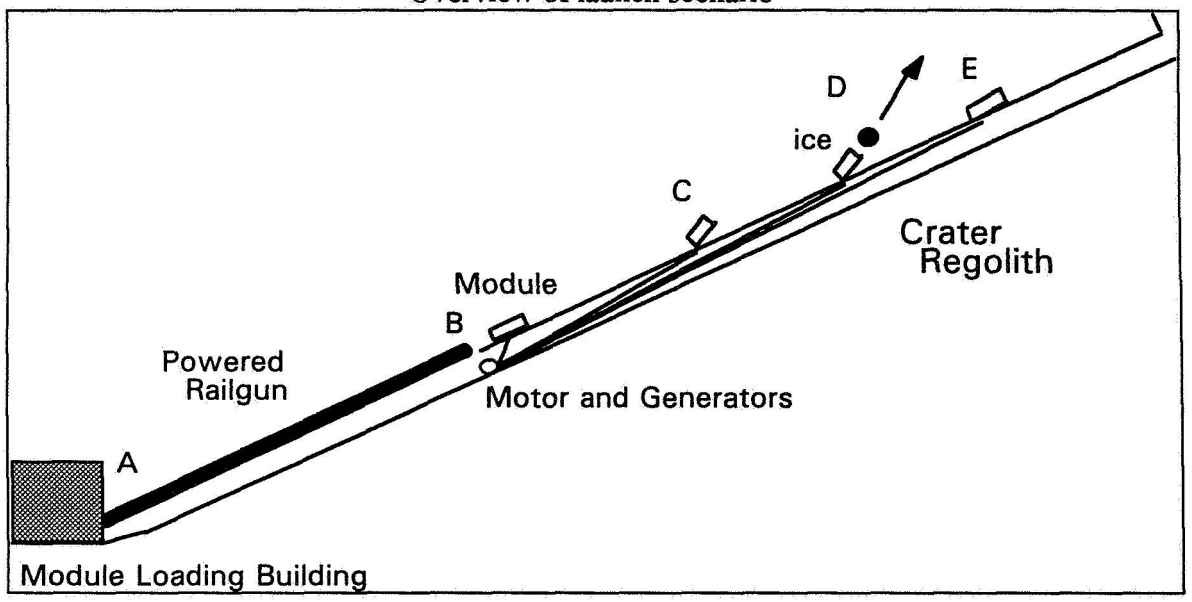

Figure 1.1.20

Assuming a super-conductive state, the capacitors can be charged instantaneously or near instantaneously by applying the necessary voltage and then removing the voltage source. The pre-launch process occurs within the Module Loading Building (MLB) where the ice pod is filled with water and then frozen. It is then placed inside the railgun bore with a thin copper sheet to serve as the plasma. The actual launch begins when the circuit bridge from the first capacitor is tripped as the projectile is given an small initial velocity (<<1 m/s) to begin the DES railgun process. The thin copper sheet that was inserted into the railgun behind the module is instantly vaporized to form the plasma (A). The module is then accelerated through the railgun until it reaches the end (B). The velocity at this point

is above the necessary limit so a more accurate means of velocity control can be achieved. Once the module leaves the bore, cables connected to the motor and generators will attach to the under side. The cables serve a dual purpose of keeping the module on the tracks as it enters an open rail design and apply an accurate, controllable braking force. While the braking process is occurring, the servo motors on the module will rotate the ice pod to the correct launch direction (C). When the correct velocity is reached by the measurement of the diode sensors on the module, a signal will be sent to the doors on the pod holding the ice in. The doors will open and the ice from the pod, through its own momentum, will exit in the predetermined direction (D). The module is then slowed down by the motors and brought back for re-launch (E). If an abort were to occur, the pod doors would not open up and the module would be decelerate with the ice payload.

Through radio signals, the velocity will be fed to a computer that will return a signal to the pod to release the ice when the correct velocity is reached. The railgun will only sense the position of the platform to discharge the capacitors at the correct time and will be unable to produce the minute changes to velocity necessary for accurate control. The braking system will produce a constant braking force and will be using a feedback control system to maintain this constant force. There will also be position sensors distributed along the launch track to mark the location of the projectile within the designated rail launch area. If it is not within this area, no signal is sent to release the ice and a mission abort takes place.

There are some assumptions concerning the state of ice through the acceleration process. Due to the fact that the acceleration of the ice is through such a small time frame and also in vacuum conditions, it has been assumed that the ice will remain a solid. There might be some sublimation at the contact surfaces but this is acceptable and is taken into account by creating a slightly larger than necessary ice carrying pod. The ice will also be strengthened by the possibility of freezing a nylon mesh within the ice structure during the molding process.

1.1.9 Railgun Configuration

The overall schematic of the railgun is shown in Fig. 1.1.20. The railgun will be placed on the side of a crater or on an artificially created mound which has been prepared with a concrete or other hard surface (regolith). The elevation angle of the railgun will be 23°. The actual angle needed for launch will vary around 24° but the extra degree will be handled by the directional control system on the ice platform. It is better to underestimate the launch elevation angle because it will be much easier to compensate for this underestimation on the module. The railgun and rails will be bolted to the prepared

concrete surface at 5 meter intervals to withstand the amount of pressure that will be applied as an outward force as the projectile progresses through the gun. This pressure is given as P_m in Table 1.1.4 and is equal to 8.07 MPa. Since this pressure is constant through the railgun and only acts on the part of the gun carrying the current, there will be a tremendous amount of force acting in the first stage. This is compensated for by increasing the strut density on the first few stages. A detail of a strut from a powered and unpowered section of the railgun is shown in Fig. 1.1.21. For reasons stated previously (Section 1.1.4), the powered railgun will be 121 m long. There will then be a 150m to 200m unpowered launch and deceleration area where the ice will be released at the correct speed and correct angle (see previous section).

Schematic of closed, powered and open, unpowered strut

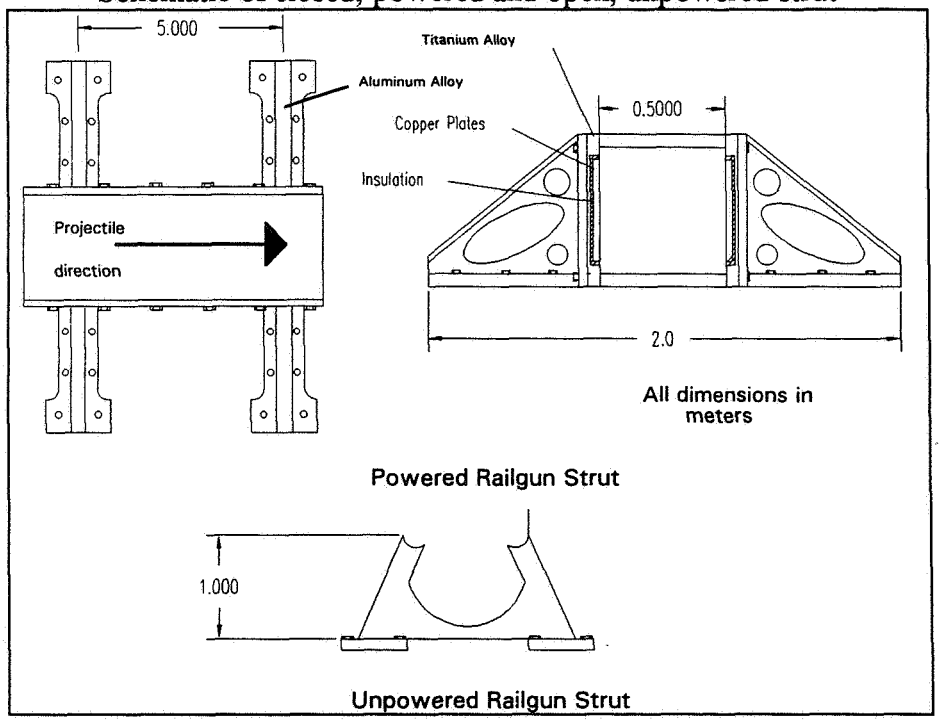

Figure 1.1.21

The actual make up of the railgun will vary from high strength aluminum alloys for the struts to titanium alloys and pure titanium for the bore. The decision to use these types of metals for the structure and bore is based on their high strength to weight ratios and ability to withstand high temperatures. The struts are made of light weight aluminum alloys because they will only need to withstand the pressure force of the railgun bore and will remain relatively protected from the space and bore environment. The railgun bore itself is made of a mixture of titanium alloys and pure titanium to withstand the high

temperatures witnessed repeatedly within the railgun bore[8]. Copper was chosen as the current carrying medium within the railgun mainly for its versatility and previous experience in experimental railgun research[3][8]. The copper will be insulated from the rest of the structure to prevent an improper current loop and serve as an expansion/contraction buffer. Also, each of the ten sections, except for the copper rails, will be insulated from each other to avoid adverse circuits that could hamper railgun operation and accommodate any expansion/contraction of the separate sections. The plates and sections will be bolted together to form the bore and gun so ease of assembly or disassembly is enhanced during construction and maintenance.

1.1.10 Power System

Earth-based research in the field of railgun experimentation use a wide variety of power sources, current generators, and energy storage devices[5][13]. Capacitors are being tested and improved to store the amount of power needed while homopolar generators (HPG), compulsators, and high energy inductive store devices are being developed to produce the high current needed for pulse powered railguns without any kind of energy storage system[5][13]. For this study, the capacitor and its future development is of particular interest.

A typical capacitor based power system is pictured in Figure 1.1.22. The energy source is a nuclear reactor based near the railgun site. Subsequently, the current may have to be cycled through a rectifier to charge the capacitors. However, the capacitors have the advantage of being compact and modular and unlike compulsators, HPG, and other rotating devices, have no adverse torques associated with charging and discharging.

Typical capacitor based power system[5]

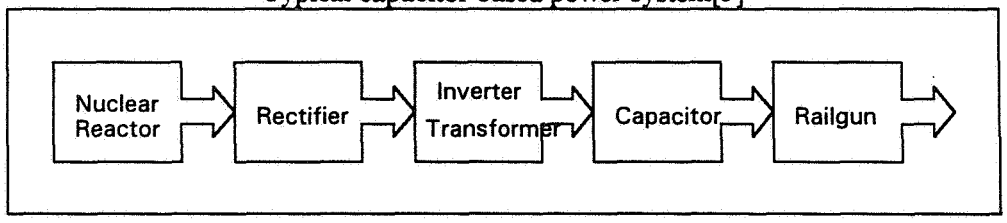

Figure 1.1.22

Energy and power densities of capacitors using new polymer and dielectric combinations are continuing to increase. Current technologies show a delivered energy density and peak power density of 9 kJ/kg and 9000 kW/kg respectively[5]. Far term energy densities for capacitors are expected to increase to 30 kJ/kg[5]. A summary on Table 1.1.5 shows the power required for each

stage of the DES railgun and the subsequent estimation of the weight of the capacitors. There are also advancements in extremely high current switching mechanisms as well.

Power Density per Stage and Estimated Capacitor Weight

	Power Density (GW)	Estimated Weight (kg)
stage 1	13.0	1444
stage 2	18.4	2044
stage 3	27.6	3067
stage 4	36.7	4078
stage 5	39.0	4333
stage 6	39.0	4333
stage 7	36.6	4067
stage 8	36.3	4033
stage 9	39.1	4344
stage 10	41.0	4556
	Total	32000

Table 1.1.5

1.1.11 Improving Railgun Efficiency

More recent studies have shown methods to improve railgun efficiency. For instance, the effectiveness of the magnetic field in the generation of a propelling force is highly dependent on when the stage is 'fired'. By delaying the 'tripping' of the stage until the projectile has traveled approximately four bore width distances past the stage entrance, the magnetic field is 99% efficient in producing a propelling force[9]. Additionally, the geometry of the stages can increase the efficiency of the railgun. Using nested chevrons, isolated from each other by insulation, may theoretically increase the effectiveness of the railgun to convert the electrical energy to kinetic energy[7].

1.1.12 Summary

Overall, the decision to pursue the railgun concept for lunar ice transport has proved feasible. The theoretical background exists for such a gun although the experimental background is somewhat sketchy. With final parameters determined, the next major concern is accuracy. As stated earlier, including every possible variable to

determine the precision of the launch mechanism is beyond the scope of this study. Currently, it is believed that the precision necessary can be achieved through a calibration process because of the predictability of the launch control system. Moreover, there are many other advantages to the railgun that cannot be overlooked. It will use little to none of the ice produced as fuel, needing only electrical energy produced by a solar or nuclear power generating system. It is a point system, not a continuous one such as a road, tramway, pipeline, or railroad. If problems occur with the railgun, they can be remedied at one point unlike the aforementioned transport possibilities which expand the trouble over a quarter of the Moon's circumference. In addition, these considerations do not even include the dust contamination and the tremendous amount of engineering and resources necessary for land transport. Finally, the railgun offers the possibility of launching projectiles into orbit or easy disassembly if ice is found at different locations.

References for Section 1.1

[1] Andreas, John C. Energy-Efficient Electric Motors: Selection and Application. Marcel Dekker, Inc., New York, NY 1982.

[2] Annet, F.A. Electric Elevators: Their Design, Construction, Operation, and Maintenance. McGraw-Hill Book Company, Inc., New York, NY 1935.

[3] Deis, Daniel W. and McNab, Ian R. *A Laboratory Demonstration Electromagnetic Launcher.* IEEE Transactions on Magnetics Vol 18, No. 1, January 1982. pp. 16-22.

[4] Donachie, Mathew J. Jr. Titanium: A Technical Guide. ASM International, Metals Park, OH 1988.

[5] Gully, J. H. *Power Supply Technology for Electric Guns.* IEEE Transactions on Magnetics Vol. 27, No. 1, January 1991. pp. 329-334.

[6] Honeycutt, Richard A. Electromechanical Devices: Theory, Applications, and Troubleshooting. Prentice-Hall, Inc., Englewood Cliffs, NJ 1986.

[7] Marshall, Richard A. *The Use of Nested Chevron Rails in a Distributed Energy Store Railgun.* IEEE Transactions on Magnetics Vol 20, No. 2, March 1984. pp. 389-390.

[8] Marshall, Richard A. *Structure of Plasma Armature of A Railgun.* IEEE Transactions on Magnetics Vol 22, No. 6, November 1986. pp. 1609-1612.

[9] Marshall, Richard A. and Barber, John P. *The 10 km/s, 10 kg Railgun.* IEEE Transactions on Magnetics Vol. 27, No. 1, January, 1991. pp. 21-27.

[10] Meetin, Ronald J. and Seifer, Howard S. *Propulsion Dynamics of Lunar Hoppers.* Journal of Spacecraft and Rockets Vol. 11, No. 12, AIAA, December, 1974. pp. 852-856.

[11] Parker, Jerald V. *Electromagnetic Projectile Acceleration Utilizing Distributed Energy Sources.* Journal of Applied Physics Vol. 53, American Institute of Physics, 1982. pp. 6710-6723.

[12] Schneigert, Zbigniew. Aerial Tramways and Funicular Railways. Pergamon Press, New York, NY 1966.

[13] Zowarka, R. C. Jr., Kajs, J. P., Pratap, S. B., Price, J. H., and Weldon, W. F. *A New Approach to a High Efficiency Inductive Store.* IEEE Transactions on Magnetics Vol. 27, No. 1, January 1991. pp. 384-389.

1.2 Rail Gun Projectile Orbital Mechanics

The mass accelerator will be required to launch ten ice "packets" every 24 hours to a collection site near the Sea of Tranquillity. If the forces on the projectile are modeled well, an accurate trajectory can be calculated which in turn will simplify the catching design. Safety considerations demand the landing site to be predicted with high precision. The science of orbital mechanics will be applied to the design of control systems to adjust for perturbations that the theoretical model will not account for and our ability to reproduce the conditions prescribed by this model.

1.2.1 Applying Fundamental Principles

During the early seventeenth century Johannes Kepler deduced from astrometric data measured by Tycho Brahe three laws of planetary motion. The first law states that the motion of a planet about the Sun can be described by an ellipse. The second law states that a line extending from the Sun to a planet sweeps equal areas in equal amounts of time. Finally, the third law states that the ratio of the cube of the semimajor axis of a planet to the square of the orbital period is a constant for all planets. Kepler also knew that the force exerted on the planets was proportional to the inverse of the square of the distance from the Sun, but was not aware of the concept of mass. It is important to remember that these laws were deduced from empirical information and were not explained theoretically until about 1656 when Issac Newton assembled his laws of motion and the universal law of gravitation. The latter can be expressed mathematically as

$$F = G\frac{m_1 m_2}{r^2}, \tag{1.2.1}$$

and Newton's second law of motion is

$$\mathbf{F} = m\mathbf{a}. \tag{1.2.2}$$

If these equations are applied to two point masses interacting with one another the equation known as the Kepler problem results as

$$\ddot{\mathbf{r}} + \frac{\mu}{r^3}\mathbf{r} = 0. \tag{1.2.3}$$

1.2.2 Describing the Trajectory

The solution to the Kepler problem is the equation,

$$r = \frac{a(1-e^2)}{1+e\cos(f)}, \tag{1.2.4}$$

which describes any of the four conic sections depending on the value of e, the eccentricity. It turns out that e equal to zero describes a circle and values between zero and one an ellipse. When e takes on values of one and greater the solution results in unbounded parabolic and hyperbolic paths. Figure 1.2.1 details the geometric interpretation of variables in the above equation. The distance r is measured from the focus to the ellipse. From an orbital mechanics viewpoint r describes the distance of the orbiting body from the center of mass of the second body; in this case, the Moon.

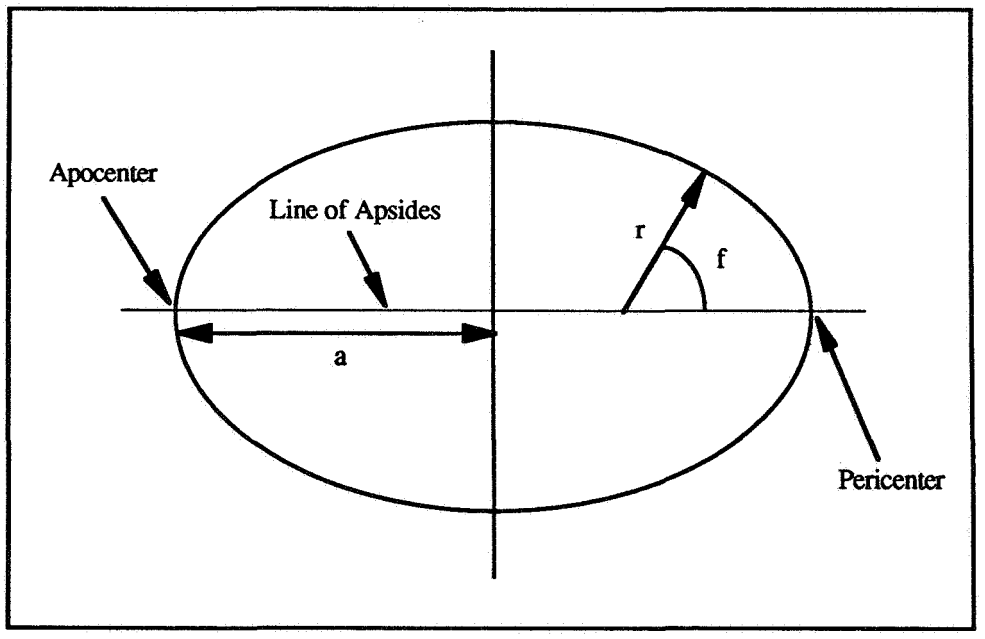

Figure 1.2.1 The Geometry of an Ellipse

The direction and magnitude of the angular momentum is an integral (constant) of motion. This implies that the satellite motion takes place entirely within a plane normal to the angular velocity vector. What remains is to find the parameters describing an ellipse intersecting the surface of the Moon at the launch and land positions.

1.2.3 Characteristics of the Sub-lunar Orbit

The equations above were derived assuming the mass of each body acts at a point. It can be shown that a homogeneous sphere acts gravitationally as a point mass; however the Moon is not quite spherical and is somewhat inhomogeneous with respect to mass distribution. The initial model will neglect these effects and assume the Moon to be a homogeneous sphere of mass 7.3532×10^{22} kg and mean radius 1738 km. With this in mind the orbit intersection points with the Moon must both be a distance of 1738 km from the lunar center of mass or focus of the ellipse. This constraint forces the Line of Apsides to bisect the angle between the vectors locating the launch and land sites on the lunar surface (see Figure 1.2.2). Pericenter will exist on this line within the lunar boundary and apocenter will be the midpoint of the flight path.

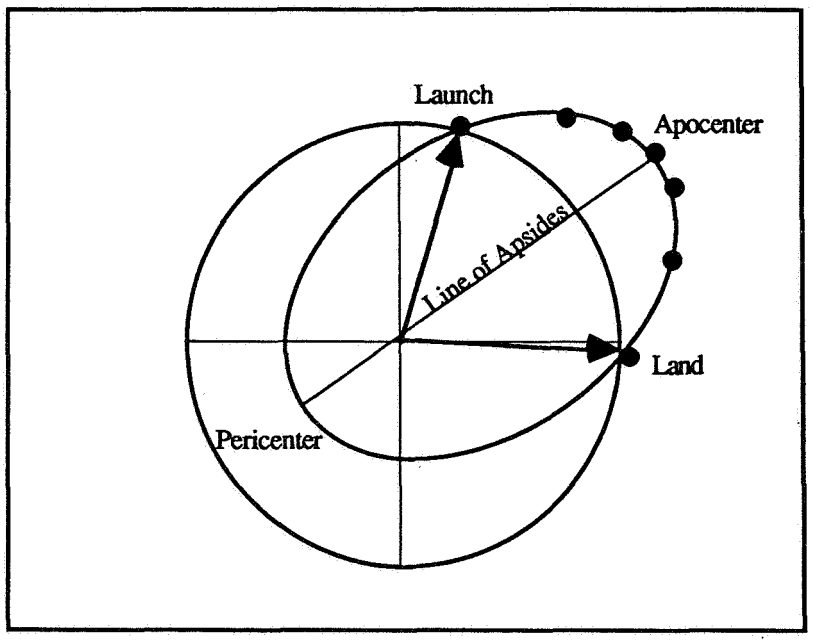

Figure 1.2.2 The Sub-lunar Orbit

1.2.4 Optimizing the Orbit

The first thing that must be accomplished is the determination of the angle between launch and land. Given that the polar site is located 150° west by 86° north and the equatorial site 42° east by 10.5° north, the Cartesian coordinates are found and a simple dot product will yield an equation for the angle between the two vectors. This is illustrated as follows:

$$
\begin{aligned}
\mathbf{r}_{launch} &= (-60.62\mathbf{i} + 104.99\mathbf{j} + 1733.8\mathbf{k})\ km \\
\mathbf{r}_{land} &= (1143.48\mathbf{i} - 1269.96\mathbf{j} + 301.8\mathbf{k})\ km \\
\mathbf{r}_{launch} \bullet \mathbf{r}_{land} &= (1738\ km)^2 \cos\phi \\
\phi &= 83.91^\circ
\end{aligned}
\tag{1.2.5}
$$

An optimal orbit in our case is one that minimizes the speed at the launch site. This will lower the power requirements of the accelerator as well as reduce the landing energy. From symmetry it can be seen that the both speeds will be equivalent. The expression for velocity at any point on the orbit is

$$v = \sqrt{m\left(\frac{2}{r} - \frac{1}{a}\right)}. \tag{1.2.6}$$

At the launch site r equals the mean radius of the Moon. Thus by minimizing a, the semimajor axis, the velocity will be reduced. Figure 1.2.3 plots injection velocity as a function of semimajor axis length.

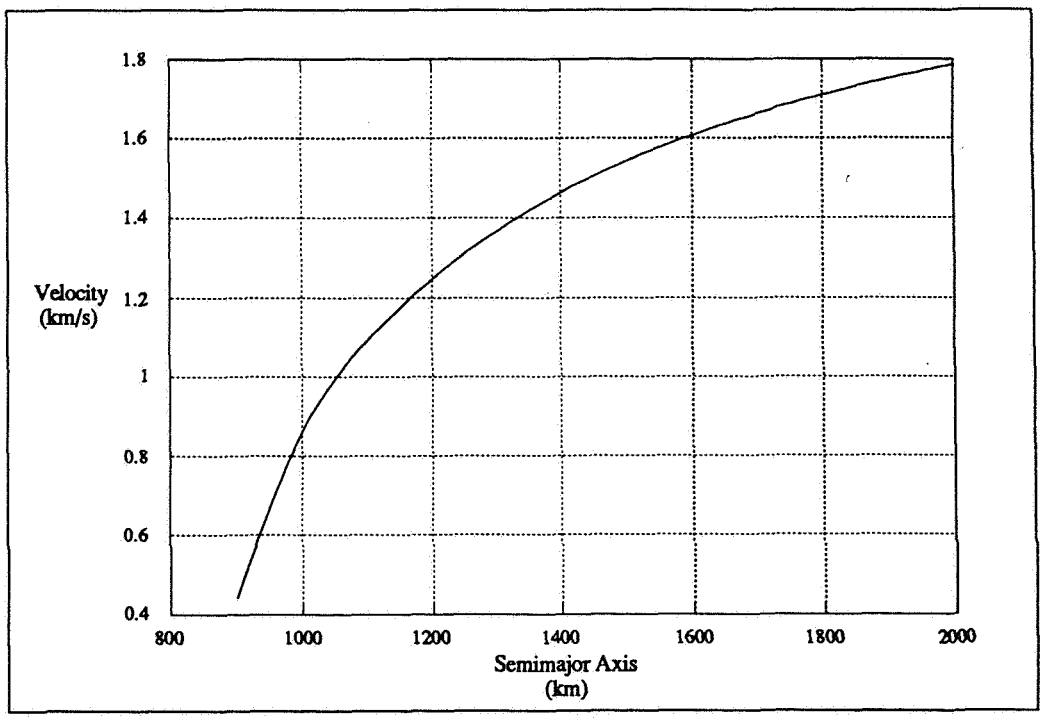

Figure 1.2.3 Rail Gun Exit Velocity Versus Semimajor Axis

The semimajor axis can be written explicitly as a function of h, the altitude of the projectile above the lunar surface at apocenter:

$$a = \frac{r_{moon} + h}{1 + e} \tag{1.2.7a}$$

$$e = \frac{h}{r_{moon}(\cos f_{launch} + 1) + h} \tag{1.2.7b}$$

$$a = \frac{1738.0 + h}{1 + \left(\frac{h}{446.41 + h}\right)} \tag{1.2.7c}$$

Differentiating and setting the resulting numerator to zero leads to the following equation:

$$h^2 + 446.41h - 288289.0 = 0. \tag{1.2.8}$$

The value of the altitude that satisfies this equation is 358.3 km which corresponds to a semimajor axis of 1450.5 km and a minimum velocity of 1.504 km/s (see Figure 1.2.4).

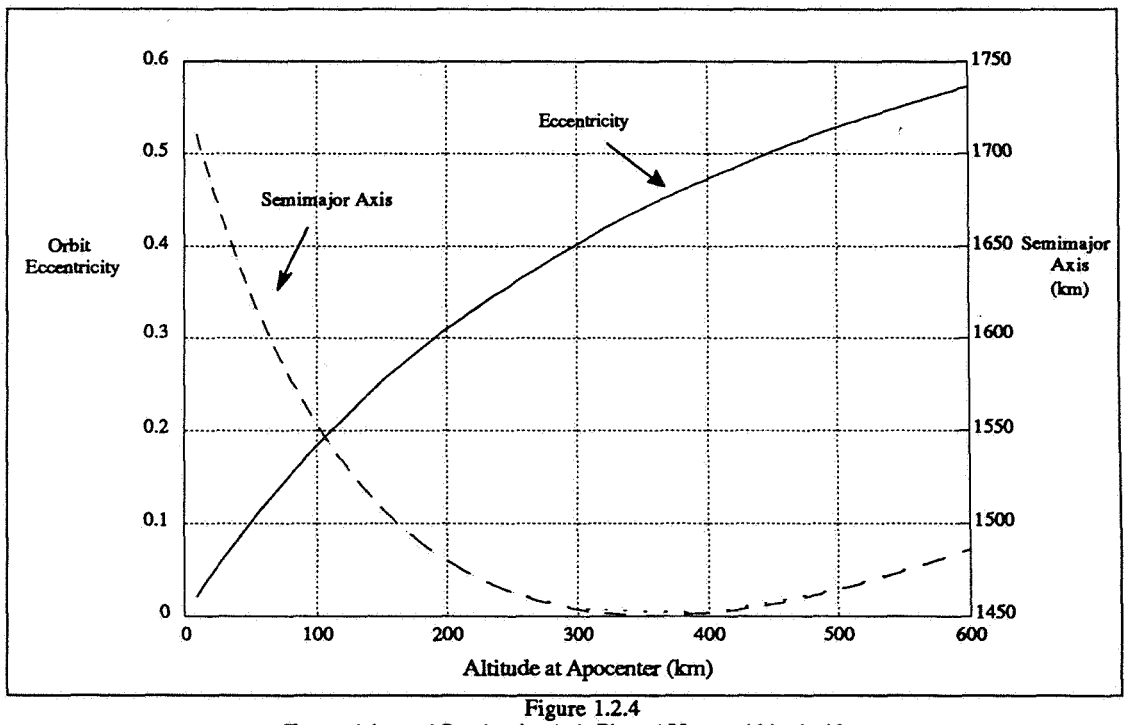

Figure 1.2.4
Eccentricity and Semimajor Axis Plotted Versus Altitude Above the Lunar Surface at Apocenter.

The eccentricity of this orbit is 0.4453 and the resulting equation for the orbital path is

$$r = \frac{1162.9\ km}{1 + 0.4453\cos(f)}. \qquad (1.2.9)$$

This function is plotted in Figure 1.2.5 with a circle of radius 1738 km, representing the lunar surface. An appropriate phase shift was added to position the orbit such that the Line of Apsides is inclined at an angle of 51.46° relative to the horizontal. Figure 1.2.5 is plotted within the orbit plane.

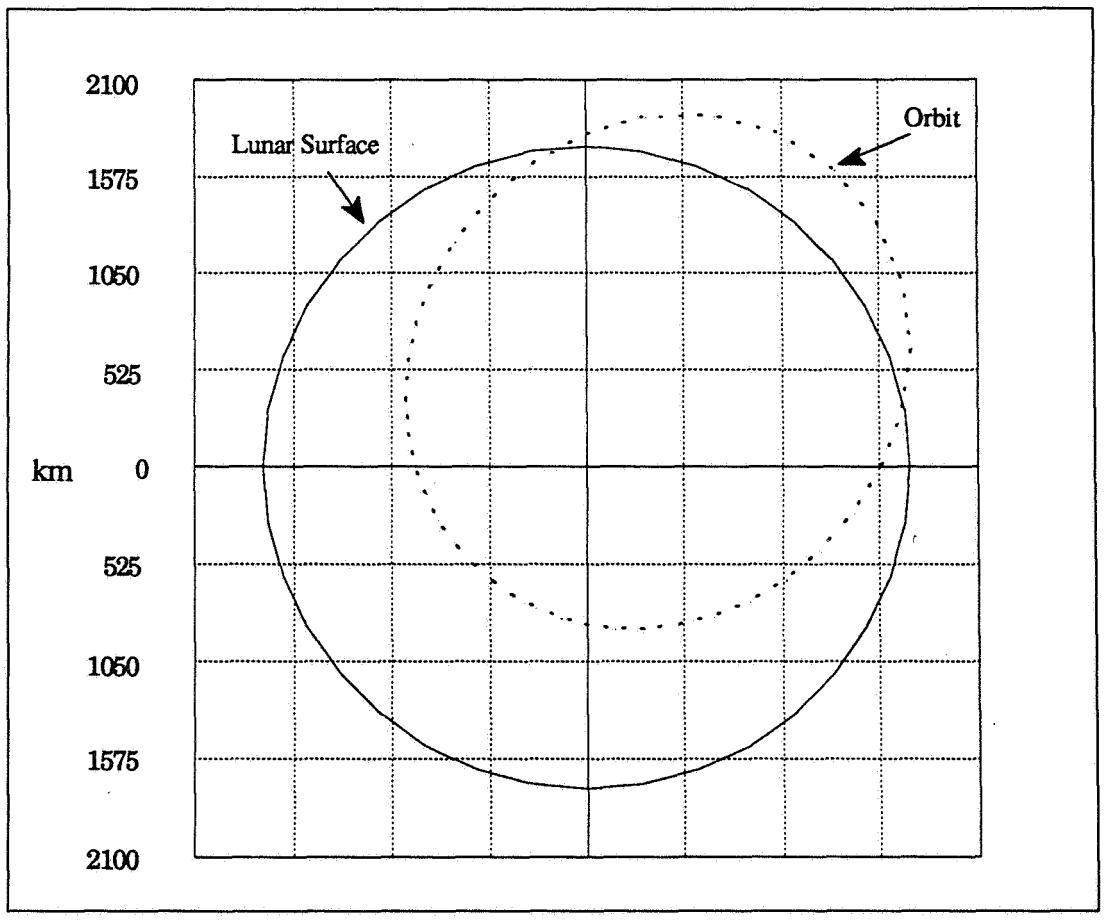

Figure 1.2.5
The Elliptical Orbit Path

1.2.5 Additional Design Parameters

Two pieces of information that will be important to the launching and landing teams are the launch angle and flight time. The launch position can be located in polar coordinates as

$$\mathbf{r} = r\hat{\mathbf{e}}_r. \tag{1.2.10}$$

Differentiating yields

$$\dot{\mathbf{r}} = \dot{r}\hat{\mathbf{e}}_r + r\dot{\theta}\hat{\mathbf{e}}_\theta. \tag{1.2.11}$$

The vector dot product of this expression in the $\hat{\mathbf{e}}_\theta$ direction yields an equation for the rail gun angle of inclination with respect to the local horizon.

$$\begin{aligned} \dot{\mathbf{r}} \cdot \hat{\mathbf{e}}_\theta &= v\cos\phi_i = r\dot{\theta} \\ \phi_i &= \cos^{-1}\left(\frac{h}{vr}\right) = 23.97^\circ \end{aligned} \tag{1.2.12}$$

Here h is the magnitude of the angular momentum vector.

Determining the flight time is not as simple. From geometry, the argument of pericenter is known for the launch and land locations: f_{launch}=138.04° and f_{land}=221.95°. Here the equations are simply outlined and the results stated.

$$\begin{aligned} &n = \frac{2\pi}{T} = \sqrt{\frac{m}{a^3}}, \ T \text{ is the orbital period.} \\ &\tan\frac{f}{2} = \sqrt{\frac{1+e}{1-e}}\tan\frac{E}{2}, \ E \text{ is the eccentric anomaly} \\ &M = E - e\sin E, \ M \text{ is the mean anomaly} \\ &t = \frac{M}{n}, \ t \text{ is the time to reach } M \end{aligned} \tag{1.2.12}$$

From these equations the time of flight is calculated to be 39.6 minutes.

1.2.6 Perturbation Effects

A fundamental question arises when using two-body celestial mechanics: can the influence of nearby bodies be neglected? The model of the ice projectile must have enough accuracy such that the feedback control system will be able to reconcile any perturbed motion. Also, calibration of the rail gun will account for any relatively constant forces not contained

within the theoretical model. With this in mind the average magnitudes of forces imposed on the ice by the Earth, Moon, and Sun are calculated:

$$\begin{aligned} \overline{F}_{earth\text{-}ice} &\approx 0.324N \\ (F_{moon\text{-}ice})_{\min} &= 133.5N. \\ \overline{F}_{sun-ice} &\approx 0.707N \end{aligned} \qquad (1.2.14)$$

The forces imposed by the Sun and the Earth are small relative to lunar influence and are second order in nature. Over an approximate flight time of 40 minutes these small forces can deviate the projectile path by an appreciable amount. To obtain more accuracy a more complete model will be constructed and numerical methods employed to solve the complex equations of motion.

Newtonian mechanics requires the use the an inertial reference frame to correctly write the vector force equation,

$$\mathbf{F} = m\ddot{\mathbf{R}}. \qquad (1.2.15)$$

During the 40 minute flight time of the projectile the motion of the Earth about the Sun is slight. For this reason an inertial frame is chosen that is fixed at the center of mass of the Earth, but does not rotate with the planet. Due to the small average eccentricity of the lunar orbit about the Earth ($\bar{e}_{moon\text{-}earth}$=0.0549) it is assumed that this motion is circular. The terrestrial orbit about the Sun is also nearly circular ($\bar{e}_{earth\text{-}sun}$=0.017) and for this reason an assumption is made that the solar gravitational force acting on the projectile is constant.

Two coordinate systems are useful in describing the dynamics of the projectile: the necessary inertial system defined by the unit vectors **i**, **j**, **k**, and a Moon fixed system with an origin at the lunar center of mass defined by unit vectors $\mathbf{e}_1$, $\mathbf{e}_2$, and $\mathbf{e}_3$. The vectors $\mathbf{e}_3$ and **k** both are normal to the eccliptic plane for all time. In reality the spin axis of the Moon is inclined at just under 2° from the eccliptic plane normal, another approximation of the model.

The Moon spins about its own axis with the same period as its rotation about the Earth. If its orbit was perfectly circular, only one of its sides would face the Earth; however, owing to the small eccentricity of the orbit, the Moon appears to sway when viewed from the Earth [1]. This back and forth motion is known as longitudinal libration. To study this effect and determine its importance, a libration angle (ξ) can be included. It should be noted that the model assumes circular motion of the Moon, but libration can be simulated if the kinematics are treated correctly [2]. Figure 1.2.6 illustrates the system described above.

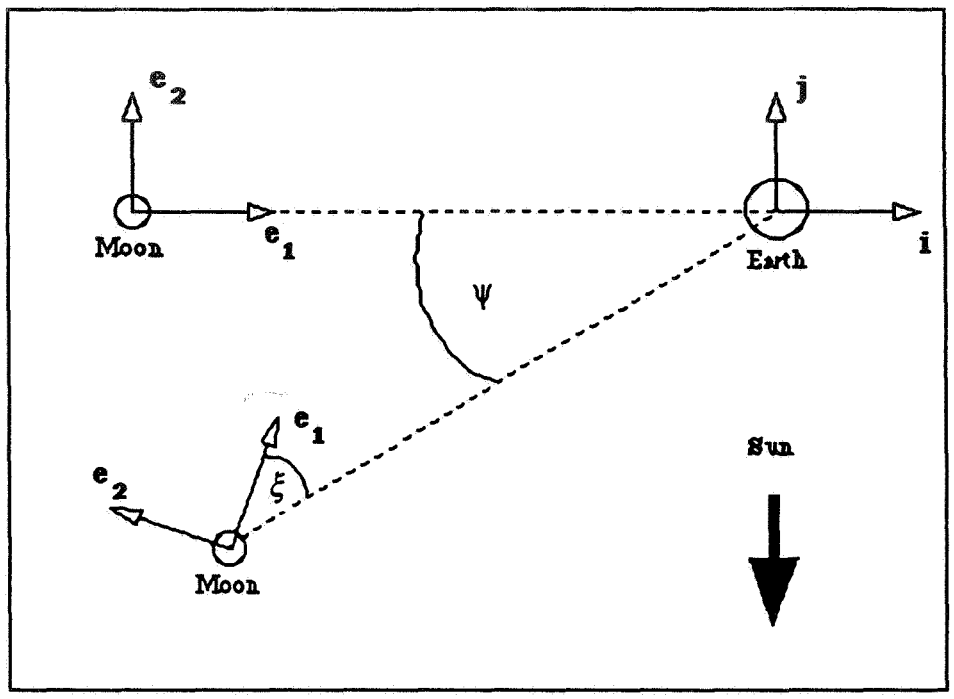

Figure 1.2.6 Geometry for Model Including Earth and Sun Effects

Newton's third law for the projectile can now be written as,

$$-\frac{GmM}{r^3}\mathbf{r} - F_s\mathbf{j} - \frac{GmM_e}{R^3}\mathbf{R} = m\ddot{\mathbf{R}} \qquad (1.2.16)$$

where,

r: locates ice from the lunar center of mass

$\mathbf{R} = \mathbf{r} + \boldsymbol{\rho}$: locates ice from the terrestrial center of mass

$\boldsymbol{\rho}$: locates the lunar center of mass from the terrestrial center of mass

m: mass of the projectile

M: mass of the Moon

M_e: mass of the Earth

F_s: constant force exerted by the Sun

After differentiation and transforming the vectors to the Moon frame the following three equations result:

$$
\begin{aligned}
&-\frac{GMx_1}{r^3}-\frac{F_s\sin(\xi+\psi)}{m}-\frac{GM_e}{R^3}(x_1-\rho\cos\xi)=\ddot{x}_1-2\dot{x}_2\dot{\psi}+(\rho\cos\xi-x_1)\dot{\psi}^2\\
&-\frac{GMx_2}{r^3}-\frac{F_s\cos(\xi+\psi)}{m}-\frac{GM_e}{R^3}(x_2+\rho\sin\xi)=\ddot{x}_2+2\dot{x}_1\dot{\psi}-(\rho\sin\xi+x_2)\dot{\psi}^2 \qquad (1.2.17)\\
&-\frac{GMx_3}{r^3}-\frac{GM_ex_3}{R^3}=\ddot{x}_3
\end{aligned}
$$

where

x_n: projection of $\mathbf{r}$ onto $\mathbf{e}_n$

ψ: the rotation angle of the Moon about the Earth.

ξ: the libration angle

These equations can be numerically integrated by a computer, but will require as input initial velocity and position of the ice. Also, it is of interest to determine the sensitivity of the landing position to rail gun initial conditions. With this in mind a new coordinate system fixed to the local terrain of the rail gun is developed. The initial conditions will be given in this convenient system and subsequently transformed to the Moon system for numerical integration.

Launch and land positions are given and can be represented as the vectors $\mathbf{r_1}$ and $\mathbf{r_2}$ respectively. The rail gun local vertical direction can be represented by normalizing $\mathbf{r_1}$,

$$\mathbf{a}_3=\frac{\mathbf{r}_1}{\|\mathbf{r}_1\|}. \qquad (1.2.18)$$

The rail gun coordinate system (a-frame) can be conveniently oriented relative to the two body orbit plane by defining $\mathbf{a_1}$ and $\mathbf{a_2}$ as follows:

$$
\begin{aligned}
\mathbf{a}_1&=\frac{\mathbf{r}_2\times\mathbf{r}_1}{\|\mathbf{r}_2\times\mathbf{r}_1\|}. \qquad (1.2.19)\\
\mathbf{a}_2&=\mathbf{a}_3\times\mathbf{a}_1
\end{aligned}
$$

The projectile initial velocity vector can now be written as

$$\mathbf{v}=v\mathbf{l}=v\cos\delta\sin\gamma\mathbf{a}_1+v\cos\delta\cos\gamma\mathbf{a}_2+v\sin\delta\mathbf{a}_3 \qquad (1.2.20)$$

where

$\mathbf{l}$: the unit velocity direction

δ: angle of elevation

γ: azimuthal angle (+ ccw about $\mathbf{a}_3$)

These components can be expressed in the e-frame through a known orthogonal transformation.

The computer code accepts as inputs the initial projectile speed, elevation angle, and azimuth angle as well as the libration angle and angular position of the Moon relative to the Earth. Initial position is known and is constant.

It is necessary to place the projectile within 0.5 kilometers of the mass catcher. Using the data generated by the computer code, the impact position sensitivity to initial conditions is found using the above constraint. To achieve this precision requires velocities to ±0.1 m/s, elevation angles to ±0.05°, and azimuth angles to ±0.03°.

To find the correct initial conditions that offset the perturbations from the two-body problem, the program described above can be modified utilizing what is commonly referred to as a shooting method. The impact position is solely a function of the initial velocity (the launch position is constant) and can be estimated by a first order Taylor series expansion in terms of these variables:

$$
\begin{aligned}
x_{1_f}(\dot{x}_{1_i}+\Delta\dot{x}_{1_i},\dot{x}_{2_i}+\Delta\dot{x}_{2_i},\dot{x}_{3_i}+\Delta\dot{x}_{3_i}) &= \left(x_{1_f}\right)_o + \frac{\partial x_{1_f}}{\partial \dot{x}_{1_i}}\Delta\dot{x}_{1_i} + \frac{\partial x_{1_f}}{\partial \dot{x}_{2_i}}\Delta\dot{x}_{2_i} + \frac{\partial x_{1_f}}{\partial \dot{x}_{3_i}}\Delta\dot{x}_{3_i} \\
x_{2_f}(\dot{x}_{1_i}+\Delta\dot{x}_{1_i},\dot{x}_{2_i}+\Delta\dot{x}_{2_i},\dot{x}_{3_i}+\Delta\dot{x}_{3_i}) &= \left(x_{2_f}\right)_o + \frac{\partial x_{2_f}}{\partial \dot{x}_{1_i}}\Delta\dot{x}_{1_i} + \frac{\partial x_{2_f}}{\partial \dot{x}_{2_i}}\Delta\dot{x}_{2_i} + \frac{\partial x_{2_f}}{\partial \dot{x}_{3_i}}\Delta\dot{x}_{3_i} \qquad (1.2.21) \\
x_{3_f}(\dot{x}_{1_i}+\Delta\dot{x}_{1_i},\dot{x}_{2_i}+\Delta\dot{x}_{2_i},\dot{x}_{3_i}+\Delta\dot{x}_{3_i}) &= \left(x_{3_f}\right)_o + \frac{\partial x_{3_f}}{\partial \dot{x}_{1_i}}\Delta\dot{x}_{1_i} + \frac{\partial x_{3_f}}{\partial \dot{x}_{2_i}}\Delta\dot{x}_{2_i} + \frac{\partial x_{3_f}}{\partial \dot{x}_{3_i}}\Delta\dot{x}_{3_i}
\end{aligned}
$$

These equations can be solved for the additive corrections needed to land the ice at a given location:

$$
\begin{pmatrix} \Delta\dot{x}_{1_i} \\ \Delta\dot{x}_{2_i} \\ \Delta\dot{x}_{3_i} \end{pmatrix} = \Phi^{-1} \begin{pmatrix} x_{1_f} - \left(x_{1_f}\right)_o \\ x_{2_f} - \left(x_{2_f}\right)_o \\ x_{3_f} - \left(x_{3_f}\right)_o \end{pmatrix}, \qquad (1.2.22)
$$

where,

$$\Phi = \begin{bmatrix} \frac{\partial x_{1_f}}{\partial \dot{x}_{1_i}} & \frac{\partial x_{1_f}}{\partial \dot{x}_{2_i}} & \frac{\partial x_{1_f}}{\partial \dot{x}_{3_i}} \\ \frac{\partial x_{2_f}}{\partial \dot{x}_{1_i}} & \frac{\partial x_{2_f}}{\partial \dot{x}_{2_i}} & \frac{\partial x_{2_f}}{\partial \dot{x}_{3_i}} \\ \frac{\partial x_{3_f}}{\partial \dot{x}_{1_i}} & \frac{\partial x_{3_f}}{\partial \dot{x}_{2_i}} & \frac{\partial x_{3_f}}{\partial \dot{x}_{3_i}} \end{bmatrix}. \qquad (1.2.23)$$

Partial differentials in the above matrix must be computed numerically. The code particular to this design uses a central difference calculation. Also note that the Taylor series is a linear approximation and that these equations will yield an accurate result only if they are applied in conjunction with iteration.

1.2.7 Implementation of Feedback and Control

The largest deviations are expected to arise from the homogeneous sphere assumption. Fortunately, lunar mass distribution will remain constant over the next century and, hopefully, will be studied well by the time this lunar facility is installed. To correct for this theoretically entails a complicated potential model of lunar mass distribution. A practical solution is to design a system that measures range and angular displacements and utilizes Laplacian orbit determination methods to predict an impact position [3]. The orbit can be sampled three times throughout its flight duration by instrumentation at the launch and land sites. This information can be transmitted to the mobile catching unit to aid in final positioning.

References

[1] Firsoff,V. A. The Old Moon and the New. Sidgwick and Jackson, London 1969.

[2] Dr. David L. Richardson. The University of Cincinnati, Department of Aerospace Engineering and Engineering Mechanics. Cincinnati, Ohio 45221.

[3] Taff, Laurence G. Celestial Mechanics: A Computational Guide for the Practitioner. Wiley-Interscience, New York 1985.

1.3 Mass Catcher

1.3.1 Introduction

The mass catcher entails many design requirements where the foremost issue is to stop an 80 kg projectile with an incoming velocity of 1500 m/s. In the interests of disposability, the launched projectile, which will traverse one fourth of the moon's circumference, will not contain a control system. Without this control system perturbations will exist; therefore, the mass catcher must be mobile to accommodate for variable landing locations. In addition, the mass catcher should use minimal power and be designed for multiple catchings.

1.3.2 Overview

Figure 1.3.1 is a simplified rendition of the major components of the mass catcher. Since the catcher must be able to translate as well as rotate, independent spherical wheels have been installed.

Major Components of the Mass Catcher

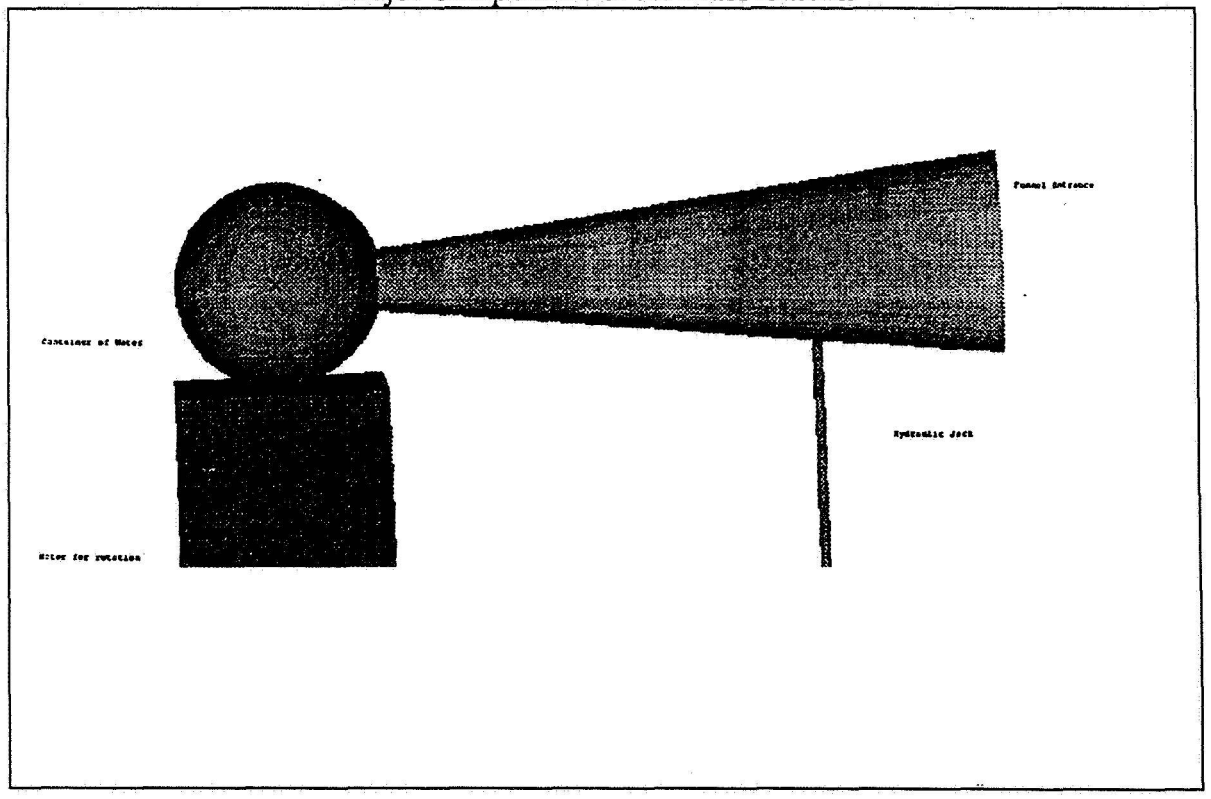

Figure 1.3.1

Figure 1.3.2 shows a probable construction of a typical wheel. By restricting the motion of certain independent rollers, the direction of the sphere (and, therefore, the catcher) can be controlled. The area will be paved in order to avoid erosive lunar soil from damaging the rolling mechanisms,

A Typical Wheel on the Catcher

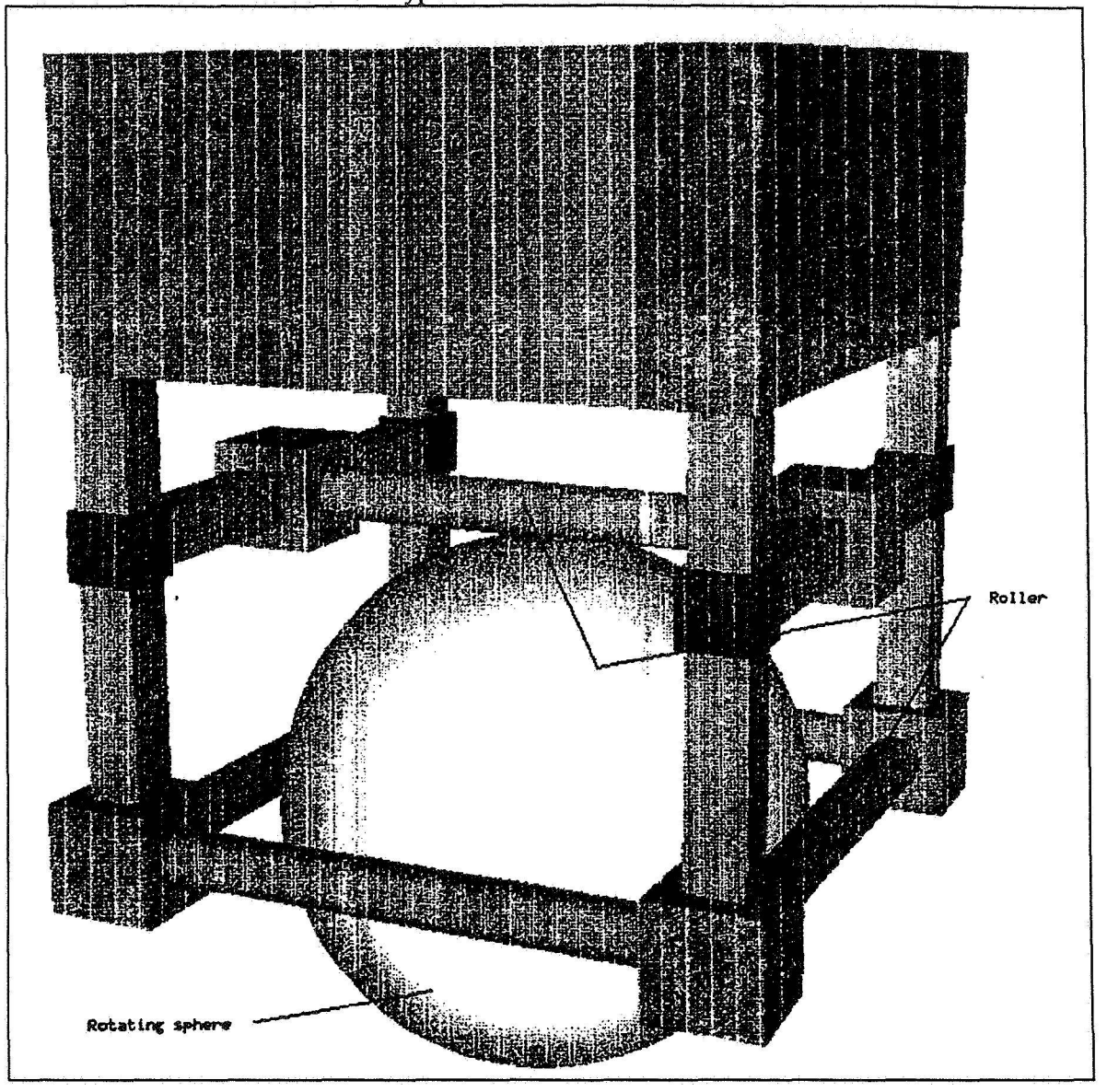

Figure 1.3.2

The ice projectile is tracked by three ground base units. At three 10 minute intervals, the catcher will be sent information using a Laplacian method of orbit

determination as to the exact impact location of the projectile. This will be sufficient time for the catcher to position itself and to allow the hydraulic jack to elevate the funnel to a pitch angle that is aligned with the incoming projectile. The ice, upon entering the funnel, is contained by a trap door installed at the entrance of the funnel. This entrapment is required to capture the vapors produced by the impacted ice. The speed of the door is dependent upon the entrance area of the funnel. The larger the area, the longer it takes to cover the opening. In all probability the door will not be fast enough to contain every molecule of ice. Once the ice has entered the funnel, it will traverse down into a lower chamber where it will impact one three possible obstructions. These three options need to be tested to verify the analytical solutions. The ice will either impact a large amount of water, a series of thick, massive, loosely hung chains, or a wall of Kevlar restricted by a spring-damper system. In the interests of this report, the lower chamber will contain a large set of chains followed by a plate attached to a spring-damper system.

Due to the scarcity of ballistic limit data of ice impacts, experiments are necessary to determine the proper configuration. A former scientist from the Sandia National Laboratories in Albuquerque, New Mexico, who had first hand experience with mass catchers of projectiles moving with velocities of up to 11 km/s, used Kevlar parachutes intermingled with sheets of steel loosely hung by chain [1]. After each run, the Kevlar chutes had to be expanded back to their original form and were quite effective for multiple runs.

The catcher will have a climate control mechanism which pressurizes the chamber with ammonia that has been extracted from each shipment of ice. The climate mechanism will also heat the chamber such that the ice will liquefy to water. The heat required will be supplied from the excess heat produced by a nuclear power source. The liquefied water will fall into a basin (for the case of the chains or Kevlar plates) ready for collection. At the end of each Earth day (800 kg of ice has been collected by then), the mass catcher will be driven back to the outer perimeter where a pipe will be located to transport the water to the processing facility.

1.3.3 Sizing the Area and Setting the Speed of the Mass Catcher

It was shown in section 1.2 that for a launch velocity error of .1 m/s a maximum deviation of ±.5 km can be expected. In order to reduce the kinetic energy of the projectile further, the mass catcher will be allowed to roll back a bit. Hence, an area with diameter of 1.5 km will be paved. This dictates that the mass catcher will need to move at a maximum speed of 1.3 m/s (3 mph) .

The lunar rover used in the Apollo 16 mission weighed approximately 700 kg and had attained a top speed of 3.1 m/s (6.8 mph) by Commander John Young [2]. The rover was powered by two 36 Volt batteries. One-quarter horsepower motors drove each wheel. This speed was attained over lunar soil. Comparably, the mass catcher will be placed on a circular shaped paved surface, require much less speed, but will weigh considerably more.

1.3.4 Impacts and the Design of the Catching Mechanism

An important factor for target damage is the ballistic limit, which is the minimum velocity required to perforate a plate of finite thickness. For projectiles moving much slower than the ballistic limit- in the specific case of a cylindrical rod- buckling would occur. Increasing the speed but remaining below the ballistic limit, the cylindrical rod deforms in a mushroom mode with little to no indentation to the target. Embedding of the projectile will soon occur with increasing velocity. Once the impacts are above the ballistic limit, an impact flash is generated at the moment of impact. High intensity stress waves propagate into the rod and target, hence cratering both surfaces immediately. Additionally, the initial impact interface pressure far exceeds the material strength of both the striker (which is the projectile) and target. Consequently, the projectile suffers hydrodynamic-like erosion while the remainder of the projectile enters the cavity undeformed. This sort of impact phenomenon shall be avoided when designing the mass catcher. Unfortunately, there has been no testing of ballistic limits for ice impacts on materials. In fact there has been very little research with high velocity ice impacts. Therefore, the approach to solving the ice projectile problem is to treat the ice as a rigid body, which is the worst case scenario.

Another concern is the effect of impacts at oblique angles. Johnson, Senguptan, and Ghosh found many similarities to normal impacts at low angles of obliquity for rods impacting on plates of the same material [3]. Low angles are considered to be less than 30°. It was observed that the depth of penetration normal to the target surface was proportional to the normal component of impact velocity. The length of cratering was proportional to the component of impact velocity parallel to the target surface. These facts lead to the formulation of impact damage both on the internal structure and the funnel.

The design point for the funnel should be one where the projectile grazes the surface. Johnson and others also observed that ricochet of long-rod projectiles occurred at angles of obliquity exceeding 75°. The critical ricochet angle was predicted reasonably well by Tate [4] to be

$$\tan^3\beta = \frac{2}{3}\frac{\rho_p \cdot V^2}{Y_p} \cdot \frac{L^2 + D^2}{L \cdot D}\left[1 + \frac{\rho_p}{\rho_t}\right]^{1/2} \qquad (1.3.2)$$

where ρ_p and ρ_t are the respective densities of the projectile and target, L and D are the length and diameter of a cylindrical projectile, and Y is the mean flow stress.

Before solving the equation, it is necessary to understand the advantages obtained from having an angle of inclination. Johnson and others noticed immediately after contact, the leading edge of the rod bends plastically and glides parallel to the target surface [3]. After traveling along the target face for some time, the leading edge of the rod lifts from the surface, due to the normal component of inertia forces, and at the same time continues to move forward. The length of time between first contact and lift-off depends on both angle of obliquity and striking velocity. For the initial impact speeds below the hydrodynamic limit, each element behind the leading edge of the projectile makes contact with the same portion of the target surface. More importantly, projectiles which ricochet intact carry little, if any, eroded target material with them. Projectiles which fragment may have ejection consisting of both projectile and target material. The rod nose used in Johnson's experiment showed a sharp decrease in velocity on contact and an increase in velocity on lift-off. If the rod was above the hydrodynamic limit, tensile stresses can cause disintegration of the rod. For impacts above the critical ricochet angle but below the hydrodynamic transition velocity, the rod was likely to ricochet intact but with increased length (In the case of ice, the elongation will be replaced with breakup). Target erosion was found to be minimal.

To calculate the obliquity, assume $\frac{\rho V^2}{Y} = 10^2$. This is generally the case for objects traveling between 800 to 3000 m/s. Table 1.3.1 depicts the critical ricochet angle for a few materials that may be likely candidates for the funnel. Notice that the angle is measured from the vertical, since equation (1.3.2) was calculated for vertical normal impacts. The length and diameter was set to .5 m.

Calculated Critical Ricochet Angle for Various Materials

Material	Critical Ricochet Angle in Degrees
Kevlar - 49	79.8
Ship Armor	79.1
Aluminum Alloy 7075-T6	79.4
Titanium Alloy 6Al-4V	79.2
Magnesium Alloy 13Li-6Al	79.7

Table 1.3.1

For a margin of safety, the angle of the funnel will be increased to 85° (i.e. almost parallel to the projectile). It is expected that with tracking, the ice will typically graze the funnel and only under the most inopportune circumstances directly impact onto the funnel. The grazing will be helpful in partially reducing the kinetic energy of the ice. However, a direct impact may occur in the funnel and will occur in the lower chamber; therefore, this problem is considered next.

1.3.5 Recht Ballistic Penetration of Ductile Media Model

Central to ballistic impact theory is the resisting force that is felt by the projectile. Components of this force are due to the inertial and flow stress properties of the target material and the friction between the sliding interface. Magnitudes of these force components are affected by penetrator size, shape and velocity.

There has been much experimentation and curve fitting of resisting force by Robins-Euler, Recht, Jacobson, Poncelet, Helie, Nishiwaki, and Burkhardt [5]. Except for Robins-Euler and Recht, all of the equations calculate the inertial pressure using a function of Bernoulli's flow pressure, $\frac{\rho V^2}{2}$. Equation (1.3.3) is the Recht Equation. The inertial pressure at an impact interface involve a rigid conical penetrator with apex half angle α and a medium. Recht multiplied the initial pressure by the empirical constants C_n and C_v, to calculate the inertial pressure. It has been shown experimentally that the Recht equation has been very accurate for both blunt and sharp bodies. In fact, it has been shown that for an α=37.5° , it very nearly models spherical impacts. The Recht equation also lends itself to a variety of ductile materials. With these reasons, the Recht equation was selected as the model for computing the force acting upon the contact interface between the projectile and medium. Note, however, that the impact in question is ice and without experimentation these results cannot be guaranteed.

$$F = -A_x\left\{C_n\left[C_v \cdot V\sqrt{K\rho}\sin\alpha + 2\tau_s \ln(2Z_m)\right]\cdot\left[1+\frac{f}{\tan\alpha}\right]\right\} \qquad (1.3.3)$$

where

$$Z_m = \frac{E}{\sigma_y}\left(1+2\cdot\frac{E}{\sigma_y}\right)^{1/2} \qquad (1.3.4)$$

A_x is the presented area of the penetrator ($\pi r^2 = \pi(.3)^2 = .283 m^2$, in this case). C_n is the empirical dimensionless constant (C_n=.62), C_v is the empirical dimensionless constant which recognizes that the inertial pressure decreases with time (C_v=.25), V is the instantaneous velocity, K is the Bulk modulus of the medium, α is the empirical result which shows that for a blunt body α=37.5°, T_s is the static shear strength of the medium, Z_m is distortion pressure, f is the dynamic friction coefficient usually set to .01 for metal-metal contacts (quite small in general for ice as well), and ρ is the mass density of the medium. Table 1.3.2 displays several common material properties, and Table 1.3.3 displays the reactive force for each material. It is important to note that the projectile is considered completely rigid.

Material	Hardness (BHN)	Mass Density ρ (kg/m^3)	Bulk Modulus K (N/m^2)	Young's Modulus E (N/m^2)	Yield Strength σ_y (N/m^2)	Compressive Shear Strength τ_s (N/m^2)
			Steel Alloys			
Structural						
soft	100	7830	158×10^9	206×10^9	172×10^6	206×10^6
mild	150	7830	158×10^9	206×10^9	309×10^6	275×10^6
Ship armor	200	7830	158×10^9	206×10^9	549×10^6	377×10^6
	250	7830	158×10^9	206×10^9	756×10^6	470×10^6
Armor	300	7830	158×10^9	206×10^9	893×10^6	549×10^6
(MIL-12560)	350	7830	158×10^9	206×10^9	1030×10^6	618×10^6
			Aluminum Alloys			
7075-0	60	2765	69×10^9	71×10^9	103×10^6	151×10^6
5083-H113	75	2765	69×10^9	71×10^9	227×10^6	185×10^6
2024-T3 (or T4)	120	2765	69×10^9	71×10^9	343×10^6	281×10^6
7075-T6	150	2765	69×10^9	71×10^9	500×10^6	330×10^6
			Titanium Alloy			
6A1–4V	285	4500	126×10^9	114×10^9	827×10^6	483×10^6
			Magnesium Alloy			
13Li–6A1	55	1720	41×10^9	45×10^9	200×10^6	152×10^6
			Other Materials			
Plexiglas	—	1180	5.2×10^9	3.1×10^9	69×10^6	76×10^6
Lexan	—	1290	3.1×10^9	2.2×10^9	69×10^6	62×10^6
Aluminum oxide	—	3750	190×10^9	303×10^9	193×10^6	1034×10^6
Glass	—	2465	36.5×10^9	69×10^9	55×10^6	483×10^6
Lead glass	—	6220	34.5×10^9	51×10^9	55×10^6	483×10^6
Reinforced concrete	—	2200	17.0×10^9	33×10^9	5×10^6	17×10^6

Table 1.3.2

Resistive Force for a Rigid Projectile Impacting at 1500 m/s (Area =.283 m^2)

Material	Yield Strength (MPa)	Force (MN)
Kevlar - 49	1380	344
Ship Armor	549	1388
Aluminum Alloy 7075-T6	500	703
Titanium Alloy 6Al-4V	827	668
Magnesium Alloy 13Li-6Al	200	524

Table 1.3.3

As can be seen from Table 1.3.3, Kevlar-49 is an excellent material for impacts. A resistive force of 344 MN can be expected upon impact with a rigid body. The area of the projectile is .283 m^2, yielding an impact pressure of 1217 MPa, which is below the yield strength of Kevlar (1380 MPa). These maximum forces should not be attained in the funnel since the ice will be entering at an angle that is not normal to the surface. Also, it is expected that since ice is not a rigid body (yield stress .5MPa), it will yield before the Kevlar. Table 1.3.4 displays the material properties of Kevlar-49 that were used in the Recht equation.

Properties of Kevlar-49 [6]

Property	Kevlar 49 Aramid
Density Kg/m^3	1380
Tensile Strength 0° MPa	1380
Compressive Strength 0° MPa	276
Tensile Strength 90° MPa	27.6
Compressive strength MPa	138
In-plane shear strength MPa	44.1
Inter laminar shear strength MPa	48.69
Poisson's ratio	.34
Tensile and compressive modulus 0° MPa	75800
Tensile and compressive modulus 90° MPa	5500
In-plane shear modulus MPa	2070
Bulk Modulus MPa	78958

Table 1.3.4

1.3.6 Determining the Thickness of the Funnel and Kevlar Plate via Recht's Penetration Equations

Recht et. al. had also computed equations of penetration using a rigid body. From equation (1.3.5), the penetration displacement x is a function of V, since the Recht equation is transcendental and cannot be resolved in terms of the independent variable.

$$\int_0^x \frac{A_x}{A_p}dx = x = \frac{2\cdot\left(\frac{M}{2A_p}\right)}{C_n b}\left[(V_o - V) - \frac{a}{b}\ln\left(\frac{a+bV_o}{a+bV}\right)\right] \qquad (1.3.5)$$

where Ax=Ap, if the penetrator is completely immersed in the medium. M is the mass of penetrator (72 kg), Vo is the initial velocity (1500 m/s), V is the final velocity, $a=2\cdot\tau_s \ln(2\cdot Z_m)(1+{}^{f}/_{\tan\alpha})$, and $b = C_v\sqrt{K\rho}(1+{}^{f}/_{\tan\alpha})\sin\alpha$.

If the final velocity is set to zero, the largest depth of penetration for Kevlar-49 is 0.4 meters. Table 1.3.5 shows the various stopping distances required for several materials.

Penetration Depth for a Rigid Blunt Body at 1500 m/s

Material	Penetration Distance (meters)
Kevlar - 49	.40
Ship Armor	.084
Aluminum Alloy 7075-T6	.16
Titanium Alloy 6Al-4V	.10
Magnesium Alloy 13Li-6Al	.29

Table 1.3.5

1.3.7 Calculating the Funnel Dimensions and the Trap Door Speed

Given the ricochet angle of 5°, mandating that the entrance be at least 10 times the area of the projectile, and requiring the exit of the funnel to have an area 1.5 times larger than the projectile allows for the calculation of the funnel geometry. Figure 1.3.3 portrays the funnel's side view. Using similar triangles, the length of the triangle for a desired cone angle can be calculated as can be seen from equation (1.3.6).

Sizing the Half Funnel

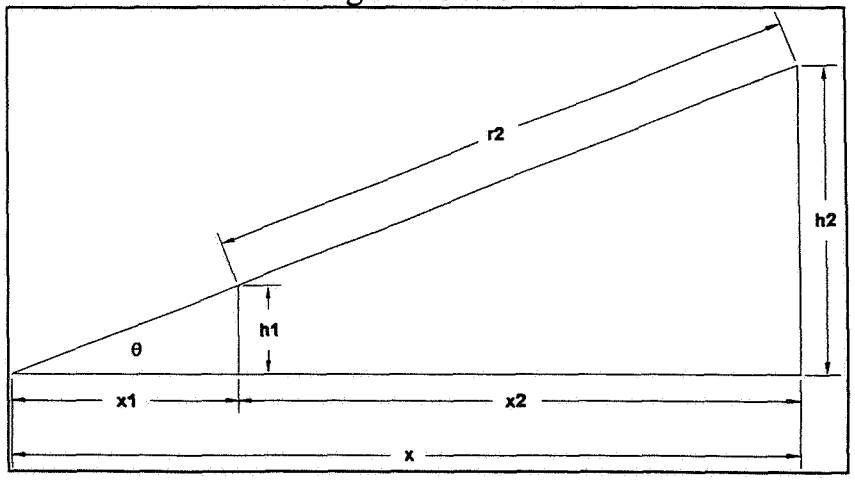

Figure 1.3.3

$$r_2 = \sqrt{\frac{1}{\tan^2 \theta} + 1} \cdot (h_2 - h_1) \qquad (1.3.6)$$

Where Θ=5°, h2=1m (half angle, half height), and h1=.32m, r2 or the length of the funnel calculates to be 9.6 meters, with a 40 centimeter thickness.

The time required to close the trap door was calculated using the assumption that the impact would occur within the chamber and not on the funnel. In addition, the impact would cause vapors of ice to exit the funnel at the same speed it had entered with (approximately 1500 m/s). Hence the time required to close the entrance is approximately .01 seconds.

1.3.8 Design of the Inner Chamber

Several methods can be used to slow the ice in the inner chamber. An easy method would be to use several hundred massive, yet loosely hung chains located within the chamber. These chains would absorb the kinetic energy of the projectile over a large distance. Unfortunately, the lack of experiments with high velocity chain impacts, as well as the complexity involved in studying the dynamics of a chain has led to a simplified solution to the energy absorbed. It is assumed that the impact will be less than the value computed by the Recht equation, since there is now a horizontal degree of freedom. This leads to the conclusion that a material for the chain is available (i.e. Armor MIL-12560).

If the assumption is made that the ice will strike the chain as in Figure 1.3.4 and will depart as shown in Figure 1.3.6, equation (1.3.7) can be formulated.

Ice Impacting a Chain

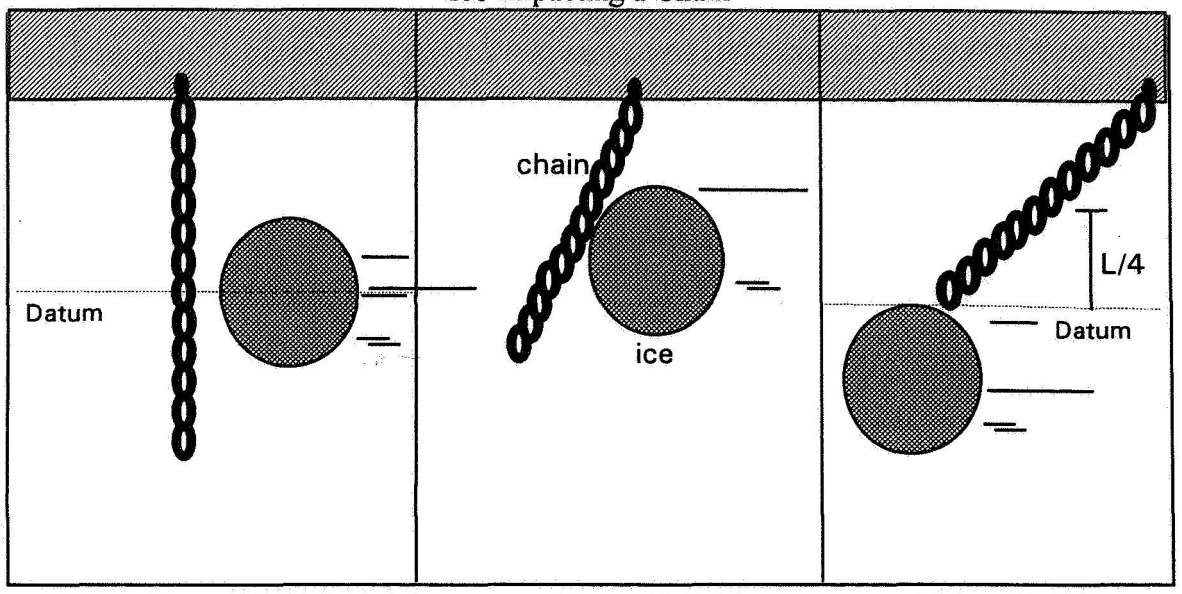

Figure (1.3.4) Figure (1.3.5) Figure (1.3.6)

$$\frac{1}{2}m_i v_{i_1}^2 = m_c gh + \frac{1}{2}m_c v_{c_2}^2 + \frac{1}{2}m_i v_{i_2}^2 \qquad (1.3.7)$$

Where the chain and ice will be moving at the same velocity ($v_{c_2} = v_{i_2}$) and the chain must reach a height of L/4 before it can "get out of the way" of the ice. Rearranging the expression yields the following equation:

$$v_{i_2} = \sqrt{\frac{\frac{1}{2}m_i v_{i_1}^2 - m_c gh}{\frac{1}{2}(m_c + m_i)}} \qquad (1.3.8)$$

Substituting $v_{i_1} = 1500\ m/s$, $\mathrm{m_i} = 80kg, m_c = 6kg, h = \frac{L}{4} = \frac{3\ \mathrm{m}}{4}$, and $g = 1.6\ \frac{\mathrm{m}}{\mathrm{s}^2}$, yields a speed of 1341 m/s after the impact. After impacting with about 10 rows of chains, the velocity should reduce to about a fourth of the initial velocity. The mass of the chain was derived from the fact that the length of the chain is 3 meters, the radius of each link (out of 118 links) is 2.54 cm and the density of the material is 7830 kg/m^3.

Even though the ice should be completely broken up, the total mass is assumed to still be moving in the same direction, where it will impact with a Kevlar plate mounted on a spring-damper. If the ice particles and the Kevlar plate are assumed to be a combined mass, the standard equation for a spring-damper system can be used.

$$m\ddot{x} + c\dot{x} + kx = 0 \qquad (1.3.9)$$

where the initial conditions are x(0)=0, and $\dot{x}(0) = 375\ m/s$. Using the Maple script in Appendix B, a stiffness k of 6000 $\frac{\text{N}}{\text{m}}$, and a damper constant c of 4000 $\frac{N \cdot s}{m}$ will yield a maximum compression of 6 meters. Figures 1.3.9, 1.3.10, and 1.3.11 depict the distance, velocity, and force response.

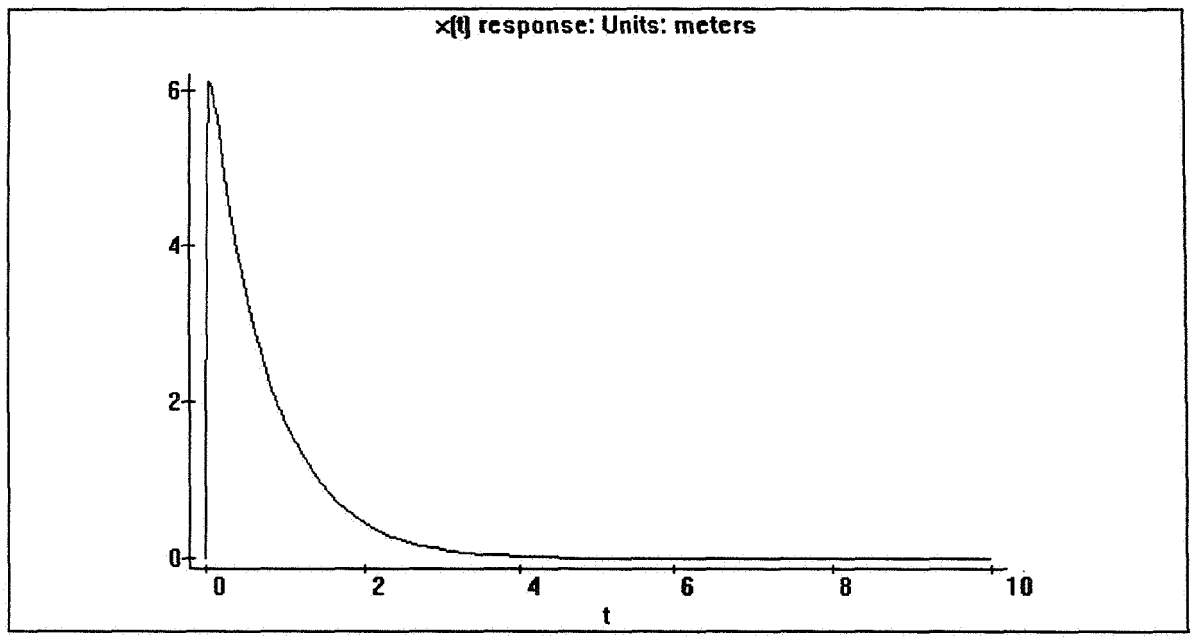

Figure 1.3.9

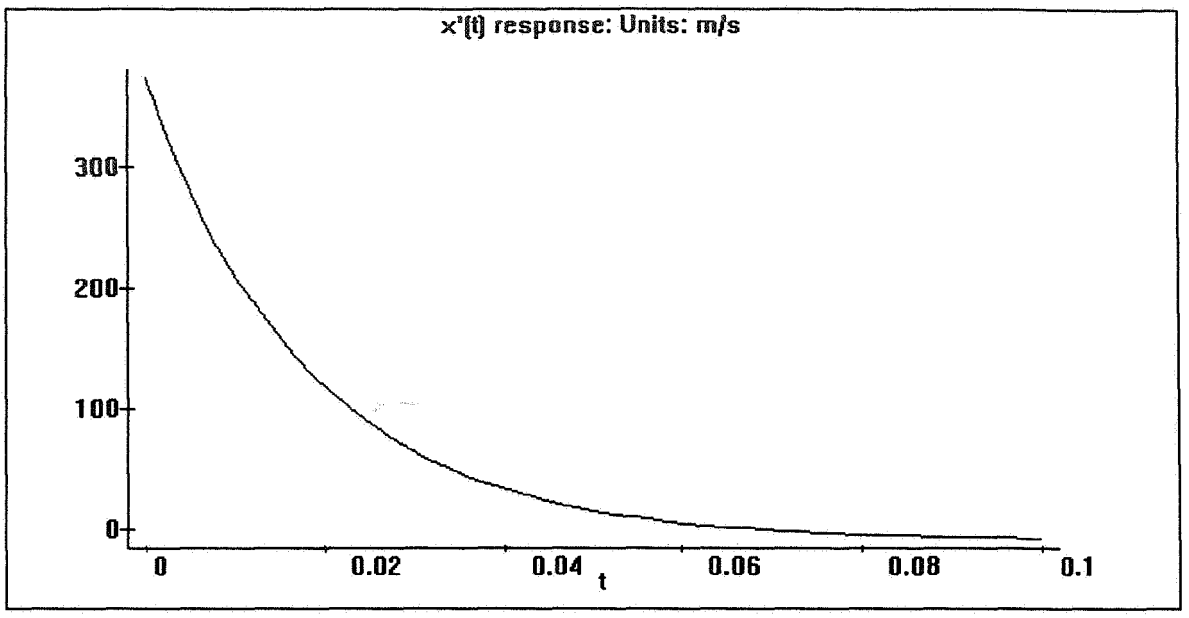

Figure 1.3.10

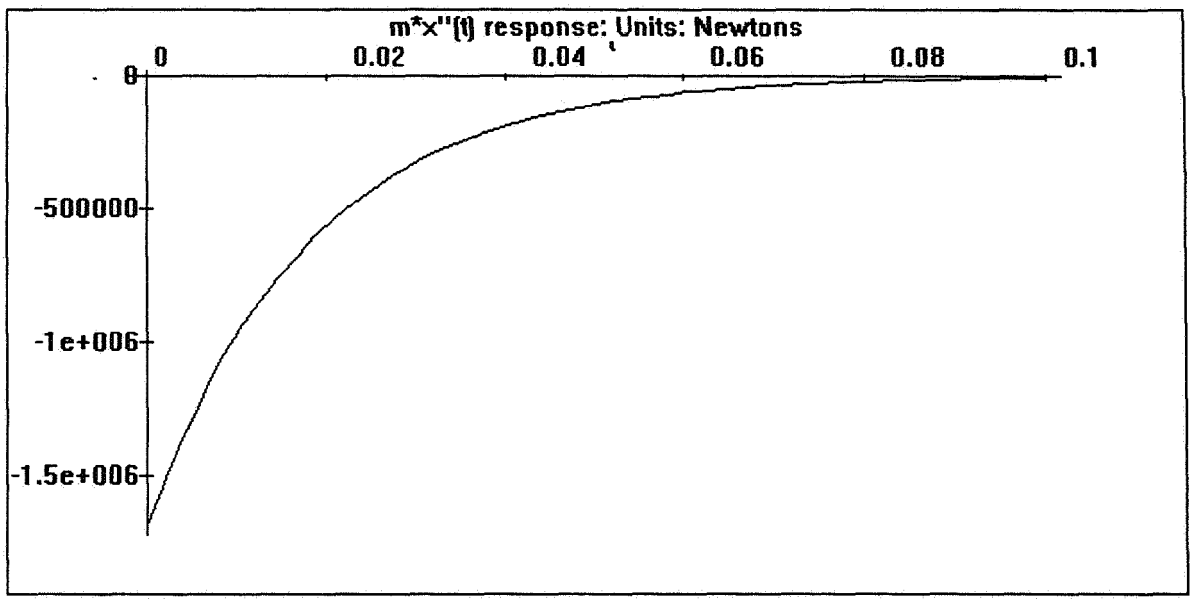

Figure 1.3.11

Another possibility for the lower chamber of the catcher is to have it filled with water or soil. Soil would be difficult to sift through for ice particles and water would entail the necessity of maintaining an environment such that during the opening of the funnel, the water would not freeze. Of course, if the upper layers of water did freeze, further structural tests would be needed to assure integrity of the catcher. There is information in regard to solid water impacts both in journals[7] and in firearm tests (since the human

body is composed of 95% water, the stopping distance of bullets is measured in inches of water).

1.3.9 Chamber Environment

In order to liquefy water, the pressure and temperature should be above its triple point which is 611 Pa (4.6 torr) and .01°C. In this instance, a pressure of 1333 Pa and a temperature of 3°C is selected. Using the ideal gas law ,

$$PV=nRT \tag{1.3.5}$$

the mass of ammonia is calculated to be 1.6 kg.

R is .08205 $\frac{\text{liter} \cdot \text{atm}}{^{\circ}\text{K} \cdot \text{mole}}$, V=170 m^3 (height=3 meters, length=6 meters), and T=276.15 °K.

References for Section 1.3

[1] Dr. Keith Keefer, University Of Cincinnati, Department of Material Engineering. Personal Correspondence.

[2] *The Kennedy Space Center Story*, Public Affairs Office, John F. Kennedy Space Center. NASA. Kennedy Space Center. Florida. 1974

[3] Johnson, W., A.K. Senguptan, and S.K. Ghosh. "High Velocity Oblique Impact and Ricochet Mainly on Long Rod Projectiles: An Overview.", *International Journal of Mechanical Science*. pp. 425-436. 1982a.

[4] Tate, A. "A Simple Estimate of the Minimum Target Obliquity Required for the Ricochet of a High Speed Long Rod Projectile." *J. Phys. D: Appl. Phys.* pp 1825-1829.

[5] Zukas, Jonas. *High Velocity Impact Dynamics*. Computational Mechanics Associates. A Wiley-Interscience Publication. John Wiley & Sons, Inc. New York, NY. 1990.

[6] Cheremisinoff. *Handbook of Polymer Science & Technology.* Vol 2. Marcel Dekker, Inc. New York, NY. 1989.

[7] Bivin, Yu. "Oblique Impact of a solid against soil or water." *Mechanics of Solids.* V24. N6. 1989. pp193-197.

[8] Heppenheimer, T.A. *Achromatic Trajectories and the Industrial Scale Transport of Lunar Resources*. Center for Space Science. Fountain Valley, CA. 1985.

[9] Bolson, P.S. ed. *Structures Under Shock and Impact,* Elsevier Science Publishers, 1989.

[10] Engel, Peter. *Impact Wear Of Materials*, Elsevier Science Publishers, 1976.

[11] Heppenheimer, T.A. "A Mass-Catcher for Large-Scale Lunar Material Transport", *Journal of Spacecraft and Rocket*s, Vol. 15, July-August 1978.

References for Section 1.3 Continued.

[12] Cointe, R. "Two-Dimensional Water-Solid Impact", *Journal of Offshore Mechanics and Arctic Engineering*, Vol. 111 pp 109-14, May 1989

[13] Frederking, R. "Ice Impact Force Measurements on a Vertically Faced Bridge Pier", *Journal of Offshore Mechanics and Artic Engineering*, Vol. 114. pp 63-5. February 1992.

[14] Xian, X. "An experimental evaluation of the tensile strength of impact ice". *Journal of Materials Science Letters*, Vol 8, pp1205-08, 1989.

[15] Chu, M.C. "Adhesive Shear Strength of Impact Ice", *AIAA Journal.*, Vol 29. No. 11. November 1991.

[16] Bogorodskii, ed. The Physics of Ice, Jerusalem, Israel Program for Scientific Translations. 1968.

Human Transportation

2.0 Discussion

The launching of scientific payloads and their propulsion systems from the lunar surface differs considerably from its counterpart on Earth. In order to provide stability for spin-stabilized payloads, especially during the thrust stage(s), the preferred shape is a large diameter-to-length ratio. This launching of rockets or orbiting vehicles from the Moon's surface is so different from the launching of such vehicles from the Earth for the following two reasons: (1) there is no atmosphere to produce aerodynamic forces on the vehicle, (2) the surface gravity is low - the acceleration due to gravity at the Moon's surface is approximately 1.58 m/s^2.

These environmental factors impose several significant consequences on the design of the vehicle and payload(s):

(1) The mass of the total system is lowered. Much of the standard equipment found on Earth-launched vehicles can be eliminated when designing a lunar-launched vehicle (e.g., a nose cone to protect the payload from aerodynamic forces, and its subsequent ejection system). One of the most important design factors taken into account by the Aerospace - LTV Design Subgroup was the minimization of the LTV's overall mass.

(2) The absence of aerodynamic forces means that the diameter of the payload, and the vehicle itself, can be made as large as desired. A large diameter would result in a simplified mechanical design and ease of assembly of the vehicle. For example, the added space resulting from the larger diameter would make layout and cabling much easier. Also, the greater accessibility would relieve troubleshooting efforts and ease replacement of fuel tanks and cargo elements.

The large diameter has one other crucial advantage in that the moment of inertia about the thrust axis of the vehicle could be made much larger than the moment of inertia about axes perpendicular to the thrust axis of the vehicle. Thus, simple spin-stabilized vehicles would satisfy the requirement for "flywheel stability". This situation is highly desirable since there is less tendency for large-angle precession of the thrust axis of the vehicle about the direction of flight.

(3) The low gravitational force on the lunar surface greatly reduces the total impulse requirement in order to acquire a given peak altitude or to attain low altitude orbital speed. In our case of a chemically-powered vehicle with rocket motors, this means that the mass of the motor plus fuel is significantly reduced compared to the terrestrial situation. A further reduction in mass follows from the absence of atmospheric drag. Because there is no need to

keep the cross-sectional area of the vehicle as small as possible, certain components can be constructed so as to maximize their volume.

All of these key characteristics were taken into account during the design of the LTV. However other factors, such as taking advantage of existing technology and ease in manufacturing, also played important roles in the design process. The Aerospace - LTV Design Subgroup tried to incorporate these differing design aspects in proposing the finest, most feasible Lunar Transportation Vehicle.

2.1 Mission Description

The main purpose of the LTV is to provide a method of personnel and/or equipment and supply transportation between the mining site and the Lunar Research Center. This mission will be accomplished via the "round trip" method. For example, the LTV would take off at the LRC, deliver its personnel and payload to the mining site, and return to the LRC without refueling (approximately 3000 mi. (4800 km)). Also, the LTV could be used for certain exploratory missions, providing they are within the specified range of 1500 mi. (2400 km).

2.2 Systems and Subsystems

In order to accomplish the mission requirement, certain systems and subsystems were implemented into the LTV's design.

2.2.1 Propulsion System

All maneuvers in the regime of space flight are propulsive in nature. Because the LTV will be traveling at high velocities, the propulsion systems must be able to produce large velocity changes. Therefore, a considerable portion of the initial vehicle weight must be invested in propellants. This large propellant supply can be broken down into the required amount for mission completion and reserve propellant to allow for unpredictable out-of-tolerance operation of the propulsion system and errors in navigation.

The propulsion system chosen for the LTV will use four (4) Pratt & Whitney RL10A-3-3A liquid oxygen/liquid hydrogen (LOx/LH_2) derivative engines. The RL10A LOx/LH_2 derivatives have a high I_{sp} and seem to be readily adaptable to meet the stated mission requirements. This engine family offers several other advantages over the others considered, most notably the extensive flight experience and reliability testing during its 34 years of use on the Atlas/Centaur launch vehicle, as well as the continuing research being conducted at Pratt & Whitney to improve the design of the RL10A and its descendants. Table 2.2.1 below presents some key specifications of the RL10A-3-3A engine.

RL10A-3-3A Specifications

Thrust vac. klbf (kN)	16.5 (73.4)
Propellants	LOx/LH_2
I_{sp}, vac(sec)	444
Max Throttle Ratio	5:1
Mixture Ratio	6:1
Expansion Ratio	61:1
PC, psia (MPa)	465 (3.21)
Total System Mass, lb (kg), (4)	556 (1226.1)
Exit Dia., in (cm)	40 (102)
Length, in (cm)	70 (178)
Gimbal Angle (deg)	±6°
Thrust to Weight	5.41

Table 2.2.1

2.2.2 Structural Elements

There were several guidelines which governed the structural design of the LTV. First the vehicle was designed for a maximum deceleration during descent of 5g's and touchdown velocities not to exceed 10 m/s. A worst-case landing load for the structural design was chosen to be a loaded, fully-fueled LTV (i.e., if the LTV had to land immediately after initial take-off). In addition, worst-case lunar surface conditions were assumed to be an effective slope of 10°, and a common safety factor of 1.4 for all structural components was incorporated into the design.

After discussions with the Materials Science and Engineering Group, Martin Marietta's lightweight Weldalite-049 Al-Li alloy was chosen as the design material for the structural components of the LTV (the truss structure and landing gear). The Weldalite alloy was chosen primarily because of its low density (2.6 g/cm^3) and excellent mechanical properties at cryogenic temperatures. The truss structure was modeled on SDRC's engineering analysis software package, I-DEAS. Figure 2.2.1 displays a solid model of the LTV, and Figures 2.2.2 and 2.2.3 are finite element models. All members of the truss structure have a 0.5 cm thickness. The top and bottom substructure members have 7.75 cm outer diameters, while the middle substructure members have outer diameters of 3.88 cm.

After calculating the total amount of propellant needed for the completion of the mission, specific amounts of LOx and LH_2 were determined using an oxidizer-to-fuel ratio of

6:1. With these amounts and the densities of LOx and LH_2 (71 and 1140 kg/m^3, respectively), sizing of the two hydrogen tanks and oxygen tank was performed on I-DEAS, using an offset-cylindrical design.

Since the LTV will be reusable, the landing gear will have to be able to withstand many landings, some on uneven terrain. Therefore, they will have to be constructed with a hydraulic spring-damper system.

2.2.3 Attitude Control

The LTV will be equipped with four small groups of thrusters in order to control its attitude about three axes of rotation, and perform delicate translational maneuvers. It is desirable to place these thruster groups in such a way as to achieve redundancy in function as a method of improving reliability. Also, ascent translation will be performed primarily by using the thrusters to pitch the LTV and then firing the main engines. However, this would only occur in extreme cases due to the gimbal ability of the engines.

The thrusters have been designed to use cold hydrogen as a working fluid. Because of the minimal amount of maneuvering required and the need to use only lunar resources, this seemed to be the logical selection. Also, since the specific impulse is proportional to the square root of the chamber temperature divided be the molecular weight, a gas with a low molecular weight, such as hydrogen, is desirable.

In determining the performance values of the thrusters the following assumptions were made: 1) The main engines will gimbal to provide for the larger adjustments during ascent. However, the thrusters may be needed for translating a maximum distance of 20 meters, for lateral maneuvering, in the final 30 meters of descent. Since the descent rate is approximately 1.6 m/s (1.7 m/s for first ascent, 1.5 m/s for second ascent) 2) The performance calculations were done using the initial take-off mass in the event of an aborted launch. 3) The hydrogen will be delivered into the thrusters at 100 K from a high pressure feed tank. Given these assumptions, the LTV's maximum horizontal velocity, due to these thrusters, is approximately 1.07 m/s (20 m/18.75 sec) for the initial take-off mass of 45,000 kg fully fueled.

The landing of the LTV at the pole was judged most demanding on its rotational motion for two reasons: (1) landing requires more complicated angular maneuverability than launching, and (2) thrusters that meet the requirements of higher mass moments of inertia (at the pole landing) will certainly meet those of a lower mass (at the equatorial landing).

A mass approximation was made, accounting only for the LTV's fuel and location. A simple computer model was then constructed and an inertia matrix calculated for landing, yielding $I_{xx} = I_{zz} = 380{,}300$ kg·m^2, and $I_{yy} = 716{,}000$ kg·m^2. These results are relative to a

principal, body-fixed coordinate system with the y-axis along the thrust vector and the origin at the center of mass.

Initially the thrusters are required to produce angular rates about each axis of 10 degrees/s^2 (0.1745 rad/s^2). Using a 9.5 kN thrust value, the moments needed to produce this motion are:

$$M_{xx} = M_{zz} = 66{,}400 \text{ N·m}$$
$$M_{yy} = 125{,}000 \text{ N·m}.$$

The resulting moment arm is 7.0 meters from the center of mass to obtain the rotational acceleration. However, the rotational acceleration about the Y axis is 5.32 degrees/s^2 (.0929 rad/s^2). The thrust and/or moment arm requirements needed to obtain the initial rates prove to be to large.

The I_{sp} calculation is as follows:

$$I_{sp} = \frac{v_{exit}}{g_0}, \tag{2.2.1}$$

where,

$$vexit = \sqrt{\frac{2\gamma R' T_C}{(\gamma-1)\cdot MW}\left[1-\left(\frac{P_{exit}}{Pc}\right)^{\frac{(\gamma-1)}{\gamma}}\right]}. \tag{2.2.2}$$

This equation simplifies drastically because p_{exit} is essentially zero is space, resulting in the maximum value for I_{sp}. The exit velocity was found to be 1705.9 m/s and this yields a maximum I_{sp} of 174.1 seconds.

Now that the I_{sp} is known, the mass flow rate can be calculated via the momentum equation,

$$\dot{m} = \frac{F}{I_{sp} \cdot g} \tag{2.2.3}$$

and in turn the required propellant mass can be determined. This was calculated to be 5.6 kg/s.

To produce the change in velocity, described by equation 2.2.3, a 5 second firing time will be required in order to translate the 20 meters for the fully-loaded LTV (as in an emergency scenario). This firing time is actually doubled to account for braking which occurs at the end of the maneuver. Allowing for approximately 30.0 seconds of thrusting for all maneuvers over the total mission equates to 168.0 kg of pressurized hydrogen. The tank needed will be approximately 2.4 m^3 in size.

2.2.4 Guidance and Navigation

The guidance and navigation (G&N) system for the Lunar Transportation Vehicle will allow for fully autonomous landing at a predetermined site with an accuracy of ±100 m. It is assumed that landing sites at both the mining facility and the Lunar Research Center have been selected, cleared, and leveled, and that there is a navigation beacon at each of the sites to assist in landing guidance. In addition, the G&N system is responsible for correcting navigational errors and providing 3-axis attitude control commands to the attitude control system.

The Guidance and Navigation system for the LTV includes a Hexad inertial navigation system (INS) with internal ring laser gyroscopes, inertial measurement units (IMU's), and accelerometers. This system provides internal redundancy by replacing multiple IMU's, gyros, and accelerometers with a single unit. However, the Hexad INS is a relatively new product and has not been space-rated at this time. It is recommended that continued studies be conducted on this product to insure its performance and reliability.

The LTV will also be equipped with several video cameras, recorders, and landing radar to provide continuous range and range rate data between the LTV and the and lunar surface. The video cameras will transmit real-time landing data to the LRC or the mining site, and could record a mission and landing during the proposed exploratory missions.

All output from the LTV's Guidance and Navigation system can be either displayed on the crew person pod control panel or on each astronaut's heads-up display incorporated into their space suit helmets. Table 2.2.2 is the Lunar Transportation Vehicle's G&N Equipment List.

LTV Guidance and Navigation Equipment List[8]

Component	*Power (W)*	*Mass (kg)*	*Mass (lb)*
Hexad INS (1)	100	22.7	50.0
Landing Radar (1)	10	7.0	15.4
Video Cameras & Recorders (4)	40	28.0	61.8
Control Electronics (1)	100	50.0	110.3
Total	**250**	**107.7**	**237.5**

Table 2.2.2

2.2.5 Communications & Data

The communications system on the LTV is one of the most important systems because it is the link between the LTV and the Lunar Research Center. The system will provide for acquisition and transmission of engineering data at a rate of 200 Kbps[8]. Again internal redundancy has been used as the baseline for all mission critical components.

The communication links will use S-band frequency to provide commonalty with similar communication situations and systems on Earth. However, Ka-band capability and compatibility with the Deep Space Network (DSN) should be implemented to provide commonalty with future manned Mars missions. The LTV will also require a low S-band antenna and transponder to be used in the acquisition and transmission of lunar tracking data.

As mentioned previously, the LTV will have a video camera and recorder system, which will relay images during landing, images of the chosen landing site (during exploratory missions), and provide visual confirmation of problems that develop during any phase of the mission.

2.2.6 Electrical Power Supply

In order to provide adequate electrical power to the Lunar Transportation Vehicle, several energy sources were considered. These were: chemical batteries, solar cells, fuel cells, chemically-powered heat engines, nuclear-powered heat engines, and thermoelectric and thermoionic converters. The electrical power system (EPS) must provide continuous operational power to the LTV throughout the mission.

Fuel cells with small start-up batteries were chosen as the electrical power supply system for the LTV. This choice was made based on the existing technology of the electrical

power systems on various orbiting satellites, and on the technology of the electrical power systems to be implemented on Space Station Freedom.

Power requirements for the LTV's various systems are listed in the following table:

LTV Power Requirements

System	Power (W)
Guidance & Navigation	250
Communications	530
Thermal Control	200
Cockpit/Cargo Manifest	300
Contingency	587
Total	**1867**

Table 2.2.3

Current projections indicate that about 1.4 kW of power will be required. However, since it is impossible to accurately account for all power requirements, a contingency was added, bringing the total power requirement to 2 kW. This contingency will account for such things as unpredictable additional power needed for other systems, as well as future changes in the design of the LTV. As another contingency factor, the EPS was designed to handle the maximum power expected for the mission (i.e., all systems functioning at full power.)

The fuel cell system consists of H_2 and O_2 preheaters, condenser, pump, cooling system, and water accumulator. The total system weighs approximately 91 kg (200 lb) and consumes 0.41 kg/kWh of fuel (H_2 and O_2). Allowing for pre/post launch powering, the total mission time is approximately 2.0 hrs. at 2kW results in a 4.0 kWh requirement. The fuel cell will then consume only 1.64 kg of fuel during the mission.

2.3 Mass Breakdown and Thrust Determination

2.3.1 Mass Breakdown

Using a circular trajectory with a height of approximately ten kilometers, mass ratios and component masses had to be determined. Initially, only the velocity differences were known from referenced historical data. Also, since 4 RL-10's were being used with an oxidizer-to-fuel ratio of six and an Isp of 444 seconds, the mass ratio could be computed using the following formula:

$$\Delta v = g I_{sp} \ln\left(\frac{m_o}{m_o - m_p}\right)$$

where, g is 9.8 m/s^2, m_O = initial mass (dry mass and propellant mass), m_p is the propellant mass, and I_{sp} is the specific impulse.

$$m_{fuel} = \frac{1}{1+\frac{O}{F}} \times m_p$$

$$m_{oxidizer} = \frac{\frac{O}{F}}{1+\frac{O}{F}} \times m_p$$

where, O/F is the oxidizer-to-fuel ratio and m_p is the propellant mass.

The next step was to determine the extra propellant needed. Sixty seconds of hovering time as well as the residual fuel had to be accounted for. This extra propellant was also determined as a percentage of the dry mass. The hover propellant was determined by finding the mass flow rate of descent and simply multiplying by sixty seconds. These results are tabulated below.

Mass Ratios

$m_O/(m_O-m_p)$	m_O/m_p	m_p/m_d	m_{fuel}/m_d	m_{oxid}/m_d	m_{pxtra}/m_d
5.58	1.22	4.58	0.65	3.93	0.25

Table 2.3.1

where, m_o is the initial gross mass (fully fueled vehicle at take-off), m_p is the propellant mass, m_d is the dry mass (unfueled vehicle), m_{fuel} is mass of the hydrogen used, m_{oxid} is the mass of the oxygen used, and m_{pxtra} is the extra propellant carried for hovering and residual.

After these ratios were determined, the structural components of the masses were also proportioned as a percentage of the dry weight. Using standard approximations from reference books and NASA designs, the mass ratios of the dry mass components were determined. For example, the landing gear was determined to be three percent of the initial weight of the vehicle. The payload was chosen to equal the mass of four 200 pound astronauts plus life support (200 pounds per astronaut), and a one thousand pound cargo. Thus, the payload mass was 1180 kilograms. The fuel and oxidizer tanks were approximated as three percent of the propellant mass.

Systems' percentage was found to be approximately fifteen due to the masses of the various components. The systems' mass includes fuel cells, guidance and navigation systems, radar as well as attitude controls (thrusters and propellant). The systems' mass total is 1176 kg which may seem high. As the design progressed, various components were researched in depth, and 700 kg (nine percent of the dry mass) may actually be closer to the actual systems' mass. However, due to the dependence of the vehicle's mass on all aspects of the report, trajectory and thrust determination, structural design, etc. the original value of 1176 kg was maintained. If this vehicle design was permitted to continue, mass reductions of all items could thus be incorporated. This is due to the strong dependence of all components on the dry mass. Since the systems' mass may be a bit conservative, all miscellaneous items could be placed under this category as well, such as extra life support, cargo, or propellant.

One important observation to make at this point is that the mass for the LTV and all components has been approximated. However, component masses were researched in depth, and these values are very close to actuality. An interesting note is that the used propellant mass (35,925 kg) approximated using the method described in this section, was remarkably accurate when compared with the used propellant mass (35,930 kg) determined in the next section, 2.3.2, which was based upon trajectory determination. Table 2.3.2 summarizes the percentages of the dry weight for each major category. The term structure in the following table represents the mass of the four engines (1226 kg) as well as the truss and astronaut seating:

Dry Mass Percentages

	STRUCTURE	TANKS	PAYLOAD	LANDING GEAR	SYSTEMS
percentage of dry mass	39.00	14.21	15.04	16.75	15.00

Table 2.3.2

Using the discussed procedure, the final results of all masses involved were calculated and displayed in the table below:

Structure Breakdown

	STRUCTURE (kg)
ENGINES	1226
TRUSS	1880
TOTAL	3106

Table 2.3.3

Payload Breakdown

	PAYLOAD (kg)
PEOPLE	726
CARGO	454
TOTAL	1180

Table 2.3.4

Table of Results

ACTUAL MASSES		
	(kg)	(lbs)
Structure (Engines + Truss + Seating)	3,060	6,740
Tanks (Fuel and Oxidizer)	1,110	2,460
Landing Gear	1,310	2,900
Payload	1,180	2,600
Systems	1,176	2,600
Used propellant	36,000	79,200
Extra propellant	1,220	2,700
TOTAL	45,000	99,000
dry mass	7,840	17,300
propellant mass	37,200	81,900
Hydrogen Mass (fuel)	5,130	11,310
Oxygen Mass (oxidizer)	30,800	67,890
Extra Hydrogen (fuel)	175	390
Extra Oxygen (oxidizer)	1,050	2,300

Table 2.3.5

2.3.2 The Journey

In order to limit fuel consumption, the scheme chosen for transportation between the equator and pole involved three distinct phases: ascent to orbit, orbital coast, and descent to the surface. During the orbital coast, which covers a vast majority of the travel distance, no main engine firing is needed; minimal thruster firings are to correct for perturbations in the orbit. The energy for any orbit is given by the expression:

$$E = -\frac{\mu}{2a}$$

where μ is the gravitational parameter for the moon and equal to 4.903×10^{12} m^3/s, and a is the semi-major axis of the orbit. Clearly, the smaller a is made, the more negative and hence smaller the energy of the orbit becomes. As low orbital energy implies low energy needed to achieve that orbit from the lunar surface, a small semi-major axis was desirable. In order to avoid impacting lunar mountains, the minimum radius of the orbit had to be 10 km. The circular orbit has the characteristic that the semi-major axis may be 10 km and the radial constraint satisfied across the entire orbit; elliptical orbits must have a semi-major axis greater than this value in order to satisfy the constraint near the launching and landing locations. Thus, a 10 km, circular orbit was the lowest energy, satisfactory orbit for the mission and was therefore selected. Such a circular orbit has two kinematic requirements for its achievement, one on the radius and another on the velocity:

$$\begin{aligned} r &= a = 10 \text{ km} \\ v &= \sqrt{\frac{\mu}{r}} = 1675 \text{ m/s} \end{aligned} \qquad (2.3.1)$$

where v is the velocity of the orbiting rocket.

Both the mass breakdown and thrust parameters are intricately linked to the dynamic parameters of the two launches and two landings, so much so that after the selection of the former, the determination of the latter may imply a readjustment of those initial values of mass and thrust. The aforementioned dynamic parameters are limited to only thrust magnitude and direction, so the profiles of the launches and landings are largely deterministic. As seen through trial and error, the allowable variability of these quantities, given that the desired end conditions of the maneuvers were obtained, was small. Within these allowable ranges, then, values may be chosen for propellant use optimization. The effect, however, of changes in the

profile resulted in very small variations in propellant use. The most simple and feasible profiles were therefore selected.

In equation form, the physical laws governing both the launch and landing are Newton's Laws. These equations of motion are expressed most conveniently in a polar (r,θ) coordinate system centered at the lunar center:

$$\begin{aligned} \frac{T}{m}\sin\alpha - g &= \ddot{r} - r\dot{\theta}^2 \\ \frac{T}{m}\cos\alpha &= r\ddot{\theta} + 2\dot{r}\dot{\theta} \end{aligned} \qquad (2.3.2)$$

Here, the design parameters are T, the thrust, and α, the thrust direction (in radians from the horizontal). Other variables are m, the vehicle mass; r, the radius from the lunar center; θ, the angle (in radians) from the radius at the start of the maneuver, and g, the lunar gravitational acceleration, which in this model varies according to Newton's Law of Gravitation. Since g varies with the distance from the lunar center and the range of these radii is small compared to their magnitude, the variation of g is quite small. Each dot above the coordinates denotes its derivative with respect to time.

These equations also illuminate the assumptions used in the formulation of the model. First, the motion of the rocket is assumed to be two dimensional. Thus, perturbations from the orbital plane are neglected. Second, only the two body problem is considered; the effects of the earth, the sun, and all other heavenly bodies are ignored. Third, the moment equation involving the attitude of the rocket is ignored. This is equivalent to assuming that the chosen time history of the thrust direction α may be generated by suitable engine gimbaling and thruster firing, both of which result in the rotation of the rocket.

For the launches, the thrust magnitude was chosen to be "large," specifically one-half the earth weight of the vehicle at take-off (this is about 3.03 times the lunar weight). This thrust magnitude was maintained for the entire duration of the launches. The thrust direction, however, was specified by the following plan:

1. Vertical ascent: $\alpha = 90°$.
2. Instantaneous α shift.
3. Gravity turn
4. Orbital kick.

The vertical ascent was specified to last until the altitude reached 20 meters. In order to obtain the desired horizontal end condition on the velocity direction, a shift in α is needed. For simplicity, the initial shift was assumed to be instantaneous, shifting from 90° to about 51°

The gravity turn stage specified that the thrust direction was to follow the velocity direction. Thus, the initial α shift caused a change in the velocity direction to a value slightly less than 90°. Since the thrust direction is equal to the velocity direction, this change in velocity causes a reduction in thrust direction, which then causes a further reduction in the velocity direction. This interaction continues until the velocity becomes horizontal. The altitude attained at this point is a function of both the vertical ascent cutoff height and the magnitude of the instantaneous shift in thrust direction. The aforementioned values for these quantities did in fact result in the attainment of the orbital altitude at the conclusion of the gravity turn stage. Other values also created this condition, but a relationship was present: the lower the vertical ascent cutoff altitude, the lower the fuel consumption for the launch. 20 meters was chosen as a lower limit on this quantity to ensure that the craft did not turn so quickly that the lower landing gear would impact with the lunar surface.

Since the velocity of the rocket when the orbital altitude is achieved is much less than ($\cong$ 1/2 times) the orbital velocity, an "orbital kick" is needed at the completion of the gravity turn. This stage maintains the orbital velocity while adding the additional velocity needed to satisfy the orbital equations 2.3.1. This is accomplished by finding the thrust direction α such that the vertical acceleration, $\ddot{r}$, becomes zero in the equations of motion 2.3.2. Its necessity is illuminated by a comparison of the energies of the orbital altitude

$$mgh \cong 1.62 \times 10^4 \cdot m$$

and the orbital velocity

$$mv^2 / 2 \cong 1.40 \times 10^6 \cdot m.$$

Clearly, the energy required to attain the orbital velocity is much higher than the energy needed for the orbital altitude.

As an analytic solution of the equations of motion, given arbitrary T and α profiles, does not exist, a numerical model was created and solved using a digital computer. The finite difference formulas used for integration were the second and third order Runge-Kutta formulas, while the accuracy was chosen to be 5 significant digits. Results for the

Equatorial Launch

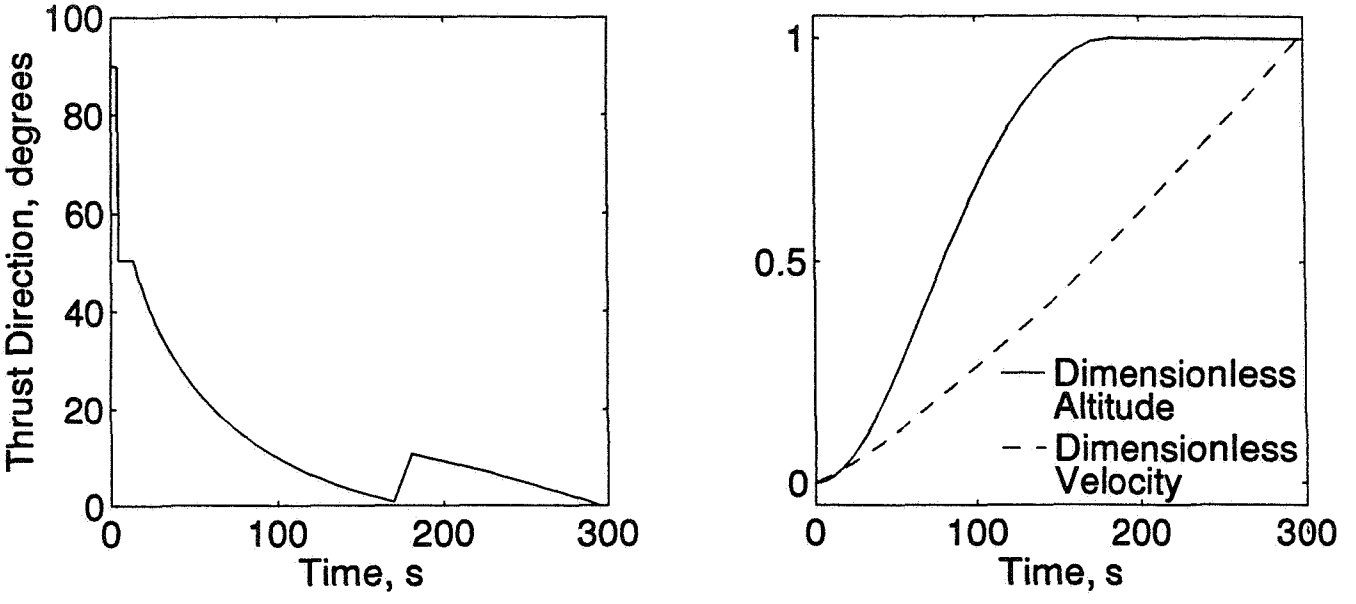

first (equatorial) launch are shown in figure 2.3.1. An inspection of the equations of motion reveals that the motion depends only on the *ratio* of thrust to mass, and therefore, an identical launch profile may be obtained for a lower take-off mass, provided that the thrust to mass ratio remains the same. This characteristic of the equations was utilized for the second launch (from the pole) and thus the plots shown in figure 2.3.1 also apply to this maneuver.

The scheme chosen for the two landings of the rocket was approximately the one used for the launches, but in reverse. Three stages were used:

1. Large, horizontal thrust.
2. Gravity turn.
3. Vertical descent.

As described in reference to the launch, the orbital velocity is much more difficult to extract than the orbital altitude, and hence the (constant) large, horizontal thrust was used to make a massive reduction in the velocity, while ignoring the need to reduce altitude. In the real scenario, this stage is quite simple since it lacks a need for kinematic measurements using sensors. The transfer to the gravity turn was specified at an arbitrary time about one quarter of the total time. The gravity turn, where the thrust direction was specified to be the same as the velocity direction, guaranteed that both the velocity direction and magnitude approached

zero simultaneously. It did not, however, specify at what altitude these quantities became zero; it was through an appropriate selection of the constant thrust magnitudes for the high thrust and gravity turn stages that the altitude at zero velocity was set. As this altitude was extremely sensitive to changes in the magnitudes of the thrusts, an "offset altitude" was desired to account for errors in thrust magnitude. Approximately 25 meters was chosen as an appropriate offset altitude from the lunar surface. The gravity turn was stopped short of its zero velocity point, leaving a small residual velocity in both the horizontal direction (< 1 m/s) and the vertical direction ($\cong 1.5$ m/s). The final stage, the vertical descent, is one where the thrust is set equal to the weight of the vehicle, and the craft slowly descends to the lunar surface. This thrust magnitude is slightly variable, since the weight of the craft decreases a small amount due to the discharge of propellant.

The results of numerical computations of the first (polar) landing are shown in figure 2.3.2. The results for the second (equatorial) landing are, as with the launches, identical. The propellant use and burn times for each of the four maneuvers are compiled in table 2.3.6. The mass of the vehicle at the final touchdown was 9070 kg, while the total propellant used for all four maneuvers was 35930 kg.

Polar Landing

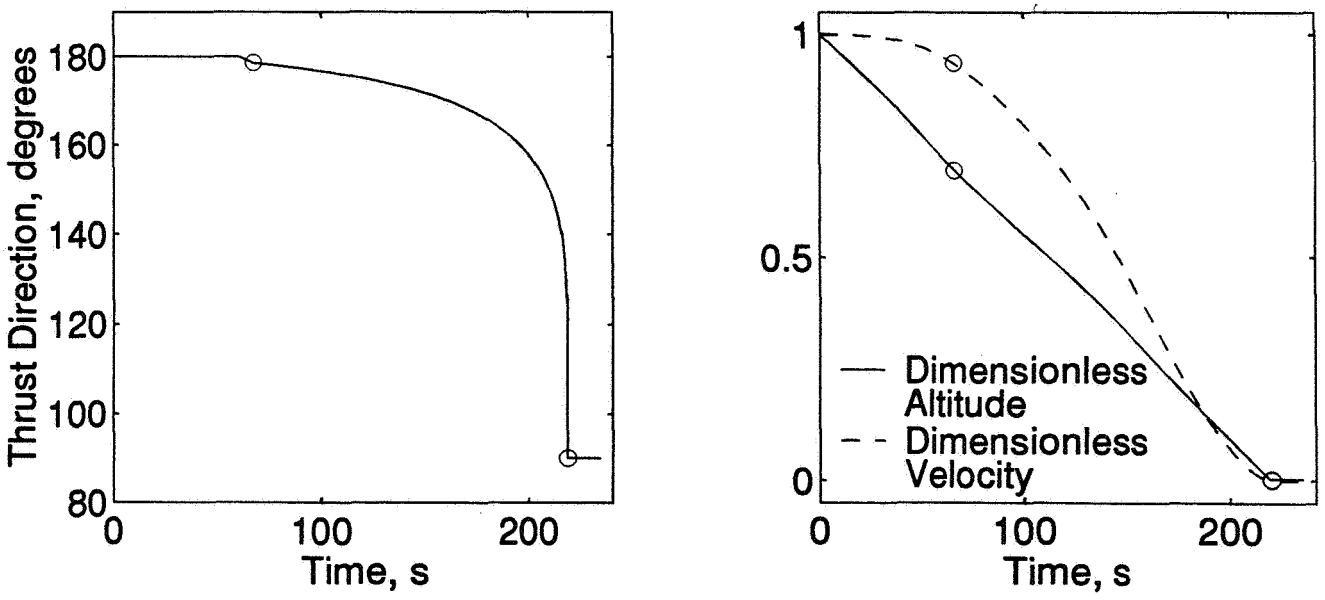

Results of the round trip between the lunar equator and pole.

	Equatorial Launch	Polar Landing	Polar Launch	Equatorial Landing
Initial mass, kg	45000	29980	20200	13460
Propellant used, kg	15020	9785	6740	4392
Burn time, s	297	234	297	234

Table 2.3.6.

2.3.3 Firing Schedule

Thrust values were calculated as discussed in the previous section. This portion of the design report specifies the firing schedule for the four main engines at the throttle capability of the engines.

As previously mentioned, four RL-10's will be used on this vehicle. However, these engines only have a maximum throttle ratio of five. To meet the thrust requirements of this design, the engine design must be slightly modified. The maximum thrust of one RL-10 engine is 73.4 kN. Thus, four engines creates a thrust of 293.6 kN. The required thrust initially for the vehicle is 220.725 kN. Using a safety factor of 1.1 the desired maximum thrust of four engines would be 240.7 kN, therefore, each engine will have a maximum thrust of 60.175 kN. Also, incorporating a maximum throttle ratio of ten, which was also used in the lunar module, all thrust specifications can be met. The "down-rating" of this engine was necessary because hovering on the second landing would be impossible without these new requirements. Also, this action prolongs engine life by reducing the maximum thrust required. Thus, by slightly lowering the maximum thrust of the engines and increasing the throttle ratio to ten, all thrust requirements are satisfied.

Table 2.3.7 summarizes the firing schedule. Note that the number of engines required and the throttle ratio are specified.

Firing Schedule Summary

Scenario	Thrust Requirement (kN)	Number of Engines Employed	Throttle Ratio (T_{max} / $T_{required}$)
Launch #1	220.725	4	1.10
Landing #1 / Stage 1	220.725	4	1.10
Landing #1 / Stage 2	183.708	4	1.31
Landing #1 / Stage 3	32.724	2	3.68
Launch #2	99.081	4	2.43
Landing #2 / Stage 1	99.124	4	2.43
Landing #2 / Stage 2	82.501	4	2.92
Landing #2 / Stage 3	14.661	2	8.20

Table 2.3.7

Stage 1 refers to the large, horizontal thrust required for the initial descent, Stage 2 refers to the gravity-turn portion of landing, and Stage 3 references the vertical descent at constant velocity. Also, for both launches there are in actuality two stages, the ascent to orbital altitude and the "orbital kick" to accelerate to orbital velocity. However, the thrust is constant for both launch stages.

References

1. Allen, Joseph P. Entering Space: An Astronaut's Odyssey, Stewart, Tabori, & Chang, New York, 1986.

2. Burgess, Eric. Assault on the Moon, Hodder and Staughton, LTD., London, 1966.

3. Kerrod, Robin. The Illustrated History of NASA, W. H. Smith, New York, 1988.

4. Lenorovitz, Jeffrey M., *G. D. Goal: Lower-Cost Manned Lunar Missions,* Aviation Week & Space Technology, January 18, 1993, pgs. 42-45.

5. LIFE in Space, Little, Brown, & Co., Boston, 1983.

6. Purser, Paul E., Faget, Maxime A., and Smith, Norman F., Manned Spacecraft: Engineering Design and Operation, Fairchild Publications, Inc., New York, 1964.

7. Sutton, George P., Rocket Propulsion Elements, John Wiley & Sons, Inc., New York, 1992.

8. Wiegmann, Bruce M., *"A Lunar Transportation System Design: The First Lunar Outpost,"* Presentation to UC Space System Design, October 21, 1992.

Appendix A

Method of Solution for the Non-dimensionalized DES Governing Equations and Code Listing

This appendix details some of the processes used to simplify the governing equations and reduce the amount of error in the code computation. It also includes the FORTRAN code used in solving the DES governing equations, including a fourth order accurate Runga-Kutta solver.

For completeness, the lossless DES railgun equations in non-dimensional form will be repeated. These equations are,

$$\lambda_i y_i'' + \Omega_i^2 y_i + \sigma_i \sum_{k=1}^{i} y_k'' - \lambda_{i+1} y_{i+1}'' - \rho_{i+1} y_{i+1}' - \Omega_{i+1}^2 y_{i+1} = 0 \qquad \text{(A.1)}$$

$$\lambda_N y_N'' + \Omega_N^2 y_N + \xi' \sum_{k=1}^{N} y_k' + (\xi - (N-1)\sigma) \sum_{k=1}^{N} y_k'' = 0 \qquad \text{(A.2)}$$

$$\xi'' = \left(\sum_{k=1}^{N} y_k' \right)^2 \qquad \text{(A.3)}$$

and,

$$\left[\sum_{k=1}^{N} y_k' \right]^2 \le \frac{P_m A S_1}{q_0 / 2C_1} \qquad \text{(A.4)}$$

where,

$$\lambda_i = \frac{2mL_i}{\ell^2 q_0^2}, \quad \sigma_i = \frac{2mS_i}{\ell q_0^2}, \quad \Omega_i^2 = \frac{C_1}{C_i}\sigma_i \qquad \text{(A.5)}$$

and,

$$\xi = \frac{2m}{\ell q_0^2} x, \quad y_i = \frac{q_i}{q_0}, \quad \tau = t \Big/ \sqrt{\ell C_1 S_1} \qquad \text{(A.6)}$$

are the non-dimensionalizing variables.

To solve the above equations using a fourth order accurate Runga-Kutta method requires the second derivatives, y'' and ξ'', as inputs. To solve for these variables, a full (n x n) matrix has to be inverted, where n ranges from 1 to the maximum number of stages. Because of the many algebraic processes required to invert such a matrix, there is a considerable amount of round off error which can result in incorrect or non-converging solutions. This problem is overcome by introducing the variables,

$$z = \sum_{i}^{n} y_i \quad , \quad z' = \sum_{i}^{n} y_i' \text{ and } z'' = \sum_{i}^{n} y_i'' \tag{A.7}$$

Substituting these variables into equations (A.1)-(A.3) produces the modified lossless DES railgun equations,

$$\lambda_i\left(z_i'' - z_{i-1}''\right) + \Omega_i^2\left(z_i - z_{i-1}\right) + \sigma_i z_i'' - \lambda_{i+1}\left(z_{i+1}'' - z_i''\right) - \Omega_{i+1}^2\left(z_{i+1} - z_i\right) = 0 \tag{A.1a}$$

$$\lambda_N\left(z_N'' - z_{N-1}''\right) + \Omega_N^2\left(z_N - z_{N-1}\right) + \xi' z' + \left(\xi - (N-1)\sigma\right) z_N'' = 0 \tag{A.2a}$$

$$\xi' = z_N'^2 \tag{A.3a}$$

From this substitution, the solution technique of the equations is greatly simplified. Where before a filled (n x n) matrix had to be inverted to construct the second derivative, y'' vector, now only a positive definite, symmetric, tri-diagonal matrix inversion is required where the variable y'' is replaced with z''. There is much less of an algebraic process so computational errors are reduced significantly.

The solution vector is then,

$$z'' = [Z'']^{-1} \cdot \left(-[Z']z' - [Z]z\right) \tag{A.8}$$

where the matrices are,

$$Z = \begin{bmatrix} \Omega_1^2 + \Omega_2^2 & -\Omega_2^2 & & & & & \\ -\Omega_2^2 & \Omega_2^2 + \Omega_3^2 & -\Omega_3^2 & & & & \\ & -\Omega_3^2 & \Omega_3^2 + \Omega_4^2 & -\Omega_4^2 & & & \\ & & \ddots & \ddots & \ddots & & \\ & & & -\Omega_{N-1}^2 & \Omega_{N-1}^2 + \Omega_N^2 & -\Omega_N^2 & \\ & & & & -\Omega_N^2 & -\Omega_N^2 & \end{bmatrix} \tag{A.9a}$$

$$Z' = \begin{bmatrix} \rho_1+\rho_2 & -\rho_2 & & & & & \\ -\rho_2 & \rho_2+\rho_3 & -\rho_3 & & & & \\ & -\rho_3 & \rho_3+\rho_4 & -\rho_4 & & & \\ & & \ddots & \ddots & \ddots & & \\ & & & -\rho_{N-1} & \rho_{N-1}+\rho_N & -\rho_N & \\ & & & & -\rho_N & \rho_N+\xi' \end{bmatrix} \qquad \text{(A.9b)}$$

$$Z'' = \begin{bmatrix} \lambda_1+\lambda_2+\sigma_1 & -\lambda_2 & & & & & \\ -\lambda_2 & \lambda_2+\lambda_3+\sigma_2 & -\lambda_3 & & & & \\ & -\lambda_3 & \lambda_3+\lambda_4+\sigma_3 & -\lambda_4 & & & \\ & & \ddots & \ddots & \ddots & & \\ & & & -\lambda_{N-1} & \lambda_{N-1}+\lambda_N+\sigma_{N-1} & -\lambda_N & \\ & & & & -\lambda_N & \lambda_N+\xi(N-1)\sigma \end{bmatrix} \qquad \text{(A.9c)}$$

where all blank spaces are considered filled with zeroes. As can be seen, all these matrices are tridiagonal and easy to invert with minimal computational error.

Following is the code listing which solves the modified, non-dimensional, simplified DES governing equations (A.1a)-(A.3a) using equation (A.8) as the second derivative vector input. It should be noted to the reader that the program is heavily commented and may be inefficient but was found to run under thirty seconds on a Sparc-2 Sun Workstation for a sixty stage railgun.

```
      program des
c
c     Program solves system of coupled linear ODE for the
c     distributed energy railgun with rail resistance
c
      parameter(nmx=1000)
c
      common/const/ sigma(nmx),zlambda(nmx),omega2(nmx),rho(nmx),g0(nmx)
      common/time/ t(nmx),delt
      common/stage/ nstage,stg,nstgmax
      common/condi/ yc(nmx),etac(nmx),xetac,zetac
c
c----------open files
c
      open(unit=8,file='desmat',status='unknown')
      open(unit=9,file='des.chk',status='unknown')
c
c----------initialize values
c
      call init(v0)
c
c----------set tolerance on zero current
c
      etol=0.0
c
c----------check for correct size of arrays
c
      if((2*nstgmax+2).gt.nmx) then
         write(*,*) '********* WARNING *********'
         write(*,*) 'Dimensions not big enough'
         write(*,*) '    Stopping Program'
         stop
      end if
c
      write(8,*) t(1),yc(1),-etac(1),zetac,xetac
c
c----------R-K 4th order approximation
c
      cmax=-100.0
      do 20 while(nstage.lt.nstgmax)
c
         call rk4
c
```

```
c----------store maximum summation current value to find beta
c
      if(abs(etac(nstage)).gt.cmax) cmax=abs(etac(nstage))
c
c----------increment to next stage if projectile past next stage
c
      if(zetac.gt.stg) then
         write(6,*) 'Done with stage ',nstage
c
c----------integrate exactly to end of stage
c
            a=zetal-stg
            b=zetac-stg
            tend=((tl-0.5*a/xetal)*b-(t(1)-0.5*b/xetac)*a)/(b-a)
            delt=abs(tend-tl)
            yc(nstage)=yl
            etac(nstage)=etal
            xetac=xetal
            zetac=zetal
            call rk4
c
c----------increment to next stage
c
            nstage=nstage+1
            stg=stg+sigma(nstage)
c
c----------set initial charge and current for each new stage
c--------------NOTE:  Values stored are summation of all values
c--------------------not actual values
c
            yc(nstage)=yc(nstage-1)+1.0/sqrt(float(nstage))
            etac(nstage)=etac(nstage-1)
c
c----------integrate up to next t(1) value
c
            delt=abs(t(1)-tend)
            call rk4
c
c----------re-initialize delt
c
            delt=0.01
         else
c
c----------store previous stage values for use if next stage
c--------------jumps past end of stage
```

```
c
            yl=yc(nstage)
            etal=etac(nstage)
            xetal=xetac
            zetal=zetac
            tl=t(1)
         end if
c
c----------write out values
c
         write(8,*) t(1),yc(nstage),-etac(nstage),zetac,xetac
c
c----------increment time
c
         t(1)=t(1)+delt
c
20    continue
c
c----------calculate effeciencies, etc.
c
      write(6,*) 'Done with stage ',nstgmax
      beta=cmax**2
      dv=(xetac**2-v0**2)/2.0
      sum1=0.0
      do 25 i=1,nstgmax
         sum1=sum1+omega2(i)*(1.0/sqrt(float(i)))**2
25    continue
      eff=dv/sum1
      synvel=sqrt(2.0*sigma(nstgmax))*cmax
      write(6,800) synvel,cmax,beta,eff,seff
c
c----------integrate until current goes to 0.0
c
      write(6,*)
      write(6,*) 'Integrating to current zero tolerance'
      do 30 while(-etac(nstage).gt.etol)
         call rk4
         write(8,*) t(1),yc(nstage),-etac(nstage),zetac,xetac
         t(1)=t(1)+delt
30    continue
c
      stop
c
c----------format statements
c
```

```
800   format(/1x,'Synchronus Velocity:                ',f8.5,
     .       /1x,'Projectile Current:                 ',f8.5,
     .       /1x,'Beta:                               ',f8.5,
     .       /1x,'Overall electrical efficiency:      ',f8.5,
     .       /1x,'Mean Space Utilization efficiency:  ',f8.5)
      end
c
      subroutine init
c-------------------------------------------------------------
c     Called by Main program:
c          Initialize sigma, lambda, omega2, rho, and g0
c          for each stage.  Usually same value except for
c          optimizing stages for better efficiencies
c-------------------------------------------------------------
c
      parameter(nmx=1000)
c
      common/const/ sigma(nmx),zlambda(nmx),omega2(nmx),rho(nmx),g0(nmx)
      common/time/ t(nmx),delt
      common/stage/ nstage,stg,nstgmax
      common/condi/ yc(nmx),etac(nmx),xetac,zetac
c
c----------set number of stages
c
      nstgmax=10
c
c----------specify initial constants
c
      sig0=1.80
      zlam0=2.0
      rho0=0.0
      g00=0.00
c
c----------fill sigma, lambda, omega2, rho, and g0 arrays
c
      do 10 i=1,nstgmax
         sigma(i)=sig0
         zlambda(i)=zlam0
         rho(i)=rho0
         g0(i)=g00*float(i)**0.25
         omega2(i)=float(i)*sigma(i)
10    continue
c
c----------fill arrays with initial conditions
c
```

```
c
      v0=0.0
      yc(1)=1.00
      etac(1)=0.0
      xetac=v0
      zetac=0.0
c
      t(1)=0.0
      delt=0.01
      stg=sigma(1)
      nstage=1
c
c----------redefine initial conditions for stages to
c--------------optimize railgun
c
c     zlambda(1)=11.0
c
      return
      end
c
      subroutine array(y,eta,zeta,xeta,r)
c-----------------------------------------------------------------
c     Called by subroutine RK4 to:
c          Compute -Z'z'-Zz solution vector, store it
c          in vector B and then invert the tridiagonal Z" array and
c          store solution in D array.  Solution in D array is then
c          moved to corresponding position in R array for use by
c          subroutine RK4
c
c     SEE NOTES FOR MORE DETAILED EXPLAINATION
c
c-----------------------------------------------------------------
c
      parameter(nmx=1000)
c
      common/const/ sigma(nmx),zlambda(nmx),omega2(nmx),rho(nmx),g0(nmx)
      common/time/ t(nmx),delt
      common/stage/ nstage,stg,nstgmax
      dimension eta(nmx),y(nmx),r(nmx),a(nmx),b(nmx),c(nmx),d(nmx)
c
c---------------r(1-->nstage)==========>etadot
c---------------r(nstage+1-->2*nstage)=>ydot
c---------------r(2*nstage+1)==========>xetadot
c---------------r(2*nstage+2)==========>zetadot
c
```

```
      if(nstage.eq.1) then
         d(1)=-(rho(1)+xeta+g0(1)*zeta)*eta(1)-omega2(1)*y(1)
         b(1)=zlambda(1)+zeta
      else
         d(1)=-(rho(1)+g0(1))*eta(1)-rho(2)*(eta(1)-eta(2))
         d(1)=d(1)-omega2(1)*y(1)-omega2(2)*(y(1)-y(2))
         b(1)=zlambda(1)+zlambda(2)+sigma(1)
      end if
      if(nstage.gt.2) then
         do 10 i=2,nstage-1
            d(i)=-omega2(i)*(y(i)-y(i-1))-omega2(i+1)*(y(i)-y(i+1))
            d(i)=d(i)-(rho(i)+rho(i+1)+g0(i)*sigma(i))*eta(i)
            d(i)=d(i)+rho(i+1)*eta(i+1)+rho(i)*eta(i-1)
            b(i)=zlambda(i)+sigma(i)+zlambda(i+1)
10        continue
      end if
      if(nstage.gt.1) then
         d(nstage)=-omega2(nstage)*(y(nstage)-y(nstage-1))
         d(nstage)=d(nstage)-
                   (rho(nstage)*(eta(nstage-1)-eta(nstage)))-
                   (xeta+g0(nstage)*
                   (zeta-float(nstage-1)*sigma(nstage)))*eta(nstage)
         b(nstage)=zlambda(nstage)+zeta-float(nstage-1)*sigma(nstage)
         do 60 i=2,nstage
            c(i-1)=-zlambda(i)
            a(i)=-zlambda(i)
60        continue
      end if
c
c----------invert A matrix
c
      call tridg(a,b,c,d,nstage)
c
c----------fill r array with rhs values after inversion
c
      do 70 i=1,nstage
         r(i)=d(i)
         r(i+nstage)=eta(i)
70    continue
      r(2*nstage+1)=eta(nstage)**2
      r(2*nstage+2)=xeta

      return
c
c----------format statements
```

```
c
900   format(2(f10.7,2x))
910   format(f10.7)
c
      end
c
      subroutine rk4
c-------------------------------------------------------------
c     Subroutine uses Rung-Kutta 4th order method to solve
c     ordinary differential eqations occuring in the R solution
c     vector.
c-------------------------------------------------------------
c
      parameter(nmx=1000)
c
      common/const/ sigma(nmx),zlambda(nmx),omega2(nmx),rho(nmx),g0(nmx)
      common/time/ t(nmx),delt
      common/stage/ nstage,stg,nstgmax
      common/condi/ yc(nmx),etac(nmx),xetac,zetac
      dimension etan(nmx),yn(nmx),r(nmx)
      dimension f0(nmx),fstr(nmx),fsstr(nmx),f1str(nmx)
c
      nx=2*nstage+1
      nz=2*nstage+2
c
c----------fill work arrays (*n arrays)
c
      do 10 i=1,nstage
         yn(i)=yc(i)
         etan(i)=etac(i)
10    continue
      zetan=zetac
      xetan=xetac
c
      do 25 nstep=1,4
c
c----------find equation array.
c
         call array(yn,etan,zetan,xetan,r)
c
c----------calculate intermediate values of eta, y, xeta, and zeta
c
         if(nstep.lt.4) then
            do 15 i=1,nstage
               ny=nstage+i
```

```
                if(nstep.eq.3) then
                    etan(i)=etac(i)+delt*r(i)
                    yn(i)=yc(i)+delt*r(ny)
                else
                    etan(i)=etac(i)+delt/2.0*r(i)
                    yn(i)=yc(i)+delt/2.0*r(ny)
                end if
15            continue
              if(nstep.eq.3) then
                  xetan=xetac+delt*r(nx)
                  zetan=zetac+delt*r(nz)
              else
                  xetan=xetac+delt/2.0*r(nx)
                  zetan=zetac+delt/2.0*r(nz)
              endif
          end if
c
c----------fill solution vector R into f0, fst4, fsstr, and f1str
c--------------depending
c--------------nstep=1------>r=f0
c--------------nstep=2------>r=fstr
c--------------nstep=3------>r=fsstr
c--------------nstep=4------>r=f1str
c
          do 20 i=1,nstage
              if(nstep.eq.1) then
                  f0(i)=r(i)
                  f0(i+nstage)=r(i+nstage)
              else if(nstep.eq.2) then
                  fstr(i)=r(i)
                  fstr(i+nstage)=r(i+nstage)
              else if(nstep.eq.3) then
                  fsstr(i)=r(i)
                  fsstr(i+nstage)=r(i+nstage)
              else
                  f1str(i)=r(i)
                  f1str(i+nstage)=r(i+nstage)
              end if
20          continue
c
          if(nstep.eq.1) then
              f0(nx)=r(nx)
              f0(nz)=r(nz)
          else if(nstep.eq.2) then
              fstr(nx)=r(nx)
```

```
            fstr(nz)=r(nz)
         else if(nstep.eq.3) then
            fsstr(nx)=r(nx)
            fsstr(nz)=r(nz)
         else
            flstr(nx)=r(nx)
            flstr(nz)=r(nz)
         end if
c
25    continue
c
c----------RK 4th order method numerical equation solution
c
      do 30 i=1,nstage
         ny=nstage+i
         etac(i)=etac(i)+delt*(1.0/6.0*f0(i)+1.0/3.0*fstr(i)+
                    1.0/3.0*fsstr(i)+1.0/6.0*flstr(i))

         yc(i)=yc(i)+delt*(1.0/6.0*f0(ny)+1.0/3.0*fstr(ny)+
     .              1.0/3.0*fsstr(ny)+1.0/6.0*flstr(ny))
30    continue
c
      xetac=xetac+delt*(1.0/6.0*f0(nx)+1.0/3.0*fstr(nx)+
     .              1.0/3.0*fsstr(nx)+1.0/6.0*flstr(nx))
c
      zetac=zetac+delt*(1.0/6.0*f0(nz)+1.0/3.0*fstr(nz)+
     .              1.0/3.0*fsstr(nz)+1.0/6.0*flstr(nz))
c
      return
      end
c
      subroutine tridg(aa,bb,cc,dd,ndim)
c-----------------------------------------------------------------
c     Called by subroutine ARRAY:
c
c     Subroutine inverts tridiagonal matrix where bb is diagonal,
c     aa is below diagonal, cc is above diagonal, dd is solution,
c     and ndim is size of matrix.  Solution stored in dd.
c-----------------------------------------------------------------
      parameter(nmx=1000)
      dimension aa(nmx),bb(nmx),cc(nmx),dd(nmx),ee(nmx)
c
c----------divide out aa diagonal
c
      ee(1)=bb(1)
```

```
      do 10 i=2,ndim
         ee(i)=bb(i)-cc(i-1)*aa(i)/ee(i-1)
         dd(i)=dd(i)-dd(i-1)*aa(i)/ee(i-1)
10    continue
c
c----------divide out cc and ee diagonal
c
      dd(ndim)=dd(ndim)/ee(ndim)
      do 20 i=ndim-1,1,-1
         dd(i)=dd(i)-dd(i+1)*cc(i)/ee(i+1)
         dd(i)=dd(i)/ee(i)
20    continue
c
      return
      end
```

Appendix B

Maple Source for Spring/Damper Response

```
# Program to plot response of spring/damper system.
# Maple Source.  Author: R.Batra
#
# Define the variables
# m=mass (kg); k=stiffness (N/m^2); c=damper constant (N*s/m)
# x=compressive distance (m); t=time (s)
m:='m';
k:='k';
x:='x';
t:='t';
c:='c';
#
# Setup the standard differential equation for a spring-damper system.
eqn := diff(x(t),t,t)+c/m*diff(x(t),t)+k/m*x(t)=0;
#
# Solve the differential equation
deqn := dsolve({eqn,x(0)=0,D(x)(0)=375},x(t));
#
# Solve for velocity (x prime)
xp := diff(deqn,t);
#
# Solve for acceleration (x double prime)
xdp := diff(xp,t);
#
# Define the stiffness and damper constants
k := 6000;
c := 4500;
m := 80;
#
# Plot out x(t) response
#
plotsetup(postscript);
interface(plotoutput=`maple1.ps`);
plot(rhs(deqn),t=0..10,title=`x(t) response: Units: meters`);
#
# Plot out the velocity response
interface(plotoutput=`maple2.ps`);
plot(rhs(xp),t=0..0.1,title=`x'(t) response: Units: m/s`);
# Plot out the Force response
interface(plotoutput=`maple3.ps`);
plot(rhs(xdp)*m,t=0..0.1,title=`m*x''(t) response: Units: Newtons`);
```

4.0 PROPELLANT PRODUCTION

Department of Chemical Engineering
William Gareau
Lawrence Kruger
William Patrizio
Kathy Reicosky
Sherif Sakr

TABLE OF CONTENTS

ABSTRACT

All disciplines of engineering at the University of Cincinnati are involved in the design of the lunar fuel processing facility. While other disciplines have engineered the mining and purifying of the ice, transportation of the ice, storage of the fuel, and support for operations, the chemical engineers have designed the fuel processing plant. The ammonia/water mixture will be separated with a distillation column. The purity of the product streams is about 99 %. A Hamilton Standard SPE Electrolyzer will be used to split the water into hydrogen and oxygen streams, which are 99.99 % pure. The ammonia stream from the distillation column will be split in a reactor. The hydrogen and nitrogen molecules will be separated via a membrane system. The splitting of the ammonia has an efficiency rate of 98 %. The liquefaction of nitrogen and hydrogen is accomplished through the use of the Linde process. The oxygen will liquefy via temperature control. The energy requirements for the entire lunar fuel processing facility is about 200 kW. The total weight of materials to be transported is about 13,000 kg, translating into a cost of $1.0 billion, not including support structures and enclosures.

4.00 INTRODUCTION

The Chemical Engineering Space Team is part of a multi-disciplinary design team comprised of Engineering Mechanics, Aerospace Engineering, Civil Engineering, Nuclear Engineering, Materials and Science Engineering, and Electrical Engineering. Each team has its own responsibilities to the success of a Lunar Fuel Production and Storage Facility.

It is believed that an ice-ammonia-dirt mixture exists at the north pole of the moon. This ice may be very useful in the production of fuel. At this time, all spacecraft must carry fuel for the return trip on their journey to the moon. There is a 5:1 ratio of fuel to weight in these missions, which results in an approximate cost of $77,000/kg to transport cargo to the moon. Therefore, it would be a major savings in cost to provide spacecraft fuel at the moon, and would increase the amount of cargo that can be carried to the moon.

All disciplines of engineering at the University of Cincinnati are involved in the design of the lunar fuel processing facility. While other disciplines have engineered the mining and purifying of the ice, transportation of the ice, storage of the fuel, and support for operations, the chemical engineers have designed the fuel processing plant. The goal of this plant is to produce liquid oxygen and hydrogen. The plant takes an ammonia/water feed, separates the mixture and splits it into its gaseous components. The oxygen from the water is liquefied as a product stream. The hydrogen from the water and the ammonia is combined and also liquefied as a product stream. The nitrogen is liquefied and used in the process for purging lines and cooling heat exchangers.

The assumptions of the design are that the plant is totally enclosed, except for storage tanks and radiation heat exchangers. It may be possible to transport the whole plant in modular sections to the moon.

Due to high costs of energy, it was decided to operate the plant during the night time only, which amounts to fourteen consecutive days of night. The capacity was therefore doubled to accommodate the monthly supply, and doubled again to allow NASA flexibility. The decision to operate at night was made in an effort to save transportation

costs and to reduce energy requirements. A large amount of heat in this process is dissipated by radiation heat exchangers, which can be made out of glass from the regolith on the moon. If the process were to operate during both the day and night, a separate refrigeration cycle would be needed to dissipate heat generated by the process. This refrigeration cycle would need to accommodate the nitrogen, hydrogen, and oxygen liquefaction cycles. The weight of equipment saved by operating continuously, would be smaller than the added weight of a massive refrigeration cycle that would be needed during the daytime temperatures of 400 K. Since the radiation heat exchangers will not be transported to the moon and do not require energy, operating during the day would be more costly than operating during the night time at double capacity.

2.00 DESIGN GOALS

The goal of the fuel processing plant is to produce liquid oxygen and hydrogen from a water/ammonia feed stream.

2.10 CONCEPTUAL DESIGN

The lunar fuel processing facility is divided into four functional sections. First is the distillation of the ammonia/water feed. Then there are two sections in parallel: the ammonia system and the water system, each geared toward separating the liquids into their elemental gaseous components. In the last stage of the process, there is a liquefaction section which converts the gases into product liquids.

The liquid feed stream from the feed tank is distilled into pure ammonia and water (see flow sheet on next page). The ammonia is sent to a reactor, where heat is used to disassociate the ammonia into its nitrogen and hydrogen components. The N_2 and H_2 leave the ammonia reactor in a gaseous mixture which is separated by a membrane system. The nitrogen is then compressed and expanded by a valve to become a saturated vapor. The saturated vapor is separated into its liquid and gaseous phases.

Fuel Processing Facility Flowsheet

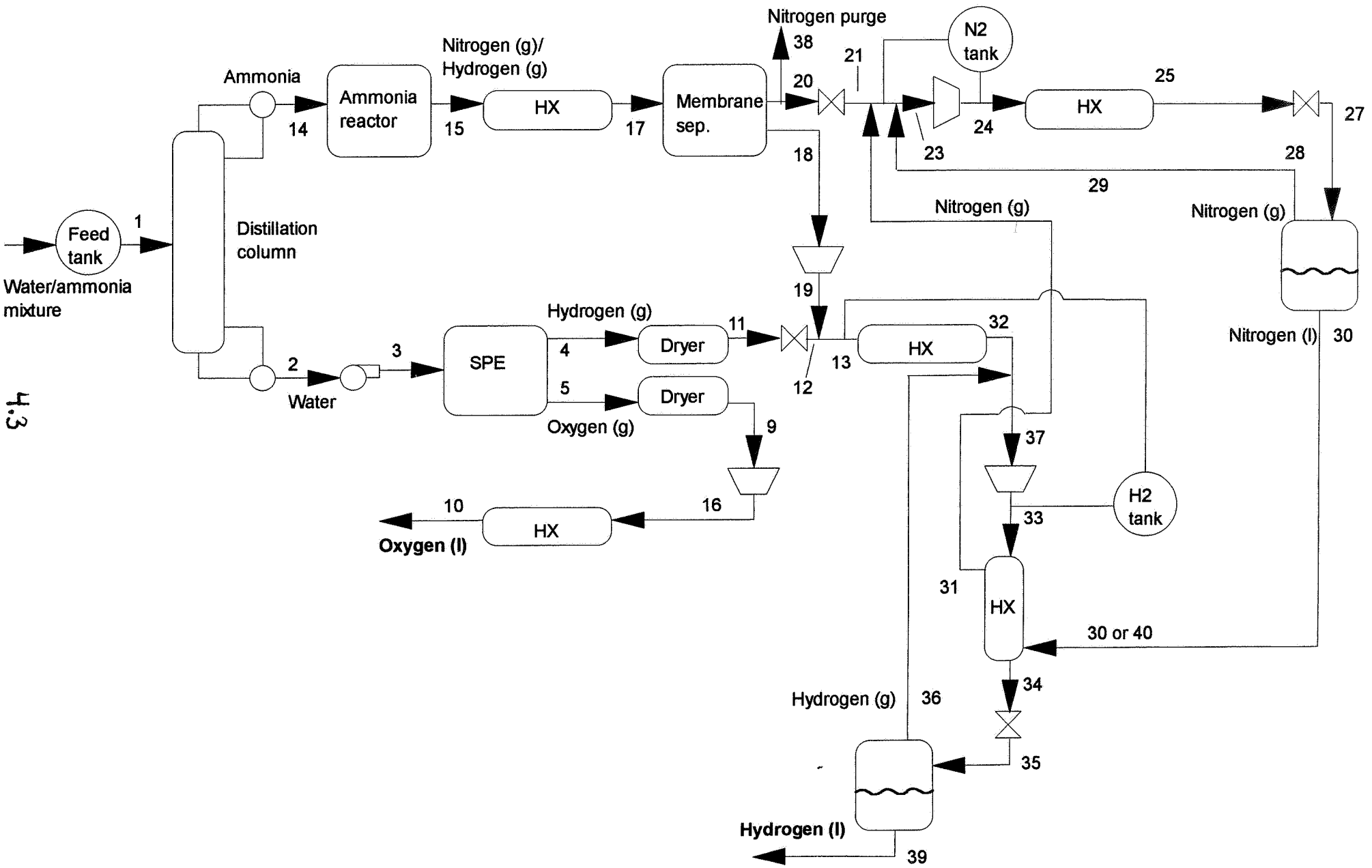

4.3

Stream #	NH3 (kg/hr)	H2O (kg/hr)	O2 (kg/hr)	N2 (kg/hr)	H2 (kg/hr)	T (K)	P (atm)
1	6.67	126.66					5
2		126.66				427	5
3		126.66					7
4		0.08			14.06	323	7
5		0.04	112.47			323	7
9			112.47			323	7
10			112.47			150	28
11					14.06	323	7
12					15.22	323.1	5
13					15.22	334.7	4.65
14	6.67						5
15				5.42	1.16	800	7
16			112.47			478	28.5
17	0.09			5.42	1.16	300	7
18					1.16	300	1
19					1.16	475	5
20					5.42	300	5
21					5.42	297.5	1
22				450		115.1	1
23				1792.8		82.73	1
24				1792.8		277.06	70
25				1792.8		130	70
26				1792.8			
27				1792.8		77.35	1
28				1342.8		77.35	1
30				450		77.35	1
31				450		97.02	1
32					15.22	120	4.65
33					108.95	40	28.5
34					108.95	87	28.5
35					108.95	27	4.65
36					93.73	27	4.65
37					108.95	40	4.65
38				5.42		297.5	1
39					15.22	27	4.65
40				450		116.7	1
41				450		120	1

The water from the distillation column is sent to an electrolysis cell that produces two product streams, O_2 and H_2. The oxygen and hydrogen are sent to separate dryers which remove traces of water vapor. The pure oxygen stream is sent through a compressor and a radiation heat exchanger to cool it to liquid form. The hydrogen streams from the ammonia reactor and the electrolysis cell are combined and sent to the hydrogen liquefaction process. A radiation heat exchanger is used to cool the hydrogen to ambient temperature. The hydrogen is further cooled by liquid nitrogen to below 100 K. The super cooled hydrogen is compressed and then expanded to become a saturated vapor. The saturated vapor is separated into liquid and gaseous hydrogen. The liquid hydrogen and oxygen are piped to the fuel storage facility, while the gaseous hydrogen is recycled.

2.20 *AMMONIA/WATER SEPARATION*

There are several methods which may be used to separate ammonia from water. Characteristics such as polarity and molecule size may be used; however, distillation was chosen because of the proven technology, the high purities needed in the effluent streams, and because of the large boiling point differences between ammonia and water. Several factors must be considered in lunar distillation design. The low gravity on the moon will result in a larger column because of the necessary residence time. Though cooling is difficult, heating is relatively cheap because heat is supplied by other engineering disciplines. Heat is the main driving force in distillation, and it is more abundant than shaft or electrical energy.

2.30 *WATER SPLITTING*

The following processes were considered for the splitting of water, which is the only source of oxygen.

2.31 RADIOLYTIC CLEAVAGE

High energy radiation of water produces H*, OH*, H2, H2O2, OH-, and H+. Due to the production of many radicals and side products, and the large amount of energy required (approximately 2 MW), this option was eliminated.

2.32 PHOTOCATALYTIC CLEAVAGE

The irradiation of water using a narrow range of the UV spectrum (Sayama et al., 1990) results in the cleavage of water. This process requires two catalysts, one for hydrogen production and one for oxygen production. A sensitizing agent as well as an electron relay compound is needed for the reaction to occur. A low evolution of hydrogen (approx. 1 % of the water could be decomposed in a 28 day period) and the transportation and handling of the catalysts eliminated this option.

2.33 THERMODYNAMIC CLEAVAGE

The application of extreme heat (5000 K) and high pressure (10 atm) on water produces oxygen and hydrogen(Etievant, 1991). Due to the low yield (max. 2.3 %) and extreme material stress, this option was eliminated.

2.34 THERMOCHEMICAL CLEAVAGE

A series of chemical reactions can split water into its elements. Three separate reactions are needed, each occurring at relatively high (1200 K) temperatures and in the presence of a metallic catalyst (PtO or MgO). With the exception of water, the reactants are regenerated within the series of reactions. With a 30% conversion and up to 39% thermal efficiency, this process is the second most probable reactor system. It was not chosen due to the large amount of initial investment of transporting three reactors, their separation systems, and reactants to the moon. (Roth et al., 1988)

2.35 ELECTROLYSIS

Electrolytic cleavage of water passes a current through an electrolytic substance. Hydrogen and oxygen are produced in a gaseous state at separate electrodes, which eliminates the need for a product separation system. The process itself is the simplest of the water-splitting technologies, and weighs the least. It can be transported to the moon pre-assembled in a module. This process is currently being discussed as the future technology for obtaining hydrogen and oxygen from water by several industrial and NASA-related studies. As electrolysis is the water-splitting technology most adaptable to the moon, it will be used for this design. (Morehouse, 1988)

2.40 AMMONIA SPLITTING

The ammonia will be thermodynamically disassociated by the addition of large amounts of heat. The resulting nitrogen and hydrogen streams could be separated by cryogenic distillation, absorption, or membrane separation. Cryogenic distillation, while capable of high flow rates and high purities, would only add mechanical equipment requiring maintenance to our plant. Our flow rates in the ammonia subsystems are low enough that cryogenic distillation is unnecessary. Carbon beds or molecular sieves are non-mechanical, but are heavy, and would require duplicate systems for periods of regeneration. Membrane systems, in contrast, are non-mechanical, have no heat load, are low-maintenance, and have extended lifetimes. The ammonia flow rates are small enough that a membrane system is feasible, and high purity is possible with multiple systems in series. For these reasons, a membrane separation system was chosen for the ammonia reactor outlet.

2.50 *LIQUEFACTION*

The use of hydrogen and oxygen as fuels for spacecraft in NASA's space program is dependent upon the liquefaction of these fuels. Liquefaction of a gas is dependent upon the temperature and pressure of the gas. In general, the lower the pressure of the gas, the lower the temperature of the gas must be for liquefaction to occur.

There are three common processes by which liquefaction can be achieved. The first of these processes involves the use of a heat exchanger to cool the gas to a temperature that is below the boiling point of the gas. This process is not feasible because it requires a cooling fluid cooler than the boiling point of the gas to be liquefied. The remaining two processes use the principle of volumetric expansion to liquefy the gas. Volumetric expansion occurs when the gas undergoes a rapid decrease in pressure. The gas maintains a constant enthalpy throughout the depressurization process while the pressure and temperature decrease. If the volumetric expansion occurs over the proper pressures, liquefaction will occur. There are two devices that induce volumetric expansion of a gas. The first is a simple pressure release valve, known as a throttling valve, and the other is an expansion turbine. Since the valve is simpler in design and has no moving parts that would require large amounts of maintenance, it has been decided that the throttling process would be the preferable expansion process. (Smith and Van Ness, 1987)

2.51 HYDROGEN

The liquefaction of hydrogen is difficult because of its extremely low boiling point. The highest temperature at which hydrogen can exist in liquid form is 33.18 K. The only fluid that can cool hydrogen to that temperature is liquid helium. In addition, the throttling process is made difficult by the unique behavior of hydrogen at low temperatures. Hydrogen will increase in temperature if it undergoes expansion at any temperature above 100 K. Since helium has a similar problem, and must be cooled to a temperature below 20 K, the heat exchanger method can not be used.

Hydrogen Liquefaction Cycle

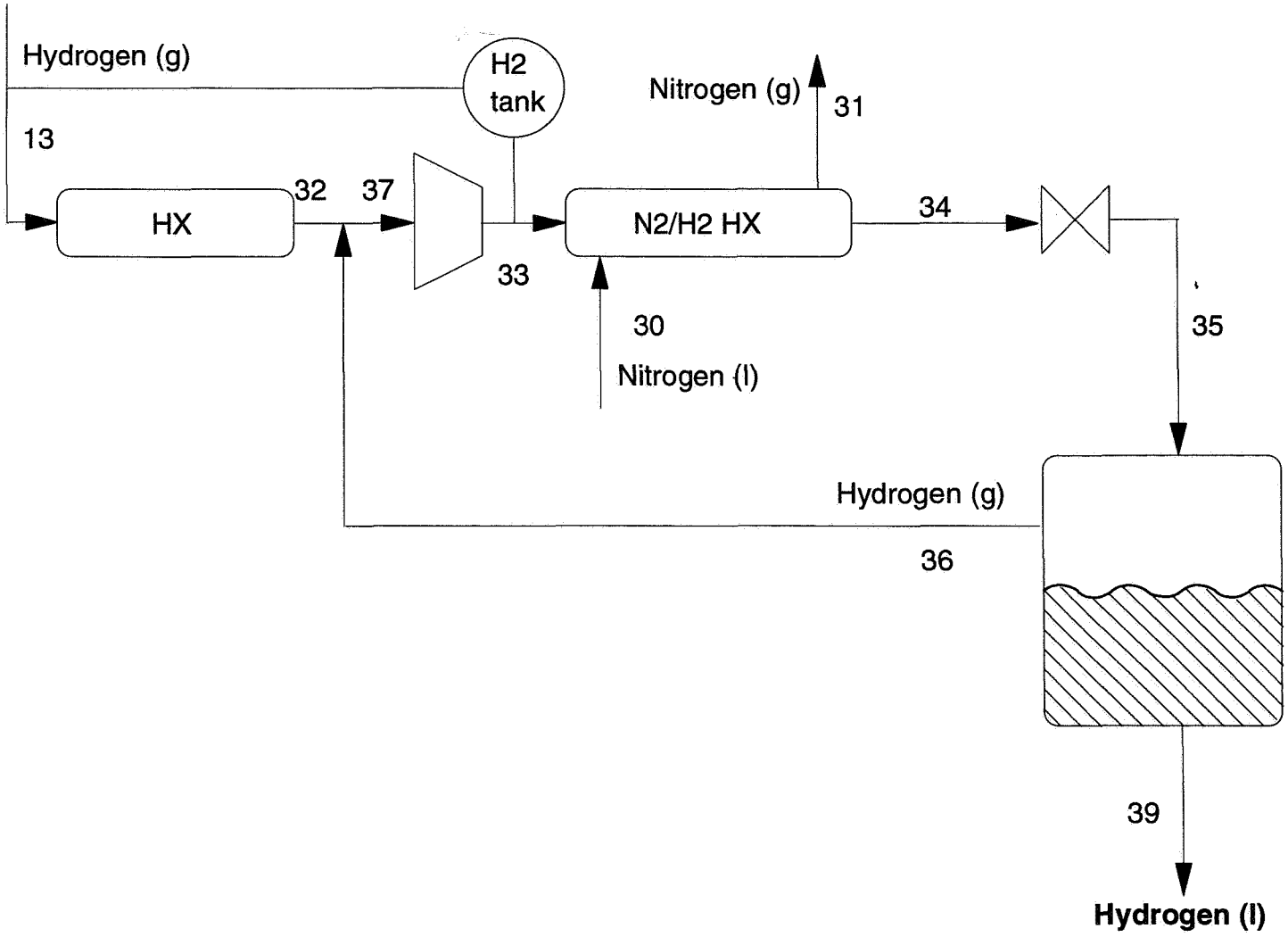

The optimum process for the lunar facility is to use a heat exchanger to cool the hydrogen to a temperature below 100 K , and then use the throttling process to liquefy the hydrogen. Liquid nitrogen can be made from the ammonia using the throttling process. Therefore, liquid nitrogen can be used to cool the hydrogen to a temperature well below 100 K.

2.52 NITROGEN

The liquefaction of nitrogen can be accomplished by using either a heat exchanger or a throttling valve. The use of a heat exchanger would require a fluid with a temperature below 67 K, so a throttling valve is the better option. The use of a throttling valve to liquefy nitrogen does not have any temperature requirements, as the hydrogen does.

When the hydrogen has reached a temperature that is close to the temperature of the nitrogen, the nitrogen liquefaction system will be shut off. Leaving the nitrogen liquefaction system on would actually hinder the hydrogen liquefaction process. This is due to the fact that the hydrogen will continue to cool in a closed loop cycle until it reaches a temperature of 40 K, which is well below the coolest temperature possible for liquid nitrogen.

2.53 OXYGEN

The liquefaction of oxygen is very easy to perform in the low temperatures of the moon during the night time. A compressor and a radiation heat exchanger will cool the hydrogen to ambient temperature. Since the temperature at night is 113 K, it is fairly easy to select operating conditions that will liquefy the oxygen without the cumbersome equipment required by the other liquefaction processes.

Nitrogen Liquefaction Cycle

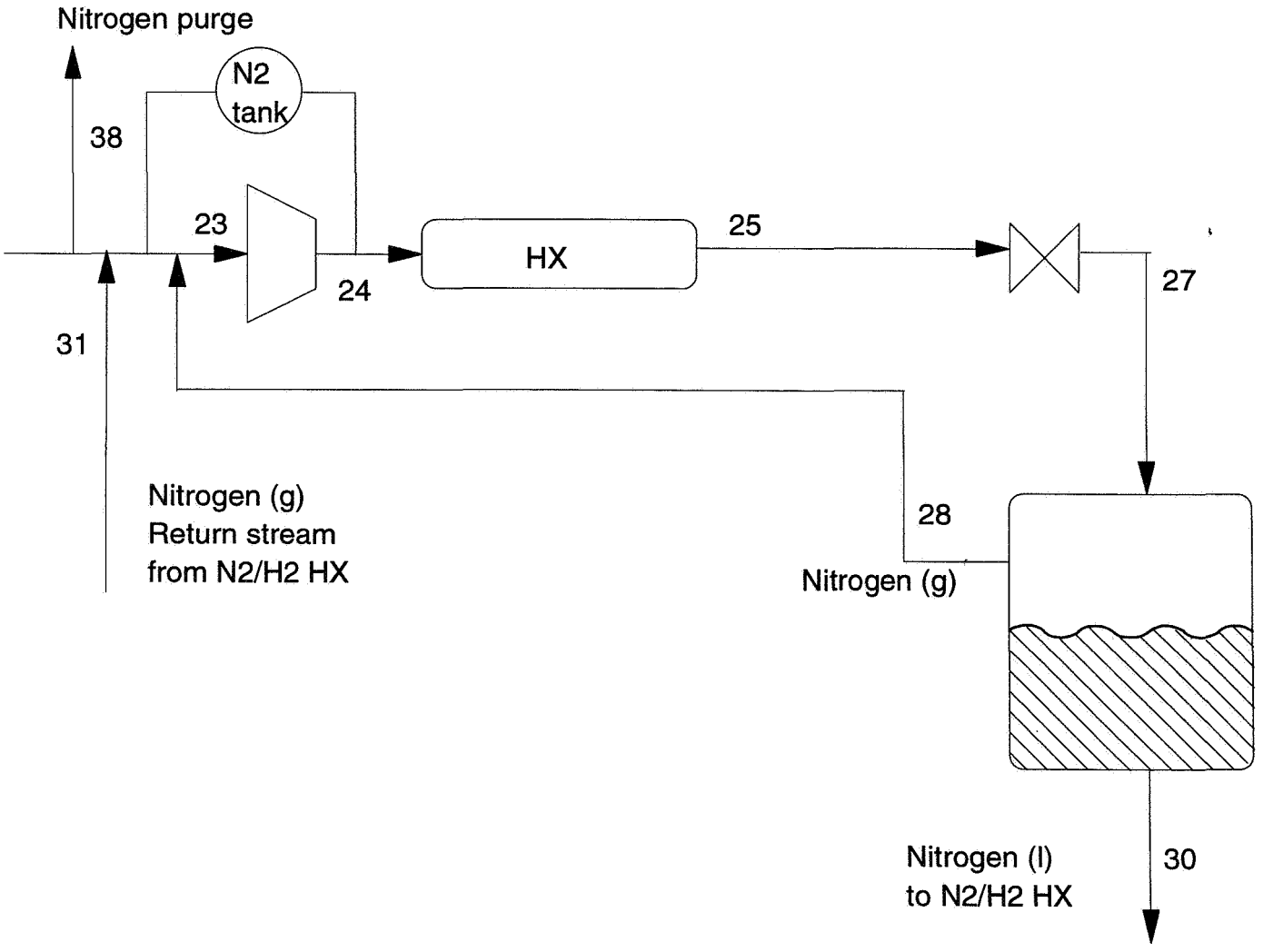

.00 DESIGN SUPPORT CONSIDERATIONS

3.*10* *SUBSYSTEMS*

The lunar fuel processing facility is divided into four functional sections: the distillation process, the ammonia system, the water splitter, and the liquefaction process.

3.110 DISTILLATION PROCESS

The distillation process consists of a feed tank with the water/ammonia mixture in it, a distillation column, a reboiler, and a condenser.

3.111 FEED TANK

A feed tank is necessary to store the water/ammonia mixture before the feed stream enters the process. The feed tank is designed to store 14 days worth of the feed stream at double capacity, approximately 22.4 m^3 (5,918 gallons). Aluminum was chosen as the tank material because of its low density and high yield stress. With a thickness of 1.96 cm, the weight of the spherical tank is 2,135 kg (4,707 lbs).

3.112 COLUMN

Since there is very little data in support of fluid behavior on the moon, distillation must rely heavily on theory. The sizing procedure was based on earth correlations, and was adjusted to the moon's lower gravity. Calculations of the column dimensions are elaborated on in the appendix.

The pressure of the column is 5 atmospheres, as dictated by processes downstream. The feed rate and the feed composition is specified by the delivery rate of ice from the lunar poles. The process temperature is 288 K. Although higher temperatures would have substantially reduced the column height, greater condenser

cooling and higher reboiler heating would negate these benefits. Sieve trays will be used for ease of maintenance.

The column diameter must be adjusted for the lunar gravity. By equilibrating the drag and buoyant forces acting on a bubble moving through a liquid, the relationship between gravity and bubble velocity is determined. Flooding velocity is assumed to have the same relationship. Knowing that area is inversely proportional to velocity, the active tray area, which is the column diameter minus the area of two downcomers, is found to be inversely proportional to the square root of gravity. Since gravity is reduced to one-sixth to that of Earth's, the active area is increased by the square root of six. The downcomer area is also enlarged by the same factor from observing gravity's effect on liquid flow rate down a vertical pipe. Therefore total column diameter increases by a factor of 2.45.

A pressure loss is observed when a vapor moves up through the column. This loss is caused by the condensation of the gas as it enters the sieve holes, by the friction with the holes, and by the resistance as the vapor passes through the liquid on the tray. Reduced gravity lowers the resistance, thereby lowering the pressure loss. Inches of liquid is proportional to gravity according to the following equation:

$$dP = \rho g h$$

where ρ = density
g = gravity
h = liquid height

Equation 1A

Vapor will travel slower through the liquid, due to the reduced gravity. As a result, bubbles will have more time to form and will be larger. An increased bubble size will decrease efficiency by reducing interfacial surface area. However, the slow movement will give greater time for mass transfer and increase efficiency. The following equation

regarding the relationship between earth and moon variables was found through the analysis of the Murphee plate efficiency:

$$\frac{\ln(1-E)_m}{\ln(1-E)_e} = 0.4089(A_m/A_e)(h_m/h_e)(d_e/d_m)^{1.5}$$

where E = tray efficiency

A = total interfacial surface area

h = liquid height on the tray

d = diameter of the bubble

Equation 2A

Dimensional analysis shows that the following relationship must exist to maintain hydraulic similarity:

$$[M \cdot g/s \cdot D]_e = [M \cdot g/s \cdot D]_m$$

where M = bubble mass

g = gravity

s = surface tension

D = Sieve hole diameter

Equation 3A

By manipulating variables in Eq.1A and Eq.2A, the effects on efficiency may be deduced. Leaving the sieve hole diameter constant results in an average 34% decrease. The bubble mass can be kept constant by reducing the sieve hole diameter to one-sixth to compensate for the gravity reduction. In this case, the increased contact time would increase efficiency by an average of 25%. As long as the pressure drop is tolerable, this option would be favorable.

The tower dimensions were calculated to be 59 feet high by 10.5 inches in diameter. A supporting truss is necessary for mechanical considerations and maintenance platforms. The weight of the distillation column using Aluminum is 1,081 kg (2,384 lbs).

The column will be designed in three to six foot sections. A replacement section

will be used when maintenance becomes necessary. The section will be connected by exterior clamps, minimizing manual labor.

3.113 CONDENSER

Condenser cooling is greatly reduced by only condensing the liquid returning to the column and not the distillate. Normal distillation draws off the distillate after condensation. In this process, the distillate, ammonia, is heated in the ammonia-splitting reaction. Therefore condensation previous to the reaction is wasteful. This process will save 1270 cal/sec. The condenser consists of a heat exchanger in which nitrogen at 73 K is used to cool the ammonia. This process assumes an overall heat transfer coefficient of 1 W/m^2, which corresponds to a heat transfer area of 1.0 m^2.

3.114 REBOILER

The reboiler will consist of a heat exchanger. Aspen calculations show that 2415 cal/sec will be transferred to the liquids from the bottom tray. The temperature and composition of the hot compound to be received from the nuclear facility is yet to be defined.

3.120 AMMONIA SYSTEM

The purpose of the ammonia system is to first split ammonia into gaseous nitrogen and hydrogen and then separate those elements from each other. The hydrogen stream is combined with the hydrogen stream from the water splitting process before being liquefied. The nitrogen stream is sent directly to be liquefied.

3.121 REACTOR

The following ammonia reaction is reversible at high temperatures:

$$\frac{1}{2}N_2 + \frac{3}{2}H_2 \leftrightarrow NH_3$$

The reaction rate constant varies with temperature. This reaction is optimized at 800 K to give a conversion of .9858. Although higher temperatures may lead to a conversion as high as .9989, this would adversely affect the radiation heat exchanger immediately downstream.

The size of the ammonia reactor was constrained by the pressure conditions and the weight transportation cost. At 7 atm, the volume of the spherical tank is 7.42 m^3 (1,960 gal). The weight is largely dependent on the width, which is related to the material strength. Titanium was chosen for its high yield stress and its non-reactivity with hydrogen. The thickness is 1.11 cm, resulting in a weight of 1,302 kg (2,871 lbs).

3.122 NITROGEN/HYDROGEN RADIATIVE HEAT EXCHANGER

The radiation heat exchanger consists of two parallel plates of glass mounted vertically through which the gas being cooled flows. Glass was chosen as the material because of its high emmisivity, and because it is a natural resource on the moon. The lack of atmosphere on the moon makes it more difficult to lose heat because there is no convective heat transfer. The heat lost by the gas throughout the length of the heat exchanger radiates off of the glass plates which is at nearly the same temperature as the gas. The heat lost by the gas is found by the following enthalpy balance:

$$Q = \dot{m} \cdot Cp \cdot \Delta T$$

where Q = heat transferred

Cp = heat capacity of the gas

ΔT = temperature drop across the heat exchanger

The previous equation is set equal to the radiation heat loss equation to find the area required to lower the temperature of the gas:

$$Q = A \cdot \varepsilon \cdot \sigma \cdot \left(Tavg^4 - Ts^4\right)$$

where Q = heat lost from gas
A = surface area of heat exchanger
ε = emmisivity
σ = Stephman - Boltzman constant
Tavg = average temperature of gas in the heat exchanger
Ts = temperature of space, 113 K

For the nitrogen/hydrogen radiative heat exchanger, the temperature of the inlet gas is 800 K , and is being cooled to 300 K. The ambient temperature of the moon during nighttime is 113 K. With a double capacity flow rate, the required area of the radiative heat exchanger is 25.86 m^2 per side. With the length four times the height, the dimensions of the heat exchanger are 2.54 m (8.34 ft) in height, 10.17 m (33.36 ft) in length, and 13 mm (0.5 in) thick per plate. The resulting weight is 1,708 kg (3,766 lbs). When the flow rate is not being operated at double capacity, the bottom half of the heat exchanger will be isolated from the gas stream.

3.123 NITROGEN/HYDROGEN SEPARATION

A membrane separation system was chosen to separate the gaseous mixture of nitrogen and hydrogen from the ammonia reactor. The diffusion rate across the membrane is a function of mass-transfer and membrane qualities.

Flux can be described by an adaptation of Fick's Law:

$$J = pH_2 \cdot A \cdot \Delta P / l$$

where J = total flux

pH_2 = H_2 permeability for a given membrane

A = surface area of membrane

ΔP = pressure drop

l = fiber length of membrane

Permeabilities are controlled by membrane characteristics. A 3,3' ODA-PMDA polyimide membrane was chosen because of the large difference in nitrogen and hydrogen selectivity (4). This difference in permeabilities causes the hydrogen to permeate through the membrane, while the nitrogen is retained.

A hollow fiber membrane design allows for greater surface area, which increases capacity. This membrane configuration is also very compact, as each fiber has a small diameter. Several fibers can be fit into a single module, a large container that houses the fibers. (see figure below). A cross-flow pattern, where the feed gas flows through the fibers on the tube side and the permeate is on the shell side, was chosen. In the flow pattern, the retentate gas experiences only one pound of pressure drop, saving the addition of another compressor.

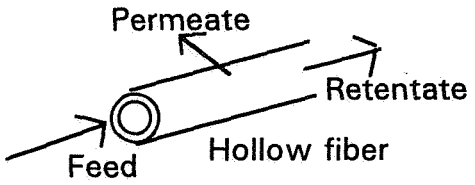

A spreadsheet modeling membrane performance (14) was used to size the membrane separation systems. Membrane characteristics, pressure drop, and flow rates were held constant, while the area and length were varied until the desired separation was achieved. Permeabilities in the analysis were defined as barrer, where:

$$\text{barrer} = 10^{-10} \frac{\text{cm}^3(\text{STP})*\text{cm}}{\text{cm}^2* \text{ cm Hg}*5}$$

The hydrogen permeability for the chosen membrane is 3.6 barrer, pressure drop set at 100 pounds, and feed rate at 11 SCFM.

From the results of these trials, diffusion through the membrane seemed to be the limiting factor, as the length of the fiber had more effect on the degree of separation than did the number of fibers in the module. The desired separation, in which 99.5% of the hydrogen was permeated, was achieved with ten million fibers 4m in length. The fiber diameter is not fixed, but the difference between the outer diameter and the inner diameter should be around 100μ. In general, fibers with larger diameters last longer.

The module itself was designed with several heuristics: a length to diameter ratio between 2 and 10; and a void area of 0.5. With an outer fiber diameter of 400μ, a single module with a 0.7 m diameter and 4 m length will suffice for the nitrogen/hydrogen system. While this module is larger than commonly found in industry, a smaller module may be possible with a more selective membrane or a higher pressure drop. Increasing pressure drop shortens membrane lifetime, and would require an additional compressor. A shorter module with a larger diameter is also possible, but would be heavier than a longer, larger module.

3.130 WATER SPLITTING

As stated earlier, electrolysis is used to split the water. This is a very efficient process and is also very safe. It minimizes the amount of chemicals which would have to be transported to the moon.

3.131 ELECTROLYSIS THEORY

The Solid Polymer Electrolyte (SPE) water electolyzer uses ion exchange membranes as its only electrolyte. This technology was originally developed for nuclear submarine oxygen production and has since been proven quite effective and reliable. The electrolysis cell contains the ion exchange membrane. It has Teflon bonded, finely divided metal electrodes. Due to its unique characteristics, no bubble point or free electrolyte, the operating pressures and hydrogen-oxygen differentials are limited only by the surrounding structures. Safety is therefore increased significantly.

The cation exchange membrane allows a cell life of 12 to 30 years. Existing cells have shown in excess of 100,000 operational hours without disassembly or modification which would amount to over 30 years of operation on the moon. Most practical applications use a number of cells stacked in a filter press arrangement, allowing the fluids to be passed through the cells in parallel. The purity of the product gases is greater than 99.99 %.

Lunar operation requires low gravity adaptability. Current technology utilizes two membrane static phase separators. Due to the low gravity environment, special membranes are used in these phase separators, namely hydrophilic, hydrophobic, and ion exchange membranes. The first passes liquid water with a small driving force, but blocks the gas. The second passes the gas with a small driving force, but blocks the liquid. And the last membrane rapidly transfers hydrogen through the membrane at a rate proportional to the electrical current draw.

3.132 SPE DESIGN

United Technologies, Hamilton Standard Division has designed a 7 atm oxygen/hydrogen generating plant for the lunar surface, based on the SPE electrolyzers. The system consists of 107 cells in eight modules, and will run at 323 K. The SPE system will require 103 kW with DC current. A copy of their report may be found in Appendix.

3.133 DRYERS

The product gases from the SPE have a dew point of 323 K. This residual water will quickly liquefy and freeze in the liquefaction system, potentially breaking lines and fouling equipment. These gases must be dried to avoid problems downstream. In the past, regenerative carbon dryers have been used. While these systems are reliable, these require redundancy, and are quite heavy. Carbon dryers can account for up to 40% of the SPE system weight.

For the purposes of this design, a coated polysulfone membrane was used. Hydrogen permeability was estimated based on polysulfone membrane qualities. Oxygen permeability was assumed to be the same as air. This membrane is capable of -100 °C dew points with a 17% recovery rate. This design uses 98.5% purity with an average 96.7% recovery rate. With further developments, better membranes need to be found that accomplish significantly better purities. For hydrogen, two million fibers two meters in length are installed in a single module 1.4m in diameter. For oxygen, one million fibers 1.5 m in length are installed in a module 0.85 m in diameter.

3.140 LIQUEFACTION

The liquefaction area of the plant will include the liquefaction of hydrogen, nitrogen, and oxygen. The liquid hydrogen and oxygen will be used as fuel propellant for spacecraft returning to Earth. The liquid nitrogen will be used in the hydrogen liquefaction process.

3.141 HYDROGEN

The hydrogen liquefaction process will begin by cooling the hydrogen to a temperature of 150 K using a radiative heat exchanger. The use of the radiative heat exchanger will reduce the size of the nitrogen/hydrogen heat exchanger as well as reduce the amount of nitrogen needed to cool the hydrogen in the process. The cooled hydrogen is sent to a compressor and cooled to 87 K in the liquid nitrogen heat exchanger. The hydrogen is then sent through a throttling valve. The hydrogen leaving the valve is a mixture of gaseous and liquid hydrogen that is separated by a phase separator. The liquid hydrogen will be sent as a product to the storage facility, while the gas is recycled.

Once the system reaches steady state, the gas recycle will combine with the incoming hydrogen and will have a flow rate of 108.95 kg/hr at 40 K and 4.65 atmospheres. At start-up, it will take approximately 8 hours to reach this steady state. Once the streams are combined, the new stream will be sent to the compressor, where it will leave at 40 K and 28.5 atmospheres. The final step of the liquefaction will throttle the hydrogen to 4.65 atmospheres and 27 K. The phase separator will produce a liquid stream of 15.22 kg/hr at 27 K and a gas stream of 93.73 kg/hr at 27 K. When the plant is shut down during the day, the gaseous hydrogen in the system will be stored in a storage tank, decreasing start-up time by half a day.

This process has been optimized by attempting to find the lowest total cost possible for the liquefaction of the process. In minimizing costs, the main effort has been to minimize the weight of the system. With the cost of transporting equipment at $77,000/kg, all other economic considerations are insignificant. It was found that the heaviest pieces of equipment in the liquefaction process are the storage tanks. With this in mind, liquefaction percentages were maximized in order to reduce the size of the storage tanks needed, for both the hydrogen and nitrogen liquefaction processes.

RADIATIVE HEAT EXCHANGER

For the hydrogen radiative heat exchanger, the temperature of the inlet gas is 334.7 K, and is being cooled to 120 K. With a double capacity flow rate, the required area of the radiative heat exchanger is 48.5 m^2 per side. With the length four times the height, the dimensions of the heat exchanger are 3.48 m (11.42 ft) in height, and 13.9 m (45.7 ft) in length, and 13 mm (0.5 in) thick per plate. The resulting weight is 3,201 kg (7,057 lbs). When the flow rate is not being operated at double capacity, the bottom half of the heat exchanger will be isolated from the gas stream.

COMPRESSOR

The hydrogen will be compressed from 4.65 atmospheres to 28.5 atmospheres. This will give a compression ratio of 6 to 1, requiring a two stage compressor. The entering hydrogen gas will have a mass flow rate of 108.95 kg/hr and a temperature of 150 K during start up and 40 K at steady state. This compressor must operate isothermally; if it does not, the heat from the compressor will make liquefaction impossible under any conditions. The inlet volumetric flow rate will be at a maximum of 2.40 cubic meters per minute (85.05 cubic feet per minute) with a maximum temperature of 150 K . The outlet volumetric flow will be at a maximum of .40 cubic meters per minute (13.88 cubic feet per minute). The compressor will have a maximum energy requirement of 9.8 kW (13.14 horsepower), which will occur when the system is at steady state.

In order for the compressor to operate isothermally, a coolant stream must expel the heat generated by the compressor. One possible method to accomplish this, is to use the liquid hydrogen from the cryogenic storage facility to cool the compressor.

N2/H2 HEAT EXCHANGER

The nitrogen/hydrogen heat exchanger will use liquid nitrogen to cool hydrogen. Hydrogen enters the heat exchanger at 150 K and is cooled to 87 K during start-up. Once

steady state has been reached, the heat exchanger will be bypassed. Nitrogen is heated in the heat exchanger from 77.35 to 115.1 K during start-up. An overall heat transfer coefficient of 20 W/M^2 was assumed, leading to a heat transfer area of 1.1 m^2.

THROTTLING VALVE

The throttling valve will decrease the pressure of the hydrogen from 28.5 atmospheres to 4.65 atmospheres. The temperature of the gas will decrease from 40 K to 27 K with enthalpy across the valve remaining constant. The resulting saturated vapor will consist of 13.97 wt% liquid and 86.03 wt% gas.

PHASE SEPARATOR

The phase separator will separate the saturated hydrogen into its liquid and gas forms. The cylindrical, titanium separator will have a volume of about 1.84 m^3 with a radius of 0.46 m, a height of 2.76 m, and a wall thickness of 4 mm. The resulting weight of the phase separator is 234 kg (516 lbs).

3.142 NITROGEN

The nitrogen liquefaction process will begin with the compression of the entering nitrogen gas stream and all the nitrogen recycle streams. After the nitrogen leaves the compressor, the gas will go through a radiative heat exchanger, where it will be cooled to ambient temperature. Next, the nitrogen gas is sent to the cooler, where it is cooled with the gas recycle stream. The final step in the liquefaction process is the throttling valve, which decreases the pressure of the nitrogen and partially liquefies it. The gas/liquid mixture is separated by a two-phase separator. The gas stream is first sent to the cooler and then recycled. The liquid stream is used to cool the hydrogen in the H_2/N_2 heat exchanger where the nitrogen is vaporized. Once the hydrogen stream reaches a temperature of 80K, the nitrogen liquefaction system will be shut off.

The process will begin with a stream of 1792.8 Kg/hr of N2 entering the compressor at 1 atmosphere and 82.3 K. The compressor will increase the pressure of the nitrogen to 70 atmospheres, and it will increase the temperature to 277.06 K. This is the optimal pressure needed to liquefy the nitrogen to a temperature of 77.35 K. Once the nitrogen leaves the compressor, it will be cooled by the radiative heat exchanger to a temperature of 130 K. The final step of the process is to throttle the nitrogen down to a pressure of 1 atmosphere and a temperature of 77.35 K, producing a saturated mixture. When the gas and liquid nitrogen are separated, the liquid stream will have a flow of 450 kg/hr, a temperature of 77.35 K, and a pressure of 1 atmosphere. The gas stream will have a flow rate of 1342.8 Kg/hr, a temperature of 77.35 K, and a pressure of 1 atmosphere. Similarly to the hydrogen system, the nitrogen will be stored in tank when the plant is shut down, thus limiting start-up time to less than an hour. Accordingly, temperature and pressure conditions have been chosen so as to maximize liquefaction in order to minimize the size of the storage tank. It has been determined that the nitrogen storage tank is the largest and heaviest piece of equipment in the nitrogen liquefaction process.

COMPRESSOR

The nitrogen compressor will increase the pressure of the nitrogen stream from 1 atmosphere to 70 atmospheres. The inlet volumetric flow will be 7.21 cubic meters per minute (255.2 cubic feet per minute) with a temperature of 82.3 K. The outlet flow will be .35 cubic meters per minute (12.4 cubic feet per minute) with a temperature of 277.06 K. The compressor will consist of four stages and will have a power requirement of 47.12 kW (63.18 hp).

RADIATIVE HEAT EXCHANGER

The nitrogen radiative heat exchanger is needed to decrease the temperature of the inlet gas from 358.85 K to 150 K. With a double capacity flow rate, the required area of the radiative heat exchanger is 451 m^2 per side. With the length four times the height, the dimensions of the heat exchanger are 10.61 m (34.83 ft) in height, and 42.5 m (139 ft) in length, and 13 mm (0.5 in) thick per plate. The resulting weight of the heat exchanger is 29,777 kg (65,647 lbs). When the flow rate is not at double capacity, the bottom half of the heat exchanger will be isolated from the gas stream.

COOLER

The nitrogen/nitrogen heat exchanger is used to supercool the incoming nitrogen, increasing the liquefaction efficiency. The incoming nitrogen is cooled from 150 K to 127 K. The recycled nitrogen is heated from 77.35 K to 138 K. For an assumed overall heat transfer coefficient of 200 W/m^2, a heat transfer area of 51.6 m^2 is needed.

THROTTLING VALVE

The nitrogen throttling valve will decrease the pressure of the nitrogen from 33.5 atmospheres to 1 atmosphere. The corresponding drop in temperature will be from 127 K to 77.35 K. This will result in a saturated mixture of 25.1 wt% liquid and 74.9 wt% gas.

PHASE SEPARATOR

The phase separator will separate the gas and liquid nitrogen from each other. This separator will include "zig-zag baffles" that will give a collection efficiency of close to 100%. The cylindrical titanium separator will have a volume of approximately 25.4 m^3 with a radius of 1.11 m, a height of 6.63 m, and a wall thickness of 4 mm. The resulting weight of the phase separator will be 1,081 kg (2,384 lbs).

3.143 OXYGEN

The incoming oxygen stream will be at 7 atmospheres and 323 K. This stream will be sent to a compressor, where its pressure will be increased to 28 atmospheres while its temperature will be increased to 478 K. The oxygen is then sent to a radiative heat exchanger that will cool it to 120 K, producing a stream of 100% liquid oxygen.

RADIATIVE HEAT EXCHANGER

The oxygen radiative heat exchanger is needed to decrease the temperature of the inlet gas from 478 K to 120 K. With a double capacity flow rate, the required area of the radiation heat exchanger is 11.4 m^2 per side. With the length four times the height, the dimensions of the heat exchanger are 1.69 m (5.53 ft) in height, 6.74 m (22.13 ft) in length, and 13 mm (0.5 in) thick per plate resulting in a weight of 751 kg (1656 lbs).

COMPRESSOR

The single stage oxygen compressor will have an inlet flow of 0.22 cubic meters per minute (7.83 cubic feet per minute) at a pressure of 7 atmospheres and a temperature of 323 K. The outlet stream will have a flow of .08 cubic meters per minute (2.9 cubic feet per minute) at a pressure of 28 atmospheres and a temperature of 428 K. This compressor will have a power requirement of 5.6 kW (7.5 horsepower).

3.20 ECONOMICS

The major cost of the Lunar Fuel Processing Facility comes from transporting the materials to the Moon. The total weight of the equipment being transported to the Moon is approximately 30,000 kg. It costs $77,000 per kg to transport materials to the Moon from Earth, so the cost of the Lunar Facility is 2.31 billion dollars. This value does not include the cost of materials, which is negligible compared to the high transportation costs, or the cost of the manned control room.

Because the Lunar Fuel Processing Facility is fully automated, workers will only be needed to monitor the process and do routine maintenance. Three workers are required for EVA jobs, with another worker to stay in the control room. A total of four workers are required per twelve hour shift, therefore a total of eight workers will be needed to operate the Lunar Facility at a cost of $80,000,000 for initial training, and $800,000 per day.

3.40 *FUTURE WORK*

Though this process has been extensively optimized, there is room for improvement in the reduction of weight of many pieces of equipment. This could be accomplished through the use of lunar glass in as many pieces of equipment as possible. A detailed study should be performed on the costs of building a lunar glass making facility and these costs should be compared to the savings that would be felt by the colony. Also, fluid flow and pipe sizing was not considered within the scope of this project. Intensive communication with the other disciplines is still required to design the support structures, enclosures, and living quarters of the plant. Process control is a vital component to the operations of this plant and may occupy the full time work of several electrical engineers for months. Finally, a detailed design of an isothermal compressor should also be made.

4.00 SUMMARY

The ammonia/water mixture will be separated with a distillation column. Heat exchangers will be used to serve as a reboiler and as a condenser. The purity of the product streams is about 99 %.

The water coming from the distillation column will be stored in a tank to allow a constant flow into to the water splitter. Electrolysis was chosen to split the water due to its efficiency, reliability, safety, and cost savings. A Hamilton Standard SPE Electrolyzer will used. It has product streams which are 99.99 % pure. Due to the new technology,

the design of this cell will be left up to the manufacturer, who has a patent on it. A report in the appendix explains the operational details and considerations.

The ammonia stream from the distillation column will be split in a reactor. The hydrogen and nitrogen molecules will be separated via a membrane system. The splitting of the ammonia has an efficiency rate of 98 %.

The liquefaction of nitrogen and hydrogen is accomplished through the use of the Linde process. This process requires two shell in tube heat exchangers, two radiation heat exchangers, two compressors, two storage tanks, and two phase separators. The oxygen liquefaction will consist of one compressor and one radiation heat exchanger. The radiation heat exchangers are made of glass to utilize the natural resources on the Moon and save on transportation costs. This process will cost 1.70 Billion dollars to transport to the moon and it will have an energy requirement of 80 kW.

6.00 APPENDIX

The following is a listing of the sample calculations as they pertain to each subsystem, the stream table, and the information of the SPE electrolyzer.

6.10 SAMPLE CALCULATIONS

6.20 STREAM TABLE

6.30 SPE CELL

REFERENCES

1. Smith and Van Ness, Chemical Engineering Thermodynamics, McGraw-Hill Inc., 1987

2. Green, Don W., Perry's Chemical Engineering Handbook, 6th edition, McGraw-Hill Inc., pp. 3-196 to 3-210, 1984

3. Brown, Royce N., Compressors, Selection and Sizing, Gulf Publishing Co., pp. 50-69, 1986.

4. Sirka, Karnalosh, Membrane Handbook, Von Nostrand Reinhold, WY,NY, 1992

5. Wssler, J., Membrane Savend

6. Wang, McCray, & co., Hollow fiber air drying, Journal of Membrane Science, 72, Elsevier Science Publishers B.V., Amsterdam, pp.231-244, 1992

7. James McElroy, SPE Electrolyzer System Design Information for Lunar Oxygen/Hydrogen Generating Plant, United Technologies, Hamilton Standard Division, 1993.

8. Peters and Timmerhaus, Plant Design and Economics for Chemical Engineers, 4th Edition, New York, McGraw Hill, Inc. 1991

9. Kister, Distillation Design, New York, McGraw Hll, Inc. 1992

10. Encyclopedia of Chemical Technology, Canada, John Wiley and Sons, Inc., 1978

11. Pettit, "Fractional Distillation in a Lunar Environment", NASA Symposium, Washington, D.C., Oct. 29-31, 1984.

12. Holman, J.P., Heat Transfer, Seventh Edition, McGraw-Hill, Inc., 1990

13. Felder and Rousseau, Elementary Principles of Chemical Processes, 2nd Edition, Wiley and Sons, Inc., 1986

ACKNOWLEDGMENTS

1. Dr. Glenn Lipscomb, Department of Chemical Engineering, University of Cincinnati

2. Dr. Amy Ciric, Department of Chemical Engineering, University of Cincinnati

APPENDIX

VARIABLES DEFINED

VARIABLE	SYMBOL	VALUE	UNITS	ORIGIN
TRAY HOLE AREA	AH	0.001174	SQ. METERS	=(h/a)*Aam
MOON ACTIVE TRAY AREA	Aam			
MOON DOWNCOMER AREA	Adm			
EARTH CROSS SECT. AREA	Ae			
BOTTOMS	B	6.556	KMOLES/HR	ASPEN
DISCHARGE COEFFICIENT	Cv	0.73		KISTER p311
DISTILLATE	D	0.8824	KMOLES/HR	ASPEN
SIEVE HOLE DIAMETER	DH	0.125	INCHES	
MOON DOWNCOMER DIAMETER	Ddm			
EARTH COLUMN DIAMETER	De			
EFFICIENCY	EFF	0.9		ASSUMPTION
FEED	F	7.4384	KMOLES/HR	GIVEN
ACTIVE AREA F-FACTOR	Fga	0.542417		=vA*(pVn+1)^.5
MOON GRAV. ACCELERATION	G	1.635	M/S2	G(earth)/6
WATER	H2O			
TRAY PRESSURE DROP	HT			PETERS p309
DRY PRESSURE DROP	Hd			
LIQUID HT. OVER WEIR	How		INCHES	
WEIR HEIGHT	Hw	2	INCHES	
FLOODING VEL. CONSTANT	Kv	0.245		PETERS p656
LIQ. TO TOP STAGE	L0	0.1447136	KMOLES/HR	L0=D*R
FEED IN LIQUID PHASE	Lf	7.4384	KMOLES/HR	ASPEN
LIQ. FROM BOTTOM STAGE	Ln	7.5831136	KMOLES/HR	Ln=L0+Lf
MASS RATE OF B	MB	118.1063	KG/HR	ASPEN
MASS RATE OF Vn+1	MVn+1	18.503445	KG/HR	=(Vn+1/B)*MB
MOLECULAR WEIGHT	MW			
AMMONIA	NH3			
PITCH	P	0.5	INCHES	=4*DH
COLUMN PRESSURE DROP	Pdc			PETERS P668
CONDENSER COOLING	Qc	1478	CAL/SEC	ASPEN
ADJUSTED COND. COOLING	Qc'	208.24055	CAL/SEC	Qc'=Qc*L0/V1
REBOILER HEATING	Qr	2415	CAL/SEC	ASPEN
REFLUX RATIO	R	0.164		ASPEN
DOWNCOMER LIQUID SEAL	S	1	INCHES	
TRAY SPACING	TS	18	INCHES	
TRAY THICKNESS	TT	0.0875	INCHES	=.7*DH
VAP. FROM TOP STAGE	V1	1.0271136	KMOLES/HR	V1=D+L0

VARIABLES DEFINED

VARIABLE	SYMBOL	VALUE	UNITS	ORIGIN
FEED IN VAP. PHASE	Vf	0	KMOLES/HR	ASPEN
VAP. FROM BOTTOM STAGE	Vn+1	1.0271136	KMOLES/HR	Vn+1=V1-Vf
VOL. RATE OF B	VoB	0.1375874	M3/HR	ASPEN
VOL. RATE OF LIQUID	VoL			
VOL. RATE OF Ln	VoLn	0.1590104	M3/HR	=Ln*MW(H2O)/pLn
VOL. RATE OF Vn+1	VoVn+1	131.50992	M3/HR	=MVn+1/pVn+1
WEIR HEIGHT	W	2	INCHES	
MOLE FRACTION	Y			
AERATION FACTOR	b	0.72		KISTER p.313
HOLE AREA/ACTIVE AREA	h/a	0.0566812		=.9069(DH/P)^2
IDEAL STAGES	n	29.5		ASPEN
ACTUAL # OF STAGES	n'	32.777778		n/EFF
DENSITY OF B	pB	858.4094	KG/M3	pB=MB/VoB
DENSITY OF Ln	pLn	858.4094	Kg/M3	pLn=pB
DENSITY OF Vn+1	pVn+1	0.1407	KG/M3	=pH20 (TABLES)
DENSITY OF LIQUID	pl			
DENSITY OF VAPOR	pv			
MAX. VAPOR VELOCITY USED	v			
ACTIVE AREA VAP. VELO.	vA	6349.4885	METERS/HR	=VoVn+1/Aam
SIEVE HOLE VAP. VELOCITY	vH	112021.01	METERS/HR	=VoVn+1/AH
MAX. VAPOR VELOCITY	vmax			

EQUIPMENT LIST

	Shape	Radius(m)	Length (m)	Height (m)	Volume (m3)	Material	Weight(kg)	Rad ht ex weight	Energy Req'd (kW)
Feed tank	sphere	1.75			22.4	aluminum	2135		
Distillation column	cylinder	0.14		18		aluminum	1081		1
Ammonia reactor	sphere	1.21				titanium	1302		
N2/H2 Radiative ht ex	plates		10.17	2.54		glass		1708	
N2/H2 membrane	cylinder	0.63	4			titanium	363		
NH3 H2 compressor							50		2
SPE cells	cylinder						545		105
H2/H20 membrane	cylinder	0.43	1.5			titanium	103		
O2/H20 membrane	cylinder	0.22	2			aluminum	220		
O2 compressor							70		10
O2 Radiative ht ex	plates		6.75	1.69		glass		751	
H2 Radiative ht ex	plates		13.92	3.48		glass		3201	
H2 Compressor							68		9.8
H2/N2 ht ex		1	11.15			titanium	2003		
H2 Phase Separator	cylinder	0.46		2.76		titanium	234		
H2 storage tank	sphere	1.55			15.7	titanium	2254		
N2 compressor							182		47.1
N2 Radiative ht ex	plates		42.47	10.62		glass		29777	
N2/N2 ht ex									
N2 Phase separator	cylinder	1.11		6.63		titanium	1081		
N2 storage tank	sphere	0.84			2.5	titanium	732		
Sub totals							12423	35437	174.9

Cost in Dollars 9.57E+08

Energy Requirements (kW) ~~174.9~~

4.34

SAMPLE Calculations

- Liquefaction percentage (isenthalpic expansion)

$$h = x h_\ell + (1-x) h_g$$

where: x = fraction liquefied
h = enthalpy (KJ/Kg)
h_ℓ = enthalpy of the saturated liquid
h_g = enthalpy of the saturated gas

(example) H_2 has $h = 706.77$
$h_g = 727.1$
$h_\ell = 360.507$

equation reduces to

$$x = \left(\frac{h - h_g}{h_\ell - h_g}\right) 100$$

$$x = \frac{706.77 - 727.1}{360.57 - 727.1} = \underline{5.55\%}$$

- mixing point temperatures (for homogeneous mixing)

$$T_{mix} = \frac{m_1 T_1 + m_2 T_2}{m_1 + m_2}$$

(example) H_2 recycle

$$T = \frac{(15.22)(120) + (259.01)(27.2)}{274.23} = \underline{32.35\ K}$$

③ Adiabatic Compressor Sizing

$$\dot{V} = \frac{nRT}{P}$$

$$T_2 = T_1 \left(\frac{P_2}{P_1}\right)^{(\gamma-1)/\gamma} \qquad \gamma \approx 1.4$$

$$\text{Power} = \frac{\Delta H}{\text{efficiency}} \qquad \Delta H = \text{change in enthalpy}$$

(example) N_2 compressor

$$\Delta H = 44.55\ KJ/Kg$$

$$\frac{44.55\ KJ}{Kg \cdot hr} \left| \frac{2927.78\ Kg}{} \right| \frac{1\ hr}{3600\ sec} = 36.23\ KW$$

$$\text{Power} = \frac{36.23}{(83\%)^3} = \underline{63.36\ KW}$$

$$\dot{V} = \frac{nRT}{P} = \frac{(104563.57\ \text{moles})(82.06)(134.5\ K}{1\ ATm}$$

$$\dot{V} = 1.15 \times 10^9\ cm^3/hr = \underline{676\ ft^3/min}$$

$$T_2 = 134.5\ K \left(\frac{33.5}{1}\right)^{(1.4-1)/1.4}$$

$$T_2 = \underline{366.8\ K}$$

Feed Tank - Aluminum sphere

Must be able to store all the liquid Ammonia/water mixture For a period of 14 days at double capacity.

$$800 \frac{kg\ ice}{day} \times 14\ days \times Double\ capacity = \underline{22{,}400\ kg\ ice}$$

$$V = 22{,}400\ kg \left| \frac{1L}{1kJ} \right| \frac{1m^3}{1000L} = 22.4\ m^3$$

$$V = \frac{4}{3}\pi r^3 \qquad \underline{r = 1.75\ m} \quad \text{Radius of Tank}$$

Thickness of Tank

$$t = \frac{P_s \cdot r}{2 \cdot S \cdot E_j - .2 P_s} + C_c$$

$$= \frac{1atm \cdot 1.75\ m}{2 \cdot 114.5 atm \cdot .8 - .2\ atm} + .01\ m$$

$$= .0096\ m + .01\ m = \underline{1.96\ cm}$$

P_s = Safety/Max Pressure = $1.15(P + 25_{psi})$

S = yield stress of metal = 114.5 atm For Aluminum

E_j = weld efficiency = 0.8

C = corrosion allowance = .01 m

ρ = density of Aluminum = $2.8 \times 10^3 \frac{kg}{m^3}$

Weight of Tank

$$\omega_V = \rho \frac{4}{3}\pi \left[(r+t)^3 - r^3\right] = \left(2.8 \frac{kg}{m^3} \cdot 10^3\right) \pi \frac{4}{3}\left[(1.75 + .0196)^3 - (1.75m)^3\right]$$

$$= \underline{2{,}135\ kg = 4{,}706\ lbs}$$

NH_3 Reactor - titanium sphere

6.67 kg/hr NH_3 $\quad NH_3 \rightarrow \frac{1}{2}N_2 + \frac{3}{2}H_2$ at 800 K

$$6.67\ \frac{kg}{1hr}\left|\frac{1000g}{1kg}\right|\frac{1mol}{17g} = 392.4 \text{ moles } NH_3 \longrightarrow \frac{1}{2}(392.4 \text{ moles})N_2) + \frac{3}{2}(392.4 \text{ moles})H_2$$

784.7 moles $N_2 + H_2$ gas

$PV = nRT$

$V = (784.7 \text{ moles})(0.082 \frac{L\,atm}{K\,mol})(800K)/7atm$

$= 7,362.8\ L$

$= 7.36\ m^3$

Spherical tank $V = 7.36\ m^3$

$V = \frac{4}{3}\pi r^3$

$r = 1.21\ m$

Hydrogen Gas Storage Tank – titanium sphere

$$\frac{109\ kg}{hr}\left|\frac{1000\ g}{1\ kg}\right|\frac{1\ mol\ H_2}{2\ g\ H_2}\left|\frac{1\ hr}{60\ min}\right|\ 15\ min\ residence\ time = 13{,}625\ moles\ H_2\ /ss$$

$PV = nRT$

$$V = \frac{(13{,}625\ moles\ H_2)\left(0.0821\ \frac{L\cdot atm}{K\cdot mol}\right)(400\ K)}{28.5\ atm} = 15.70\ m^3$$

$V = \frac{4}{3}\pi r^3$ $\quad r = 1.55\ m$ $\quad t = 1.48\ cm$ $\quad w_v = 2{,}254\ kg$

$= 4{,}970\ lbs$

Hydrogen Phase Separator – Titanium Cylinder

$$\frac{93.73\ kg}{hr}\left|\frac{1000\ g}{1\ kg}\right|\frac{1\ mol\ H_2}{2\ g\ H_2}\left|\frac{1\ hr}{60\ min}\right|\ 5\ min\ residence\ time = 3{,}905.42\ kg$$

$$V = \frac{nRT}{P} = \frac{(3{,}905.42\ kg)\left(0.0821\ \frac{atm\cdot L}{K\cdot mol}\right)(270\ K)}{4.7\ atm} = 1.84\ m^3$$

$V = \pi r^2 \cdot h$ $\quad r = .46\ m = 1.5\ Ft$ $\quad t = 5.0\ mm$

$6 \cdot r = h$ $\quad h = 2.76\ m = 9.1\ Ft$ $\quad w_v = 234\ kg$

$= 516\ lbs$

CALCULATIONS

DISTILLATION COLUMN DESIGN

STEP 1: MAXIMUM VAPOR VELOCITY

EQ.1: vmax=Kv((pl-pv)/pv)^.5

		FEET/SEC	METERS/HR
FOR BOTTOM:			
vmax=Kv((pLn-pVn+1)/pVn+1)^.5=		19.1	20997
USE v=vmax*2/3	v=	12.8	13998

STEP 2: DIAMETER OF COLUMN

EQ.2: Ae=Vo/v EQ.3: D=(4Ae/Pi)^.5

		SQ. INCHES	SQ. METERS
FOR BOTTOM: Ae=VoVn+1/v	=	14.562441431125	0.0093951047137
		INCHES	METERS
De=(4Ae/Pi)^.5	=	4.3059814558354	0.10937192897822

STEP 3: CONVERT EARTH TRAY SIZE TO MOON

EQ.4: Am=Ae*6^.5 EQ.5: Dm=(4Am/Pi)^.5

		SQ. INCHES	SQ. METERS
FOR BOTTOM:	Am=	35.670550915422	0.02301321262859
		INCHES	METERS
	Dm=	10.547457408683	0.26790541818056

CALCULATIONS

DISTILLATION COLUMN DESIGN

STEP 4: DOWNCOMER AND ACTIVE TRAY SIZE

EQ.6: Adm=0.05Am EQ.7: Ddm=(4Adm/Pi)^.5

	SQ. INCHES	SQ. METERS
Adm=	1.7835275457711	0.00115066063143

	INCHES	METERS
Ddm=	1.5069365615049	0.03827618866222

EQ.8: Aam=Am-2(Adm)

	SQ. INCHES	SQ. METERS
Aam=	32.10349582388	0.02071189136573

STEP 5: RESIDENCE TIME

EQ.9: Rt=Adm*TS/VoL

FOR BOTTOM: Rt=Adm*T S/VoLn = 11.910510418859 SECONDS

CALCULATIONS

DISTILLATION COLUMN DESIGN

STEP 6: PRESSURE DROP

EQ.10: Ht=Hd+Hl

EQ.11: Hd= 0.186*(pv/pl)*(vH/Cv)^2

FOR BOTTOM:

Hd=0.186*(pVn+1/pLn)*(vH/Cv)^2= 0.59625341742627 INCHES

EQ.12: Hl=b*(Hw+How) EQ.13: How=0.20*(VoL*4.4029/(Ddm))^(0.704)

FOR BOTTOM:

How=	0.11658613157116	INCHES
b=	0.72	INCHES
Hl=	1.5239420147312	INCHES
Ht=Hd+Hl=	2.1201954321575	INCHES/TRAY

EQ.14: Pdc=pL*G*Ht*n'

FOR BOTTOM: Pdc=pLn*G*Ht*n'= 2.4774296915672 KPa

N2-H2 MEMBRANE

Material Properties		Feed Conditions		BoreSide Crossflow Version 2.6
PH2 :	1.72E-07	T (C) :	30.0	
Alpha :	180.00	Fraction n2:	0.2500	
OD ,Micron :	400.0	Rate ,Scfm :	1.10E+01	
ID ,Micron :	300.0	Shell ,Psia:	14.7	
Fiber # :	5.00E+06	Bore ,Psia :	114.7	
Length ,Cm :	400.0	Mu ,Poise :	1.80E-04	
Discretization		**Results**		
Increments		DP ,Psia :	2.92E-03	
		N2 RETENTATE	0.2449	
Numerical		RE-TATE SCFM	2.69E+00	
Error ,% :	1.96E-03	Area ,Cm2 :	2.51E+08	

5/2 10:55

R = 0.632 m

L = 4 m

O2-H2O MEMBRANE				
Material Properties		Feed Conditions		BoreSide Crossflow Version 2.6
PH2O	2.30E-03	T (C) :	50.0	
Alpha :	30000.00	H2	0.9800	
OD ,Micron :	600.0	Rate ,Scfm :	4.90E+01	
ID ,Micron :	500.0	Shell ,Psia:	14.7	
Fiber # :	5.00E+05	Bore ,Psia :	114.7	
Length ,Cm :	200.0	Mu ,Poise :	1.80E-04	
Discretization		Results		
Increments		DP ,Psia :	2.34E-02	
		Inert Rec. :	0.9625	
Numerical		Inert ,Scfm:	4.72E+01	
Error ,% :	5.18E-10	Area ,Cm2 :	1.88E+07	

5/2 11:15

R=0.212

L=2m

H2-H2O MEMBRANE				
Material Properties			Feed Conditions		BoreSide Crossflow Version 2.6
PH2O		2.30E-03	T (C) :	50.0	
Alpha	:	30000.00	H2	0.9800	
OD ,Micron	:	600.0	Rate ,Scfm :	9.80E+01	
ID ,Micron	:	500.0	Shell ,Psia:	14.7	
Fiber #	:	1.00E+06	Bore ,Psia :	114.7	
Length ,Cm	:	150.0	Mu ,Poise :	1.80E-04	
Discretization			Results		
Increments			DP ,Psia :	1.76E-02	
			Inert Rec. :	0.9718	
Numerical			Inert ,Scfm:	9.52E+01	
Error ,%	:	1.30E-10	Area ,Cm2 :	2.83E+07	

5/2 11:15 pm

Retentate = 0.985 H_2

R = 0.424 m

L = 1.5 m

Radiation Heat Exchanger: Stream 24					
Nitrogen					
1.03	Cp (kJ/kg K)		Q=m*Cp*dt		
			75.4329564	kJ/s	
277.06	Temp. in (K)				
130	Temp. out (K)		A=Q/(e*sigma*(Tavg^4-Ts^4))		
113	Temp. space (K)		901.7791297	m^2	
203.53	Temp. avg (K)				
			Cp=6.5+.001*T	(cal/K*mol)	
0.95	emissivity				
5.67E-11	sigma (kJ/s m^2 K^4)				
0.498	m (kg/s)				
2-sided radiation heat exchanger					
901.77913	Total Surface Area (m^2)				
450.889565	Area of HX (m^2) per side				
10.6170802	Height of HX (m)	34.8325166	Height of HX (ft)		
42.4683207	Length of HX (m)	139.3300664	Length of HX (ft)		
Radiation Heat Exchanger: Stream 13					
Hydrogen					
14.43	Cp (kJ/kg K)		Q=m*Cp*dt		
			13.09885559	kJ/s	
334.7	Temp. in (K)				
120	Temp. out (K)		A=Q/(e*sigma*(Ti^4-Ts^4))		
113	Temp. space (K)		96.9381051	m^2	
0.95	emissivity		Cp=6.62+.00081*T	(cal/K*mol)	
5.67E-11	sigma (kJ/s m^2 K^4)				
4.23E-03	m (kg/s)				
2-sided radiation heat exchanger					
96.9381051	Total Surface Area (m^2)				
48.4690525	Area of HX (m^2) per side				
3.48098594	Height of HX (m)	11.42041868	Height of HX (ft)		
13.9239438	Length of HX (m)	45.68167473	Length of HX (ft)		

Radiation Heat Exchanger: Stream 16					
Oxygen					
0.858	Cp (kJ/kg K)		Q=m*Cp*dt		
			9.596417688	kJ/s	
478	Temp. in (K)				
120	Temp. out (K)		A=Q/(e*sigma*(Ti^4-Ts^4))		
113	Temp. space (K)		22.75458529	m^2	
0.95	emissivity		Cp=8.27+.000258*T-187,700/T^2		
5.67E-11	sigma (kJ/s m^2 K^4)				
3.12E-02	m (kg/s)				
2-sided radiation heat exchanger					
22.7545853	Total Surface Area (m^2)				
11.3772926	Area of HX (m^2) per side				
1.68651213	Height of HX (m)	5.533108993	Height of HX (ft)		
6.74604852	Length of HX (m)	22.13243597	Length of HX (ft)		
Radiation Heat Exchanger: Stream 15					
Nitrogen/Hydrogen					
3.39	Cp (kJ/kg K)		Q=m*Cp*dt		
			254.48052	kJ/s	
800	Temp. in (K)				
300	Temp. out (K)		A=Q/(e*sigma*(Ti^4-Ts^4))		
113	Temp. space (K)		51.7215635	m^2	
550	Temp avg (K)				
0.95	emissivity		Cp=8.27+.000258*T-187,700/T^2		
5.67E-11	sigma (kJ/s m^2 K^4)				
1.50E-01	m (kg/s)				
2-sided radiation heat exchanger					
51.7215635	Total Surface Area (m^2)				
25.8607817	Area of HX (m^2) per side				
2.54267486	Height of HX (m)	8.342007677	Height of HX (ft)		
10.1706994	Length of HX (m)	33.36803071	Length of HX (ft)		

5.0 PROPELLANT STORAGE

Department of Aerospace Engineering and Engineering Mechanics
J. Matt Campbell
Chris Staneluis

TABLE OF CONTENTS

THE CRYOGENIC LUNAR STORAGE FACILITY

The design of the lunar storage facility considers many of the requirements needed for a safe, cheap, and efficient facility for a lunar base. The design comprises of common materials used in cryogenics on the earth, a simple construction, flexibilty of storage, product conservation, and human and safety factors.

From the cryogenic production facility, a 110 m pipeline will carry the product to the tank farm. The pipeline has a 10 m section between two 50m straight sections that runs perpendicular to these straight sections (see Figure 1). This layout considers a 100 m distance from the production facility for safety purposes and the perpendicular section for expansion relief for the broad lunar temperature range. Also for safety and ease of maintenance, the LOX and LH lines are seperated 25 m. This distance, combined with the lack of lunar atmosphere, will adequately decrease the probability of an explosive interaction between the two materials. All parts of the facility will be well spaced to allow freedom of maintenance and safety. The piping itself will be layed out in 10 m secitons. These secitons are easy to transport but are long enough to reduce connection leakage. The pipe will be made of 304L stainless steel for its availability, compatiblity with both cryogenic fluids, strength, and a relatively small coefficient of thermal expansion. The piping will have an inner pipe within which the product will be transported and an outer pipe to add protection and an extra radiation shield to the inner pipe.

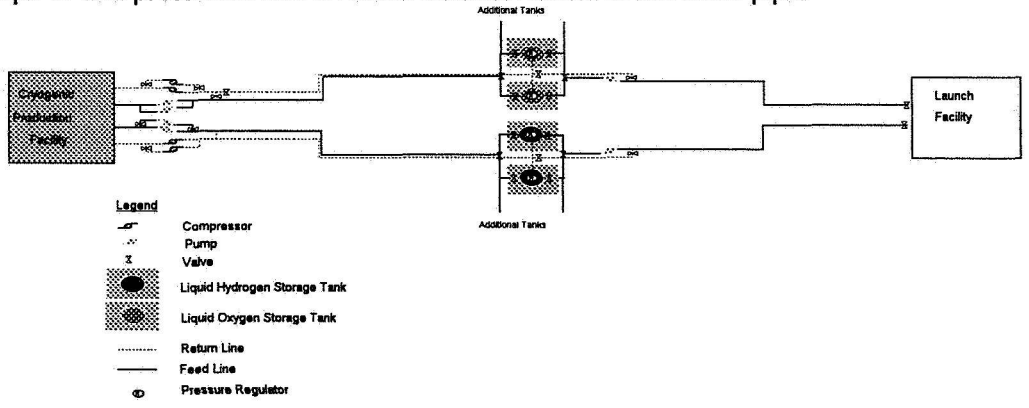

Figure 1

Fluid will be propelled by centripetal pumps capable of raising pressures up to 7000 kPa and using dc motors driven by 2983 W. In the case of pump or compressor failure, a spare pump or compressor will be located at each pump and compressor location. Fluid will be controlled by two way valves capable of stopping or allowing fluid passage, three way valves which only direct flow, and

release valves to maintain correct system pressure. These valves will computer controlled from the lunar base and will only require one technician to overview the operation. Also at the control facility, product flow will be monitored via a doppler ultrasonic flow meter oriented in a diagonal fashion coupled with a third transducer to measure changes in fluid density. Strain gagues on a pressure sensing tube will measure tank pressure, and an ultrasonic level sensor will measure fluid level within the tanks.

The storage tank and hexagon shell system is designed for projectile and radiation protection, conservation of boiloff product, and ease of lunar construction. The storage tank for the liquid oxygen will be made of stainless steel because of its good compatability with oxygen. The liquid hydrogen tank will be made of titanium because of its strength to weight ratio and its good compatability with hydrogen. The tanks are cylindrical in shape with hemispherical ends. A multi-layered aluminized mylar heat shield surround each tank to reflect radiation. A support structure with four verticle legs reinforced by eight cross members are attached to the lower hemisphere of each storage tank. This support structure will be welded on earth before launch. The shell system consists of six flat panels, six verticle beams, and a cover. The panels slide into a grove in the beams and the panel will be fastened to the top of the beams. This construction will ease assembly and maintence. The panels will be fabricated from stainless steel and polished to a shine. The beams will also be fabricated from stainless steel and are grounded to reduce any charge on the shell surface. A reduced charge should reduce dust build up on the shell surface. Both the beams of the shell system and the verticle support legs will be fastened to a concrete surface produced on site.

Product is to be fed into the storage tank through the side of the tank, released to the launch pad through the bottom of the tank, and the boiloff will be guided back to the production plant from the top of the tank. The boiloff product is returned to the production facility by a compressor driven system originating at the production facility.

3.0 ANALYSIS

3.1.0 Pressure Vessel

The pressure vessels was analyzed using the Ansys 4.4a finite element program. Several tests were performed to insure the model's integrity. Among the verifications performed are a free edge check, to verify that there are no "cracks" in the model, and an element warping check, to verify that there are no poorly shaped elements. Also, for this model the legs were not modeled and are assumed to hold the vessel rigidly. The vessel thicknesses were varied to account for the different expansion rates of a cylinder and a hemisphere under a uniform pressure. Therefore, different thicknesses are imposed to help create an even welded joint. The piping joints are modeled as a hole cut in the vessel wall without a filleted connection. This results in elevated stresses in the joint regions. The true stresses in the pipe joint regions are lower than those predicted by this analysis because a filleted connection is in the actual design. The modeling parameters and results are tabulated below:

Pressure Vessel	Liquid Oxygen	Liquid Hydrogen
Material	304 Stainless Steel	Ti-5 Al-2.5 Sn Titanium
Young's Modulus	174E9 Pa (25.3 ksi)	126E9 Pa (18.3 ksi)
Yield Strength	151E10 Pa (220 ksi)	148E10 Pa (215 ksi)
Poisson's Ratio	0.28	0.28
Density	8.0E3 kg/m^3 (0.75E-3 lbm/in^3)	4.49E3 kg/m^3 (0.42E-4 lbm/in^3)
Nodes	1,795	1,795
Elements	1,852	1,855
Degrees of Freedom	10,390	10,390
Weight	17,540 N (3,943 lbs; half model)	9,808 N (2,205 lbs; half model)
Volume	18 m^3	18 m^3
Fluid Storage Pressure	5.5E6 Pa (800 psi)	2.1E6 Pa (300psi)
Von Mises Stress	1.42E9pa (20,600psi)	3.41E8 Pa (49,500 psi)
Safety Factor	1.1	4.3
Max. Displace. - upper hemisphere	3.81 mm (0.15 in)	2.03 mm (0.08 in)
Max. Displacement - cylinder	3.56 mm (0.14 in)	1.52mm (0.06 in)
Von Mises (psi) - Input pipe	206,000	49,500
Factor of Safety - Input pipe	1.1	4.3
Von Mises (psi) - Output pipe	120,000	30,000
Factor of Safety - Output pipe	1.8	7.2
Von Mises (psi) - General Model Surface	84,000	20,000
Factor of Safety - General Model Surface	2.6	10.8

Table 1: Pressure Vessel Analysis Results (see figures 9-12)

Pressure Vessel	Liquid Oxygen	Liquid Hydrogen
Nodes	36	36
Elements	44	44
Degrees of Freedom	216	216
Mass	0.647 kg (1.39 lbm)	0.307 kg (0.6778 lbm)
Volume	18 m^3	18 m^3
Axial Force (P)	1.14E5 lbf	7.5E5 lbf
Axial Stress	63,513 psi	39,790 psi
Buckling Ratio (P/P_{cr})	0.74	0.76
Max. Displace - Vertical	.14 in	.12 in
Max. Displace. - Horizontal	.14 in	.08 in

Table 2: Support Structure Pressure Vessel (See figures 13-14)

2.0 Heat Transfer

The heat transfer analysis performed for this project was done by modeling each area of interest. Thus, with the proper assumptions made, the heat flux was calculated applying the Newton-Raphson numerical method using a FORTRAN code with a mesh size of .0001.

The six-sided shell is considered to be oriented with two of the six points on the equator and two of the six panels are parallel to it. To find the heat flux through the shell and vessel, the temperature of the outer surface of the shell is needed as well as the temperature of the inner wall of the pressure vessel. During the lunar day of 14 earth days, in general, this temperature is the result of the solar load on the shell and the load from the radiation of the lunar surface. This daytime temperature flux changes on the shell as a function of the sun's angle. During the lunar night of 14 earth days, the temperature of the shell is the result of the lunar heat flux radiating into space. The temperature of the inner vessel wall is considered to be the minimum temperatures of 33.25 K for hydrogen and 154.34 K for oxygen.

To find the shell temperature during the lunar day, a proper model needs to be constructed. The heat balance equation is solved using data from the Surveyor 6 lunar mission,

$$\varepsilon_S \sigma T_S^4 = \varepsilon_S \varepsilon_L F_{SL} \sigma T_L^4 + \alpha_S S(\cos\beta + A F_{SL} \sin\psi) \qquad (2.1)$$

Shell Temperature = Lunar Load + Solar Load

Where the subscripts S and L are for the shell and lunar surface respectively, ε is the emisivity of the surface, σ is the Stefan-Boltzman constant, T is the temperature, F is the view factor, α is the absorbtivity

(for a diffuse system $\alpha/\varepsilon=1$), S is the solar flux (1430 W/m^2), β is the angle of solar incidence, A is lunar albido, and ψ is the lunar sun angle. The lunar surface temperature is solved by the Lambertian temperature profile for the lunar day,

$$\sigma T_L^4 = (1-A)S\sin\psi \qquad (2.2)$$

The variables of (2) correspond to those of (1). The lunar night temperature data is interpolated from the Surveyor 6 and Apollo 11 with the thermal constant, γ=800, where γ is the inverse of the thermal inertia.

The shell temperatures are solved by considering the heat flux "seen" by each of the six side panels and by the top panel of the shell. The shell is assumed to be located directly on the equator such that only the panels skewed to the equator and the top of the shell see direct solar flux. With this consideration, the view factors for each panel are found to be 0.33. The heat balance equation also considers the lunar surface and the shell surface to be completely diffuse (i.e. the amount of radiation absorbed is equal to the amount of radiation reflected). Although the shell will have a highly polished surface, the worst case of dust accumulation is considered in the analysis.

With the shell surface temperature known, the heat balance of the shell and vessel system can now be solved. This balance describes the energy entering the vessel and the proportional amount of vaporizing liquid product. The assumptions made for this system are as follows: (1) Constant Q, (2) Conduction through all layers, (3) Reflectivity between layers, (4) Infinite parallel plates, (5) Mylar layers considered to be seperate radiation shields, (6) gray body radiation, (7) all metallic surfaces are highly polished, and (8) the pipes do not conduct into the system.

The assumptions help form the heat flux resistance model (figure 2) that is in the computer code.

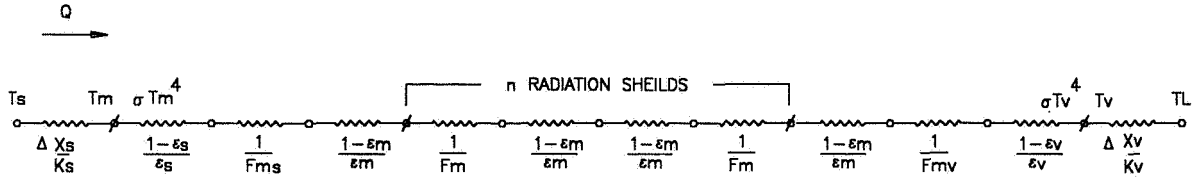

Heat Flux Resistance Model
Figure 2

The design of the structure is optimized by considering an average maximum loss of 0.1% of volume per day for both liquid oxygen and liquid hydrogen. This value is a commercially accepted loss rate. Thus, using the wall thicknesses found in the structures analysis, the mylar thickness is 2.15 cm for hydrogen and .38 cm for oxygen (1cm=100 layers of mylar). The heat flux results corresponding to the maximum loss rate are found in figures 3 and figure 4.

The results for the liquid oxygen are,

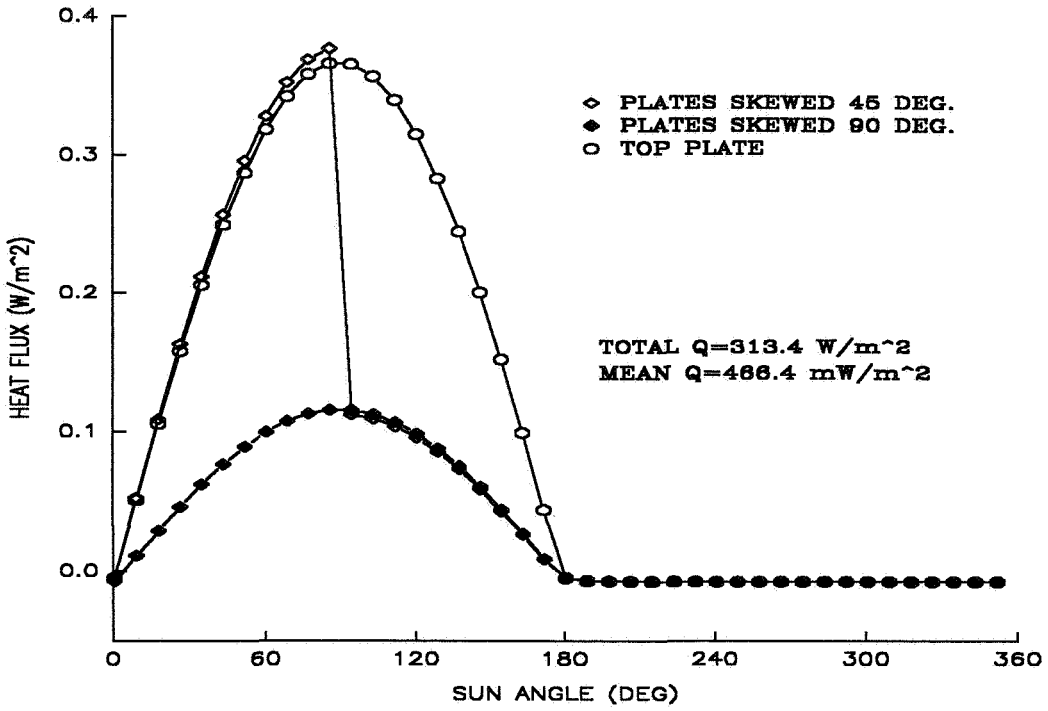

Heat Flux of Liquid Oxygen
Figure 3

The results for the liquid hydrogen are,

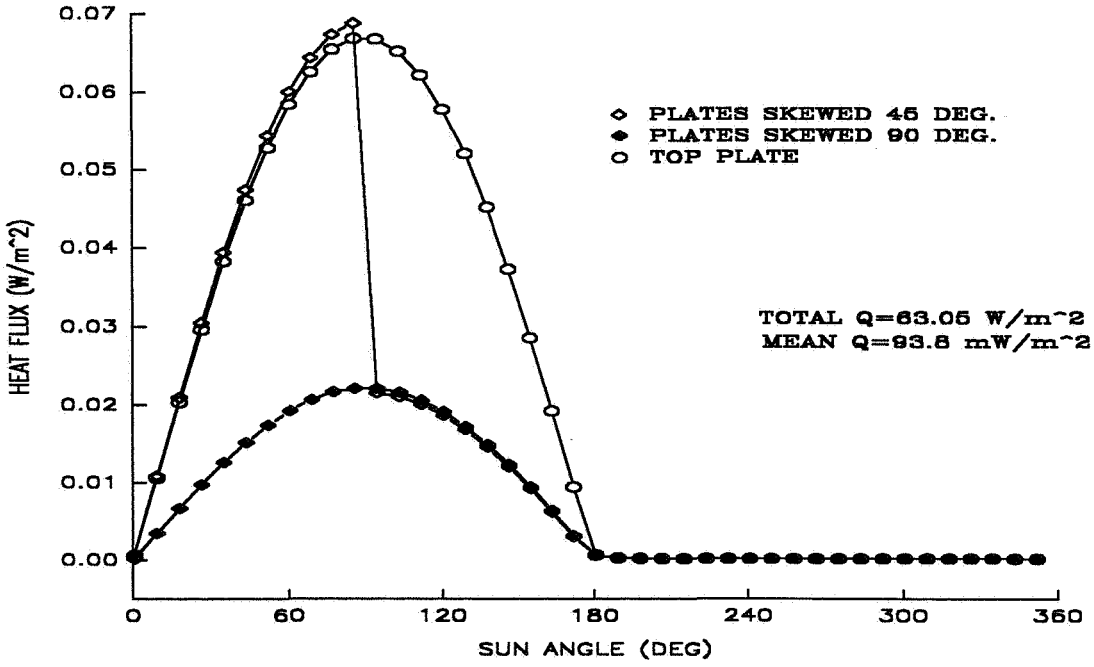

Heat Flux of Liquid Hydrogen
Figure 4

The support heat flux is calculated to complete the total energy balance of the shell and vessel system. Since the support surface area contacting the vessel is much smaller than the surface area of the vessel, the heat flux from supports is considered very small and only simple hand calculations were performed. The supports are modeled considering their geometry and also considering the concrete pad below it. Thus, the final results for the heat flux through all four supports are .01 Watts. Because of the small contact area, the amount of product affected will be minimal.

3.0 Piping system

A thermal stess analysis was conducted for the oxygen and hydrogen piping systems to determine the allowable stress range, the pipe thickness, schedule, reaction forces, bending moments, and expansion stresses at each support and elbow. The assumptions made in order to simplify the piping analysis are: each connection is a right angle, the pipes have a constant cross sectional area, the number of full temperature cycles is 240 cycles for a twenty year period, the operating temperatures are -101 ^{o}C and 141 ^{o}C, and there are only two anchors and no intermediate restraints. This analysis computed the allowable stress from expansion, minimum wall thickness, the reaction forces and moments in the piping system, the rotations and deflections, and the minimum distance for the piping supports.

3.1 Pipe Sizing

In order to minimize frictional losses, the diameters of the pipes were chosen such that the flows through the pipes would be laminar. The production rates of liquid hydrogen and liquid oxygen are 8.2 kg/hr (18 lb/hr) and 63.6 kg/hr(140 lb/hr) respectively. The volumetric flow rates derived from these weight flow rates are 5.24e-5 m^3/s and 2.60e-5 m^3/s for hydrogen and oxygen respectively. Laminar flows have Reynold's numbers which are less than 2000. To insure laminar flow the Reynold's number was set at 1800. Employing equations 3 -5 the pipe diameters were determined to be .16 m (6.33 in) for the hydrogen and .25 m (9.85 in) for the oxygen.

$$\mathrm{Re} \equiv \frac{\rho V d}{\mu} \tag{3.1}$$

$$V = \frac{4Q}{\pi d^2} \tag{3.2}$$

$$d = \frac{4\rho Q}{\pi \mu \mathrm{Re}} \tag{3.3}$$

Where :
V = Fluid Velocity
d = Pipe Diameter
Q = Volumetric Flow Rate
ρ = Fluid Density
μ = Fluid Viscosity

ASME piping standards recommend that these diameters be changed to .15 m (6.06 in) and .26 m (10.25 in) respectively. A more elaborate description of the selection of these diameters will be given in section 2.4.

As previously mentioned, repairability is a key design parameter. For this reason, most sections of pipe will have a length of 10 m. With this length, transporting spare piping sections to repair locations will be easier than transporting sections of pipe which are larger. At the same time, minimizing the number of pipe connections provides less opportunity for leakage. Thus, 10 m pipe sections are more advantageous than smaller sections of pipe.

3.1.1 Pumps and Compressors

Before pump selection was performed, the pressure differential required to transport the fluids was determined. In this analysis pressure losses occuring from pipe friction and turning of the flow were modeled. In figure 5, the points of interest in the piping system are numbered. The subscipts of the variables of equations (3.4-1), which were used to determine the pressure differential, are the same as the numbers in figure 5.

Key Analysis Points of Piping System

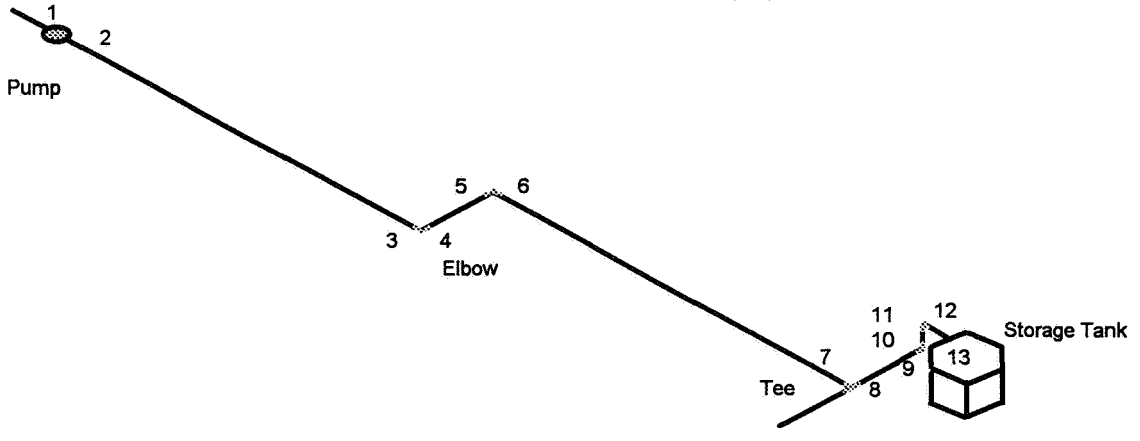

Figure 5

The following assumptions were made in order to determine the required pressure differential that the pump must produce :

- The pressure of the fluid as received from the plant (station 1 in above figure) is the same as the pressure within the tank (station 13.)
- Assume fluid is incompressible. Therefore, since piping diameter is contant, the fluid velocity at each of the stations is constant.
- All elbows and tees are modeled with equivalent (l/d) ratios.

From the volumetric flow rates and the pipe diameter the velocity of the flow for the hydrogen and the oxygen lines was determined using the relationship describe in equation (3.4).

$$V = \frac{4\rho Q}{\pi d} \tag{3.4}$$

$V_H = 2.57 \times 10^{-3}$ m/s

$V_O = 5.29 \times 10^{-4}$ m/s

The ith station and the next station in the piping system are related by equation (3.5)

$$P_i + \frac{\rho V_i^2}{2} + \rho g Z_i + \rho g H_{p_i} - \rho g H_{f_i} = P_{i+1} + \frac{\rho V_{i+1}^2}{2} + \rho g Z_{i+1} \tag{3.5}$$

Where :
P = Fluid Static Pressure
ρ = Fluid Density
V = Fluid Velocity
g = Gravitational Constant
H_p = Pump Head
H_f = Frictional Head

The frictional head is expressed with equation 3.6.

$$H_f = f \frac{l}{d} \frac{V^2}{2} \tag{3.6}$$

Because the flow is laminar this equation can be simplified to equation 3.7.

$$H_f = \frac{32 \mu l V}{\rho d^2} \tag{3.7}$$

Combining equation 3.7 with equation 3.5 allows for the determination of the required differential pressure or pump head. With the assumptions mentioned previously applied, equation 3.8 is the used to determine the pump head.

$$Hp = \frac{1}{\rho g}\frac{32\mu V}{d^2}(l_{2:3} + 4l_{elbow} + l_{tee} + l_{4:5} + l_{6:7} + l_{10:11} + l_{12:13}) + (Z_{13} - Z_1) \qquad (3.8)$$

Where :
l_{elbow} = Equivalent length of elbow (30*d)
l_{tee} = Equivalent length of tee (60*d)
$l_{2:3}$ = Length from station 2 to station 3

The pressure differential required to transport the cryogenic fluids are:

ΔP_O = 2290 Pa

ΔP_H = 146 Pa

After determining the required pressure differential, the next step is to find pumps and compressors which will satisfy are needs. After consulting with several companies for information regarding cryogenic pumping, pump specifications regarding pumps are determined. The pumps to be used in the design are centripetal pumps capable of raising pressures up to 7000 kPa. Flow rates of 0.132 m^3/s (3.5 gal/min) can be handled. The pumps are driven by 4 hp motors dc motors.

The return line will use 13.6 Mpa compressors with a storage capacity of 60.6 m^3.

3.2.0 Piping Problem Definition

A thermal stress analysis was conducted for the oxygen and hydrogen piping system to determine the allowable stress range, the pipe thickness, schedule, reaction forces, bending moments and expansion stresses at each support and elbow. The deflections and rotations are calculated for points' b and c (refer to figure 2.1). By comparing the expansion stress to the allowable stress for each connection, any modifications that may be required to reduce the expansion stress can be determined. In order to insure that the material selected is safe against the internal effects due to pressure and temperature conditions, and to provide sufficient flexibility for the thermal expansion of the pipe system, some corrections to the piping system are covered in the conclusion section to help reduce the expansion stress. The distance between piping supports is also calculated.

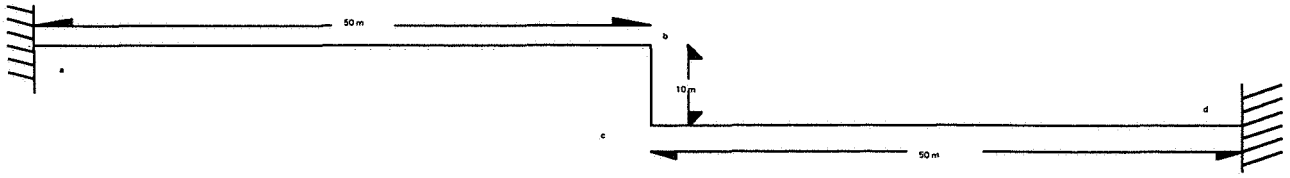

Figure 6: Geometry and Supports

Assumptions

Several assumptions are made in order to simplify the piping analysis (refer to figure 6).

- Each connection is a right angle
- The pipe has a constant cross sectional area
- The number of full temperature cycles:

  1 cycle/month x 12 months/year x 20 years = 240 cycles
- The operating temperatures are -150 °F and 285 °F
- There are only two anchors and no intermediate restraints

3.2.1 Material Selected

The piping material is stainless steel 304 (piping grade ASTM A312 TP 304L) due to its ability to withstand extreme conditions brought on by the lunar environment. It is easy to weld, has low heat conductivity, and requires no stress relief. The properties being used in this analysis are:

- Thermal Expansion Range: 6.5×10^{-6} / °F
- Modulus of Elasticity: 24.1×10^{6} psi = 8.398×10^{9} N/m^2
- Poisson's Ratio: 0.3

3.2.2 Allowable Stress

Expansion stress (Se) is the maximum stress due to thermal changes. It is based on the modulus of elasticity in the cold condition and for the total expansion range from the maximum to the minimum operating temperatures.

Allowable stress (Sa) = f (1.25 x Sc + 0.25 x Sh)

Where

Sc = Basic material allowable stress at the minimum operation temperature (-150 °C)
= 20,000 psi

Sh = Basic material allowable stress at the maximum operating temperature (120 °C)
= 18,400 psi

f = Stress range reduction factor for cyclic conditions for total number N of full temperature cycles over total number of years during which the system is expected to be in operation. There are 240 full temperature cycles (from above).

f = 1.0 for 7,000 full temperature cycles of less

Sa = 29,600 psi = 2.0391 x 10^8 N/m^2

3.2.3 Computation of Minimum Pipe Wall Thickness

By using the internal service pressure and the nominal pipe diameter (calculated from section 3.1), the thickness of the pipe wall is calculated.

$t_{min} = P D_o / (2 (S + P y) + C$
$t_{nom} = t_{min} / M$

Where

t_{min}= Minimum required wall thickness (in)
P = Internal design service pressure (plus 10% over)
Plus atmospheric pressure to compensate for no atmosphere
730 x (1.10) + 15 psi = 813 psi
D_o = Nominal Diameter of pipe (in)
S = Maximum allowable stress (psi)
C = Allowance for threading or corrosion (in)
0.065 in for stainless steel
y = 0.4 for stainless steel
t_{nom}= Nominal or standard wall thickness (in)
M = Manufacturers tolerance
0.876 for steel pipes

Using this thickness and nominal pipe diameter the schedule may be chosen from the ASTM piping guidelines. Their properties are listed below.

	Schedule	O.D. (in)	I.D. (in)	Thickness (in)	Moment (in^4)	Section Modulus (in^3)
Hydrogen	40	6.625	6.065	0.280	28.14	8.50
Oxygen	20	10.750	10.250	0.250	113.52	21.12

Table 3: Pipe Thickness and Diameter

3.2.4 Calculate Reaction Forces

The reaction forces at the supports (refer to figure 7) is directly related to the expansion of the pipes as well as the geometry of the pipe system. These relationships are shown below.

$$F_x = \frac{I_y (\Delta_x EI) + I_{xy} (\Delta_y EI)}{I_x I_y - I_{xy}^2}$$

$$F_y = \frac{I_x (\Delta_y EI) + I_{xy} (\Delta_x EI)}{I_x I_y - I_{xy}^2}$$

3.2.5 Calculate Reaction Moments

The reaction moments at each support and elbow are calculated to determine the expansion stress. The relation of the reaction moments to the reaction forces is given below.

$M = F_x * y + F_y * x$

	Fx (N)	Fy (N)	Ma (N-m)	Mb (N-m)	Mc (N-m)	Md (N-m)
Hydrogen	8.57	2.466	166.15	42.85	42.85	166.15
Oxygen	34.41	9.9025	667.175	172.05	172.05	667.175

Table 4: Pipe expansion forces and moments

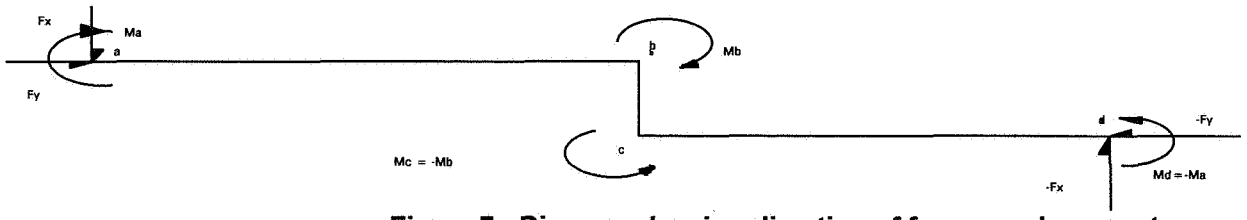

Figure 7: Diagram showing direction of forces and moments

3.2.6 Calculate Forces and Moments in Cold Condition

To calculate the moments and forces in the cold conditions, the factor Ec/Eh which is the ratio of the modulus of elasticity in the cold condition to the modulus of elasticity in the hot condition is multiplied by the forces and moments in the hot condition.

$F = F(E_c/E_h)$
$M = M(E_c/E_h)$

$E_c/E_h = 27.9 \times 10^6 / 24.1 \times 10^6 = 1.158$

For hydrogen:
$M_a = -667.17 \times 1.158 = -772.58$ N-m
$M_b = -49.62$ N-m
$M_c = 49.62$ N-m
$M_d = 772.58$ N-m
$F_x = -9.92$ N
$F_y = -11.47$ N

For oxygen:
$M_a = -166.15 \times 1.158 = -192.4$ N-m
$M_b = -199.23$ N-m
$M_c = 199.23$ N-m
$M_d = 192.4$ N-m
$F_x = -39.85$ N
$F_y = -2.86$ N

3.2.7 Calculate Expansion Stresses

The expansion stress should not exceed the allowable stress calculated from above. The expansion stress equal to the reaction moment divided by the section modulus.

$S = M / Z$
Z = Section Modulus (m^3) = I/c

For hydrogen:
$Z = 4.9 \times 10^{-4}\ m^3$
$S_a = 1.58 \times 10^6\ N/m^2$
$S_b = 4.067 \times 10^5\ N/m^2$
$S_c = 4.067 \times 10^5\ N/m^2$
$S_d = 1.58 \times 10^6\ N/m^2$

For oxygen:
$Z = 1.393 \times 10^{-4}\ m^3$
$S_a = 1.3812 \times 10^6\ N/m^2$
$S_b = 3.562 \times 10^5\ N/m^2$
$S_c = 3.563 \times 10^5\ N/m^2$
$S_d = 1.3812 \times 10^6\ N/m^2$

With an allowable stress of $2.0391 \times 10^8\ N/m^2$, there is no risk of the expansion stress exceeding this value for either material.

3.2.8 Calculations for Rotation and Deflection

The sum of static moment about the x-axis S_x, and the y-axis S_y, is calculated from the fixed point for which the rotation and deflection is to be computed. The relation between forces and rotation is given below.

$S_x = \Sigma Ly$
$S_y = \Sigma Lx$
$- F_x S_x + F_y S_y = \theta EI$

Rotation is equal to:
$\theta = 1/EI\ (- F_x S_x + F_y S_y)$

Deflection is equal to:
$\Delta_x EI = F_x I_x - F_y I_{xy} + \theta EI\ y'$
$\Delta_y EI = F_y I_y - F_x I_{xy} - \theta EI\ x'$

Due to symmetry of the system the deflection and rotation are calculated for only point b.

For hydrogen:
Rotation of point b from point a.

$S_x = 250\ m^2$
$S_y = 1250\ m^2$
$\theta = 0.5451$ deg

Deflection of point b from point a:

$\Delta_x = 0.0404$
$\Delta_y = 0.282$

For oxygen:
Rotation of point b from point a:

$\theta = 0.5456$ deg

Deflection of point b from point a:

$\Delta_x = 0.0404$
$\Delta_y = 0.282$

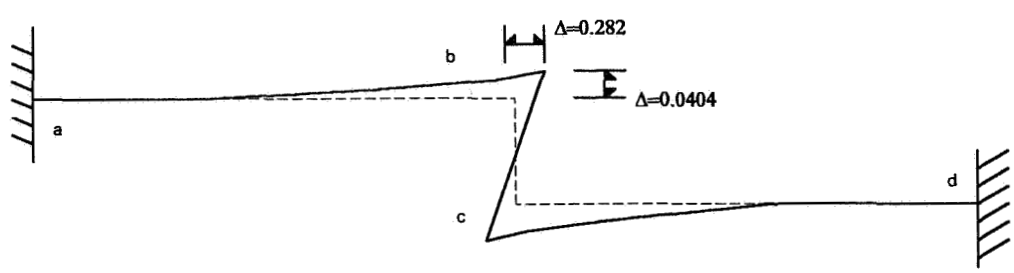

Figure 8: Diagram showing displacements for both piping systems

3.2.9 Piping Supports

The oxygen pipe is modeled since it is the heavier of the two pipe lines.

Running load due to pipe mass

Density x π ($R2^2$ -$R1^2$) = 408.69 N/m

Running load due to liquid oxygen
2214.2 N/m^3 x 3.14 x $.1301^2$ = 117.8 N/m

Total running load = 117.8 N/m + 408.69 N/m = 526.5 N/m

The maximum stress is equivalent to the bending moment at the supports (refer to figure 4). The relation is given below.

$$\sigma_{max} = \frac{My}{I}$$

$$M = \frac{qL^2}{12}$$

$$I = \pi r_{avg}^3 t$$

I = 4.722×10^{-5} m^4
σ_{max} = 24,000 psi = 1.6547×10^8 N/m^2 = 526.5 N/m * X^2 * 0.1365 m / (12* 4.722×10^{-5} m^4)

X = 36.12 m apart

This is the maximum distance the supports should be from one another. Placing the supports only 10 m apart, due to shipping concerns, adds stability to the piping as well as durability from any shock or vibration in the system.

FIGURE 1.1
VESSEL DIMENSIONS AND GEOMETRY

NOTE: ALL DIMENSIONS IN CENTIMETERS
HYDROGEN VESSEL - Ti-5 Al-2.5 Sn
OXYGEN VESSEL - 304L Stainless Steel

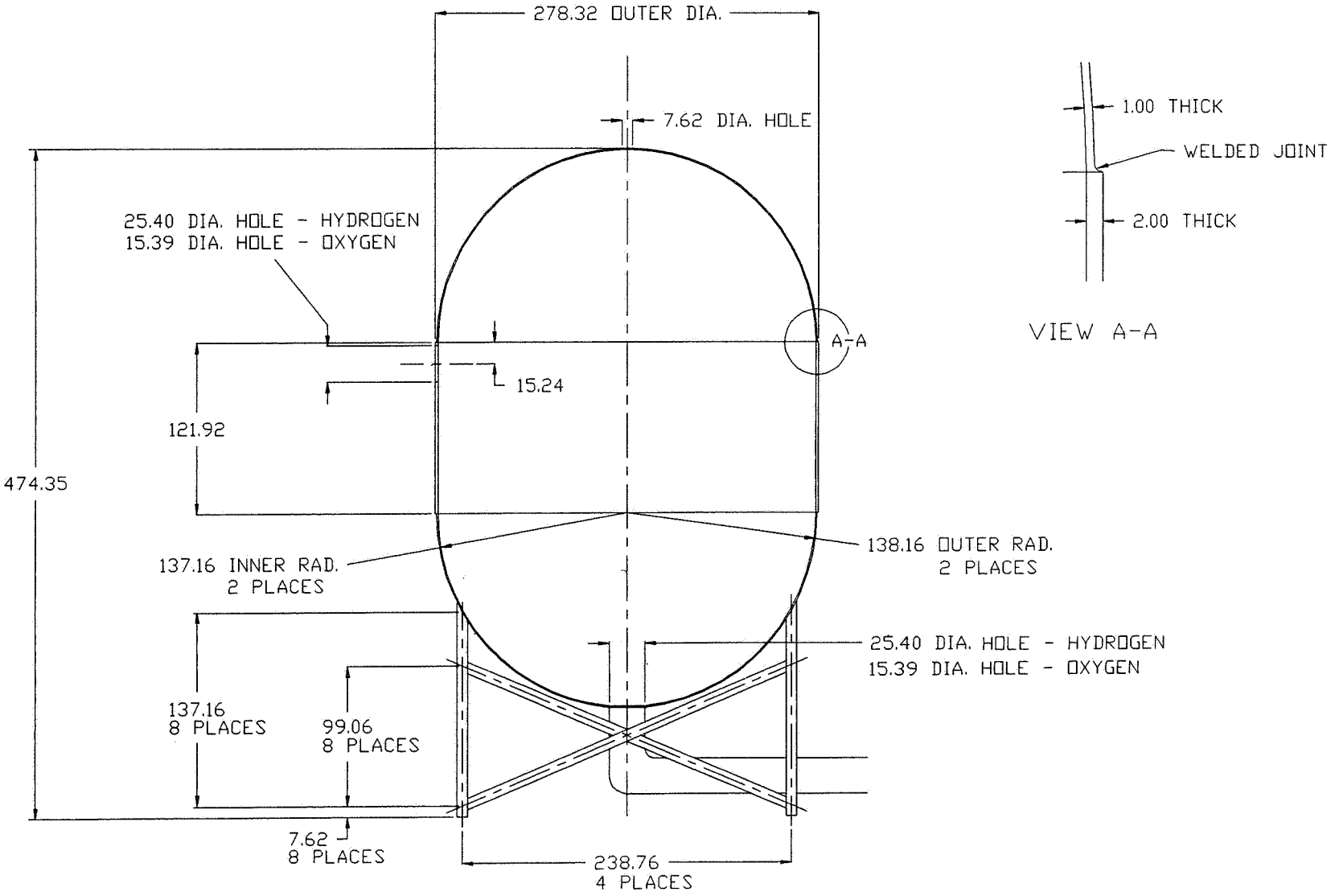

5.16

FIGURE 1.2
SHELL DIMENSIONS AND GEOMETRY

MOTE: ALL DIMENSIONS IN CENTIMETERS
MATERIAL: 304L – Stainless Steel

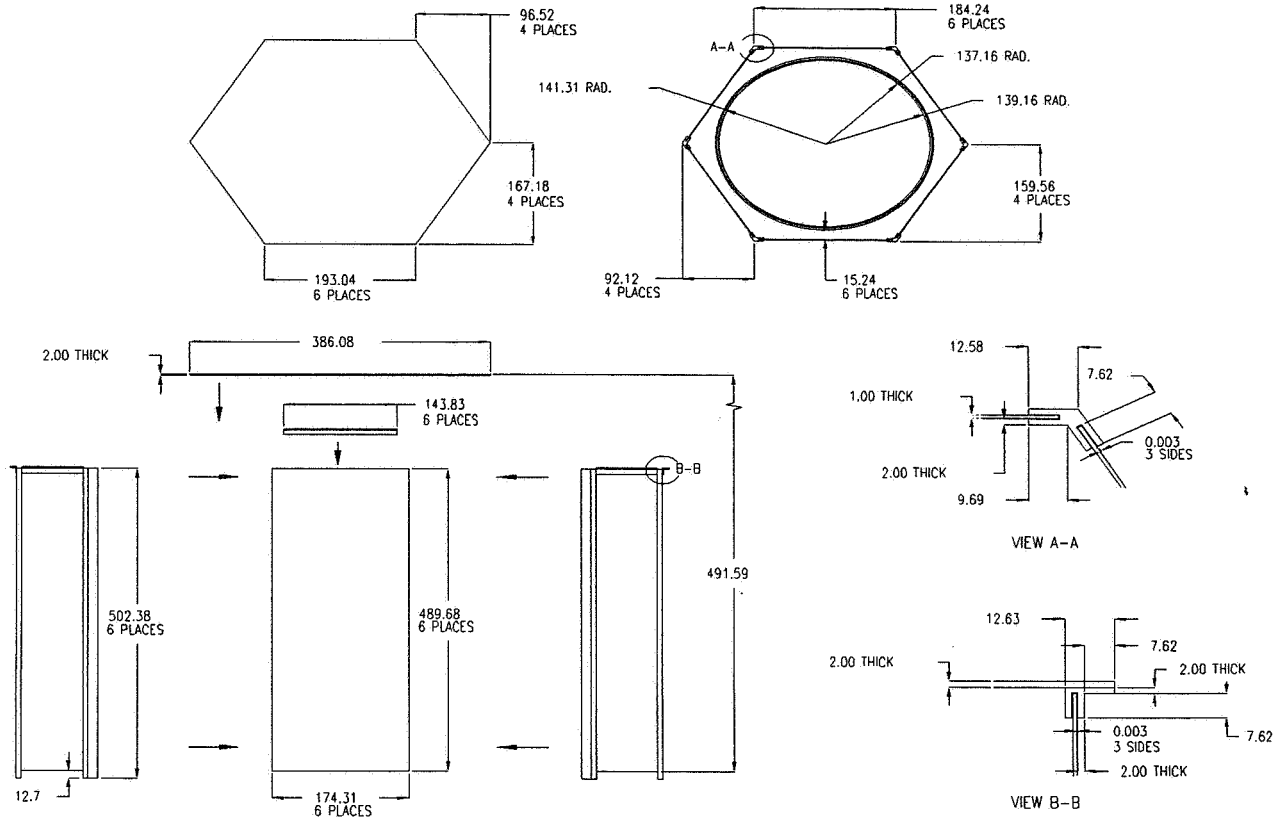

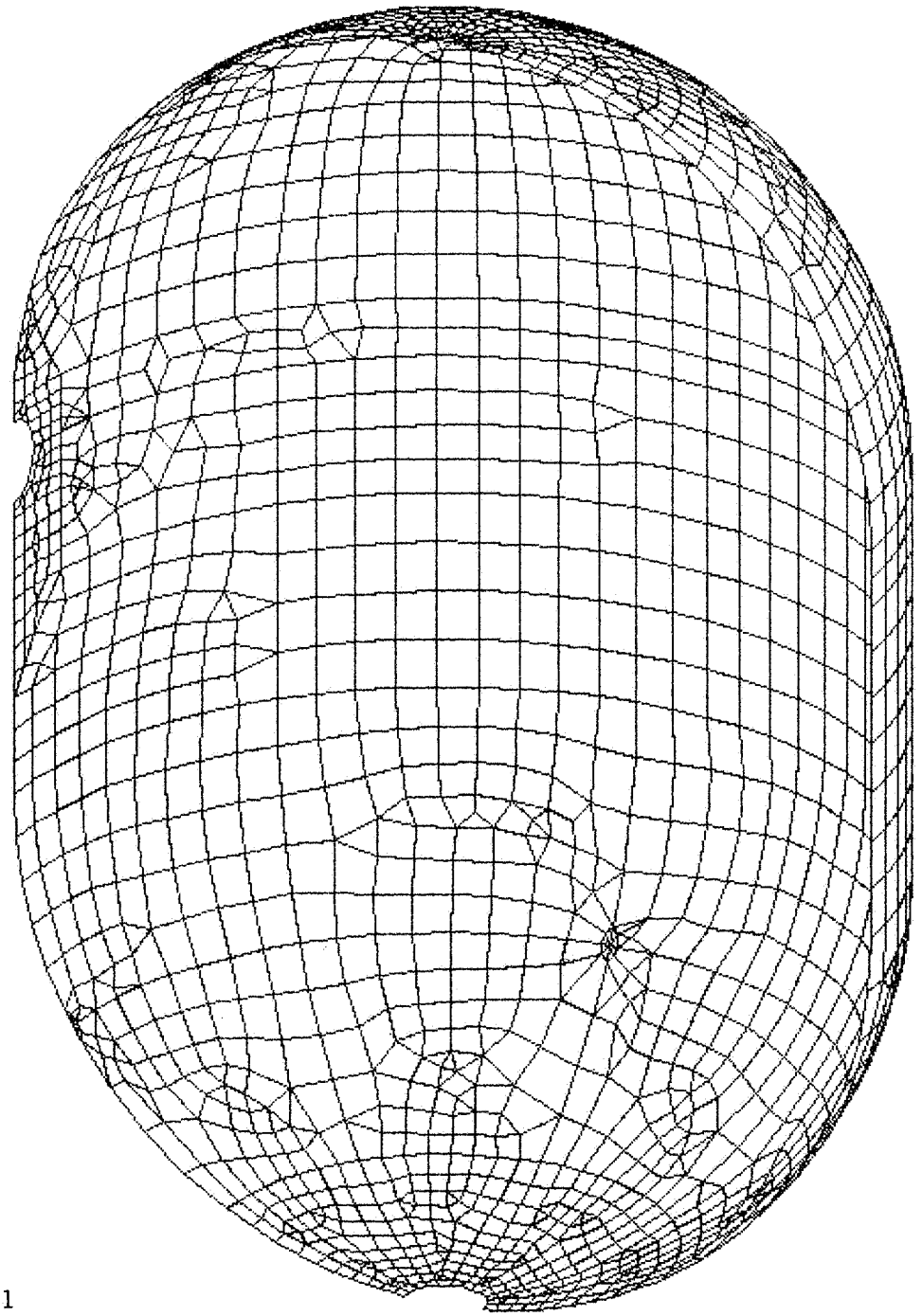

Figure 2.1

OXYGEN PRESSURE VESSEL FE MODEL

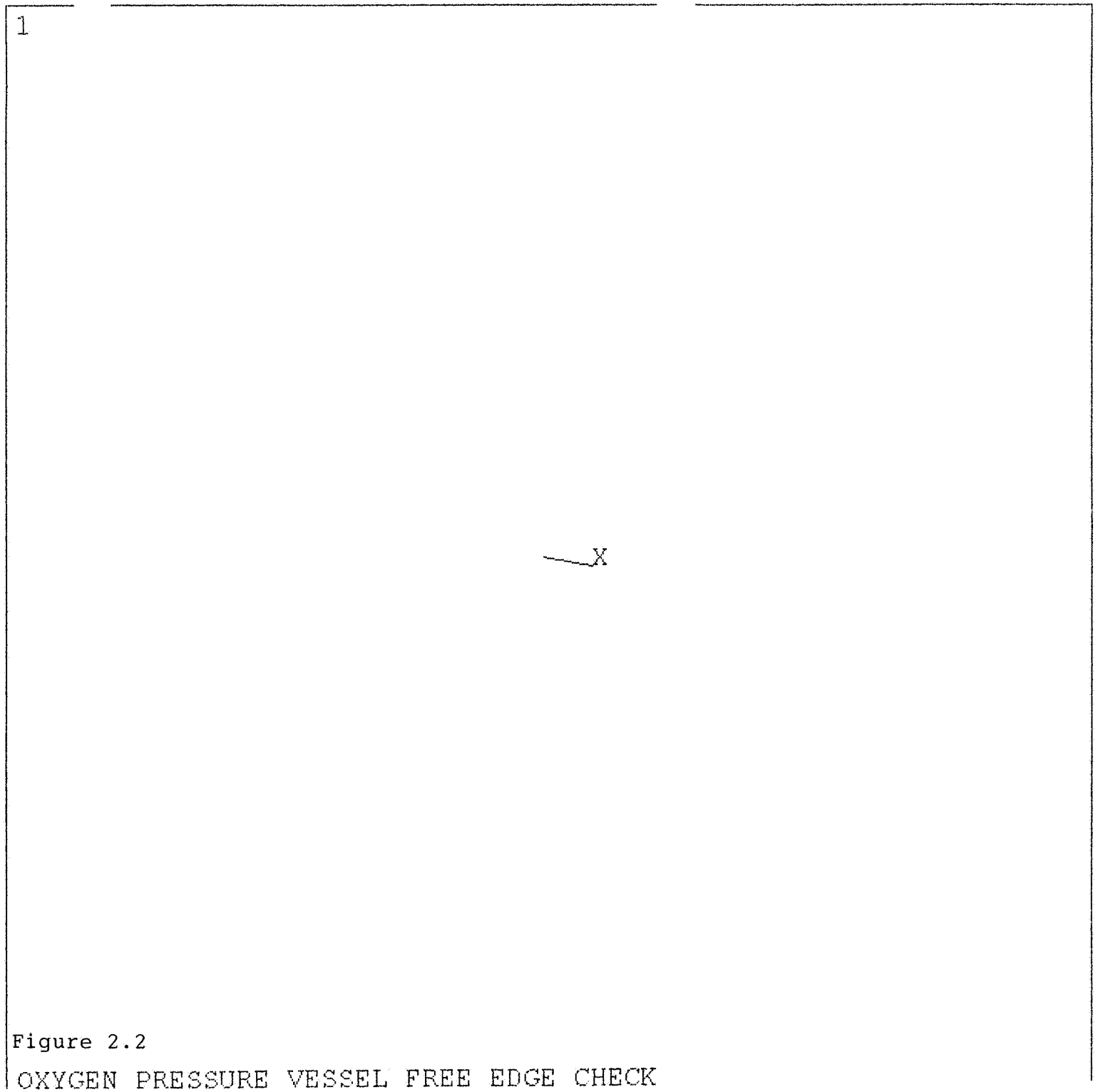

Figure 2.2
OXYGEN PRESSURE VESSEL FREE EDGE CHECK

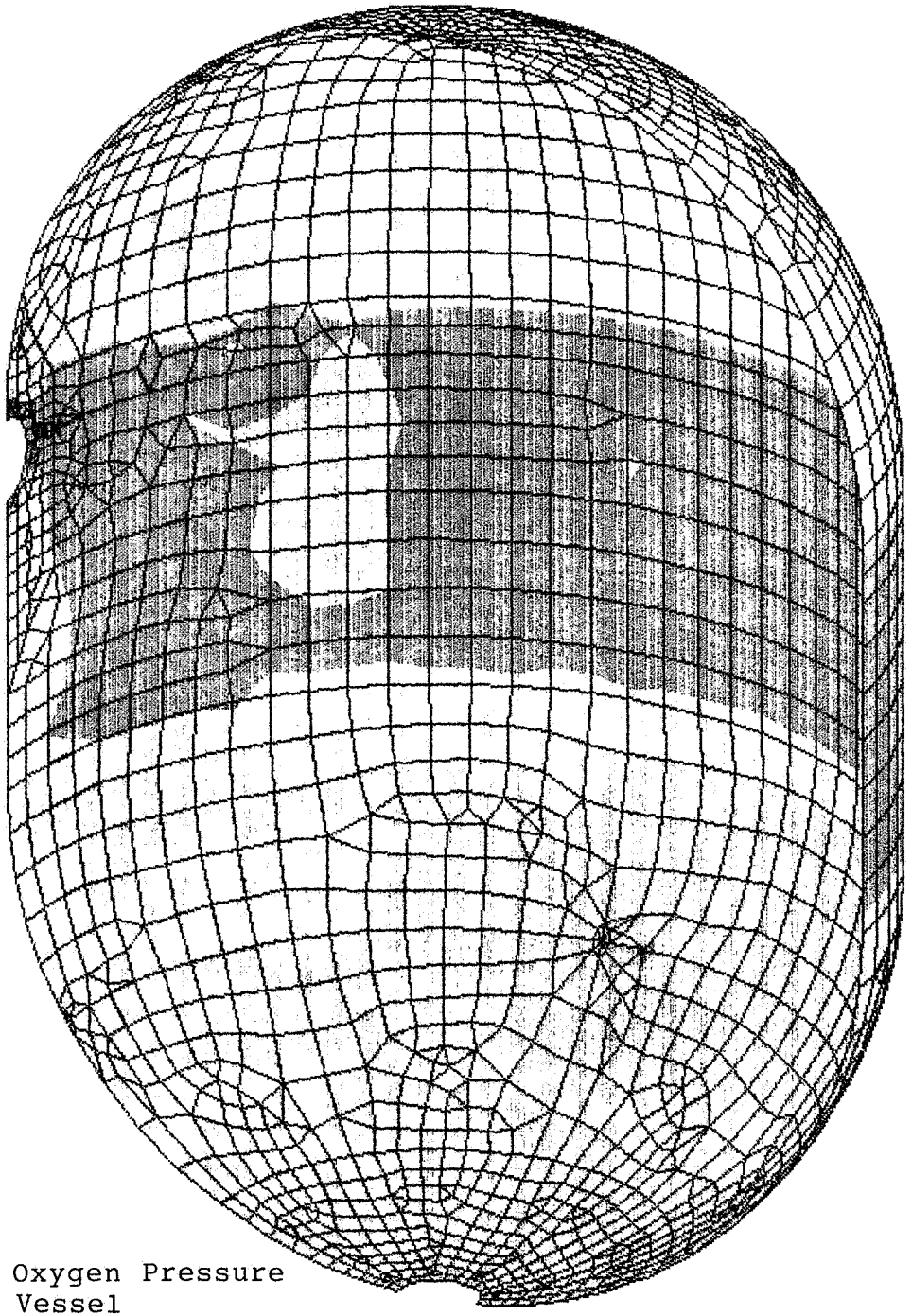

Figure 2.3 Oxygen Pressure Vessel

VON MISES STRESS CONTOUR - 800 Psi 1/6 G ACCELERATION

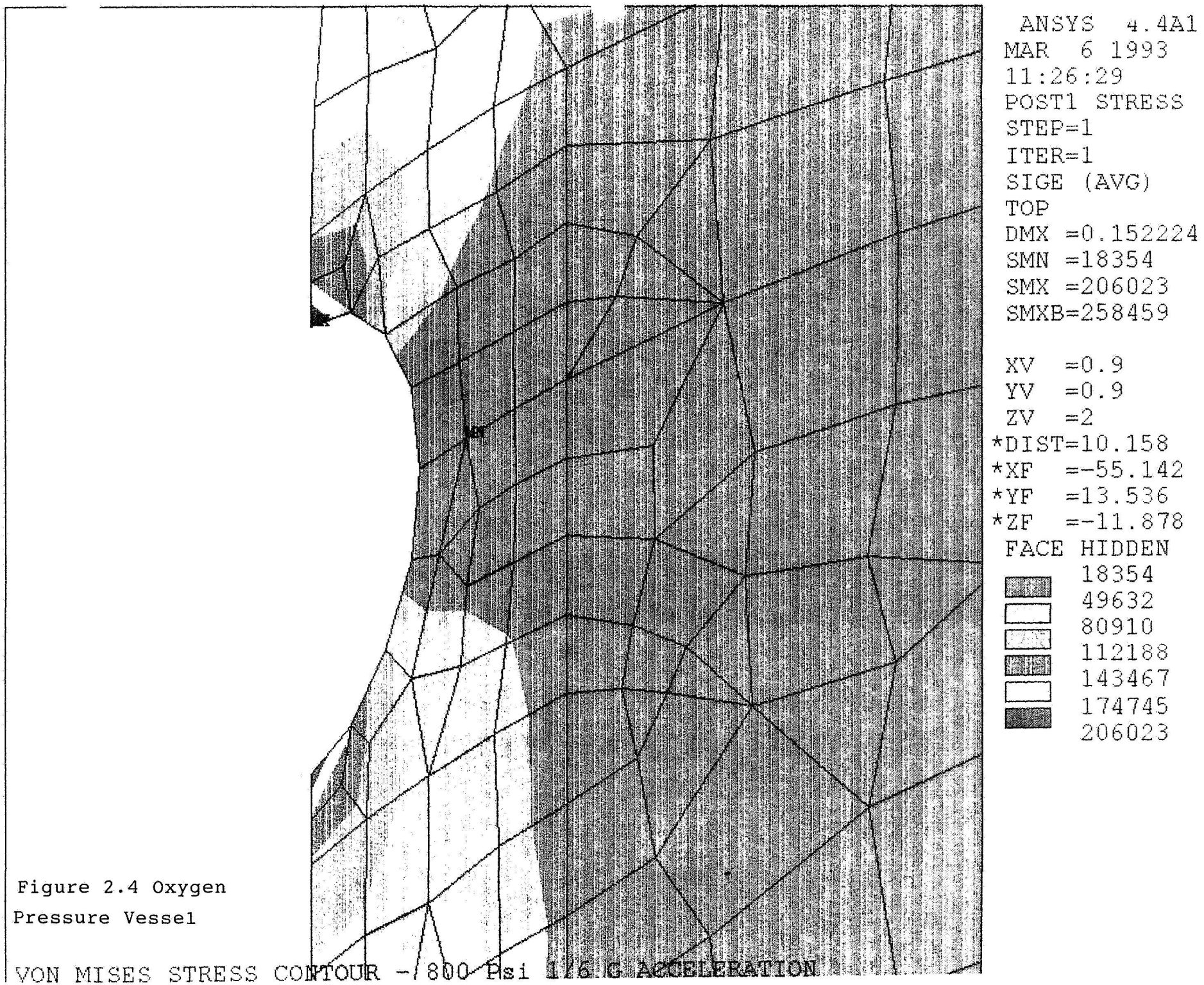

Figure 2.4 Oxygen
Pressure Vessel

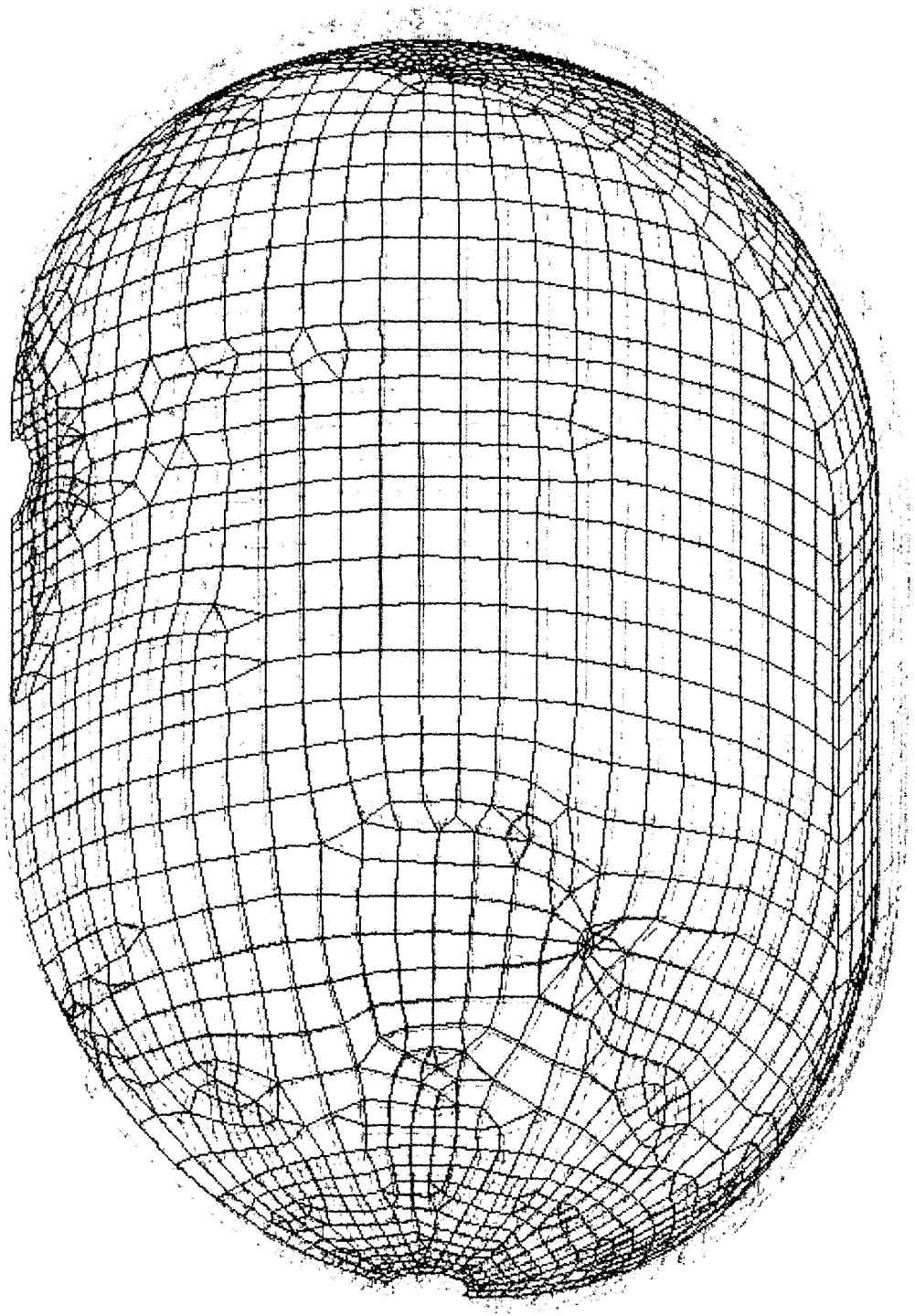

Figure 2.5

DEFORMED GEOMETRY PLOT OF OXYGEN PRESSURE VESSEL

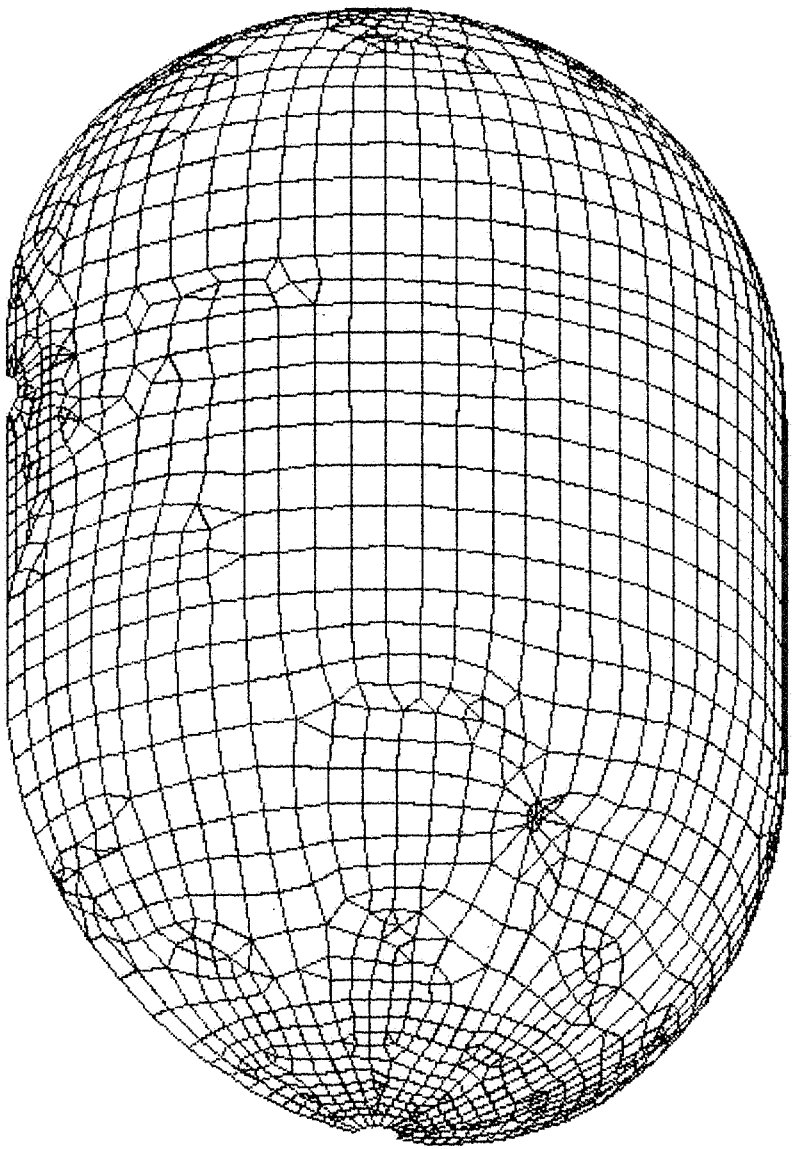

Figure 3.1

HYDROGEN PRESSURE VESSEL FE MODEL

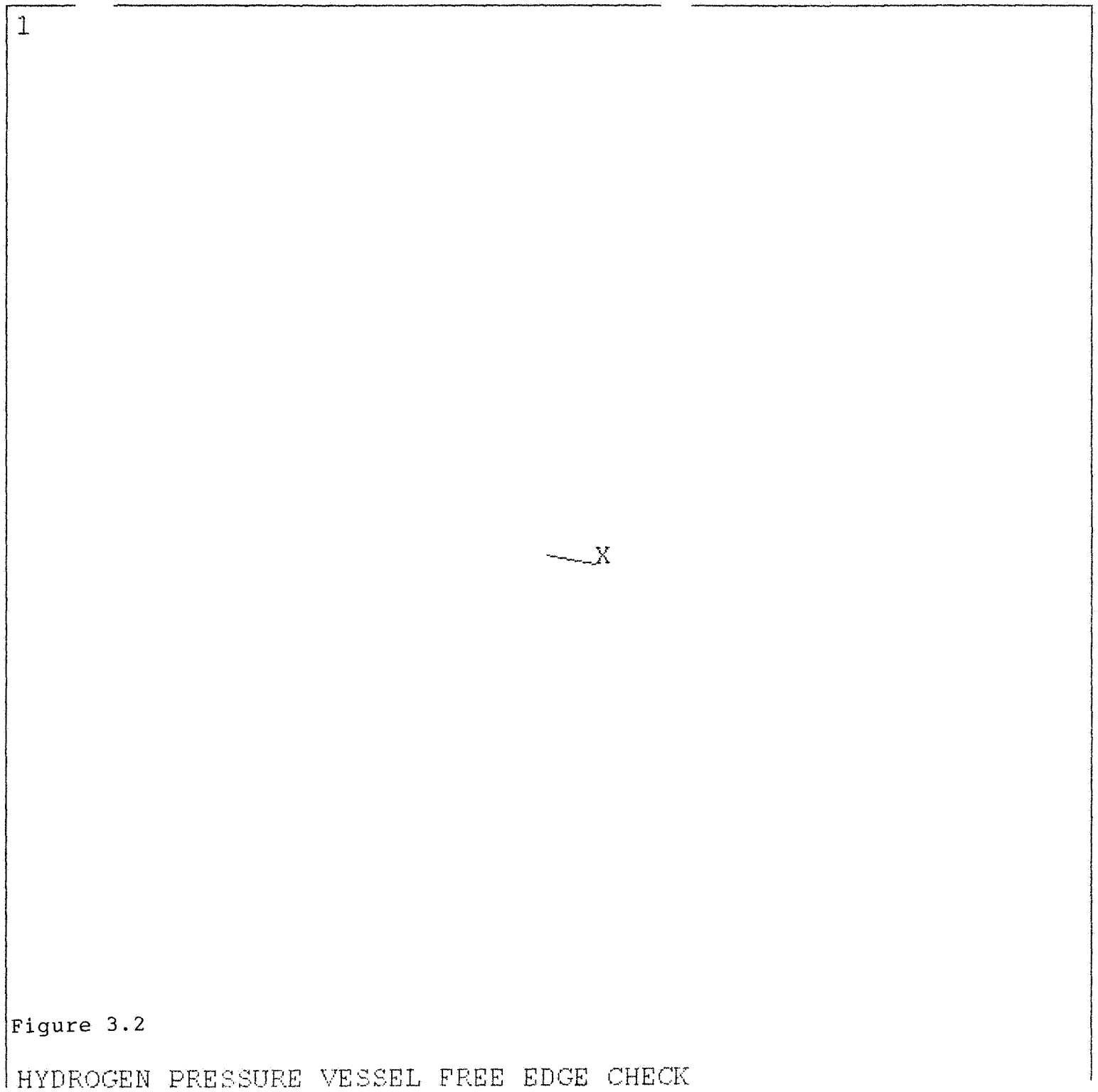

Figure 3.2

HYDROGEN PRESSURE VESSEL FREE EDGE CHECK

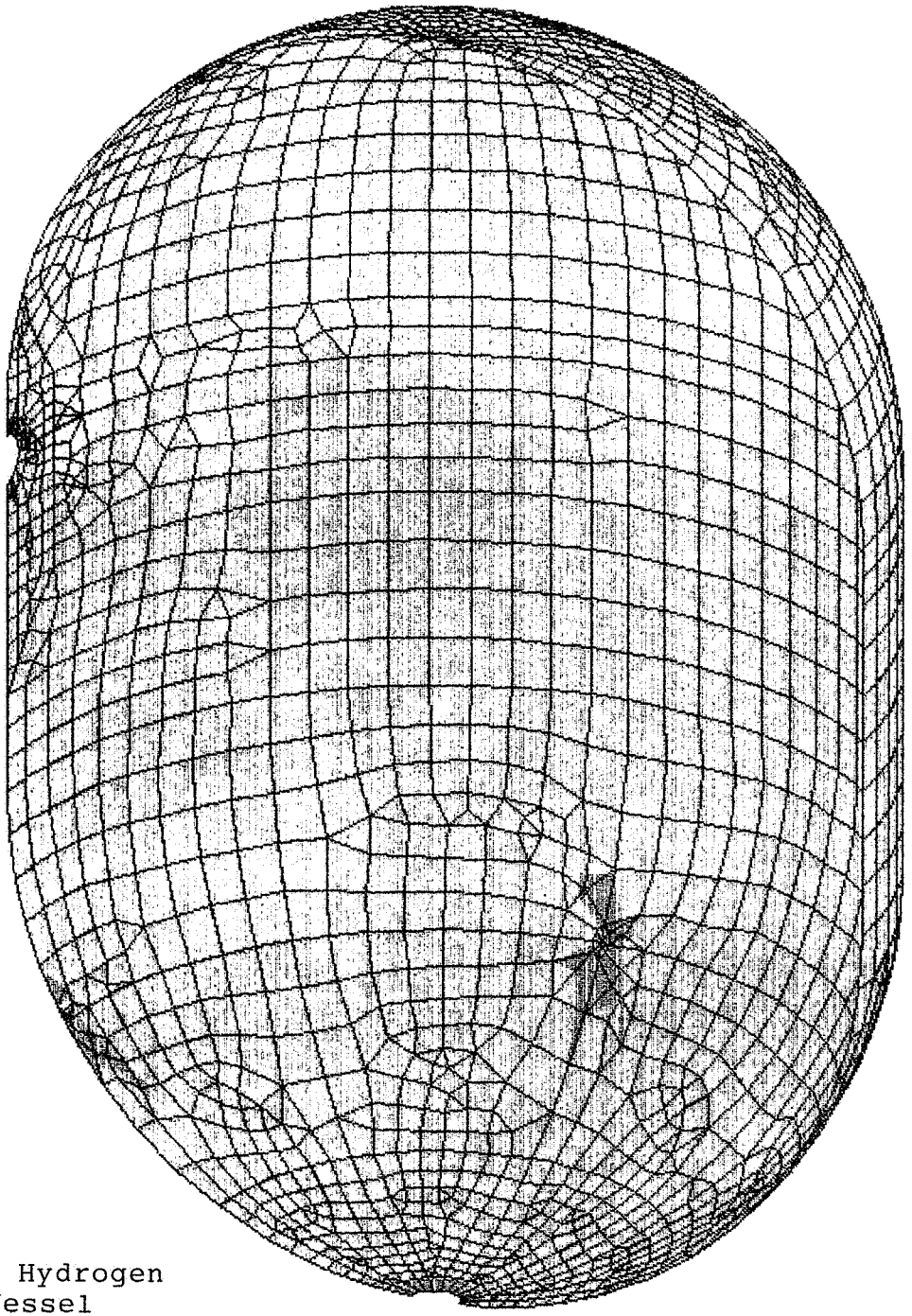

ANSYS 4.4A1
MAR 6 1993
13:48:26
POST1 STRESS
STEP=1
ITER=1
SIGE (AVG)
TOP
DMX =0.082241
SMN =7096
SMX =49508
SMXB=58830

XV =0.9
YV =0.9
ZV =2
*DIST=83
*YF =-8
*ZF =-27
FACE HIDDEN

7096
8255
16510
24765
33020
41275
49530

Figure 3.3 Hydrogen Pressure Vessel

VON MISES STRESS CONTOUR - 300 PSI 1/6 G ACCELERATION

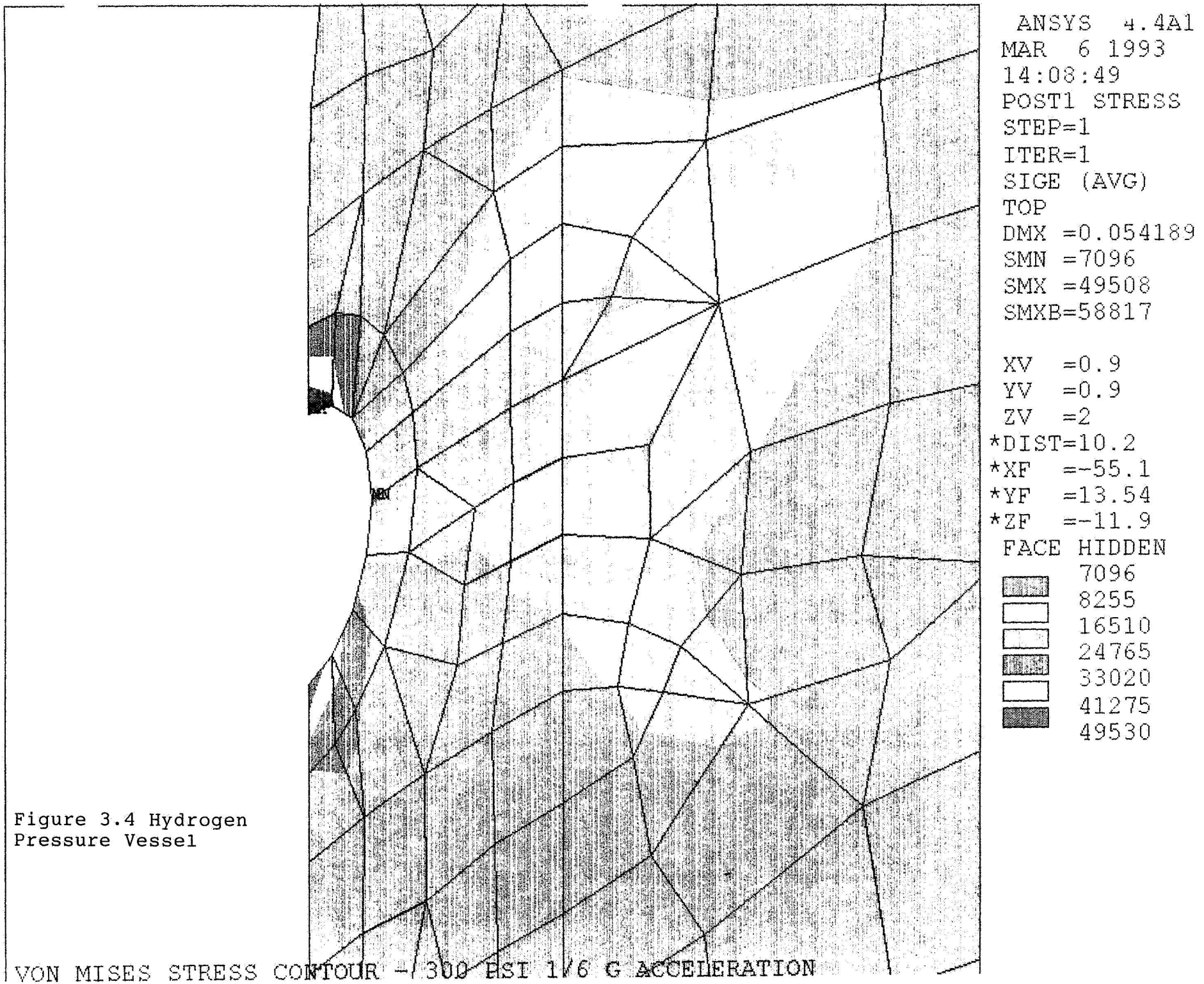

Figure 3.4 Hydrogen Pressure Vessel

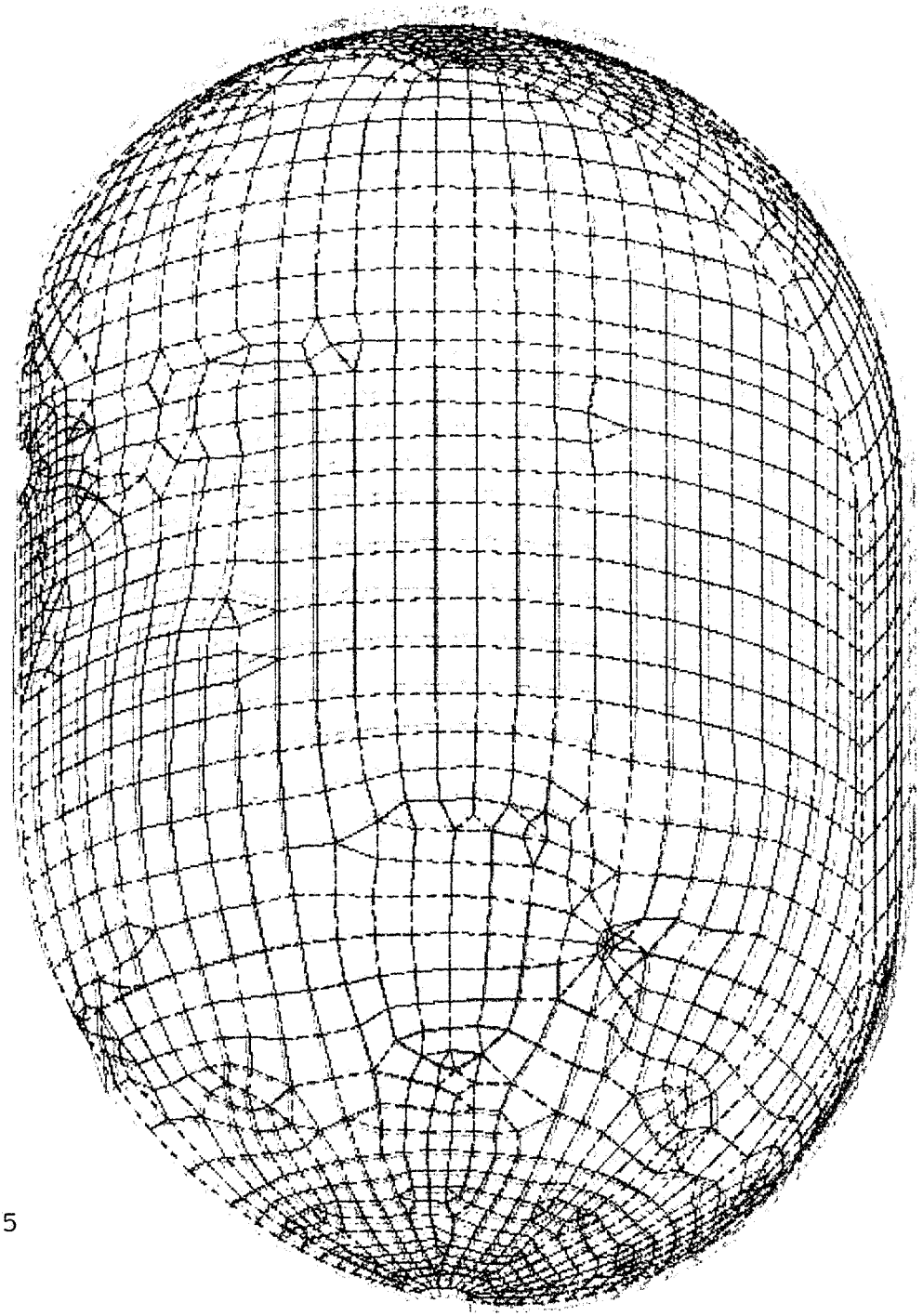

ANSYS 4.4A1
MAR 6 1993
13:52:19
POST1 DISPL.
STEP=1
ITER=1
DMX =0.082241
ERPC=11.823

*DSCA=30
XV =0.9
YV =0.9
ZV =2
*DIST=83
*YF =-8
*ZF =-27
PRECISE HIDDEN

Figure 3.5

DEFORMED GEOMETRY PLOT OF HYDROGEN PRESSURE VESSEL

Database: leg4
View : No stored View
Task: Beam Properties
Model: 1-FE MODEL1

Associate

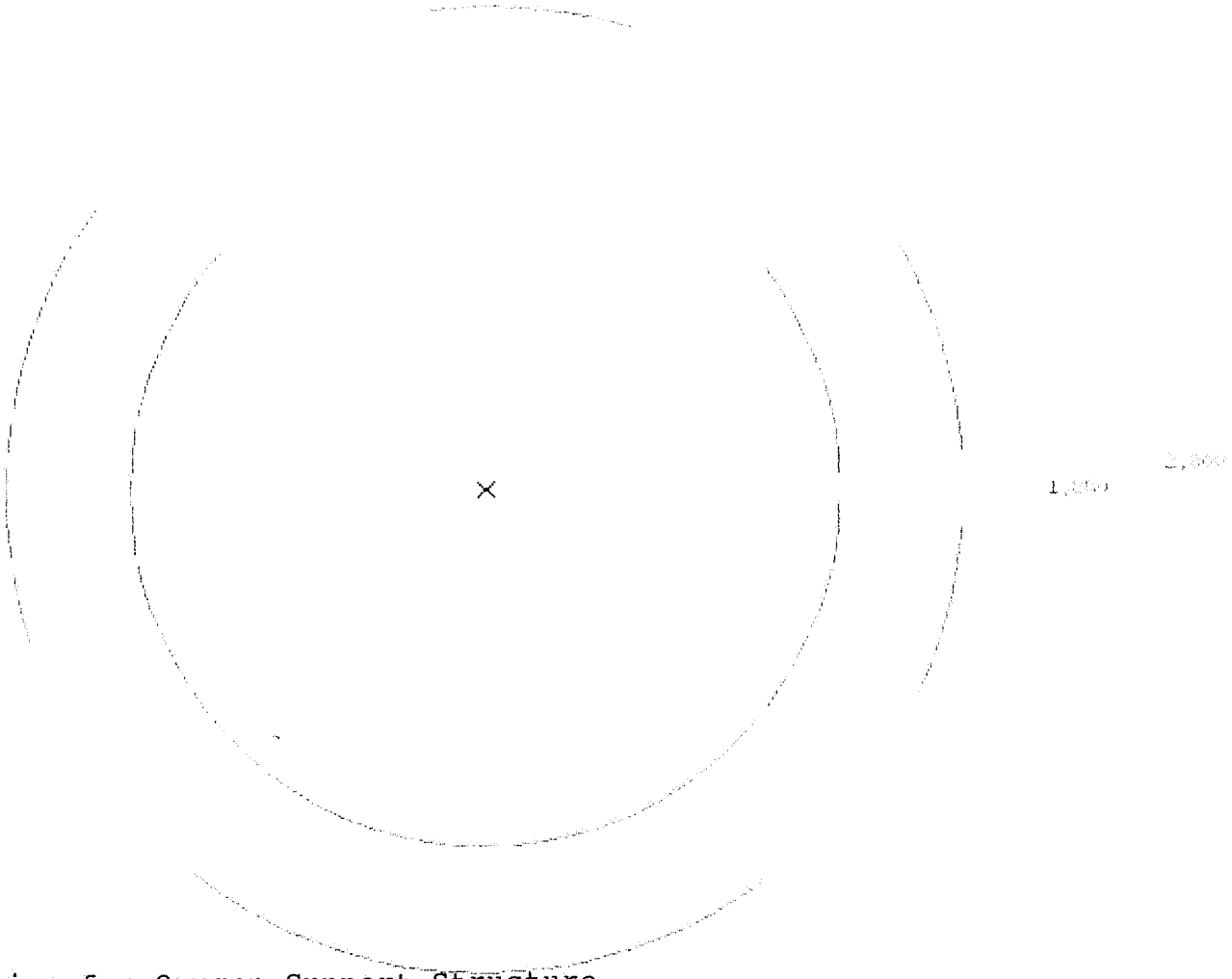

Figure 4.1 Leg Cross Section for Oxygen Support Structure.

Database: leg2
View : No stored View
Task: Boundary Conditions
Model: 1-FE MODEL1

Associat

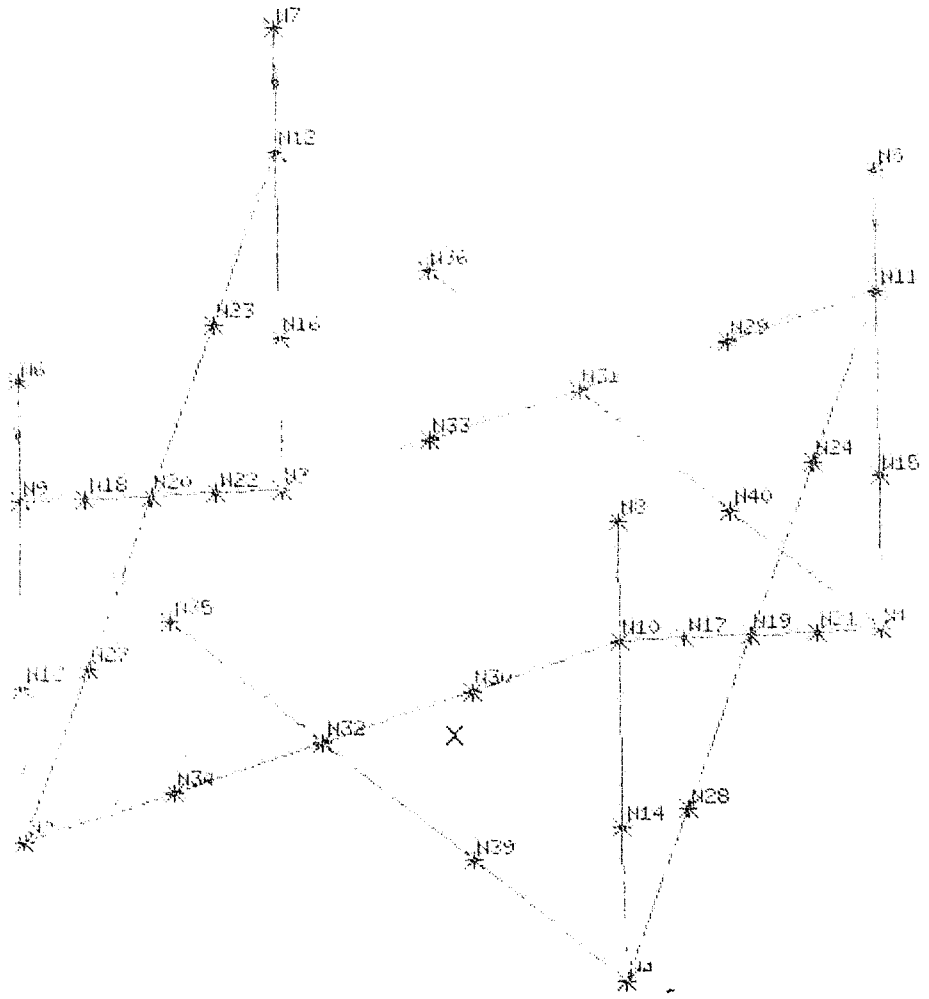

Figure 4.2 Finite Model Plot with BC's and Loading for Support Structure.

Database: leg4
View : VIEW1
Task: Post Processing
Model: 1-FE MODEL1

Units : I
Display : No stored Optio
Model Bin: 1-MAIN
Associated Workset: 1-WORKING_SET1

leg4

LOADCASE:1
DISPLACEMENT - MAG MIN: 0.00 MAX: 0.199434

Displacements scaled by 20

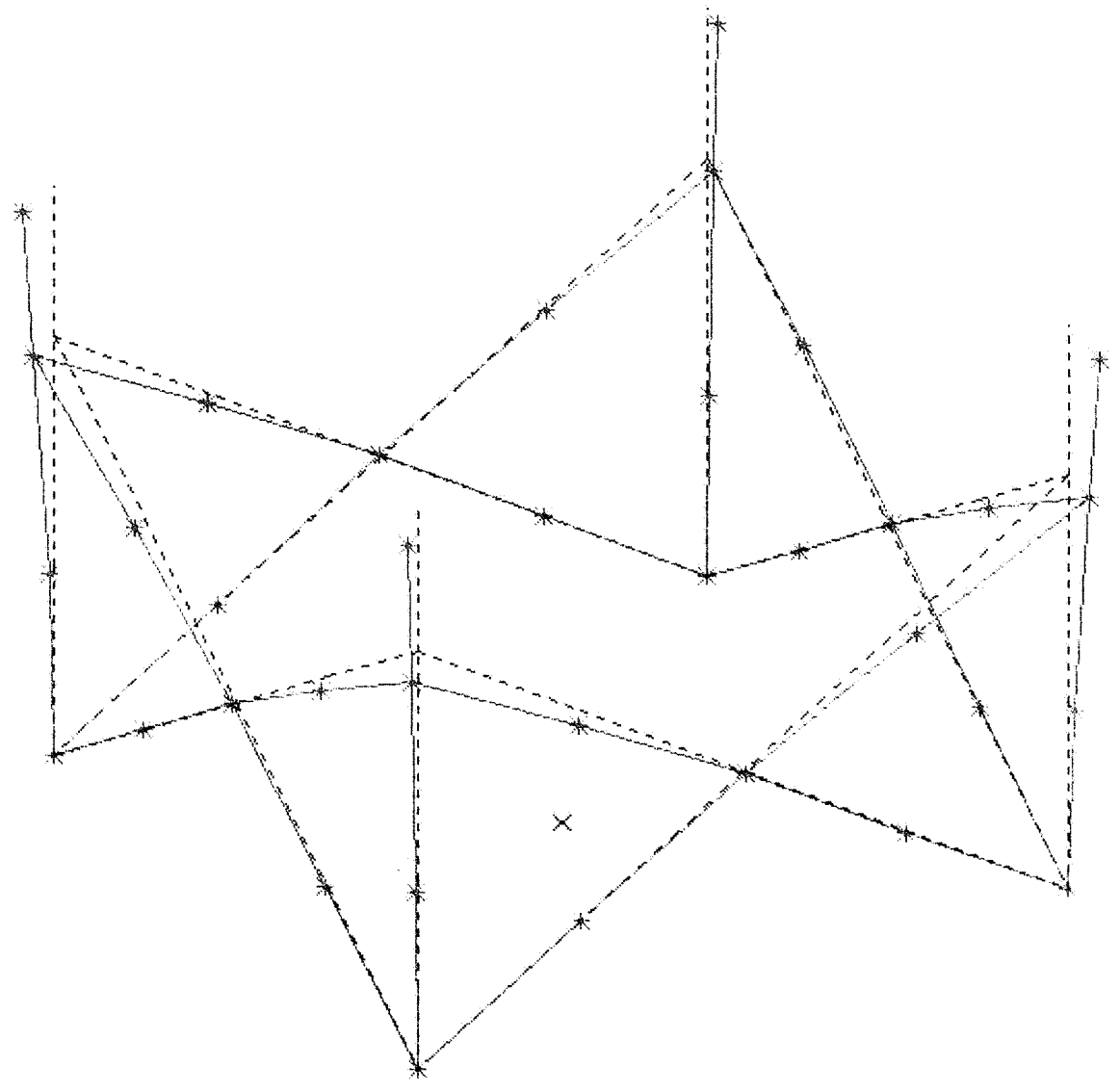

Figure 4.3 Deformed Geometry Plot for Oxygen Support Structure.

Database: leg4
View : No stored View
Task: Beam Properties
Model: 1-FE MODEL1

Associat

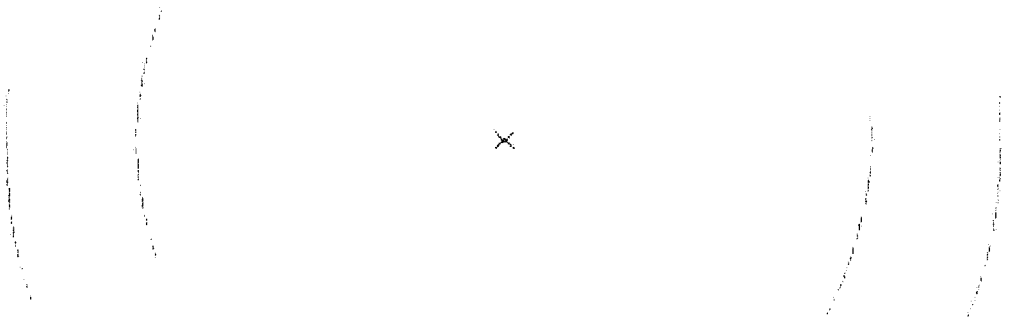

Figure 5.1 Leg Cross Section for Hydrogen Support Structure.

I = 0.963 in^4

Database: leg4
View : No stored View
Task: Post Processing
Model: 1-FE MODEL1

Units : IN
Display : No stored Option
Model Bin: 1-MAIN
Associated Workset: 1-WORKING_SET1

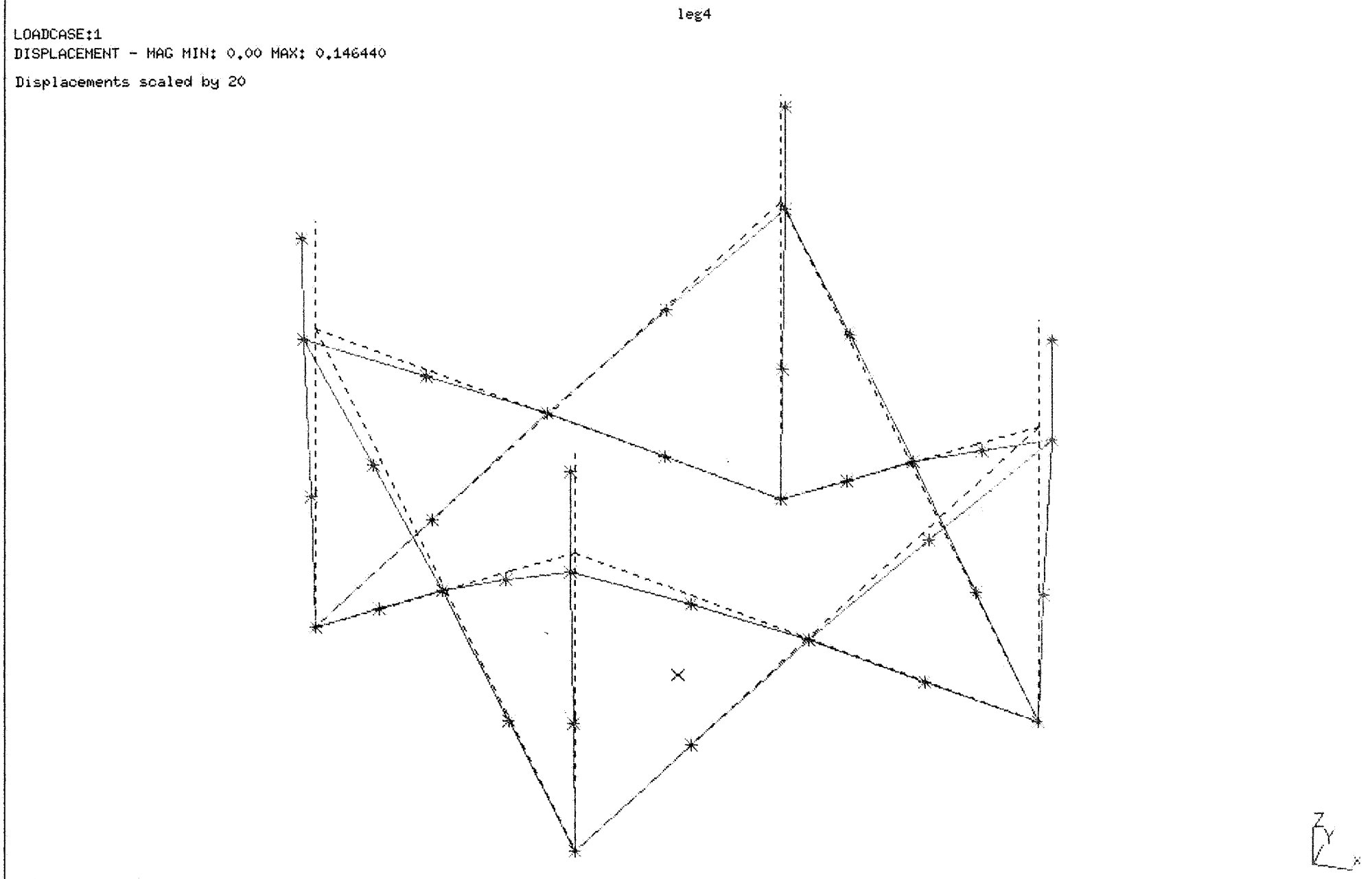

Figure 5.2 Deformed Geometry Plot for Hydrogen Support Structure.

Database: fun
View : 1, 1
Task: OBJECT
Object: 1-WORK1, Workbench

Units : IN
Display : none, none
Bin: 1-MAIN
Update Level: Full

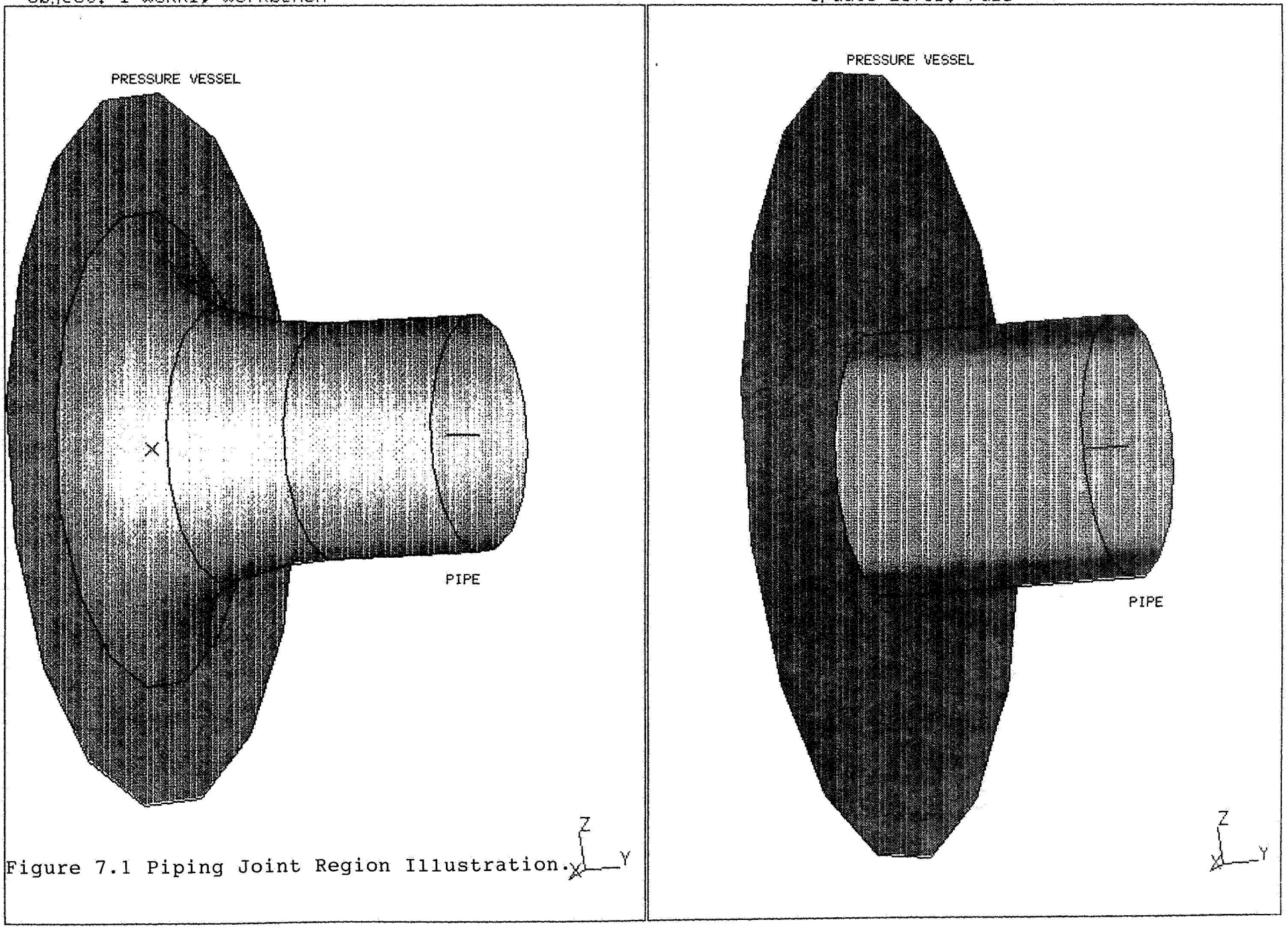

Figure 7.1 Piping Joint Region Illustration.

6.0 STRUCTURES

Department of Civil and Environmental Engineering
Steve Hudepohl
Greg Schreppel

TABLE OF CONTENTS

1.0 Introduction.

The goal of the project presented to the University of Cincinnati by National Aeronautics and Space Administration (NASA) is to investigate the utilization of lunar resources. More specifically, our goal will be to design a mining and processing facility on the lunar surface to extract ice from the polar regions and convert it into oxygen and hydrogen. These elements will then be used for rocket propellant. Most disciplines within the College of Engineering have been involved in the design of the lunar base. Each major system of this project will be designed by the engineering discipline with the most related expertise.

The Civil Engineering Department will coordinate the design of the structural components required for the lunar processing facility. Components such as habitats, equipment supporting structures, communication towers, and launch platforms are all of structural significance, however, the focus of this report will be on the design of the habitat and the supporting structure for the rail gun.

1.1 Lunar Structural Systems

In the design of all lunar structural systems, numerous factors were considered so that the designs would be as efficient as possible. These considerations include the weight of the structure, transportation of materials to the lunar surface, construction of structural systems, maintenance, and radiation protection. The following sections summarize these topics.

1.1.1 Weight (Mass) of Materials

Due to the high cost required to transport materials from earth to the lunar surface, mass is one of the most important design factors in our project. To limit the amount of materials imported from earth, structural members were designed to resist the loads as

efficiently as possible. Materials with high strength to weight ratios were chosen, and indigenous materials were used whenever feasible.

1.1.2 Cargo Space Requirements for Transportation of Structural Systems

The ability to transport structural members from the earth to the lunar surface using the least possible space will be extremely beneficial. Members that can be nested or folded together during transportation were used in the design of all structures.

1.1.3 Construction of Structural Systems and Equipment Requirements

One important factor in the design procedure was to develop structures using the simplest types of connections possible. The process of welding and bolting members together is to be avoided due to the working enviroment and the limited dexterity of the astronauts caused by the space suits. Simple connections such as slip, hinged or ball and joint will be investigated.

For construction of the lunar structures, equipment capable of moving/carrying regolith, lifting structural members, and driving piles into regolith will be required. It would be beneficial and realistic to have one piece of equipment to perform all of these tasks.

1.1.4 Maintenance Requirements

The design life of the lunar base has been specified to be 20 years. However, structures with static loads should easily exceed this time requirement at no additional initial expense.

1.1.5 Micrometeorite and Radiation Protection

Since the frequency of a meteorite impacting the lunar habitat is extremely small and since the energy and resultant force of impact are nearly impossible to resist, no

attempt was made to design against such an event. However, limiting devastation to the site of impact was deliberated. Micrometeorite (0.001 mm in diameter) impacts are much more frequent and must be a design consideration. Shielding must therefore provide resistance to these impacts, as well as, provide protection against radiation.[1]

1.2 Method of Analysis and Design

The analysis and design of the lunar structures was in accordance with the Allowable Stress Design method (AISC-ASD). In this method, the maximum stress in any structural element is limited to a percentage of the yield stress of the material. Although this design procedure was developed for terrestrial structures, data concerning material reliability and construction quality is not available; therefore, the safety factors used in the ASD was used for design of the lunar structures.

According to ASD procedures, the allowable stress (F_b) for a fully braced element in bending is 0.66 F_y, where F_y is the yield strength the material (Factor of Safety = 1.5). The allowable stress (F_t) for a tension member, according to ASD, is limited to 0.6 F_y (F.S. = 1.66) on the gross area and 0.5 F_u (F.S. = 2.0) on the effective net area, where F_u is the ultimate strength of the material.[2] For other safety factors, refer to the AISC-ASD design manual.

2.0 Lunar Habitat

2.1 Introduction

The establishment of a lunar habitat early in the construction of the lunar processing facility is a high priority. Since the cost of transporting personnel to and from the lunar surface is high, an open life support system capable of sustaining life for long periods must be established on the lunar surface to initiate construction of the facility. The lunar habitat must also be able to accommodate the gradual increase of occupants as the lunar facility nears completion.

Two independent designs were initiated for the lunar habitat. Prior to commencement of the designs, characteristics considered important to both designs were discussed. These characteristics are discussed in the following sections.

2.1.1 Preliminary Design Considerations

In order to expedite construction of the facility, the habitat must accommodate any number of occupants as efficiently as possible, and it must be assembled in a short period of time. To meet these criteria, a modular design was chosen for the habitat. In this type of design, one habitat is capable of supporting three personnel. To accommodate more people, multiple habitats, arranged in any configuration, can be established either as one large habitat at a central location or as several smaller habitats placed throughout the processing and mining sites. Unlike a single habitat designed to support the maximum number of personnel, a modular habitat can be established in a relatively short period of time, thereby, reducing the construction time of the entire facility. In addition, the size of a modular habitat can be increased throughout the construction as the need for more personnel increases. Although not the focus of this report, the habitat can be rearranged and enlarged should future expansion of the facility be desired.

Each habitat was equipped with facilities for sleeping, eating, hygiene and recreation, as well as, facilities for communications and laboratory work. Space was also

provided within the habitat for storage of food, water, oxygen and heating and cooling units.[3] Although power will ultimately be provided by a separate facility, power during initial construction of the processing plant must be provided by batteries and/or solar cells. These habitats will be transported to the lunar surface and assembled at various phases of construction until the number of habitats provided satisfies the occupant space required for operation of the completed facility.

2.1.1.a Habitat Design Capacity

As stated previously, each module was designed to accommodate three personnel. This was number chosen because it is the minimum number of personnel required for an extra-vehicular activity (EVA). Habitats will be required at both the polar mining site and the processing facility located at the equator.

2.1.1.b Habitat Shielding

Safety of the personnel within the habitat was another consideration that had to be addressed before beginning design. The primary threats to habitat occupants are micrometeorites (0.001 mm in diameter) and radiation (including solar flares). Through research, we established that two meters of regolith would provide adequate protection from these threats[4]. Although the habitats were not designed to withstand the impact of large meteorites, habitats can be separated far enough apart to limit damage to a single structure. If several habitats are connected together, pressure locks were needed to withstand sudden pressure drops should a breach in the structure occur.

2.1.2 Design Parameters and Material Properties

The following data and material properties were used in the design:

Habitat Design Pressure = 82.75 kPa (12 psi)

Design Occupancy = 3 personnel

Maximum Deflection = L / 180 (L = span of member)

- **Soil Properties ***

Unit Weight of Lunar Soil (γ)	31.41 N/m^3 (20.00 lb/ft^3)
Friction Angle (ϕ)	40°
Relative Density (D_R)	74%
Allowable Bearing Capacity	95.76 kPa (2000 lb/ft^2)

* assumed

- **Material Properties** [5]

Aluminum Alloy

Material Name	6061-T6 or 6062-T6
Yield Strength (F_y)	241.3 MPa (35 ksi)
Ultimate Strength (F_u)	262.0 - 289.6 MPa (38 - 42 ksi)
Modulus of Elasticity (E)	68,950 MPa (10,000 ksi)

Steel Alloy

Material Name	A514 *
Yield Strength (F_y)	689.5 MPa (100 ksi)
Ultimate Strength (F_u)	785.4 to 896.32 MPa (110 to 130 ksi)
Modulus of Elasticity (E)	200,000 MPa (29,000 ksi)

* Structural members less than 6.35 cm (2.5 inches) thick.

Steel Alloy (Rods)

Material Name	A490
Yield Strength (F_y)	1034.2 MPa (150 ksi)
Ultimate Strength (F_u)	1241.1 MPa (180 ksi)
Modulus of Elasticity (E)	200,000 MPa (29,000 ksi)

2.2 Lunar Habitat -- Alternative 1

2.2.1 Foreword

In this design, the habitat consists of two structural systems. The first system is designed to carry the gravity loads and lateral pressures generated by the regolith shielding. The second system is designed to resist an internal pressure of approximately 82.75 kPa (12 psi) using some type of strong fabric (possibly nylon) fortified with a system of cables. These two systems will work simultaneously to provide an adequately large, shielded, economically feasible habitat. Refer to figures 5.1.1 and 5.1.2 (Appendix A) for a conceptualized view of the proposed habitat.

2.2.2 Design

The system required to support the regolith shielding consists of eighteen hollow, cylindrical columns designed as hollow steel piles filled with lunar regolith. All columns will have an embedment length of 18.90 m (62 feet). This gives total column lengths of twelve - 22.87 m (75 feet) lengths and six - 22.36 m (73.33 feet) lengths. Twelve of these columns (see figure 5.1.3) will have a height of 3.96 m (13 feet) above grade while the remaining six columns will be 3.45 m (11.33 feet) above grade. These piles will all be 61.0 cm (24 inches) in diameter having a thickness of 9.5 mm (0.375 inches).

Six typical steel joists spanning approximately 9.15 m (30 feet) will be placed on top of these columns which will in turn support a standard type of steel roof decking.

Steel panels are used to resist the lateral pressures created by the regolith shielding. These panels are spanning between all the columns and are fastened to the columns using slots already fabricated into the columns.

The system used to constrain the internal pressure of 82.75 kPa (12 psi) will consist of some type of fabric that is required to resist a tensile force of about 254 N/cm (145 pounds per inch) length of fabric. This fabric must also have a low gas permeability

in order to constrain oxygen and filter out volatiles. This fabric will be held in place by sixteen steel cables capable of withstanding a high tensile force of approximately 622 kN (140 kips) per cable. The internal pressure of 82.75 kPa (12 psi) creates a large upward and inward force on the columns due to the cables and it creates a large bearing pressure on the floor and underlying regolith. The floor system consists of aluminum decking (see figure 2.2.1) which will be bearing on the regolith and also on each column using a typical shear connector.

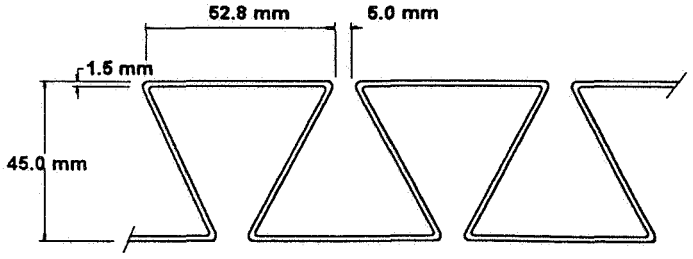

Figure 2.2.1

2.2.2a Required Materials

Materials needed will include the hollow steel columns, steel joist and deck, high tensile strength fabric and cables.

Specifications

Column/Pile

Material	Welded or Seamless Tubing, A514
Size	61.0 cm (24 in.) O.D.
Thickness	9.5 mm (0.375 in.)
Section Modulus (S)	2653 cm^3 (161.87 in^3)
Weight	31.6 kN (7.1 k)
Required Strength	747 N-m (551.2 k-ft)
Allowable Strength	841 N-m (620.5 k-ft)

Joist

Joist Name*	20LH9 (cap. = 12.60 kN/m (859 lb/ft))
Span	9.15 m (30 ft)
Load	11.73 kN/m (798 lb/ft)
Weight	308 N/m (21 lb/ft)

* From Steel Joist Catalog

Decking: Roof (steel)

Decking Type *	1.5B16 (three span condition)
Span	1.68 m (5.5 ft)
Moment of Inertia (I)	0.505 cm^4/cm (0.370 in^4/ft)
Weight	165 Pa (3.44 lb/ft^2)

* From Steel Decking Catalog

Floor (aluminum)

Decking Material	Aluminum
Span	0.589 m (1.93 ft)
Moment of Inertia (I)	1.52 cm^4/cm (1.11 in^4/ft)
Weight	125 Pa (2.61 lb/ft^2)

Cables

Cable Type	7-wire strand (14.3 mm (.563 in) diameter)
Span	1.68 m (5.5 ft)
Weight	9.55 N/m (0.65 lb/ft)
f_{pu}	1.86 MPa (270 k/in^2)
Required Strength	205.9 kN/cable (46.3 k/cable)
Allowable Strength	230.4 kN/cable (51.8 k/cable)

Pipe Beams

Material	Welded or Seamless Tubing, A514
Size	20.3 cm (8 in.) O.D.
Thickness	5.56 mm (0.219 in.)
Section Modulus (S)	165.5 cm^3 (10.10 in^3)
Weight	135.8 N/m (9.24 lb/ft)
Required Strength	73.45 N-m (54.17 k-ft)
Allowable Strength	75.33 N-m (55.55 k-ft)

Wall Plates

Material	A514
Thickness	4.93 mm (0.194 in.)
Weight	379 Pa (7.92 lb/ft^2)

Fabric

Material	fabric w/ low gas permeability
Quantity	108.7 m^2 (1170 ft^2)
Thickness	< 3.18 mm (0.125 in.)
Weight *	11.8 Pa (0.25 lb/ft^2)
Required Strength	254 N/cm (145 lb/in.)

* assumed

Total Weight of Structure

Columns/Piles

Total Length	Weight per Habitat
408.5 m (1340 ft)	563.6 kN (126.7 k)

Joist

Total Length	Weight per Habitat
54.9 m (180 ft)	16.8 kN (3.78 k)

Decking: Roof (Steel)

Total Area	Weight per Habitat
76.6 m^2 (825 ft^2)	12.63 kN (2.84 k)

Floor (Aluminum)

Total Area	Weight per Habitat
76.6 m^2 (825 ft^2)	9.56 kN (2.15 k)

Cables

Total Length	Weight per Habitat
190 m (624 ft)	1.81 kN (0.406 k)

Steel Plates/Walls

Total Area	Weight per Habitat
69.0 m^2 (742 ft^2)	26.17 kN (5.88 k)

Pipe Beams

Total Length	Weight per Habitat
10.7 m (35.1 ft)	1.44 kN (0.324 k)

Fabric

Total Area	Weight per Habitat
108.7 m^2 (1170 ft^2)	1.30 kN (0.292 k)

Total Weight of Structural Materials (approx.) -- 633 kN (142.3 k)

Since the length and weight of the columns make them difficult to manage, they will be cut into thirds producing lengths of 7.62 m (25 feet) weighing about 10.54 kN (2.37 kips).

In order to make the fabric reinforcing cables easier to work with during construction, the required area of each steel cable was divided by three to create two additional cables that attached between each of the six columns. This gives a total of sixteen cables altogether. These additional cables are attached to pipe beams with a length of 1.07 m (3.51 feet), having a diameter of 27.9 cm (11 inches) and a thickness of 7.06 mm (0.279 inches). These beams span between the six columns and are attached at the bottom of the columns.

2.2.2.b Construction of Habitat and Equipment Requirements

The initial step in the construction of this habitat is to excavate an area of 148.6 m^2 (1600 square feet) to a depth of about 3.05 m (10 feet). Sides of excavation must slope at a 45^o angle to ensure slope stability.

Before the columns are transported to the lunar surface, they will be fabricated in two halves. These two halves will be connected together using high strength hinges. Once on the lunar surface, these halves are flipped together and latched using prefabricated clasps. The initial lengths of 7.62 m (25 feet) are driven into the regolith using the appropriately sized hammer and crane. The three 7.62 m (25 feet) lengths are simply spliced together using a prefabricated coupler. Once the piles have been driven securely into the regolith to the specified depth, the remaining hollow column above the floor height will be filled with regolith. Steel plates, having the same dimensions as the inner diameter of the columns, are then placed in the top of each column in such a way that the plates will be bearing on the regolith and the columns. The joists can then be laid across and fastened to these plates in the columns. Rectangular steel plates, used to resist the lateral regolith pressure, are then placed and fastened into prefabricated slots in the columns. These plates are also fastened to the hollow beams (see figure 5.1.1 in appendix A) which are, in turn, attached to the base of the columns. Both the upper and lower decking can be laid into place followed by the fastening of the cables and the placement of

the interior lining. During this construction time, ducts and pipes for air, water, etc. can be placed into the structure, along with the 1.52 m (5 feet) diameter entrance pipe (pressure lock).

Once everything is constructed and checked, the structure can be backfilled and protected with a layer of regolith no more than 2.13 m (7 feet) thick on the roof surface, sloping the sides downward on a 3:1 slope. The entrance pipe will protrude horizontally through the regolith cover.

2.3 Lunar Habitat (Alternative 2)

2.3.1 Foreword

In this design, the habitat is comprised of multiple modules. Figures 5.1.4 and 5.1.5 (see appendix A) illustrate five of these modules. Although identical in structure, each module serves a specific function so that together they form a suitable habitat. Figure 5.1.6 illustrates these functions, as well as, shows dimensions of the modules. The number of modules varies with the number of personnel to be sheltered, however, since the minimum design capacity of the habitat is three personnel, a minimum of five modules will be required. The modules can be arranged in numerous configurations and modules can be added to create additional habitable space. The modules are connected together by a short network of cylindrical passageways. The habitat shown in figures 5.1.4 and 5.1.5 (see appendix A) illustrates one possible module arrangement.

2.3.2 Design

Most of the analysis of this structure was performed using a computer structural analysis program called Structural Analysis and Design III (STAAD-III). This program uses a finite element analysis to determine stresses in structural elements. Structural members were then chosen to limit these stresses to an allowable stress specified by ASD procedures.

For Aluminum Alloy - 6061-T6

$$F_b = 0.66\ (241.3\ \text{MPa}) = 159.3\ \text{MPa}\ \ (23.1\ \text{ksi})$$

Although most of the material in the module is aluminum, high strength steel was required for four tension members.

For Steel Alloy - A490

$$F_t\ (\text{for gross area}) = 0.6\ (1034.2\ \text{MPa}) = 620.5\ \text{MPa}\ \ (90.0\ \text{ksi})$$

The modules described in the foreword are composed of aluminum decking reinforced with I-shaped aluminum members. The aluminum decking was designed by analyzing a plate spanning one-direction, with a moment of inertia (I) = 49,867 mm^4 per 32.6 mm of decking, This is identical to the moment of inertia of the decking shown in figure 2.3.1. The maximum span of the decking for this habitat is 0.589 meters.

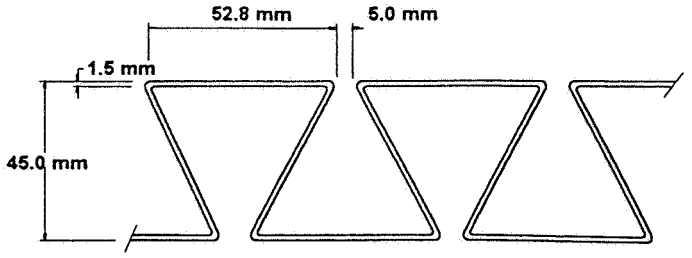

Figure 2.3.1

I-shaped members were designed to provide the decking with addition strength. From analysis, a structural member with the dimensional properties illustrated in figure 2.3.2 is required.

The aluminum decking is welded to the grid of reinforcing members resulting in the plates illustrated in figure 2.3.3. Although a module is made up of 26 reinforced plates, there are only five different sized plates as shown in this figure.

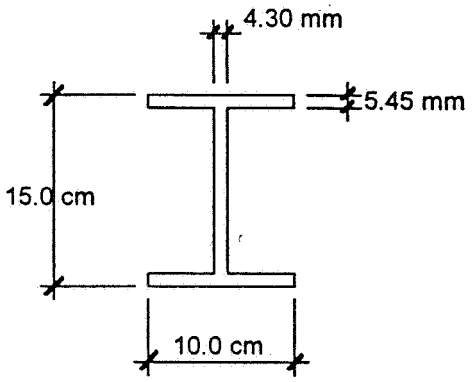

Figure 2.3.2

Hinge connections will be used to connected the system of plates together. This gives the structure some degree of flexibility and allows the structure to be folded together during transportation. Four hinges will be provided on each edge of the plates at the point of convergence of the I-shaped sections. Double shear pins (A-490 steel alloy) with a diameter of 1.58 cm (0.625 inches) will be used for the hinges.

In order to create more usable space within a module, steel rods were used to draw the top and bottom plates together. This reduces the structure's height, but increases the horizontal dimensions. Four, A-490, 1.58 cm (0.625 inches) diameter rods located at

the corners of the top and bottom plates were used to achieve this. (see figure 5.1.6 in appendix A)

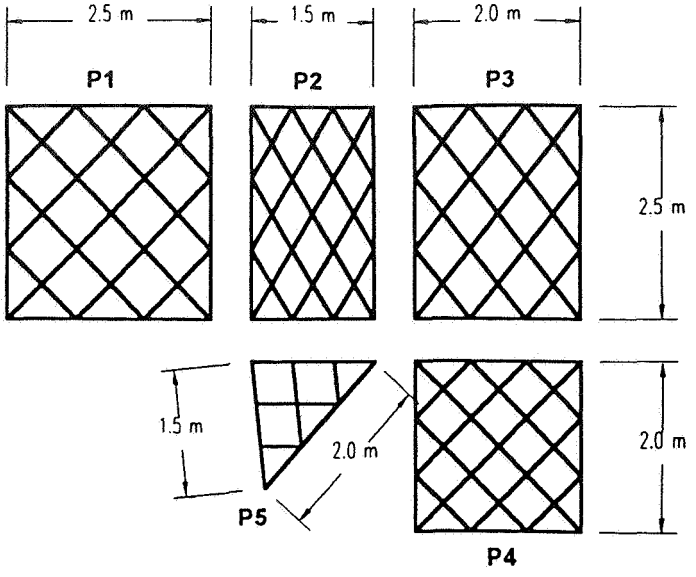

Figure 2.3.3

Due to the hinging of the plates, the structure is not likely to be air tight. Therefore, a lining will be needed to seal the module. The tensile strength of the fabric is not critical since the aluminum decking will be resisting the pressure loads, however, the fabric must have a low gas permeability.

As stated previously, the modules are connected together by a short network of cylindrical passages. The diameter of the cylinders is 1.75 m (5.74 feet) and the walls are 5 mm (.1875 inches) thick. The entrance (pressure lock) into the habitat is also cylindrical. Because the pressure lock is subjected to cyclical pressures changes, the materials that make up to pressure lock are subject to fatigue. Since the walls of a pressurized cylinder are in tension and not in bending, they are more resistant to fatigue failure.

2.3.2.a Material Requirements

The required structural materials for a habitat designed to support three personnel (five modules) is listed in the following tables.

Aluminum Decking

Material	Quantity	Weight of Material	Total weight per Module	Total weight per Habitat
6061-T6	92.9 m^2	52.31 lb/m^2	11.61 kN (2.61 k)	58.05 kN (13.05 k)

Aluminum I-shaped Members

Material	Quantity	Weight of Material	Total weight per Module	Total weight per Habitat
6061-T6	535.09 m	9.94 lb/m	23.67 kN (5.32 k)	119.9 kN (26.95 k)

Steel Tension Rods

Material	Quantity	Weight of Material	Total weight per Module	Total weight per Habitat
A-490	16.0 m	3.42 lb/m	0.24 kN (0.055 k)	1.21 kN (0.273 k)

Aluminum Cylindrical Passages

Material	Quantity	Weight of Material	Total weight per Module	Total weight per Habitat
6061-T6	17.5 m	79.83 lb/m	--	6.18 kN (1.39 k)

Pressure Fabric

Material	Quantity	Weight of Material	Total weight per Module	Total weight per Habitat
--	92.9 m^2	1.5 lb/m^2 *	0.62 kN (0.14 k) *	3.11 kN (0.70 k) *

* assumed weight

Total Weight of Structural Materials (approx.) -- 188.4 kN (42.36 k)

2.3.2.a Construction of Structure and Equipment Requirements

To construct this habitat, an area approximately 14 m (45.9 feet) x 16 m (52.5 feet) must be leveled on the lunar surface. Each module will then be folded together (with the help of a crane) and pins will be inserted into the remaining hinges. Once all the hinges are secured, the four steel rods can be installed followed by the pressure lining. The modules can then be arranged into the desired configuration and connected together by the cylindrical passageways. Finally, a 2 m thick cover of regolith will be placed over the habitat with the entrance tunnel protruding through the cover horizontally.

One of the primary advantages of this design is the small amount of cargo space required to transport the modules to the lunar surface. Because the plates are connected by hinges, they can be folded together during transportation. Upon arrival at the intended destination, the modules can be unfolded and assemble relatively easy. Figure 2.3.4

illustrates the 26 hinged plates. Figure 2.3.5 gives the overall dimensions of the folded plates. Since the depth of each plate is 19.5 cm (7.68 inches), the total depth of the folded plates in figure 2.3.5 is approximately 39 cm (15.3 inches).

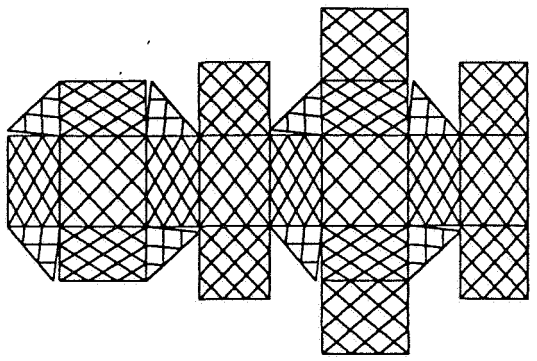

Figure 2.3.4

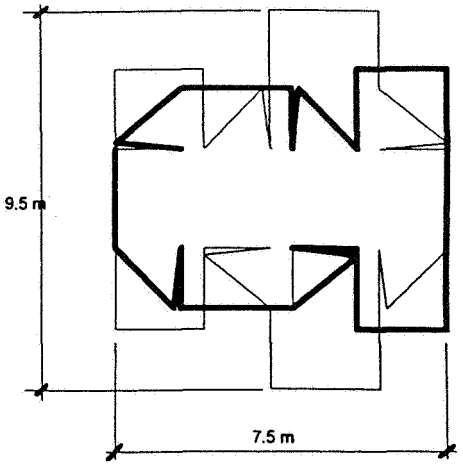

Figure 2.3.5

3.0 Railgun Supporting Structure

3.1 Foreword

The supporting structure for the railgun was designed according to information provided by the Aerospace Design Team. The main purpose of the supporting structure is to resist the large longitudinal forces generated by the accelerating projectile. The proposed design will involve the use of an existing crater's side slope for the support of the railgun. By using large amounts of regolith to achieve the required angle of 24 degrees, the amount of materials needed to be imported from earth will be significantly reduced.

3.2 Design

The following information has been provided by the Aerospace Design Team:

1. Muzzle angle of 23 degrees
2. 100 meters of platform length will be required for acceleration of projectile.
3. 200 meters of platform length will be required for deceleration of the projectile's sled.

The total mass of the projectile and platform is 120 kg. This mass will be accelerated over a 100 m length track to a velocity of 1650 m/s. This results in an acceleration of 13,612 m/s^2. The resultant force of the accelerating mass that must be resisted by the supporting structure is 1633 kN. Using an allowable soil bearing capacity of 95.76 kPa, 22 steel plate footings (1.45 m x 1.45 m) are required. Figure 3.1.1 shows the location and orientation of the footings.

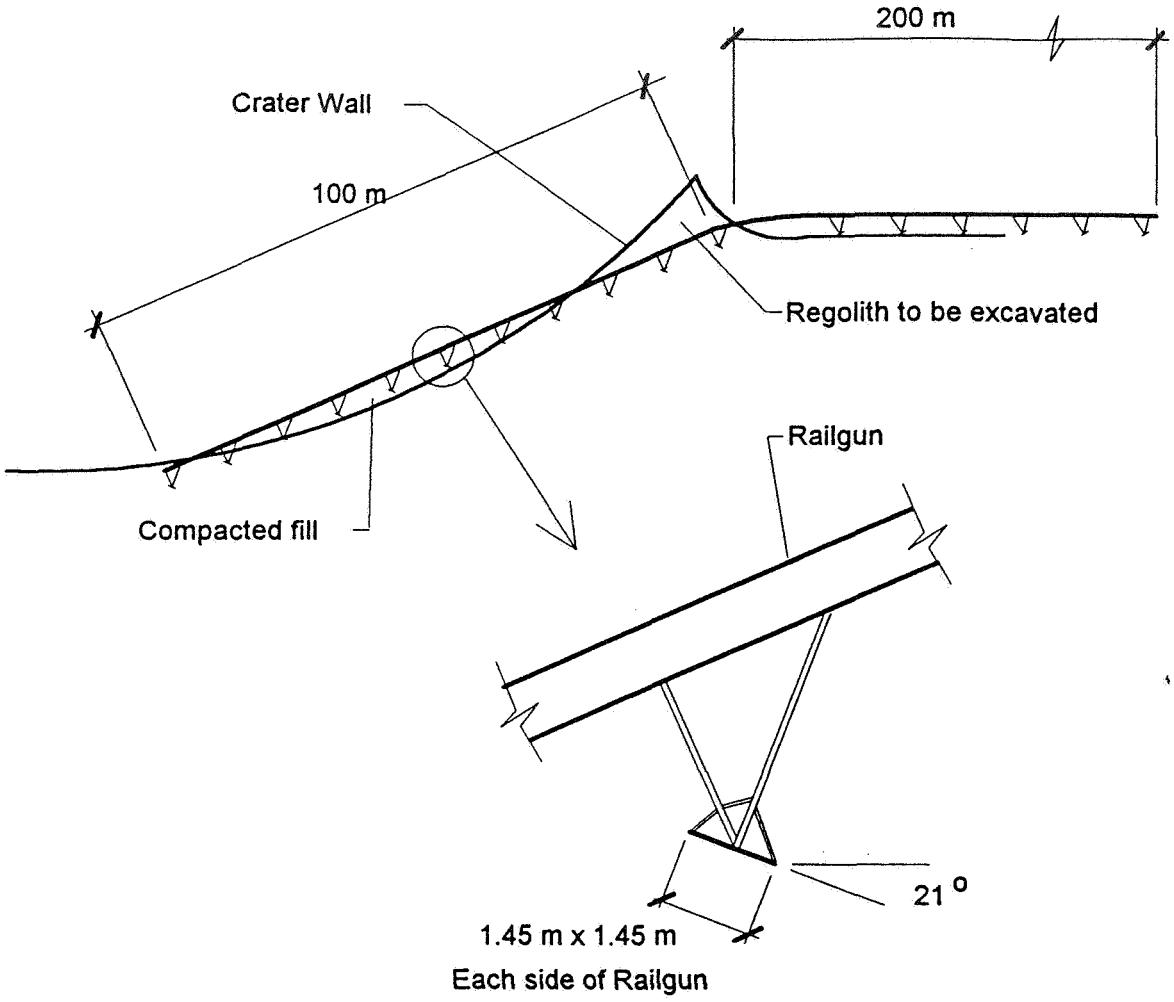
200 m
Crater Wall
100 m
Regolith to be excavated
Railgun
Compacted fill
21 °
1.45 m x 1.45 m
Each side of Railgun

Figure 3.1.1

4.0 Conclusion

The main goal of the Civil Engineering Design Team was to design the structural systems required for the lunar processing facility. The focus of this report was on the design of the habitat and the supporting structure for the railgun. Many design considerations were many including weight of materials, cargo space requirements for transportation of structural systems, construction of systems and equipment requirements, maintenance and radiation protection.

Two habitat designs were initiated in this report. In both of these designs, a modular design was chosen so that the size of the habitat could be increased as the need for habitable space increased. Since radiation and micrometeor bombardment were safety concerns, a minimum of 2 m of regolith was used to shield the habitats from their harmful effects. The structures were also designed to support this regolith cover should the habitats need to be depressurized.

The supporting structure for the railgun was design to support both the self weight of the structure and the large resultant force of the accelerating projectile. To accomplish this, an angled footing was used. By angling the footing, it could more efficiently resist the lateral force.

A possible change to the habitat (Alternative 1) would be to reduce the length of the 75 feet long piles. This would reduce the weight of the structure significantly. To do this, the diameter of the pile would have to be increased to accommodate the large bending moment. To increase the upward thrust resistance of a shorter column, the bottom of the column would have to be widened or flared.

In this report, the structures have been designed to resist the loads as efficiently as possible, however, because data on some material properties was not well defined, assumptions were made resulting in a more conservative design.

5.0 Appendix A

Illustrations

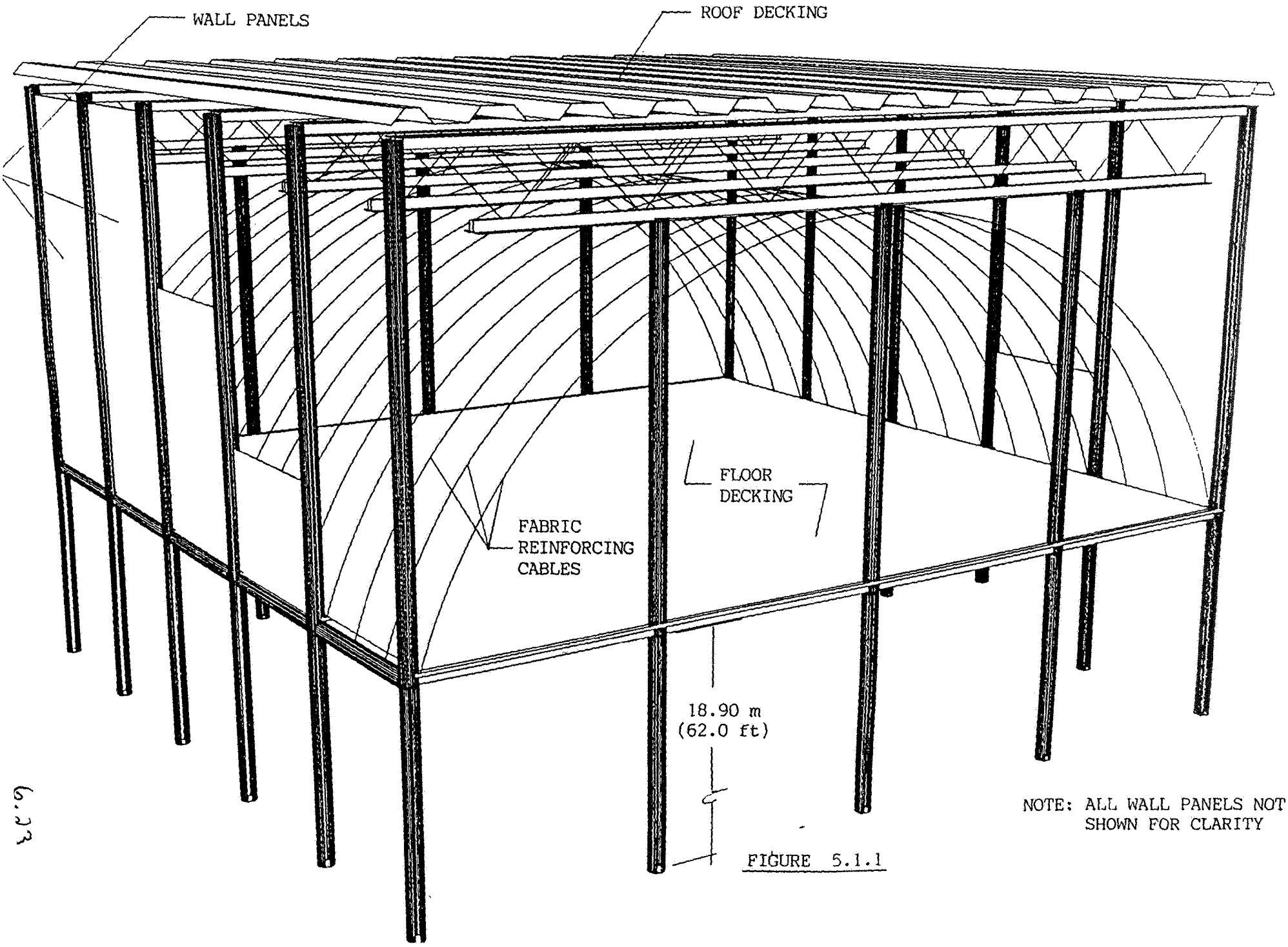

NOTE: ALL WALL PANELS NOT SHOWN FOR CLARITY

FIGURE 5.1.1

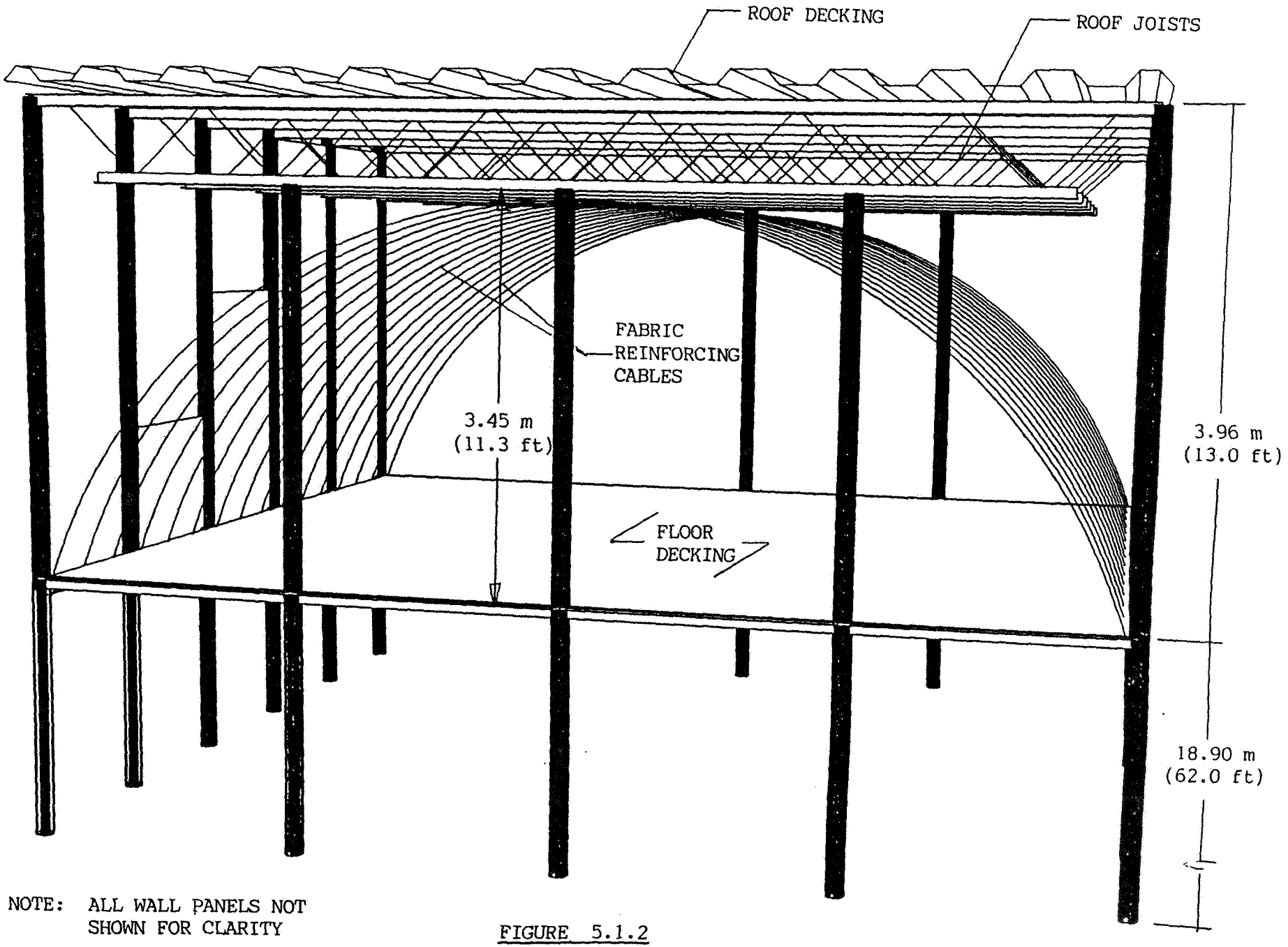

NOTE: ALL WALL PANELS NOT SHOWN FOR CLARITY

FIGURE 5.1.2

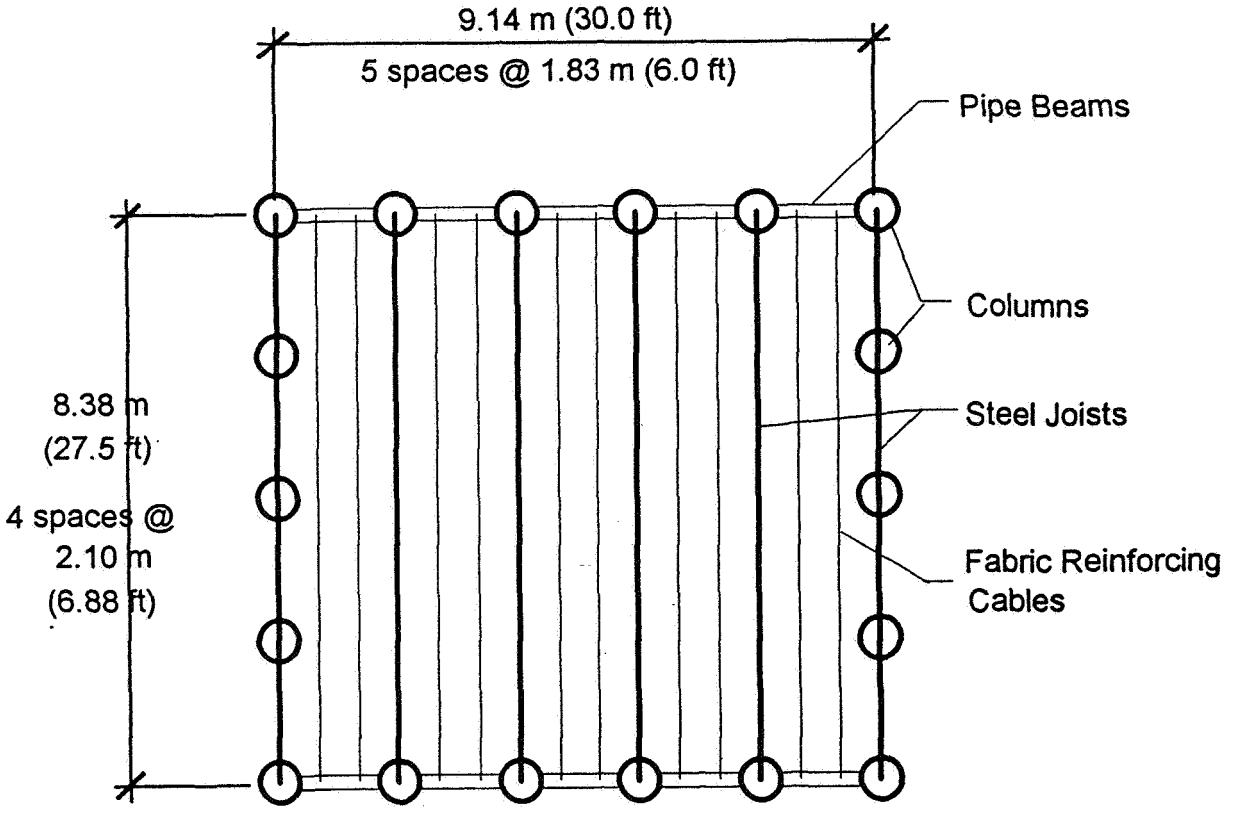

Plan View of Habitat Alternative #1

Figure 5.1.3

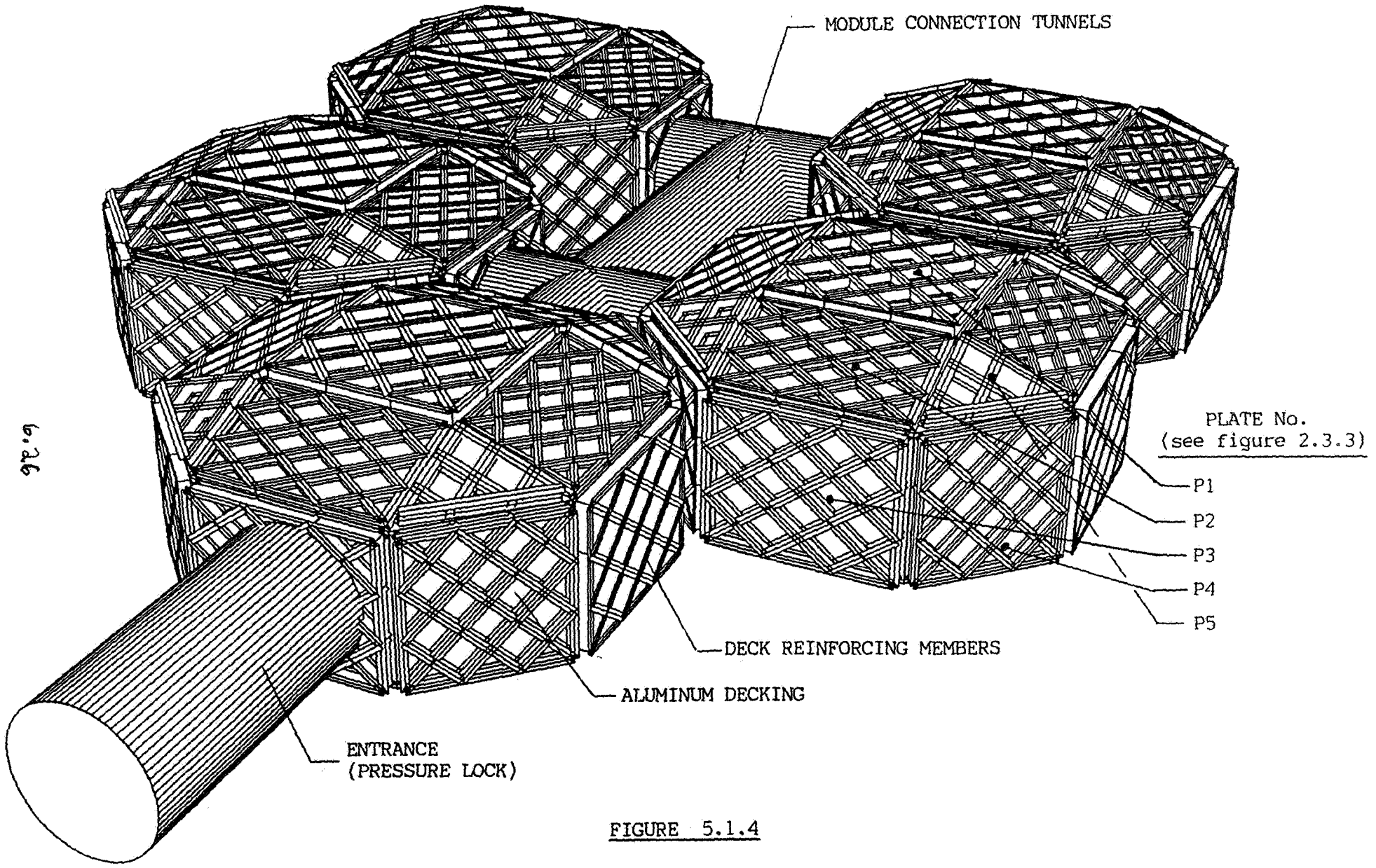
MODULE CONNECTION TUNNELS
PLATE No.
(see figure 2.3.3)
P1
P2
P3
P4
P5
DECK REINFORCING MEMBERS
ALUMINUM DECKING
ENTRANCE
(PRESSURE LOCK)

FIGURE 5.1.4

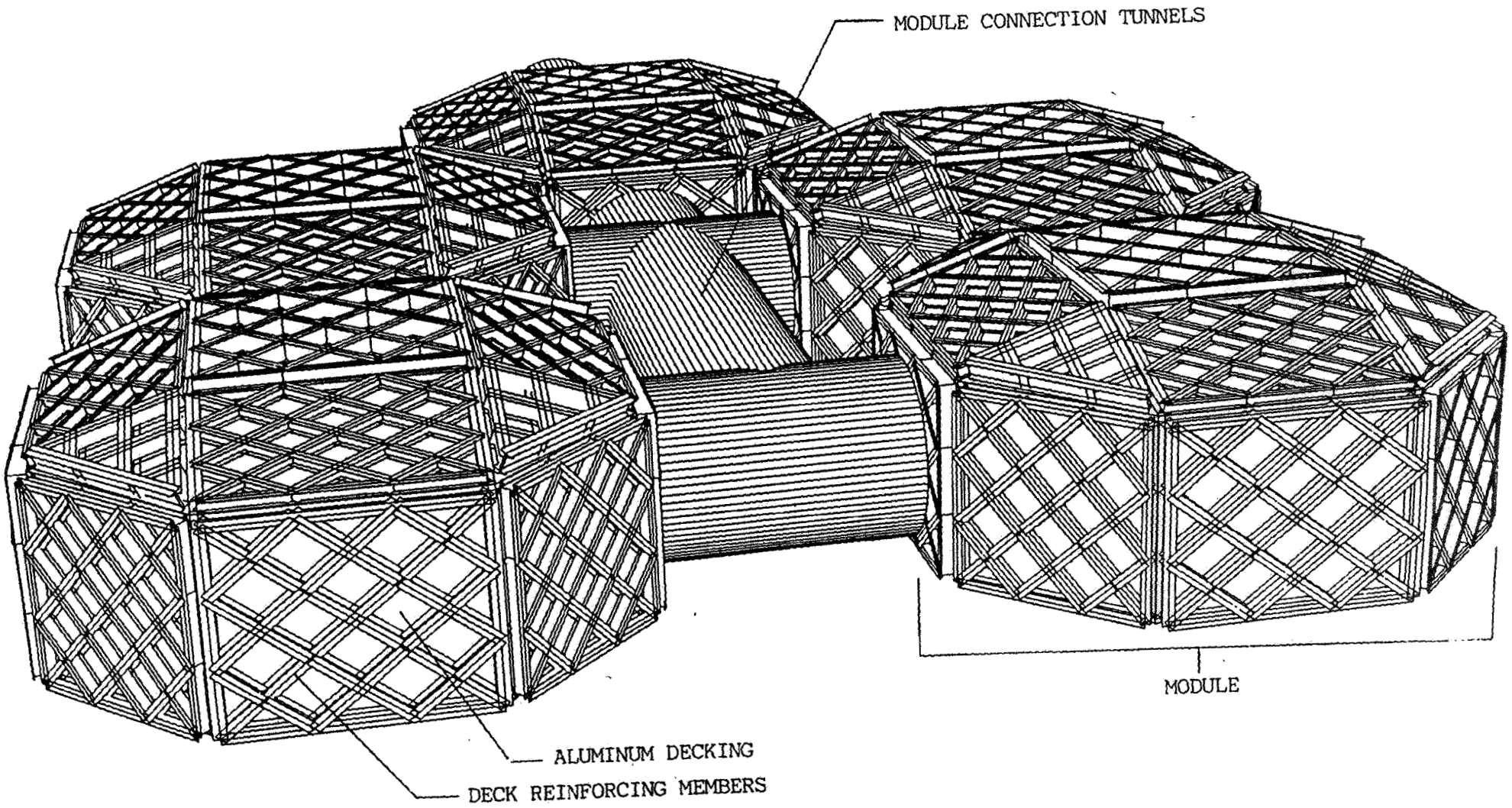
MODULE CONNECTION TUNNELS
MODULE
ALUMINUM DECKING
DECK REINFORCING MEMBERS

FIGURE 5.1.5

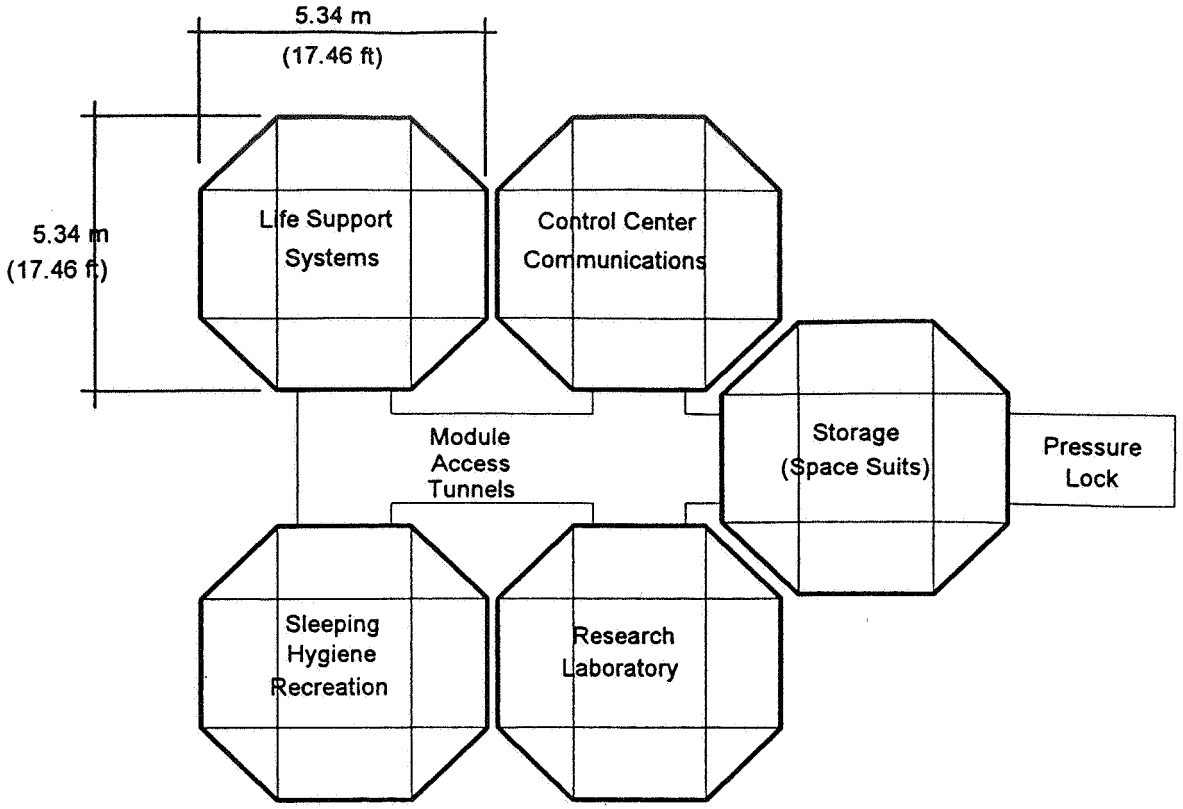

Plan View of Habitat Alternative #2

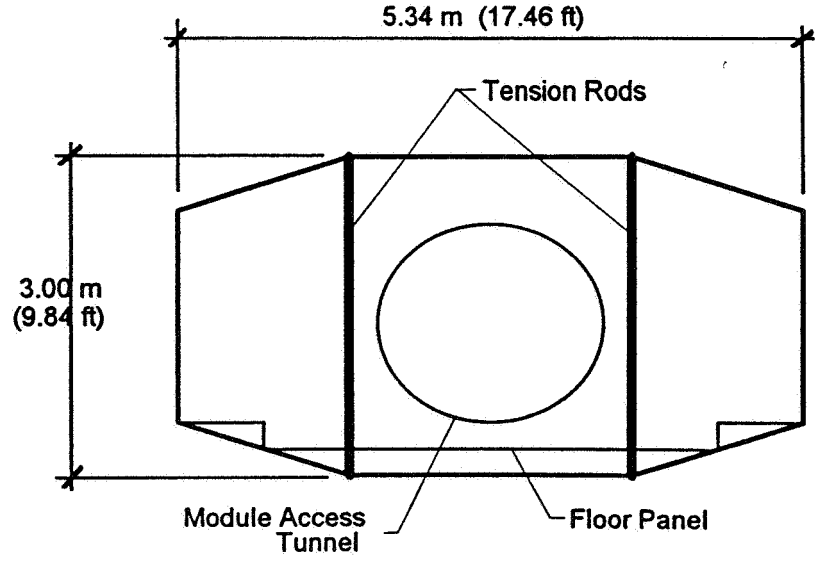

Section View of Module

Figure 5.1.6

6.0 Appendix B

Supporting Calculations

JOIST AND DECK DESIGN (ROOF)

LOOSE ROCK UNIT WEIGHT ≅ 65 pcf

HARD ROCK UNIT WEIGHT ≅ 175 pcf

WE WILL USE 120 pcf ÷ 1/6 = 20 pcf
for moon gravity

7 FEET OF REGOLITH

TOTAL WEIGHT OF REGOLITH ONTO DECK = (7 ft)(20 pcf) = 140 psf

ROOF DECK:

THREE SPAN, 1.5B16 spanning 5'-6"

WT = 3.44 psf
I = 0.370 in⁴/ft

JOIST!

SPAN = 30'

LOAD ON JOIST = 145 psf * 5.5 ft = 798 plf

CHOOSE A 20LH9, CAPACITY = 859 plf

WEIGHT = 21 plf

CABLE DESIGN

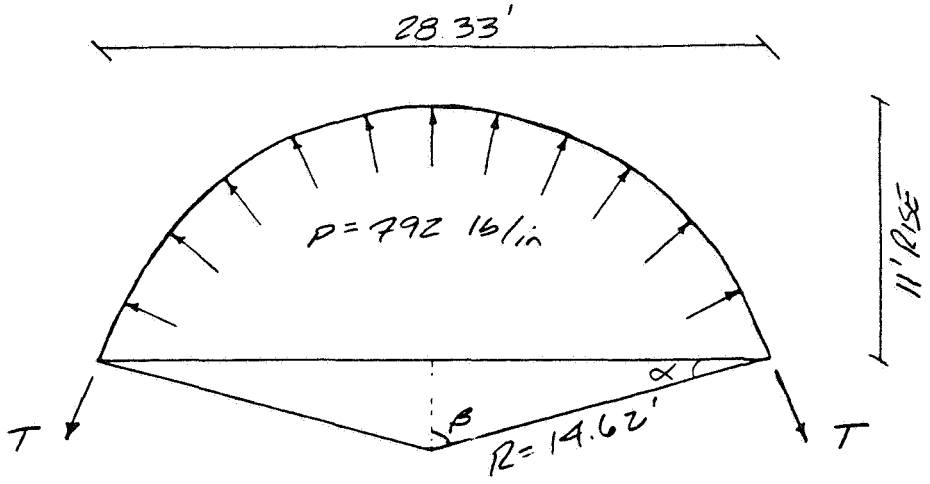

RADIUS $R = \frac{4b^2 + c^2}{8b} = \frac{4(11^2) + 29^2}{8(11)} = 14.62'$

$\beta = \cos^{-1}\frac{3.6}{14.62} = 75.74°$, $\alpha = 14.26°$

PRESSURE = 12 psi * 66" = 792 lb/in = P

HORIZONTAL COMPONENTS OF PRESSURE CANCEL OUT.

$$\int_{-\beta}^{\beta} p\cos\theta R\,d\theta = RP\sin\theta\Big|_{-\beta}^{\beta} = 2RP\sin\beta$$

VERTICAL REACTION AT EACH END OF CABLE = $RP\sin\beta$

TENSILE FORCE $= \frac{RP\sin\beta}{\cos\alpha} = \frac{(14.62)(12")(792\#/in)\sin 75.74}{\cos 14.26}$

$= 138,949$ lb/cable

DIVIDE BY 3 FOR 3 AREAS $= 138,949/3 = 46,316$ lbs/cable

$f_{pu} = 270$ ksi

$f_{pu} A_p = 51.8$ kips > 46.3 kips Area $= 0.192\,in^2$, $\phi = 9/16"$

wt = 0.35 plf

INTERIOR LINING STRENGTH DESIGN

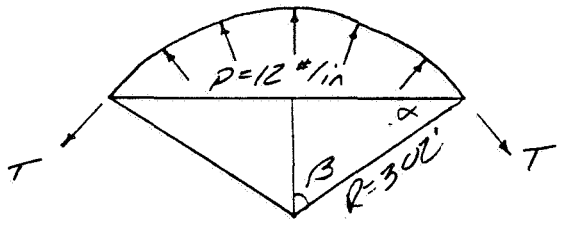

$$\text{RADIUS } R = \frac{4b^2 + c^2}{8b} = \frac{4(1.5) + (5.5)^2}{8(1.5)} = 3.02'$$

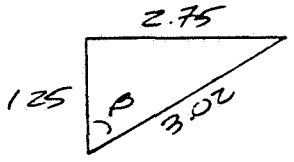

$$\beta = \cos^{-1}\frac{1.25}{3.02} = 65.55^\circ \qquad \alpha = 24.45^\circ$$

$$\text{PRESSURE} = 12\,\text{psf} * 1' = 12\,\#/\text{in} = P$$

$$\text{TENSILE FORCE} = \frac{\left(\frac{3.02'}{3}\right)(12'')(12\,\#/\text{in})\sin 65.55^\circ}{\cos 24.45^\circ}$$

$$= \frac{135}{3}\ \#/\text{inch length of fabric}$$

$$= 145\ \#/\text{in}$$

HOLLOW BEAM DESIGN

THIS HOLLOW BEAM IS USED TO RESIST THE TWO CABLES PLACED BETWEEN EACH COLUMN. THESE HOLLOW BEAMS SPAN 3.51', THE DISTANCE BETWEEN THE COLUMNS, AND ARE ATTACHED AT THE BASE OF THE COLUMNS. EACH CABLE LOAD = 46.3 k.

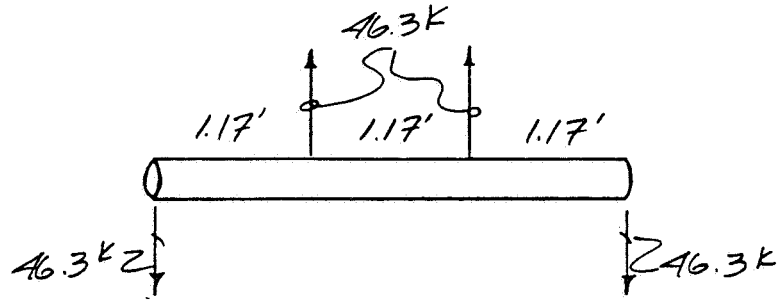

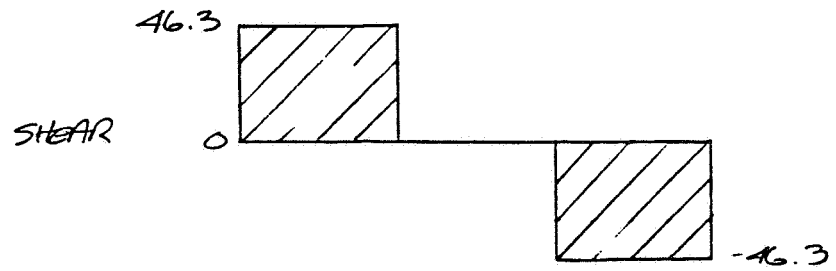

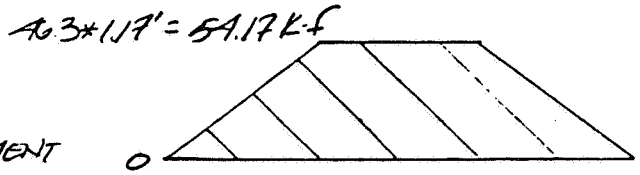

USING YIELD STRENGTH = 0.66(100ksi) = 66ksi

CHOSE AN 8" DIAMETER, HOLLOW STEEL PIPE, WITH SECTION MOD. = 10.10 in^3 AND THICKNESS = 0.219 in.

$$M_{all} = (66\,ksi)(10.10\,in^3)\left(\frac{1\,ft}{12\,in}\right) = 55.55\ k\text{-}f$$

$M_{all} > M_{req'd}$, OK ✓

WT. OF BEAM = (18.19 plf) * 3.51' = 63.8 lbs = 0.064 kips/beam

STEEL PANEL DESIGN

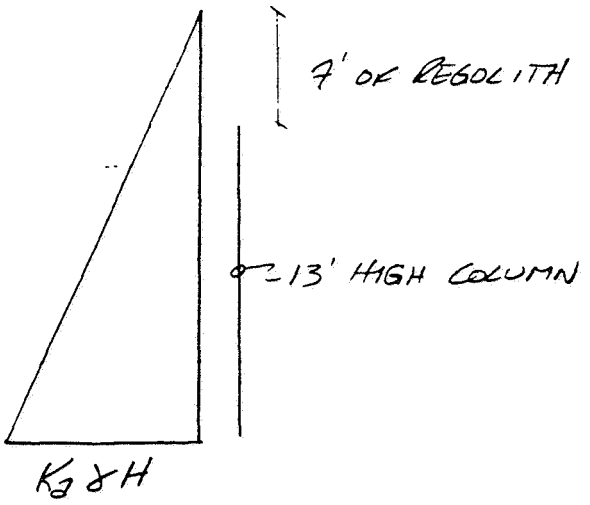

$K_a \gamma H = 0.2174(20\,pcf)(20') = 86.96\,psf$

ASSUMING A 2' HIGH PANEL, THE LOAD ON THE PANEL ALONG THE 5.5' LENGTH OF PANEL (INTO THE PAPER)

$= (86.96\,psf)(2') = 173.92\,plf$

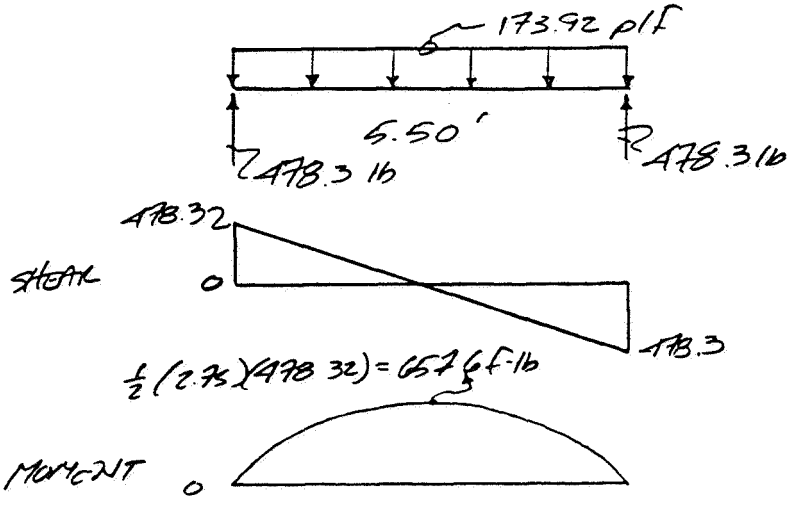

STEEL PANEL DESIGN, CONT'D.

TRY A 0.1793 in THICK PIECE OF GAGE 7 STEEL

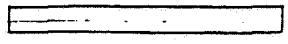

$$I = \frac{bh^3}{12} = \frac{(2')(12'')(.1793)^3}{12} = 1.15\times10^{-2}\ in^4$$

$$c = d/2 = .1793/2 = 0.0897\ in$$

$$\sigma = \frac{Mc}{I} \qquad M_{all} = \frac{\sigma I}{c} = \frac{(0.66)(100ksi)(1.15\times10^{-2}\ in^4)}{0.0897}$$

$$M_{all} = 8.46\ k\text{-}in = 0.7051\ k\text{-}ft = 705.1\ lb\text{-}ft$$

$$M_{ALL} > M_{REQ'D} = 705.1\ ft\text{-}lb > 657.6\ ft\text{-}lb \quad \underline{OK} \checkmark$$

WT. OF PANEL = (2' HIGH) * (5.5' LONG) * $\left(\frac{0.1793''}{12''}\right)$ * (490 lb/ft³)

5.5' LONG

= 80.5 lbs

WT OF PANEL = (2' HIGH) * (3.51' LONG) * (0.1793/12) * (490 lb/ft³)

= 51.4 lbs

ON 27'-6" SIDE, (6 panels) * (5 rows) * (51.4 lbs) * 2 SIDES = 3084 lbs

ON 30'-0" SIDE, (6 panels) * (4 rows) * (80.5 lbs) * 2 SIDES = 3864 lbs

TOTAL PANEL WT. = 6,948 lbs = 6.95 KIPS

COLUMN/PILE DRAWING

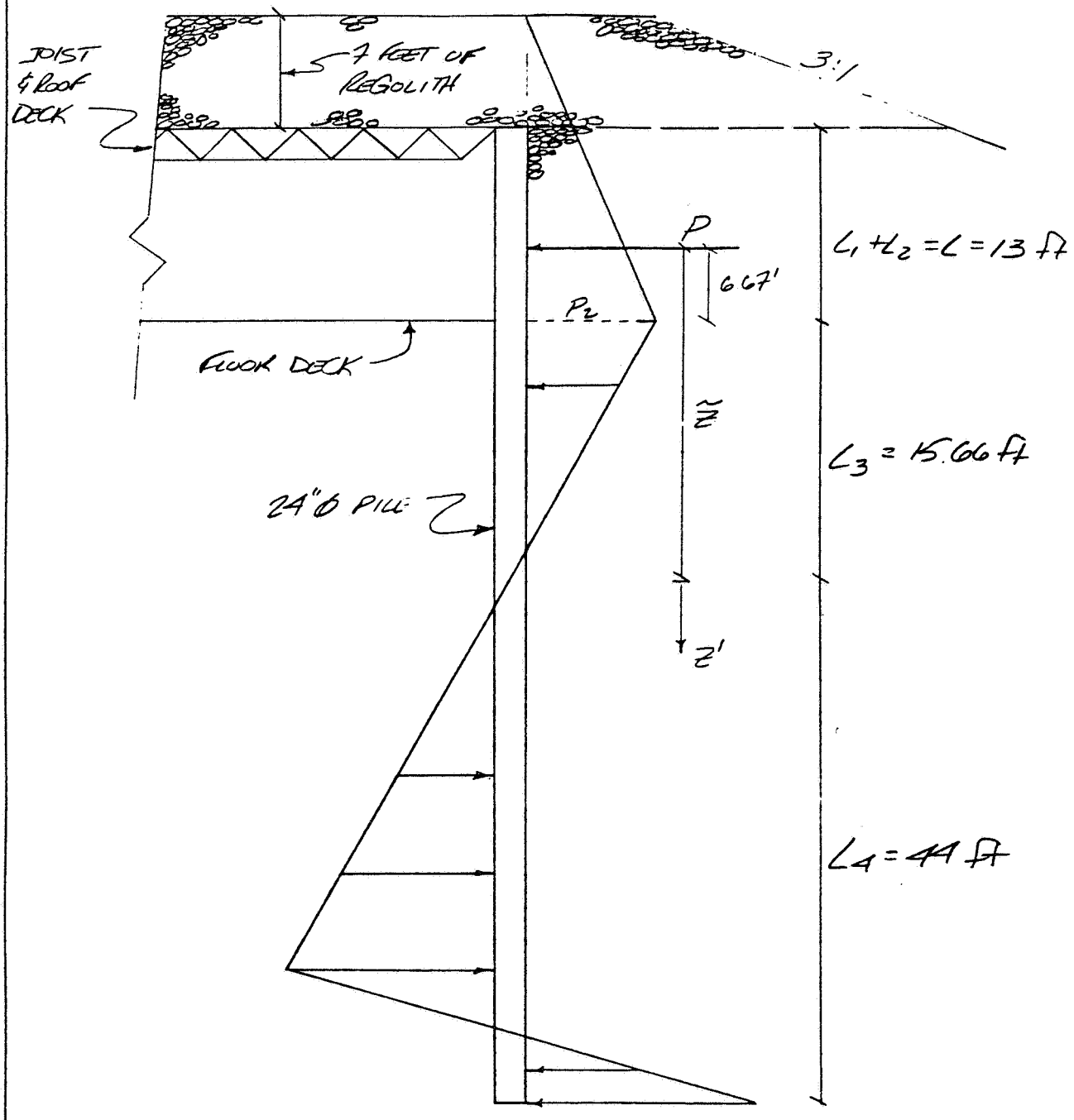

FIGURE

COLUMN/PILE DESIGN

ALL EQUATIONS TAKEN FROM PRINCIPLES OF FOUNDATION ENGINEERING AND PRINCIPLES OF GEOTECHNICAL ENGINEERING, DAS, SECOND EDITION.

UNIT WT. OF SOIL = 20 pcf AND $\phi = 40°$ FROM INFORMATION PROVIDED BY

$$K_a = \tan^2(45 - \phi/2) = \tan^2(45 - 40/2) = 0.2174$$

$$K_p = \tan^2(45 + \phi/2) = \tan^2(45 + 40/2) = 4.5989$$

TO BE MORE CONSERVATIVE, $K_{p(DESIGN)} = \frac{K_p}{FS}$ IS USED

$$K_{p(DESIGN)} = \frac{4.5989}{2} = 2.30$$

REFER TO FIGURE ON PREVIOUS PAGE

$$P_2 = \gamma H K_a = (20pcf)(10ft)(0.2174)(7.5ft) = 652.2 plf$$

$$L_3 = \frac{P_2}{\gamma'(K_p - K_a)} = \frac{652.2}{20(2.30 - .2174)} = 15.66 ft$$

$$P = \tfrac{1}{2}(652.2)(20) = 6522 lbs$$

$$P_5 = (\gamma L_1 + \gamma' L_2) K_p + \gamma' L_3 (K_p - K_a)$$

$$= (20*20)\,2.3 + 20(15.66)(2.3 - 0.2174) = 1572.3 plf$$

$$A_1 = \frac{P_5}{\gamma'(K_p - K_a)} = \frac{1572.3}{20(2.3 - .2174)} = 37.75$$

$$A_2 = \frac{8P}{\gamma'(K_p - K_a)} = \frac{8(6522 lbs)}{20(2.3 - 0.2174)} = 1252.7$$

COLUMN / PILE DESIGN, CONT'D.

$$\bar{z} = L_3 + \tfrac{1}{3}h = 15.66' + \tfrac{1}{3}(20) = 22.33 \text{ ft}$$

$$A_3 = \frac{6P[2\bar{z}\gamma'(K_p - K_a) + P_S]}{\gamma'^2(K_p - K_a)^2} = \frac{6(6522)[2(22.33)(20)(2.3 - .2174) + 1572.3]}{20^2(2.3 - 0.2174)^2}$$

$$A_3 = 77422.67$$

$$A_4 = \frac{P(6\bar{z}P_S + 4P)}{\gamma'^2(K_p - K_a)^2} = \frac{6522(6 * 22.33 * 1572.3 + 4 * 6522)}{20^2(2.3 - 0.2174)^2}$$

$$A_4 = 889{,}999$$

$$L_4^4 + A_1 L_4^3 - A_2 L_4^2 - A_3 L_4 - A_4 = 0$$

BY TRIAL & ERROR, $L_4 = 44$ feet

CALCULATE MAXIMUM MOMENT ON PILE:

$$M_{MAX} = P(\bar{z} + z') - \left[\tfrac{1}{2}\gamma' z'^2 (K_p - K_a)\right]\left(\tfrac{1}{3}\right) z' + \text{(HORIZ. COMP CABLE LOAD)}(L_3 + z')$$

where $z' = \left(\frac{2P}{(K_p - K_a)\gamma'}\right)^{1/2} = \left(\frac{2 * 6522}{(2.3 - .2174) * 20}\right)^{1/2} = 17.7 \text{ ft}$

$$M_{MAX} = 6522(22.33 + 17.7) - \left[\tfrac{1}{2}(20)(17.7^2)(2.3 - .2174)\right]\tfrac{1}{3}(17.7) + (35{,}260\#)(15.66 + 17.7)$$

$$= 222{,}580 \text{ f-lb} + 1{,}176{,}274 \text{ f-lb}$$

$$= 1{,}399 \text{ f-K}$$

$$M_{REQ'D} = 1399 \text{ f-K}$$

COLUMN/PILE DESIGN, CONT'D.

PILE MATERIAL: WELDED OR SEAMLESS TUBING, A500, COLD-FORMED, ROUND, GRADE C

CHOSE 24 IN OUTER DIAMETER

THICKNESS = 0.375 IN.

SECTION MODULUS = $161.87\ in^3$

YIELD STRENGTH = 100 KSI, (NO REDUCTION FACTOR USED SINCE F.S. = 2 WAS USED IN PILE DESIGN)

ALLOWABLE MOMENT = $\sigma S = (100 ksi)(161.87 in^3)\left(\frac{1 ft}{12 in}\right)$

$M_{ALLOW} = 1349\ f\text{-}k$

M_{ALLOW} IS SLIGHTLY LESS THAN $M_{REQ'D}$

THEREFORE, A YIELD STRENGTH EQUAL TO 104 KSI WOULD BE ADEQUATE. OK ✓

WT. OF PILE = $(94.62\ plf)(75 ft) = 7.1\ KIPS/PILE$

LOADS ON EACH COLUMN:

CABLE LOADING AT BASE OF COLUMN:

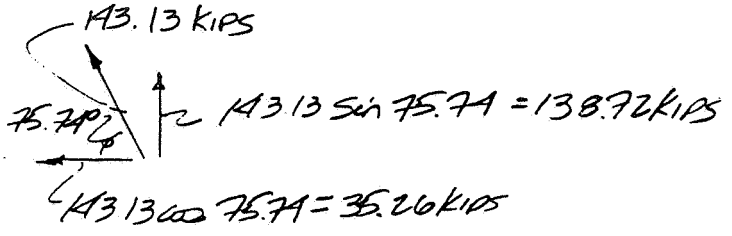

VERTICAL LOAD AT TOP OF COLUMN FROM SHIELDING:

$$(6.5\text{ft} * 7.5\text{ft}/2) * 145\text{psf} = 3.0\text{KIPS}$$

VERTICAL LOAD AT BASE OF COLUMN FROM FLOOR LOADING:

$$\left[\left(12\text{psi} * \frac{144\text{in}^2}{1\text{ft}^2}\right) + \underset{\text{LL}}{150\text{psf}}\right] * 5.5 * \frac{7.5}{2} \approx 39\text{ KIPS}$$

NOTE! SOME OF THIS LOAD ONTO REGOLITH

WEIGHT OF COLUMN = 7 KIPS

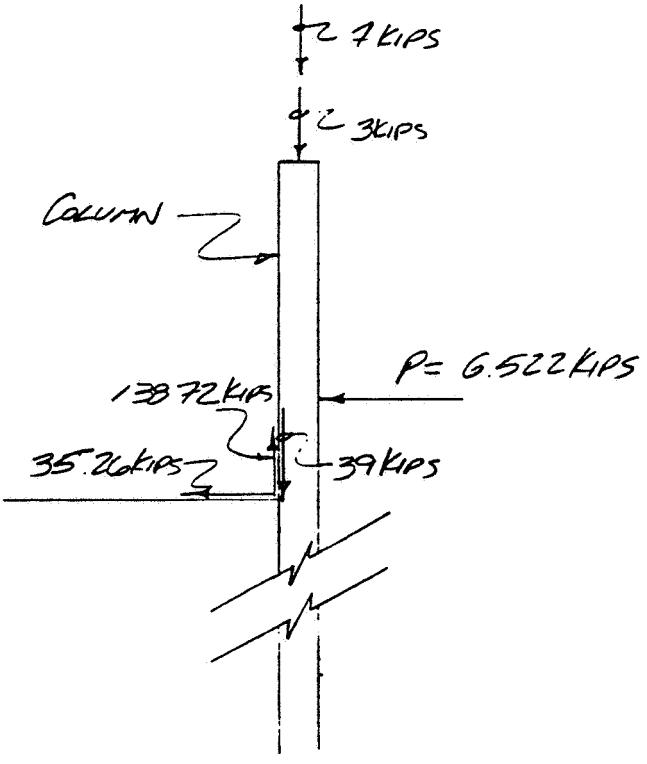

Σ VERTICAL = -7 - 3 - 39 + 138.7 = 90 KIPS UPWARD WHICH MUST BE HANDLED BY SKIN FRICTION.

SKIN FRICTION

$$Q_S = \Sigma p \Delta L f$$

$\Delta L = 13$ feet

$p = \pi D = \pi(2') = 6.28$ ft

$f = K\sigma_v' \tan\delta$

$K \tan\delta = 0.18 + 0.0065 D_r$

$= 0.18 + 0.0065(.74) = 0.185$

$\sigma_v' = 652.2$ psf FOR INITIAL 13 ft.

$f = 0.185 * 652.2 = 120.66$ psf

$Q_S = (6.28)(13)(120.66) = 9.85$ kips FOR FIRST 13'

FOR REMAINING LENGTH OF PILE,

$\sigma_v' = \gamma(h)K_\delta = 22(63')(.2174) = 274$ psf

$Q_S = (6.28)(62')(274) = 106.7$ kips

TOTAL FRICTIONAL RESISTANCE = 9.85k + 106.7k = 117 kips

117 kips > 90 kips. PILE OK ✓

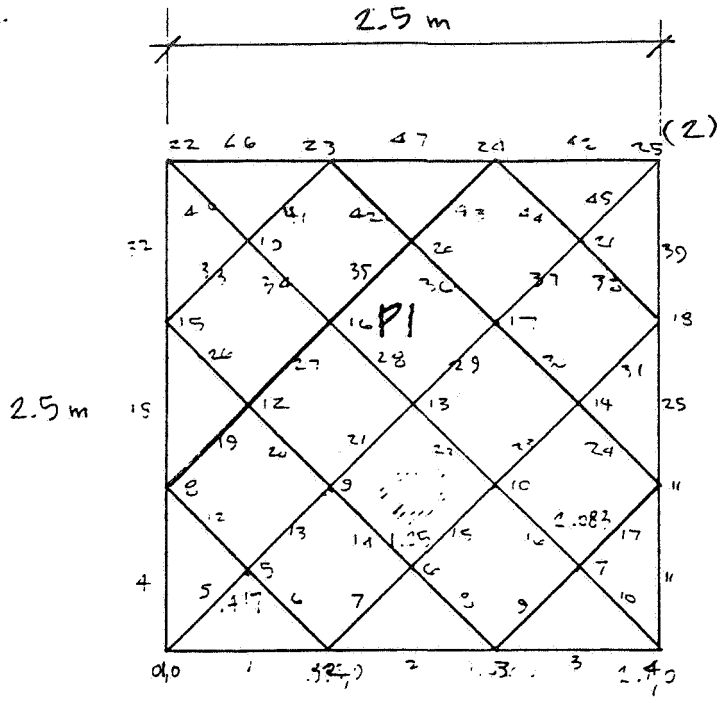

2.

62.43 ft m

L/180

.589

21.21

1.80 m

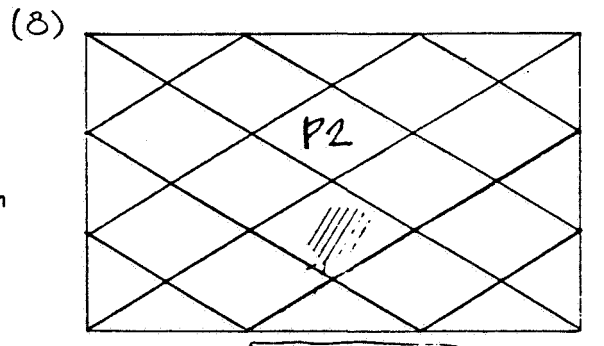

195.94 ft

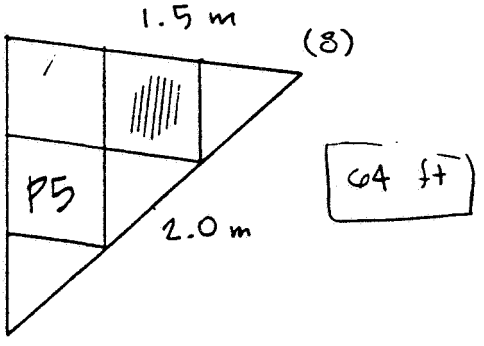

64 ft

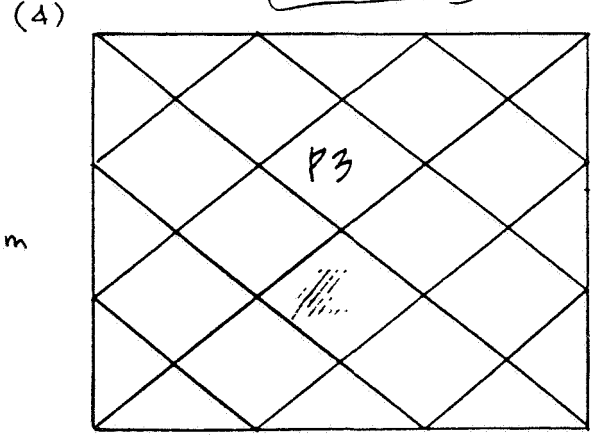

112.89 ft

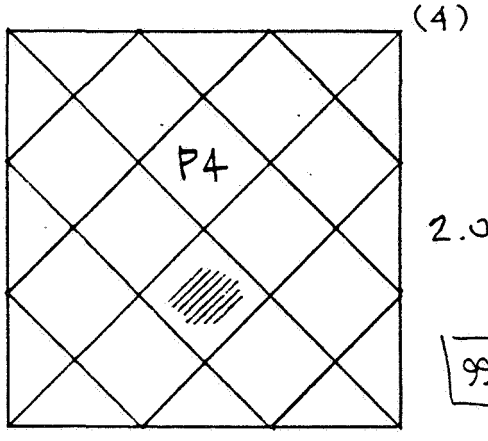

99.88 ft

ELEMENT PROPERTY
1 TO 24 TH 0.025

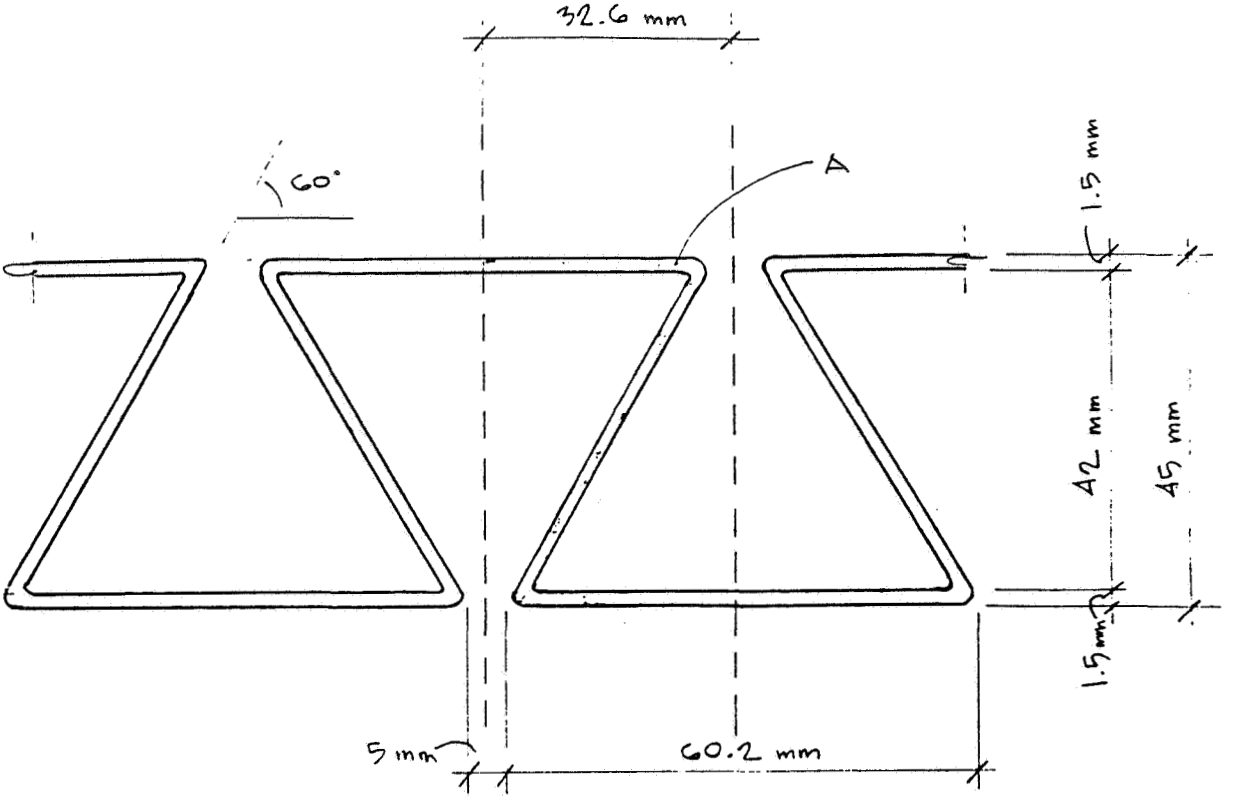

5. THICKNESS – 1.5 mm (≈16 GA.)

I_A = 49,867 mm^4 > 42,447 mm^4 (SOLID 2.5 cm THICK PLATE)

A_A = 1.57 cm^2

VOLUME OF 1m x 1m

.00482 m^3 = .170 ft^3

ALUMINUM DECKING – 28.05 lb/m^2 = 2.61 lb/ft^2

STEEL DECKING – 83.3 lb/m^2 = 7.74 lb/ft^2

PLATE NO.	DIMENSIONS(m)	AREA (m^2)	QUANTITY
P1	2.5 × 2.5	6.25	2
P2	1.5 × 2.5	3.75	8
P3	2.0 × 2.5	5.00	4
P4	2.0 × 2.0	4.00	4
P5	Δ1.5×1.5×2.0	1.80	8

TOTAL ~~AREA~~ WEIGHT — 92.9 m^2 (52.31 lb/m) = ~~4.86~~ 4.86 K

NEW DECKING

USING 1.5 mm (≈16 GA.) THICK SHEETS

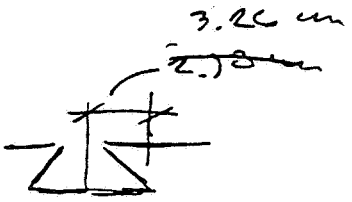

AREA = ~~1.404~~ 1.57 cm^2 1.404 cm^2

VOLUME = .00471 m^3 = .166 ft^3

= 27.4 lb/m^3 = 2.55 lb/ft^2

TOTAL WEIGHT — 92.9 m^2 (27.4 lb/m^2) = ~~2.54~~ 2.60 K

$\frac{2.86 \quad 45 - 42^3}{12}$ = 28,700 mm^4

4221

38,802 SOLID 2.5 cm DECK

40,604

49,865 mm^4

42,447 mm^4 SOLID

QUANTITY OF MATERIALS

ALUMINUM DECKING — 92.9 m^2

15 cm DEEP I-section (9.94 $^{lb}/_{m}$ or 3.03 $^{lb}/_{ft}$) — 535.09 m

WEIGHT

AL. DECKING — 92.9 m^2 (28.05 $^{lb}/_{m^2}$) = 2.606 K

I-sections — 535.09 m (9.94 $^{lb}/_{m}$) = 5.319 K

MODULE WEIGHT

7.925 K

DESIGN OF TENSION RODS & HINGES

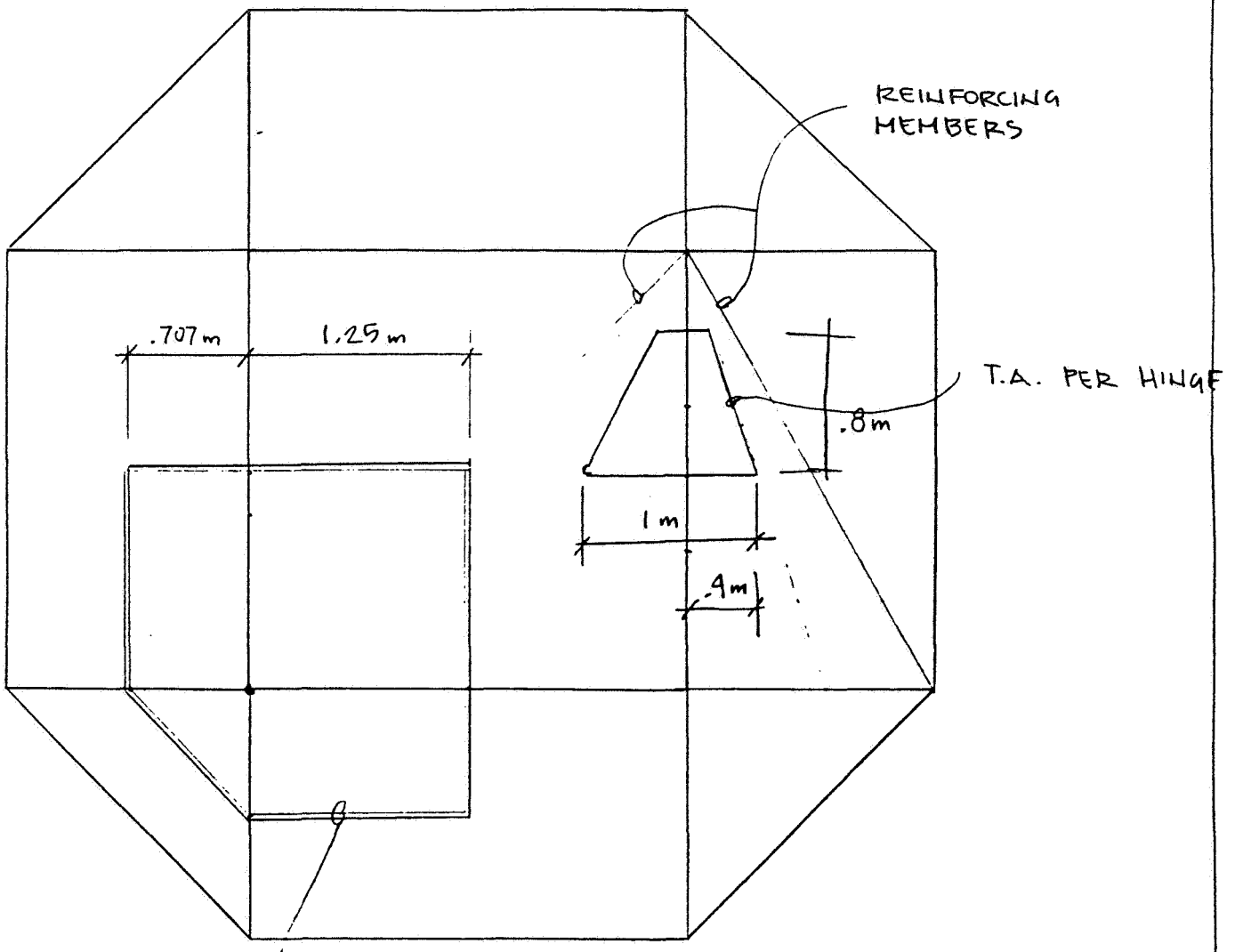

— RODS

$T.A. = (.707 + 1.25)^2 - .25\ m^2 = 3.57\ m^2 = 11.7\ ft^2$

$LOAD = 11.7\ (1728\ lb/ft^2) = 20.2^K$

$A_{REQ} = P/F_t = \frac{20.2^K}{150\ ksi\ (.6)} = .22\ in^2$

use 5/8" ROD
$A = 30.7\ in^2$

5/8" = .625 = 1.58 cm.

— HINGE

RESULTANT SHEAR ON PIN - CONVERSION TO ENGLISH UNITS

SHEAR FORCE $= .4_n(.8\ m)\ (10.764)(1728)\ (1.41/.5) = 16.78^K$

PIN IN DOUBLE SHEAR (A490)
FROM TABLE 1-D (ASD) USE 5/8" CAP = 24.5^K

DESIGN OF CYLINDRICAL PASSAGES

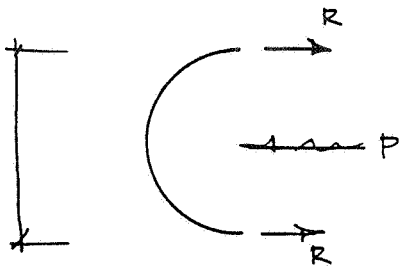

INTO PAGE

$P = 5.74' (1') (1728\ lb/ft)$

$= 9918$

$R = P/2 = 4.95\ K$

$F_T = .6 (F_Y) = .6 (35\ ksi) = 21\ ksi$

$w \times t = \frac{R}{F_T} = \frac{4.95}{21} = .235$

$t = \frac{.235}{12} = .019$ inches use minimum of 5 mm ($3/16$")

WEIGHT

LENGTH OF TUBING +5m (PRESSURE LOCK)

$= 2.5 (2) + 5.5\,m + 2.0\,m) = 17.5$

~~WEIGHT/m~~. VOLUME PER METER LENGTH

$= .0137\ m^3$

WEIGHT

$= .0137\ m^3 (5826.8\ lb/m^3)\ 17.5\ m = 997.8$ lbs.

$79.83\ lb/ft$

DESIGN OF RAILGUN SUPPORT

$$a = \frac{V_0^2}{2s} = \frac{(1650\ m/s)^2}{2\,(100\ m)} = 13{,}612\ m/sec^2$$

$$F = ma = 120\ kg\ (13{,}612) = 1633\ KN\ (367\ k)$$

assuming allowable soil pressure is $2000\ lb/ft^2$ ($95.76\ KPa$)

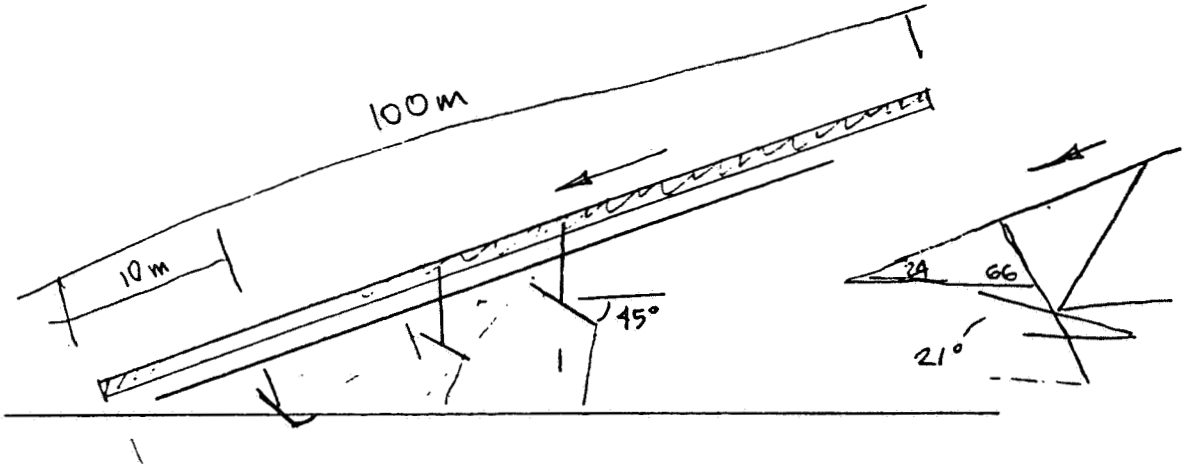

required area of footing

$$367 / 2.0\ k/ft^2 = 183.5\ ft^2$$

PROVIDE 11 steel footings each side

FOOTING size $3' \times 3' = 9\ ft^2$ TOTAL area $= 9\,(22) = 198 > 18$

HOWEVER, SINCE FOOTINGS ARE PLACE @ 45° angl, twice area required ($18\ ft^2$) per footing

- use $4.5' \times 4.5'$ footing

ALUMINUM DECKING ANALYSIS


```
 ****************************************************
 *                                                  *
 *           S T A A D - III                        *
 *           REVISION 16.0 (VERSION 16 LEVEL 0)     *
 *           PROPRIETARY PROGRAM OF                 *
 *           RESEARCH ENGINEERS, INC.               *
 *           DATE=    APR 25, 1993                  *
 *           TIME=    22:44: 5                      *
 *                                                  *
 ****************************************************

  1. STAAD SPACE          PLATE
  2. UNIT KNS MET
  3. INPUT WIDTH 79
  4. OUTPUT WIDTH 79
  5. JOINT COORDINATES
  6.     1        0.000        0.000        0.000
  7.     2        0.833        0.000        0.000
  8.     3        1.666        0.000        0.000
  9.     4        2.500        0.000        0.000
 10.     5        0.417        0.417        0.000
 11.     6        1.250        0.417        0.000
 12.     7        2.083        0.417        0.000
 13.     8        0.000        0.833        0.000
 14.     9        0.833        0.833        0.000
 15.    10        1.666        0.833        0.000
 16.    11        2.500        0.833        0.000
 17.    12        0.417        1.250        0.000
 18.    13        1.250        1.250        0.000
 19.    14        2.083        1.250        0.000
 20.    15        0.000        1.666        0.000
 21.    16        0.833        1.666        0.000
 22.    17        1.666        1.666        0.000
 23.    18        2.500        1.666        0.000
 24.    19        0.417        2.083        0.000
 25.    20        1.250        2.083        0.000
 26.    21        2.083        2.083        0.000
 27.    22        0.000        2.500        0.000
 28.    23        0.833        2.500        0.000
 29.    24        1.666        2.500        0.000
 30.    25        2.500        2.500        0.000
 31. MEMBER INCIDENCES
 32.     1     1     2
 33.     2     2     3
 34.     3     3     4
 35.     4     1     8
 36.     5     1     5
 37.     6     2     5
 38.     7     2     6
 39.     8     6     7
  0.     9     3     7
 41      10     4     8
 42.    11     4    11
 43.    12     5     9
 44.    13     8     9
 45.    14     9    10
```

```
 49.      18      8     15
 50.      19      8     12
  1.      20      9     12
 52.      21      9     13
 53.      22     10     13
 54.      23     10     14
 55.      24     11     14
 56.      25     11     13
 57.      26     12     15
 58.      27     12     16
 59.      28     13     16
 60.      29     13     17
 61.      30     14     17
 62.      31     14     18
 63.      32     15     22
 64.      33     15     19
 65.      34     16     19
 66.      35     16     20
 67.      36     17     20
 68.      37     17     21
 69.      38     18     21
 70.      39     18     25
 71.      40     19     22
 72.      41     19     23
 73.      42     20     23
 74.      43     20     24
 75.      44     21     24
  6.      45     21     25
 77       46     22     23
 78.      47     23     24
 79       48     24     25
 80. ELEMENT INCIDENCES
 81.      49      1      2      5
 82.      50      2      3      6
 83.      51      3      4      7
 84.      52      1      5      8
 85.      53      2      6      9      5
 86.      54      3      7     10      6
 87       55      4      7     11
 88.      56      5      8     12      8
 89.      57      6     10     13      9
 90.      58      7     11     14     10
 91.      59      8     12     15
 92.      60      9     13     16     12
 93.      61     10     14     17     13
 94.      62     11     14     18
 95.      63     12     16     19     15
 96.      64     13     17     20     16
 97       65     14     18     21     17
 98.      66     15     19     22
 99.      67     16     20     23     19
100.      68     17     21     24     20
  1       69     18     21     25
102.      70     19     22     23
103       71     20     23     24
104       72     21     24     25
105. MEMBER PROPERTY INFORMATION
106  1 TO 18 TA ST  MEMB
107  ELEMENT INCIDENCES
```

```
109. CONSTANT
110. E ALUMINUM ALL
  .. BET 90.  ALL
112. SUPPORT
113. 1 TO 4 8 11 15 18 22 TO 25 PINNED
114. LOAD 1 PRESSURE
115. ELEMENT LOAD
116. 19 TO 72 PR GZ 82.74
117. PERFORM ANALYSIS PRINT ALL
```

P R O B L E M S T A T I S T I C S

NUMBER OF JOINTS/MEMBER+ELEMENTS/SUPPORTS = 25/ 72/ 12
ORIGINAL/FINAL BAND-WIDTH = 7/ 7
TOTAL PRIMARY LOAD CASES = 1, TOTAL DEGREES OF FREEDOM = 150
SIZE OF STIFFNESS MATRIX = 7200 DOUBLE PREC. WORDS
TOTAL REQUIRED DISK SPACE = 0.00 MEGA-BYTES

Endnotes

[1] Sadeh Willy Z., et al. eds. Engineering, Construction, and Operations in Space III. 2 vols. (New York: American Society of Civil Engineers, 1992) 1: p. 7.

[2] American Institute of Steel Construction, Inc. Manual of Steel Construction, Allowable Stress Design, 9th Edition. (1989): pp. 2-4 - 2-5.

[3] Mendell, W. W. ed. Lunar Bases and Space Activities of the 21st Century. (Houston: Lunar and Planetary Institute, 1985): p. 72.

[4] Sadeh, Willy Z. Engineering, Construction, and Operations in Space III. p. 7.

[5] Gaylord, Edwin H. Jr. et al. Steel Structures Third Edition. (New York: McGraw-Hill, Inc. 1992): pp. 50-58.

Bibliography

Sadeh, Willy Z., Sture, Stein, and Miller, Russell J., eds. Engineering, Construction, and Operations in Space III 2 vols. New York: American Society of Civil Engineers, 1992.

Mendell, W. W. , eds. Lunar Bases and Space Activities of the 21st Century. Houston: Lunar and Planetary Institute, 1985.

Gaylord, Edwin H. Jr., et al. Steel Structures Third Edition New York: McGraw-Hill, Inc., 1992.

American Institute of Steel Construction, Inc. Manual of Steel Construction, Allowable Stress Design 9th Edition. 1989.

7.0 POWER

Department of Nuclear and Power Engineering
Mark Gleckler
Scott Hakel
Randall Hardin
Bobbi Hartwell
Jeff Kellar
Richard Listo
Jeff Long
Jenna McNanie
Chris Pickrell
Bill Reinwald
Ed Schulte
Scott Snider
Tim Taulbee
Grover Wilson

TABLE OF CONTENTS

1.0 INTRODUCTION

The National Aeronautic and Space Administration (NASA) has sponsored several Senior Engineers at the University of Cincinnati in a design project. The project is to design a facility to convert ice in the regolith that was found at the northern pole of the Moon and convert it to liquid propellant at the equator of the Moon. To do this, the ice needs to be removed from the mined regolith and then transported to the equator. There it can be further separated and converted to rocket fuel. This project is being designed by several engineering groups at the University of Cincinnati which are: Aerospace, Chemical, Civil and Environmental, Electrical and Computer, Materials Science, Engineering Mechanics, and Nuclear. Each group was assigned a different task in this project.

The Nuclear Engineering Group has been assigned to provide the needed stationary and mobile power for this mission. Our group has also assumed the responsibility of environmental, safety, and health management of humans and equipment involved because of our knowledge in the area with radiation. We have been working with the other groups to get a estimate on the range of power that will be needed. With this information we were then able to decide on the type of power and conversion system to best meet these needs. Other issued that have been addressed are safety, cost, room for expansion, loss of power demand, setup, and shutdown. Another objective of our group was to maximize our resources. For example, we can use excess heat from our reactor to directly heat the water in a chemical separation facility or use the lunar regolith as a shield for radiation.

To meet the stationary power demands, we have decided to provide electricity from SP-100 nuclear reactors. These reactors are coupled with dynamic conversion systems to produce electricity that will then be sent to a grid system to be used as needed. For mobile power needs, such as rovers and bulldozers, we have designed a DIPS

(Dynamic Isotope Power Supply) system that uses radioactive isotopes as the power source. These DIPS can also be used for items such as habitats or backup power.

2.0 POWER SUPPLY ON THE MOON

To meet the base stationary power demands we are using a modified SP-100 reactor. These reactors use a stirling engine system to convert heat to electricity. Some of the reactors will also be coupled with an in-core thermionic power conversion. Using the coupled system will enhance the efficiency to over 36% and increase the power output another 125kW. The reactors are of a standard modular design and more can be added to meet any future power demands. For any remote or mobile power needs, we plan to use DIPS to meet the power demands.

2.1 STATIONARY POWER AT THE POLAR SITE

To meet the stationary power needs at the northern polar region, we have designed a setup to use three SP-100 reactors. The reactors will supply a total of over 2.025MW which was based on our power estimate from the information from the other groups with a 50% backup supply. All three reactors will be using the thermionic conversion system. The reactors will be hooked up in a triangular area in a ring bus design and connected to a grid where the electrical power can be controlled.

2.2 STATIONARY POWER AT THE EQUATOR SITE

Jordy City is the lunar colony assumed to already exists at the equator. The power for the additional facilities to be built at the equator are to have their own independent system and distribution. We do, however, plan to connect the power sources for the new facilities and Jordy City. This will allow back-up emergency power to both locations. The power demand for the new facilities are relatively small. It primarily consists of the rail

gun catching mechanism and the chemical separation facility. We plan to provide the power there by using two SP-100 reactors with a stirling system and no thermionic topping system. We decided not to use the thermionic topping system since there is not a large power demand, and using the thermionic topping system with the SP-100 reactor will only increase the cost.

2.3 MOBILE POWER

Not all of the power needs of the mission can be met from a central power station and a fixed distribution grid. Power will be needed at communication relay stations, remote science outposts, mining sites, and other miscellaneous locations. Power will also be needed for an assortment of surface rovers, construction vehicles, and mining vehicles. The power required will range from a couple of kilowatts to around thirty kilowatts. Some typical power requirements are shown in Table I.

Table I: Typical Power Applications[a]

Application	Power Needed
Fixed Elements:	
• communication station	1 kW_e
• early power base	5-15 kW_e
• science outpost	2-10 kW_e
Mobile Elements:	
• robotic rovers	3 kW_e
• robotic payload unloaders	up to 10 kW_e
• robotic construction equipment	up to 10 kW_e
• unpressurized manned rovers	3 kW_e
• pressurized manned rovers	7 kW_e average, 12kW_e peak
• regolith haulers[b]	3kW_e average, 10-12 kW_e peak

a. This table is adapted from "Versatile Dynamic Isotope Power Systems for the Exploration of Space," Proceedings of the Eight Symposium on Space Nuclear Power, ed. Mohammed S. El-Geuk and Mark D. Hoover (Albuquerque, NM: American Institute of Physics, 1991), 547.

b. The regolith hauler may be thought of as a combination dump truck and bulldozer.

It is not feasible to try to custom design power supplies for each of these applications. Instead, a modular power unit has been designed (a 2.5 kW_e Dynamic

Isotope Power Supply, DIPS). Previous studies have shown that 2.5 kW_e is the optimum power output for the range of interest[1]. Four alternatives to mobile power were examined to be used before the DIPS option was chosen. They were chemical batteries, fuel cells, RTGs, and DIPS. These modules can be combined to meet a wide variety of power requirements. The 2.5 kW_e DIPS units will be used during all phases of the lunar mining project.

2.4 ELECTRICAL POWER SUPPLY

The distribution grid consists of a series of transmission lines, transformers, and switch gear that connect facilities needing electric power to reactors generating power. The grid must provide/remove power efficiently and reliably.

The pattern of power line connections and protective devices is determined by the need for reliability. Reliability is determined by failure rate, mean time to repair individual components, as well as the redundancy of components. The lines will be connected in a modified ring bus configuration to maximize redundancy in the system. On the lunar surface, find and correcting a problem in a buried electric line could result in a very high mean time to repair. To reduce this problem, the electric lines are divided into 100 meter, line maintenance segments.

Each line maintenance segment (LMS) has ten conduit sections. The condition of the lines at each section can be checked from the beginning of the LMS. Line crews would only have to travel to the beginning of the LMS, connect an electronic meter and within seconds any problems in the line would be narrowed down to a ten meter section. This not only reduces the mean time to repair, it also reduces the exposure to personnel.

---

[1] Maribeth E. Hunt, William D. Otting, and Richard D. Rovang, "2.5 kWe Dynamic Isotope Power Systems for Lunar and Mars Surface and Remote Power," in Nuclear Technologies for Space Exploration, (Jackson, WY: American Nuclear Society, 1992), Vol. 1, 140.

The reliability of the distribution grid is important to the entire fuel production process. The grid is the lifeline of power to the processing facilities. It also removes power from the reactors to prevent the need for emergency cooling. The accessibility of the maintenance segments improves this reliability and assures the continued supply of power to the fuel processing facilities.

3.0 SP-100 REACTOR SYSTEM

The SP-100 reactor program was started in the U.S. in the early 1980's to meet the further need for higher power in space. The payload cost for this system is expected to be around $3,663,870,000 and weigh a total of 52,341 kg. The preferred emplacement strategy is to bury the reactor 5 meters and deploy a shield blanket under the heat rejection subsystem radiators to capture neutrons and to prevent radiator scattering. With the reactor buried 5 meters and the shield blanket deployed, the dose rate for a single reactor unit is greatly reduced, thus making working conditions more favorable.

3.1 DESCRIPTION OF REACTOR AND SUB COMPONENTS

Each SP-100 lunar power module includes the following eight subsystems; 1) Reactor, 2) Reactor Instrumentation and Control (RI&C), 3) Shield, 4) Heat Transport, 5) Converter, 6) Heat Rejection, 7) Power Conditioning Control and Distribution (PCC&D), and 8) Mechanical/Structural.

The Reactor subsystem is the heat source where a controlled nuclear reaction produces thermal power at high temperatures. The RI&C subsystem consists of temperature and neutron sensors, control drums and safety rod actuators, and the computer hardware and software necessary to control the reactor thermal power. The

Shield subsystem consists of lithium hydride, tungsten and beryllium materials configured to reduce the neutron and gamma flux emitted from the reactor and protect vital electrical components. The Heat Transport subsystem includes lithium coolant, niobium alloy piping, thermoelectric electromagnetic (TEM) pump, and the gas separator/accumulator which are necessary to transfer the thermal power at high temperature from the reactor to the hot side of the thermoelectric converter. The Converter subsystem continuously converts the thermal power from the reactor to electrical power with silicon germanium thermoelectric multicell converters. The Heat Rejection subsystem includes lithium coolant, titanium piping, ducts and heat pipes to radiate the waste heat from the cold side of the converter to space. The PCC&D subsystem consists of a one kilowatt auxiliary solar cell/battery power generator, electric power cables, control cables, power electronics, power module controller, shunt dissipater, computer hardware and software required to collect, control and distribute the electrical power from the power module to the lunar base control switching station. The Mechanical/Structural subsystem includes the structure required to support, deploy and protect the refractory metal from the lunar dust and mechanically interface the power system with the launch vehicle and the lunar landing and placement vehicle.

Safety

The SP-100 reactor design contains inherent safety features with negative temperature and power reactivity coefficients. The lunar reactor includes two independent shutdown systems with built-in redundancy, a passive cooling system capable of preventing loss of structural integrity in the unlikely event of a loss-of-coolant accident, a double-contained lithium loop to eliminate single point failures and other design features that assure sub criticality under all accident conditions.

To properly predict how the core design a set of criticality experiments have been conducted by Argonne National Laboratory. The Zero Power Physics Reactor was built

to measure the neutronic features of a variety of critical assemblies. A mockup of the SP-100 core design was assembled and tested at this facility. These tests validated all key neutronic predictions of the design, including its safety in the unlikely event of a launch or re-entry accident.

An important element within the reactor core is the auxiliary coolant loop (ACL). Its purpose is to remove the residual heat produced by the reactor after shutdown in the unlikely event of accidental loss of the primary coolant following operation. This cooling loop will maintain the structural integrity of the core and prevent core disruption because of overheating. The key to the design is a set of tubes strategically inserted throughout the core pin bundles and coupled to a common manifold. Detailed three dimensional thermal analysis have shown that this ACL design keeps the peak fuel temperature well below its limit even with a postulated instantaneous loss-of-coolant accident at full power.

Reactor Shielding

The preferred emplacement strategy is to bury the reactor 5 meters and to deploy a shield blanket under the heat rejection subsystem radiators to capture neutrons and to prevent radiator scattering. The exclusion boundary, or distance where the dose rate is 5 rem/yr with the reactor buried 5 meters and the shield blanket deployed, is 180 meters for a single reactor unit. Because there is multiple SP-100 reactors in a relatively small area, additional shielding is being designed to enable work on electrical transmission lines.

Heat Transport Subsystem

The heat transport subsystem components are located in the region between the reactor and the support feet attachment points. There are six reactor inlet pipes and six reactor outlet pipes to circulate lithium. There are six linked Thermoelectric Electromagnetic (TEM pumps). The pumps require a temperature gradient to operate.

This gradient is provided as heat and is transferred to the heat rejection subsystem across twelve power converter assemblies.

The flow path for a single loop is as follows: lithium exits the reactor, passes through the primary duct of the first TEM pump, enters two paralleled power converter assemblies, enters the primary duct of the second TEM pump, and finally, returns to the reactor. A gas separator/accumulator (GSA) is attached to each of the six loops. The GSA makes use of lunar gravity for gas separation.

Thaw of the heat transport subsystem is accomplished by natural circulation and a series of bypass lines. "Natural circulation is driven by both the density difference between hot and cold lithium and lunar gravity. It is estimated that the thaw of the LSPS can be accomplished in less than 24 hours."

Power Assembly Enclosure

All LSPS components fabricated from PWC-11 are enclosed in a dust sealed Power Assembly Enclosure for safety and material compatibility considerations. For postulated non-energetic core melt events, this confinement ensures that core solids would remain in the vicinity of the reactor. The confinement also ensures that the lunar soil does not chemically or mechanically react with niobium based alloys.

Heat Rejection Subsystem

For the LSPS, there are 12 independent segments in the heat rejection subsystem. Heat is transferred from the primary to the heat rejection subsystem (secondary) lithium loops in the power converter assemblies. The secondary lithium acts as the cold sink for the thermoelectric materials. The lithium is then pumped by the secondary side of the TEM pumps through fixed titanium piping, through a flexible joint required for radiator deployment, and through the radiator panel lithium supply duct. At the end of the radiator, the radiator panel supply ducts act as return ducts. The lithium then flows back

to the TEM pump through the return duct, flexible joint, and fixed piping. The TEM pump supplies pressure head and adds some rejected heat to the secondary lithium.

Thermal Shield Subsystem

A multi-layer aluminum thermal shield is located below the heat rejection subsystem radiators. This shield is needed to reflect thermal radiation to space and to provide a cooler environment for the cavity cooling subsystem radiators.

Cavity Cooling Subsystem

The cavity cooling subsystem (CCSS) is required to maintain the shield and control reflectors within their operating temperature range and to maintain the lunar soil below 870K, at which temperature offgassing could become a problem. The CCSS radiators operate at a lower temperature than the heat rejection subsystem radiators. The CCSS is a naturally circulating NaK system that is designed to dissipate 40 kW_t.

The CCSS consists of six independent closed loops fabricated from titanium. Each loop consists of the following four regions: lower annulus surrounding the reactor vessel and control reflectors, piping passing through the shield and connecting to the heat rejection radiators and return piping. The maximum NaK operating temperature is 605 K. The CCSS is thawed by natural circulation in approximately three days.

Optional Dust Cover

To prevent the build-up of lunar dust on radiator surfaces, and the subsequent degradation in radiator performance, an optional dust cover is provided for each reactor unit. It is designed to be inflated and then back-filled with a structural foam.

Monitoring and Control

The monitoring and control of each reactor unit utilizes fiber optic links to the habitat. Override control of the reactor is maintained by earth mission control. The astronauts can monitor reactor performance, issue global commands (i.e. start up, shutdown, go to x% power) and scram the unit in case of an emergency. Reactor control, however, is designed to be autonomous.

3.2 DESCRIPTION OF POWER CONVERSION SYSTEMS

An integration study was performed by Rocketdyne in coupling an SP-100 reactor to either a Brayton, Stirling, or K-Rankine power conversion system. The application was for a surface power system to supply power requirements to a lunar base. A power level of 550 kWe was chosen as the desired power output (Harty 1992, 221). The Stirling has a full power operating lifetime of approximately 10 years, while the Brayton and K-Rankine have lifetimes of 7.6 and 7.4 years, respectively. The Stirling and Brayton are simple to startup and shutdown, while the K-Rankine is complex to control. The Brayton is capable of load following, while the Stirling can load follow only in discrete power increments.

Based on much research and study, we chose to use the Stirling as the dynamic conversion system. The Stirling system has the highest efficiency and is the easiest to integrate, while the Brayton and K-Rankine systems have lower efficiencies and are harder to integrate. Unlike the K-Rankine, the Stirling is simple to operate and is capable of allowing discrete power changes. Although the Stirling has the greatest mass, it is capable of operating at full power for approximately 10 years (2 years longer than the Brayton or K-Rankine system). In addition, the radiator area of the Stirling is 36% less than the Brayton system. A smaller radiator area is beneficial in respect to the possibility of occurring from meteor showers. The Stirling is an intelligent choice for the dynamic conversion system for the SP-100 space reactor.

4.0 DYNAMIC ISOTOPE POWER SUPPLY SYSTEM

A 2.5 kW_e DIPS module has been developed for use in remote and mobile power situations. The 2.5 kW_e DIPS module has four basic systems: the fuel pile (Pu-238), the power conversion unit (based on the Stirling cycle), the waste heat rejection unit (radiators), and the power conditioning unit.

The fuel pile contains 54 General Purpose Heat Sources (GPHS). Each GPHS has a mass of 1.5 kg and produces 250 watts of thermal power at the beginning of its life. Heat is removed from the fuel pile through the use of heat pipes imbedded in the molybdenum structural material. Na is the working fluid in the heat pipes. The heat pipes connect to a common manifold before going to the power conversion unit. The mass of the GPHS and structural materials is 117 kg.

From the manifold heat pipes lead to eight independent Free Piston Stirling Engines (FPSE) modules that are used to produce electricity. Each module can produce 0.5 kW_e and has a mass of 7 kg. The mass of all 8 modules is 56 kg. Heat enters the FPSE at 1300 K from the fuel and is rejected from the engines at a temperature of 650 K. The FPSE modules operate with an efficiency of 24% at this temperature range. Eight FPSE modules are used to provide a margin of safety. Up to three of the eight modules can fail before the power output falls below 2.5 kW_e.

Waste heat from the FPSE is removed to the radiators. The radiators have a combined area of 1.5 m^2 and a mass of 14 kg. The power conditioning unit couples the electrical output of the FPSEs to the load. This unit has a mass of 73 kg. The total mass of the 2.5 kW_e DIPS module is 260 kg. The transportation cost of each module approximately $29 million to the polar region and $20 million the equator from earth in both cases. Table II highlights some of the key characteristics of the 2.5 kW_e DIPS.

Table II: Reference 2.5kW$_e$ DIPS Performance

System Specific Power	9.6 W$_e$/kg
System Mass	260 kg
System Life	15 years
# of GPHS	48
Efficiency of FPSE	25%
BOM Power (year 1)	2.88 kW$_e$
EOM Power (year 15)	2.5 kW$_e$

The 2.5 kW$_e$ DIPS modules are able to function with very little human interaction. Once the modules have been emplaced they require no regular maintenance. The only element that has any moving parts is the FPSE and this has only two moving pistons floating on gas bearings in a sealed unit. Control of the DIPS module is handled by what load the modules are connected to. The DIPS modules can be run autonomously and be abandoned at a site for months or longer.

5.0 SETUP PROCEDURE

Since power will be crucial to do anything at the pole, the procedure for setting up the site will be important. Since there is no prior development, it will be necessary to send communication equipment and survey probes to examine the site more thoroughly. Unmanned cargo ships can then be sent to the area before the astronauts arrive to reduce their time there. The cargo ships will contain items like self-powered rovers and any other equipment the astronauts may need. Next, the people that will be starting the construction will need to be deployed at the pole. They will arrive in a space capsule that will provide them with life support for the time needed and a means to get back to the equator or Earth. Once at the pole, these people will excavate holes for the SP-100 reactors with the provided equipment. Once they complete the site and are ready for the next shipment, the SP-100 reactor can be sent to their spot. Two reactors units will be sent for this phase since the third will not be needed until the site is completed. Along with the reactors, the

materials for the grid will be needed to be sent along with any equipment needed to control the reactor. Next, we will be sending a large habitat that will house all the construction workers present. This habitat will be used as the life support for the entire ten year lifetime of the mining site. This habitat should also contain the control room for the grid and reactor control. This way the astronauts will not have to leave the habitat to control the reactors. This habitat should also contain the control for the rail gun. It should be designed to protect any one from the environment, especially solar flares. Once the grid and the habitat are set up, the reactor can be started to provide the needed power for the habitat and the upcoming construction. With the power ready to go, the other facilities can be sent up to the site along with any extra construction workers needed. The previous workers can stay at the site and move into the large habitat. The space capsule that was used previously can now be used as a backup life support and means of escape. While construction is going on, the other SP-100 systems can be sent up and placed into the desired locations. Prior to doing this though, holes will need to be excavated similar to the previous reactors.

6.0 CONCLUSION

As design preparations come to a close, we can observe an overall view of the power systems for this project. Stationary power will be provided by SP-100 reactor systems, some of which will be modified with an in-core thermionic power conversion system. For mobile power systems a modular power unit has been designed in the DIPS system which was the most appropriate for our needs. Also important is the power distribution grid which delivers power to all facilities. This is especially important in this space power application since a high reliability is required. The entire facility is designed to be set up efficiently, continuously provide power for the railgun system, and for hydrogen recovery processing, as well as backup power for the existing colony if

necessary. We have designed this these power systems to fulfill all these requirements, keep damage to the lunar environment to a minimum, and ensure maximum safety to all personell. With these designed systems, these goals are realistic and will be achieved.

8.0 COMMUNICATIONS

Department of Electrical and Computer Engineering
John Penix

TABLE OF CONTENTS

Abstract

Due to the additions to the Lunar Industrial Park and the introduction of activities at the lunar pole it will be necessary to upgrade the existing communications system on the moon. The upgraded system should support the communication, data acquisition, and command needs of the lunar mining facilities.

The existing system is assumed to support only the current Lunar Research Center activities using the Deep Space Network here on Earth. It is also assumed that the existing support covers only the area around the research center and not the entirety of the lunar near-side surface.

The proposed upgrade consists of adding an additional transmitter at the Lunar Research Center as well as a transmitter at the lunar pole mining site. A lunar relay satellite will then be placed in a halo-like orbit over the near-side surface. This will then be in contact with the Deep Space Network here on Earth. There is also the possibility of adding a pair of geostationary satellites to allow centralization of the earth based communications and control systems.

Table of Contents

List of Figures

Introduction

The existence of mining and propellant processing operations on the moon introduces a need for expanded communications coverage and bandwidth. The existing communications resources at the Lunar Research Center and the Lunar Industrial Park will not be sufficient to support the communication needs of the chemical processing plant and the propellant storage facilities being added to these sites. In addition, the mining operations and the benefication activities at the lunar pole represent an area that is not covered by the current communications system. There is also a preference to centralize the earth based communications center with the continued expansion of lunar activities.

By predetermining the needs of the mining and propellant processing operations, a communications system upgrade is proposed that support the needs of the new facilities. The types of services needed between the various sites and the corresponding data rates have been take into account. The system upgrade will consist of additional transmitters at both the equatorial and lunar pole sites as well as a lunar relay satellite to provide a link between these two sites and earth. The lunar relay satellite will reside in a halo-like orbit to provide lunar near-side coverage that will allow for communications and navigational information to be received by rovers. Coverage of the entire lunar near-side cannot be achieved with the existing Deep Space Network alone because the beam widths of the antennas are too narrow. The ability to centralize the earth based communications and control operations will be supported by the addition of two geostationary

satellites working with the Deep Space Network. There will also be a need for greater redundancy in the system due to the higher importance of the propellant processing operations.

Proposed Conceptual Design

The main assumption made in the design of the communication system is that it is an upgrade to an existing system. The basis for the specifics for the existing system and the upgrade options come from a NASA presentation outline describing the work that has been done in proposing a Telecommunications, Navigational, and Information Management (TNIM) system architecture for operations on Mars and the moon. The assumption is made that the current operations at the Lunar Research Center are small and are of scientific, not processing or manufacturing nature and the existing system architecture would reflect this. It is also assumed that use of the Deep Space Network will be available due to its utilization by the NASA proposal.

This level of operation would require only a minimum or moderate capability system as described by NASA. This system would involve the use of the current Deep Space Network and a single lunar surface terminal located at the research center's equatorial site. This assumption does not require any technological development beyond current levels and uses an upgrade that is currently underway for the Deep Space Network, taking it from S-band (2-4 GHz) to X-band (8-12 GHz). This minimum capability system is depicted in Figure 1.

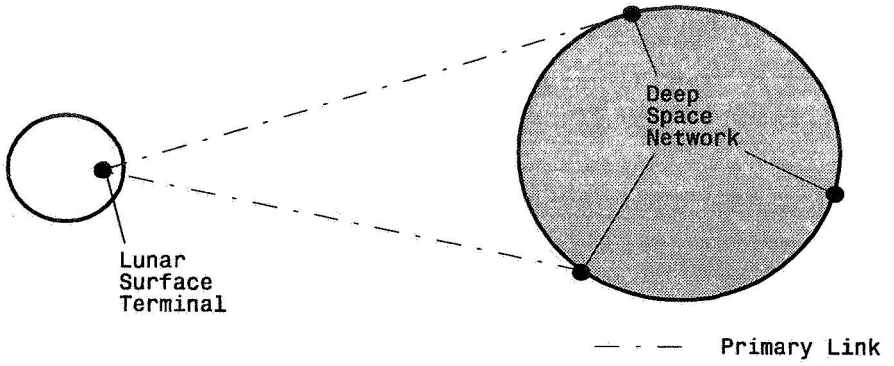

Figure 1. Existing Lunar Research Center TNIM architecture

The two basic objectives to be achieved by the communications system upgrade are to support the additions to the Lunar Industrial Park and the new operations at the lunar pole. Both of these requirements will be met with the addition of lunar surface terminals at the corresponding sites. These terminals will have both transmitting and receiving abilities capable of communicating with earth and with a relay satellite orbiting the moon.

To allow for communication between the two lunar sites and to add redundancy to the overall communications system, there will be a lunar relay satellite poised in a halo orbit over the near side of the lunar surface. This satellite will also provide the capability of covering the entire near side lunar surface, which was not possible using the Deep Space Network. With the use of phased-array antennae, the lunar relay satellite will be able to track and monitor vehicles roving on the near-side. This may include tracking and navigational assistance for the rail-gun projectile that is being sent from the pole to the equator for further processing. The proposed upgrade of the lunar systems is shown in figure 2.

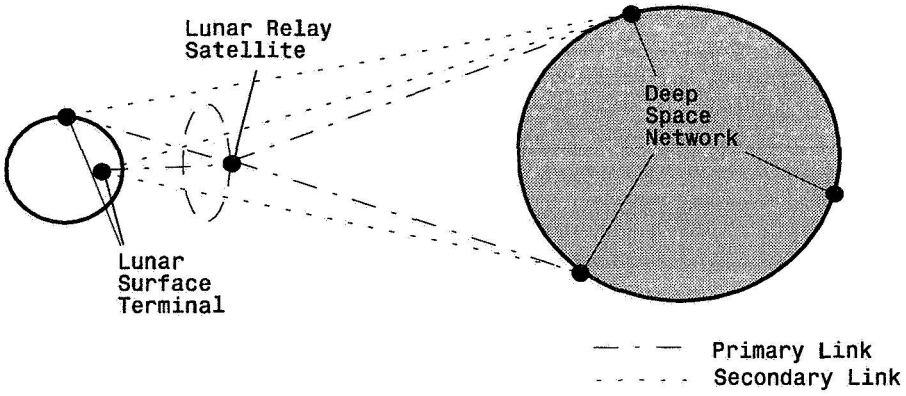

Figure 2. Proposed Lunar Communication Support System

There may also be the preference of having a centralized command and control location here on Earth. To accommodate this preference there will have to be additional upgrades to the Deep Space Network link to the lunar end of the communication system. This addition would consist of two geostationary satellites working with one surface terminal on Earth. This architectural geometry would provide a constant communications link to the lunar end of the system from one earth based location.

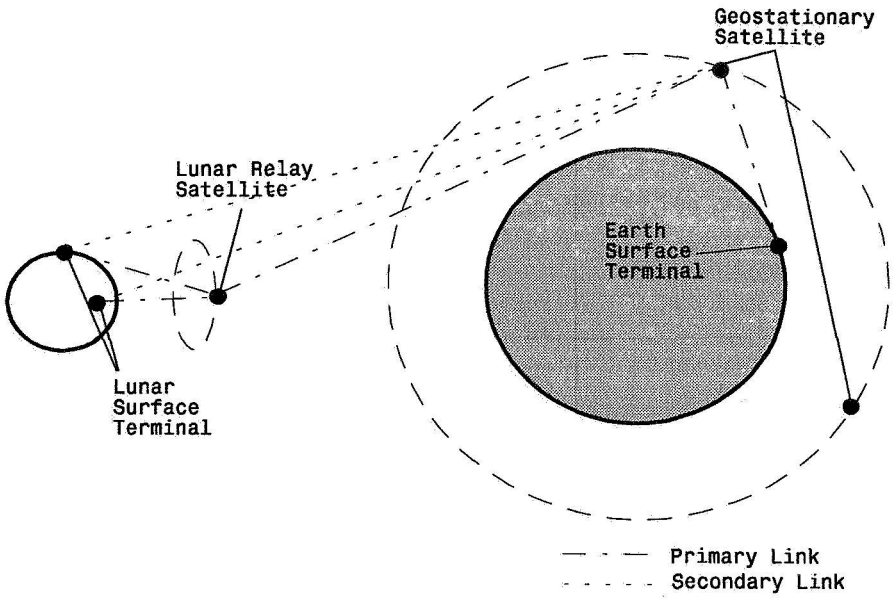

Figure 3. Proposed Communication System With Centralized Earth Command-Control Location

This second system architecture could be implemented with the first system architecture as a backup for redundancy in the communication links.

Design Support Considerations

There are four basic system elements in the existing and upgraded communication system architecture presented. These are the Deep Space Network and their corresponding earth surface terminals, the geostationary relay satellites, the lunar relay satellite, and the lunar surface terminals.

The first of the four, the Deep Space Network, is an already established communication system whose resources will be utilized for the lunar mining and propellant processing operations. At present, an upgrade is underway that would convert the Deep Space Network from S-band to K-band operations. It may eventually be necessary to convert the system to Ka-band (27-40 GHz) to facilitate even larger data requirements from the Lunar Industrial Park.

The geostationary relay satellites will consist of a microwave receiver and transmitter powered by a solar array. This will require two transmitter antennae about 1-2 meters in diameter operating in the range of 50 - 100 watts, depending on the operational frequency. There will also have to be resident storage cells to insure link availability when the satellite moves through the shadow of the Earth each day. The mass of this satellite is estimated in the range of 600-1000 kilograms.

The lunar relay satellite will be very similar in configuration to the geostationary satellites. There will be the need of a third 1-2 meter transmit antenna to allow for communications between the pole, the equator and Earth without repositioning the satellite. There is also the possible addition of a phased-array antenna to handle communications on the near-side surface. This will require an additional power source

in the range of 100 watts, again depending on the frequencies desired. The mass of this satellite is estimated to be 800 - 1200 kilograms.

The lunar surface terminals will also consist of a microwave receiver and transmitter pair. These will require antennae approximately 1-2 meters in diameter, depending on the frequency of operation. The power source will be in the range of 200 watts.

During the buildup phase of the lunar sites, the system will be able to operate using only the lunar surface terminals and the Deep Space Network. The lunar relay satellite can be added when a larger bandwidth or higher frequency of communication is needed between the two lunar sites. During the operational phase, the lunar relay satellite will definitely be needed for the larger bandwidth, navigational assistance, and to introduce link redundancy. It will also be during the operational phase that the need for a centralized Earth control center may arise. This would be when the two geostationary satellites would be deployed.

Summary

The proposed communication upgrade is designed to support the foreseeable needs of the lunar propellant processing operations. The basic operational system utilizes the undergoing upgrade of the Deep Space Network and introduces lunar surface terminals at both lunar sites, a lunar relay satellite and two geostationary satellites.

The power requirement for keeping the lunar relay satellite in a halo orbit over the near-side has yet to be determined. It is also not known if the necessity of centralizing the earth based operations will be worth the cost of deploying and maintaining the two geostationary satellites.

Appendix I

Transmit Power vs. Antenna Diameter Data

OPERATIONAL L2 LRS-ERS (2-2-2)

Rb=500 Mbps, NF=1.0 dB, Dr=2.0, QPSK

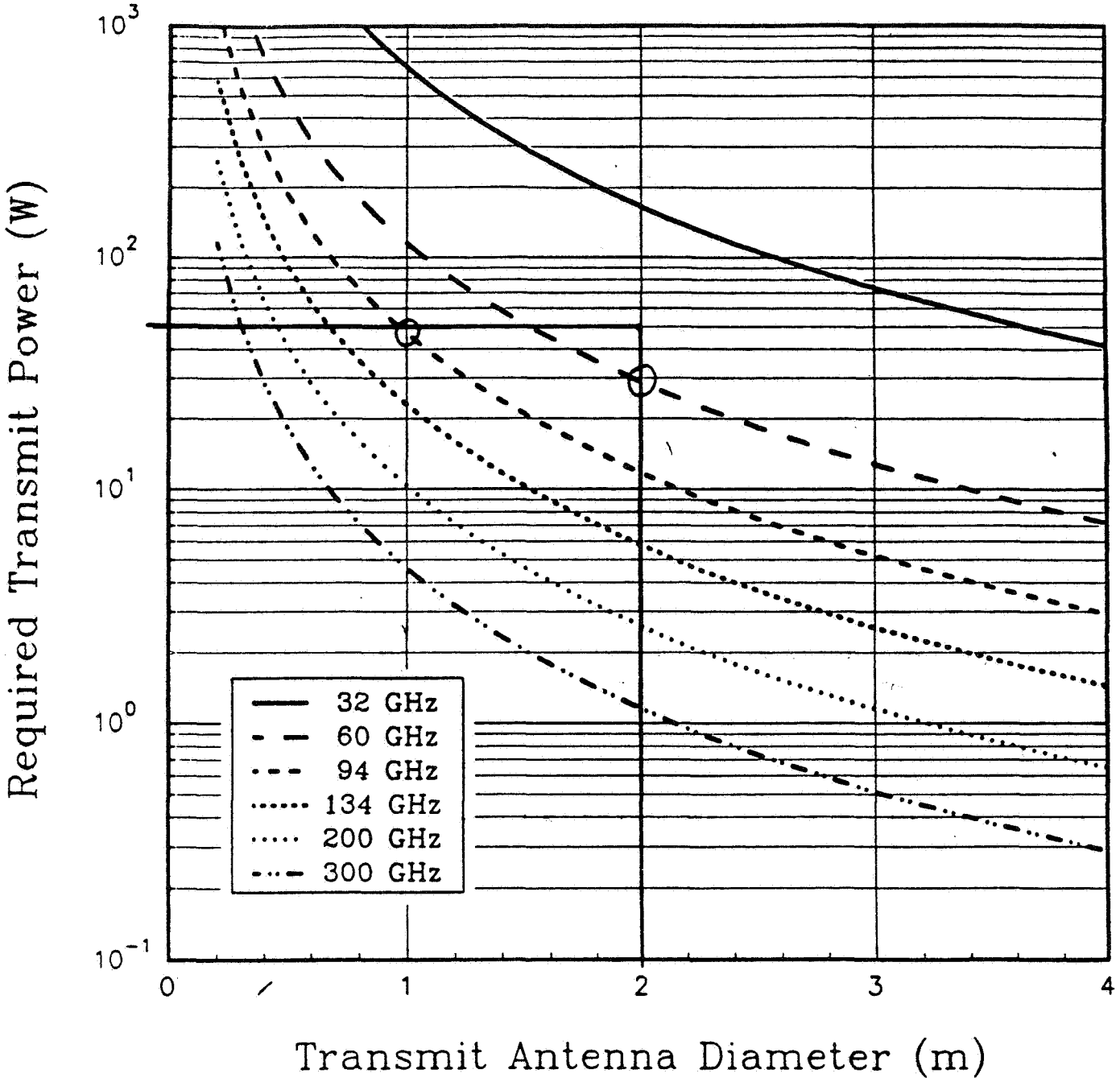

EVOLUTIONARY LR-LRS (3-13-3)

Rb=100 Mbps, NF=0.5 dB, Dr=1.0 m, QPSK

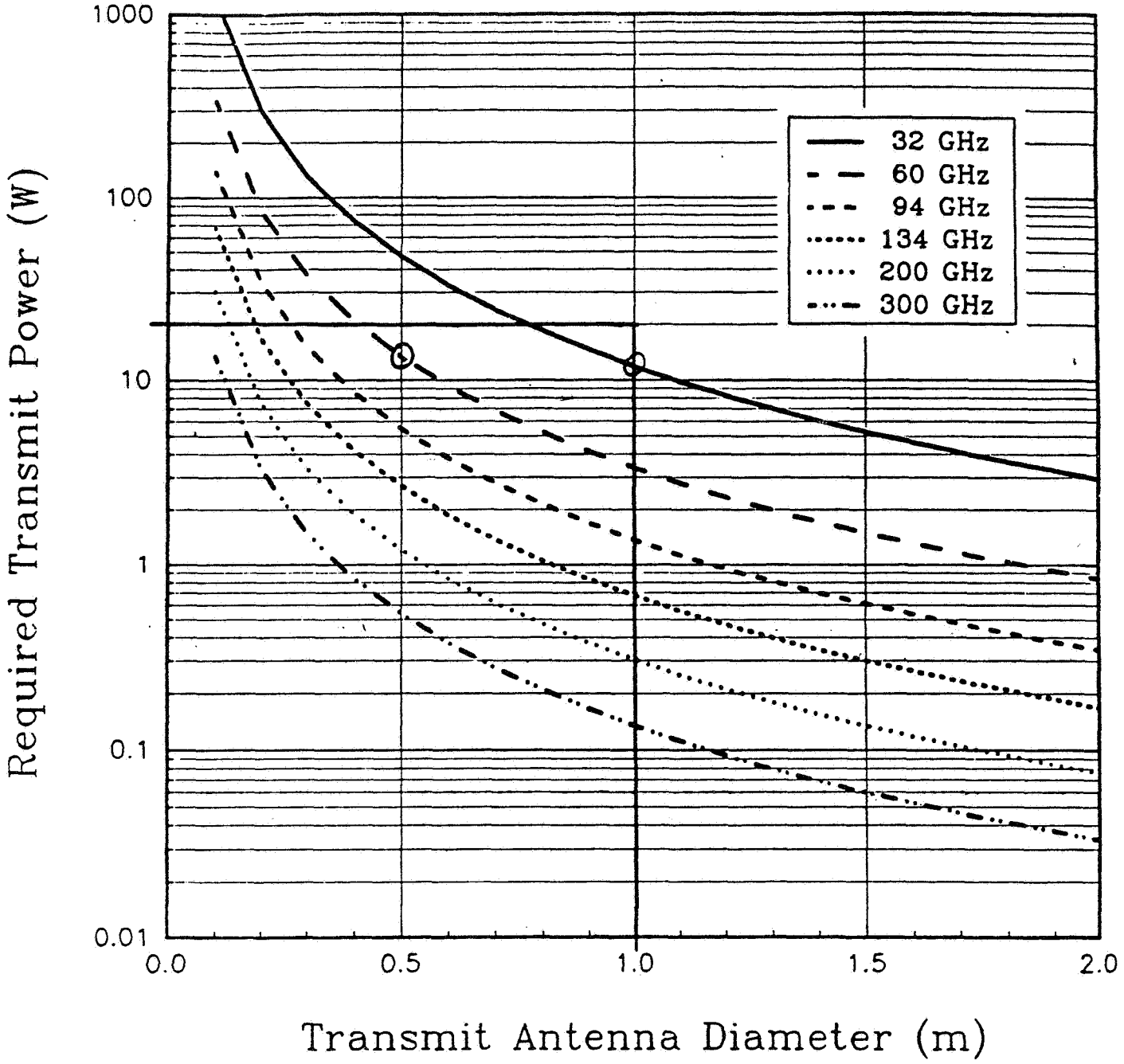

References

Zuzek J. Space Communications Seminar - Seminar notes. NASA Lewis Research Center, Cleveland, Ohio

Sanders, K.F. 1987 Microwave Components and Systems Addison-Weslsy